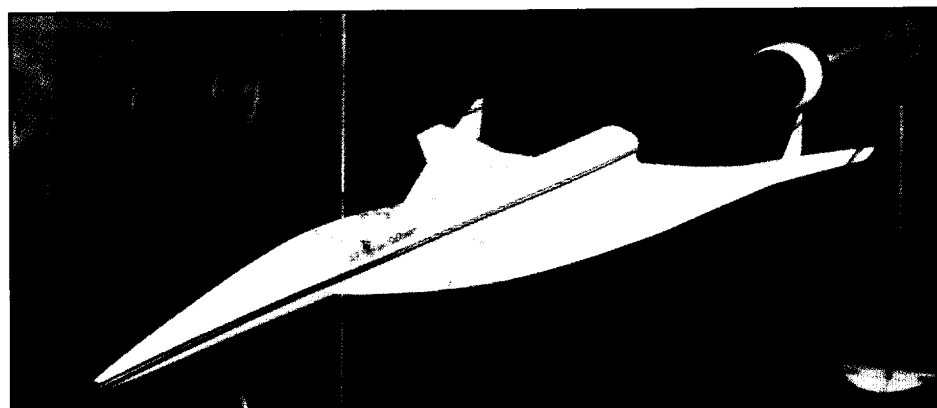
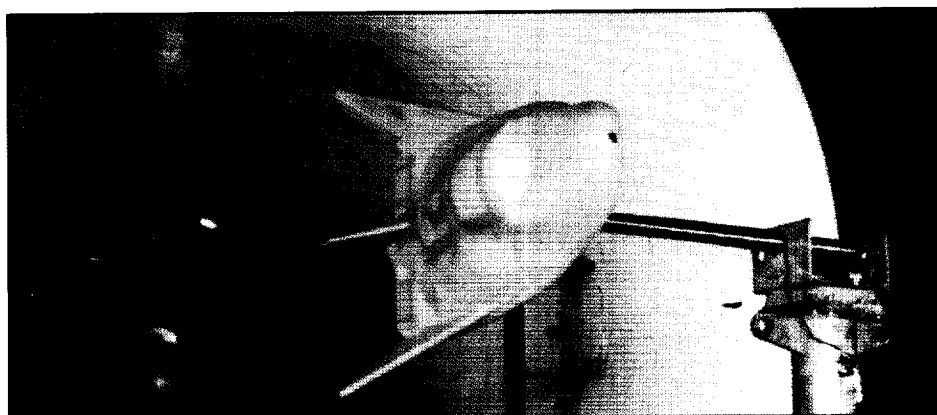


# Langley Aerospace Test Highlights



# 1990

Langley Research Center  
NASA Technical Memorandum 104090

ORIGINAL PAGE  
BLACK AND WHITE PHOTOGRAPH

LANGLEY AEROSPACE TEST CELL 95P  
NASA 104 090

Unclas  
65/99 0021405

W91-25112



# Langley Aerospace Test Highlights 1990



National Aeronautics and  
Space Administration

**Langley Research Center**  
Hampton, Virginia 23665-5225

**Langley Research Center**  
NASA Technical Memorandum 104090



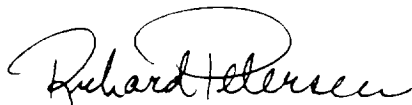


# Foreword

---

The role of the NASA Langley Research Center is to perform basic and applied research necessary for the advancement of aeronautics and spaceflight, to generate new and advanced concepts for the accomplishment of related national goals, and to provide research advice, technological support, and assistance to other NASA installations, other government agencies, and industry. This report highlights some of the significant tests that were performed during calendar year 1990 in the NASA Langley Research Center test facilities, a number of which are unique in the world. The report illustrates both the broad range of the research and technology activities at the NASA Langley Research Center and the contributions of this work toward maintaining United States leadership in aeronautics and space research. Other highlights of Langley research and technology for 1990 are described in *Research and Technology 1990—Langley Research Center*.

Further information concerning both reports is available from the Office of the Chief Scientist, Mail Stop 105-A, NASA Langley Research Center, Hampton, Virginia 23665 (804-864-6062).



Richard H. Petersen  
Director

# Availability Information

---

For additional information on any highlight, contact one of the individuals identified with the highlight. This individual is either a member or a leader of the research group. Commercial telephone users may dial the listed extension preceded by (804) 86. Telephone users with access to the Federal Telecommunications System (FTS) may dial the extension preceded by 928.

Numerous photographs and figures were submitted in color by the authors. Please contact the Langley Research Center Photographics Section to determine if a color version is available. Langley (L) numbers are provided where available.

# Contents

---

<b>Foreword .....</b>	<b>iii</b>
<b>Availability Information .....</b>	<b>iv</b>
<b>30- by 60-Foot Tunnel (Building 643) .....</b>	<b>1</b>
Free-Flight Tests of Supersonic Persistence Fighter .....	2
X-31 Wind-Tunnel Free-Flight Tests .....	2
Stability and Control Research on Generic NASP Configuration .....	3
HL-20 Static and Dynamic Wind-Tunnel Tests .....	3
Forebody Controls Research .....	4
Tail Buffet Research .....	5
<b>Low-Turbulence Pressure Tunnel (Building 582A) .....</b>	<b>6</b>
Three-Component Laser Velocimeter Development for LTPT .....	7
High-Lift Airfoil Research .....	8
Reynolds Number Effects on Delta Wing of 65° .....	8
Subsonic Aerodynamics Characteristics of HL-20 Lifting-Body Configuration .....	9
Subsonic Aerodynamics Characteristics of HL-20A Lifting-Body Configuration in LTPT .....	10
<b>20-Foot Vertical Spin Tunnel (Building 645) .....</b>	<b>11</b>
Tumbling Research .....	11
Pressure Distributions in Rotational Flow .....	12
<b>7- by 10-Foot High-Speed Tunnel (Building 1212B) .....</b>	<b>13</b>
Effect of Winglets on Induced Drag for Low-Aspect-Ratio Wing .....	13
F-18 Forebody/LEX Test .....	14
High-Alpha Gritting to Simulate Flight Reynolds Numbers .....	15
Subsonic Control Effectiveness of HL-20 Lifting-Body Configuration .....	15
<b>14- by 22-Foot Subsonic Tunnel (Building 1212C) .....</b>	<b>17</b>
Rotor Inflow Research .....	18
Powered Ground Effects Investigation of a Single-Stage-to-Orbit Vehicle .....	19

---

<b>8-Foot Transonic Pressure Tunnel (Building 640)</b> .....	<b>20</b>
Fiber Optic-Based Laser Vapor Screen System .....	22
Wind-Tunnel Investigation of Generic High-Speed Civil Transport .....	23
 <b>Transonic Dynamics Tunnel (Building 648)</b> .....	 <b>24</b>
Flutter Tests of A-12 Advanced Fighter .....	25
Flutter Characteristics of Trail-Rotor Model .....	26
Aeromechanical Stability of Hingeless Rotors .....	27
Statically Unstable Model on Cable Mount System .....	28
NACA 0012 Benchmark Model Test .....	29
Transonic Shock-Induced Dynamics of Flexible Wing in TDT .....	30
 <b>16-Foot Transonic Tunnel (Building 1146)</b> .....	 <b>33</b>
 <b>National Transonic Facility (Building 1236)</b> .....	 <b>34</b>
Mach Number Calibration on National Transonic Facility Test Section .....	35
Reynolds Number Effects on High-Speed Civil Transport at Takeoff Speeds .....	36
Reynolds Number Effects on Commercial Transport .....	36
 <b>0.3-Meter Transonic Cryogenic Tunnel (Building 1242)</b> .....	 <b>38</b>
Half-Wing Test in Adaptive-Wall Test Section .....	40
 <b>Unitary Plan Wind Tunnel (Building 1251)</b> .....	 <b>41</b>
Flow Field Survey Apparatus for Unitary Plan Wind Tunnel .....	41
Sonic Boom Tests .....	42
Supersonic Aerodynamic Characteristics of Sidewinder Missile Variant Configurations .....	43
Incipient Leading-Edge Separation Study .....	43
Experimental Analysis of Optimized Waveriders .....	44
Supersonic Aerodynamics Characteristics of HL-20A Lifting-Body Configuration in UPWT .....	45
Supersonic Dynamic Stability Characteristics of NASP Test Technique Demonstrator Configuration .....	46
 <b>Hypersonic Facilities Complex (Buildings 1247B, 1247D, 1251A, 1275)</b> .....	 <b>47</b>
Flow Field Calibration of 15-Inch Mach 6 High-Temperature Tunnel .....	48
20-Inch Mach 6 Tunnel Laser Velocimeter Measurements .....	48
Aerothermodynamic and Aerodynamic Testing of Propulsion/ Avionics Module .....	50

---

Evaluation of Infrared Thermography for Hypersonic Heat-Transfer Measurements .....	50
Wind-Tunnel Blockage Tests of Scramjet Inlet at Mach 10 .....	51
Tests of Large Slender Bodies in 31-Inch Mach 10 Tunnel .....	52
Aerothermodynamic Measurement and Prediction for Modified Orbiter at Mach 6 and 10 in Air .....	53
Lateral-Directional Stability Characteristics of AFE Vehicle Configuration .....	55
Thermal Mapping Data Obtained With Thermographic Phosphors .....	56
Application of Focusing Schlieren Photograph for Flow Visualization .....	57
Thermal Effects on Flow-Through Balance Used in Hypersonic Scramjet Exhaust Flow Simulation Studies .....	58
Testing of Metric Forebody-Inlet Test Technique Demonstrator Model .....	59
Pitot-Rake Survey of Simulated Scramjet Exhaust Flow Field of 2-D Nozzle Model .....	59
Advanced Mach 6 Axisymmetric Quiet Nozzle in Nozzle Test Chamber .....	60
Mach 6 Powered Testing of Test Technique Demonstrator .....	61
Shock Interaction Heating in Generic Hypersonic Engine Inlet .....	62
<b>Scramjet Test Complex (Buildings 1221C, 1221D, 1247B) .....</b>	<b>63</b>
Transpiration Cooling in Vicinity of Fuel Injectors .....	66
Static Temperature Surveys in Scramjet Combustor .....	67
Subscale Scramjet Engine Tests .....	67
<b>Aerothermal Loads Complex (Building 1265) .....</b>	<b>69</b>
<b>Acoustics Research Laboratory (Building 1208) .....</b>	<b>71</b>
Simulation of Sonic Booms .....	72
Fatigue Crack Growth of Acoustic/Mechanical Loads in Aircraft Structures .....	72
High-Temperature Sonic Fatigue Testing .....	73
Active Control of Interior Noise in Large-Scale Fuselage Using Piezoceramic Actuators .....	74
Near Inplane Tilt-Rotor Noise .....	75
Duct Liner In Situ Tuning With Gas Percolation .....	76
Noise Propagation for Unique Helicopter Operational Characteristics .....	77
BVI Noise Prediction Validation .....	78
ASTOVL Acoustic Loads .....	79
Supersonic Elliptic Nozzle Acoustics .....	81
Rotor Noise Reduction Using Higher Harmonic Control .....	81
F-18 HARV Aeroacoustic Loads .....	83
Active Sound Attenuation Across Double-Wall Fuselage Structure .....	83
Active Control of Multimodal Random Sound in Ducts .....	84

---

<b>Avionics Integration Research Laboratory (AIRLAB)</b>	
<b>(Building 1220)</b> .....	<b>86</b>
Validation of Formally Verified Clock Synchronization Theory .....	87
<b>Aerospace Controls Research Laboratory (Building 1232A)</b> .....	<b>89</b>
Control Moment Gyro Steering Law Testing on SCOLE .....	90
<b>Transport Systems Research Vehicle (TSRV) and TSRV Simulator</b>	
<b>(Building 1268)</b> .....	<b>92</b>
Flight Tests Using Data Link for Air Traffic Control and Weather	
Information Exchange .....	93
Knowledge-Based Flight Display Information Management .....	94
<b>Crew Station Systems Research Laboratory (Building 1298)</b> .....	<b>96</b>
Ambient Lighting Simulator Experiment for High-Brightness TFEL Display .....	97
<b>Human Engineering Methods Laboratory (Building 1268A)</b> .....	<b>98</b>
Brainmap Analysis Identifies States of Awareness for System	
Monitoring Tasks .....	98
Multi-Attribute Task (MAT) Battery for Pilot Strategic Behavior .....	99
<b>General Aviation Simulator (Building 1268A)</b> .....	<b>101</b>
Easy-to-Fly General-Aviation Airplane Concept .....	101
<b>Differential Maneuvering Simulator (Building 1268A)</b> .....	<b>103</b>
One-Versus-Two Air Combat Study .....	103
Velocity-Vector Display in High-Alpha Air Combat Situations .....	104
<b>Visual Motion Simulator (Building 1268A)</b> .....	<b>106</b>
<b>Space Simulation and Environmental Test Complex</b>	
<b>(Buildings 1295 and 1250)</b> .....	<b>108</b>
Gas Response Test for HALOE Instrument Verification .....	109
Acceptance Testing of Aeroassist Flight Experiment Pressure Distribution/	
Air Data System Transducers .....	111
LITE Load Path Verification Test .....	111
Laser Doppler Velocimeter Measurements of Solar-Simulated Laser .....	112

---

<b>Advanced Technology Research Laboratory (Building 1200)</b>	<b>114</b>
Diode Laser Laboratory	114
Hydrogen Transport Barriers in Ti-Aluminides	115
Efficient Laser Medium for Solar Pumping in Space	116
<b>Structural Dynamics Research Laboratory (Building 1293B)</b>	<b>117</b>
Completion of CSI Mini-Mast Guest Investigator Test Program	118
Fabrication of DSMT Hybrid-Scale Space Station Model for Structural Dynamic Testing	119
Phase-Zero CSI Evolutionary Model Test-Bed	120
Experimental Validation of Dissipative Control Laws for CSI Evolutionary Model	121
<b>Materials Research Laboratory (Building 1205)</b>	<b>123</b>
Mixed-Mode Delamination Fracture Tests Using MMB Fixture	124
Evaluation of Fatigue of Thin-Sheet Aluminum With Multi-Site Damage	125
Inelastic Stress-Strain Response of Organic Matrix Composites at Elevated Temperatures	126
<b>Structures and Materials Research Laboratory (Building 1148)</b>	<b>127</b>
Space Crane Articulating Joint Test-Bed	128
Failure Modes of Composite Laminates Subjected to Bending	128
Evaluation of Oxidation-Resistant Carbon-Carbon Composite Materials	129
Aluminum-Lithium Alloy Built-Up Structure Development	130
Precision Composite Reflector Panels	131
<b>Polymeric Materials Laboratory (Building 1293A)</b>	<b>132</b>
Characterization of Polymer Molecular Weight	133
LaRC TPI Dry Powder Towpreg Process	134
<b>NDE Research Laboratory (Building 1230)</b>	<b>135</b>
Infrared Measurements of Heat-Transfer Coefficient for Global Imaging of Flow Fields	136
<b>Vehicle Antenna Test Facility (Building 1299)</b>	<b>137</b>
Design and Testing of X-31 Aircraft Drop Model Antenna System	138
<b>Experimental Test Range (Building 1299F)</b>	<b>141</b>
Measurements of 1-m Almond Test Body Radar Backscatter	142

---

<b>Impact Dynamics Research Facility (Building 1297)</b> .....	<b>144</b>
Beam Column Data to Verify Analysis Tools .....	144
Effect of Floor Location on Failure of Composite Fuselage Frame .....	146
<b>Aircraft Landing Dynamics Facility (Building 1257)</b> .....	<b>148</b>
Variable Yaw System .....	149
Definition of Cornering Characteristics of Radial-Belted and Bias-Ply Aircraft Tires .....	149
Effect of Rain on Airfoil Performance at Large Scale .....	150
<b>Basic Aerodynamics Research Tunnel (Building 720A)</b> .....	<b>153</b>
Experimental and Computational Study of Helicopter Rotor Tips .....	153
NACA 0012 Flow Field Survey Using Particle Image Velocimetry .....	154
<b>Flight Research Facility (Building 1244)</b> .....	<b>156</b>
In-Flight Off-Surface Flow Visualization Using Infrared Imaging .....	158
Boeing 757 Hybrid Laminar-Flow Control Flight Tests .....	159
Airborne Wake Vortex Detection .....	159
Transport High-Lift Flight Experiment .....	160
Wing Leading-Edge Vortex Flap Flight Experiment .....	161
<b>16- by 24-Inch Water Tunnel (Building 1234)</b> .....	<b>162</b>
Flow Visualization Study of Vortex-Generating Devices .....	162
Shear-Driven Three-Dimensional Boundary-Layer Studies .....	163
<b>Scientific Visualization System (Building 1268A)</b> .....	<b>165</b>
Applications of Scientific Visualization System .....	165
<b>13-Inch Magnetic Suspension and Balance System (Building 1212)</b> .....	<b>168</b>
<b>Supersonic Low-Disturbance Pilot Tunnel (Building 1247D)</b> .....	<b>170</b>
Relaminarization of Supersonic Attachment-Line Boundary Layers .....	171
<b>Pyrotechnic Test Facility (Building 1159)</b> .....	<b>172</b>
Hazardous Testing of HALOE Hardware .....	172





## 30- by 60-Foot Tunnel

---

*The Langley 30- by 60-Foot Tunnel is a continuous-flow open-throat double-return tunnel powered by two 4000-hp electric motors, each driving a four-blade 35.5-ft-diameter fan. The tunnel test section is 30 ft high and 60 ft wide and is capable of speeds to 100 mph. The tunnel was first put into operation in 1931 and has been used continuously since then to study the low-speed aerodynamics of commercial and military aircraft. The large open-throat test section lends itself readily to tests of large-scale models and to unique test methods with small-scale models.*

*Large-scale and full-scale aircraft tests are conducted with the strut mounting system. This test method can handle airplanes to the size of present-day light twin-engine airplanes. Such tests provide static aerodynamic performance and stability and control data, including*

*the measurement of power effects, wing pressure distributions, and flow visualization.*

*Small-scale models can be tested to determine both static and dynamic aerodynamics. For all captive tests, the models are sting mounted with internal strain-gauge balances. The captive test methods include conventional static tests for performance and stability and control, forced-oscillation tests for aerodynamic damping, and rotary tests for spin aerodynamics. Dynamically scaled subscale models, properly instrumented, are also freely flown in the large test section with a simple tether to study their dynamic stability characteristics at low speed and at high angles of attack. A small computer is used in this free-flight test technique to represent the important characteristics of the airplane flight control system.*

*The Langley 12-Foot Low-Speed Tunnel, which is used extensively for static tests prior to entry in the 30- by 60-Foot Tunnel, is an atmospheric wind tunnel with a 12-ft octagonal cross section for model testing. The tunnel serves as a diagnostic facility for exploratory research primarily in the area of high-angle-of-attack stability and control studies of various airplane and spacecraft configurations. Preliminary tests are conducted in the 12-Foot Low-Speed Tunnel on simple models prior to testing in higher speed facilities on more sophisticated models to obtain more efficient test planning and effective use of occupancy time in such facilities.*

## Free-Flight Tests of Supersonic Persistence Fighter

The emphasis on efficient supersonic cruise capability for fighter aircraft has raised interest in configurations with high-fineness-ratio fuselages, highly swept low-aspect-ratio wings, and highly integrated control surfaces. These features, although attractive because they are conducive to low supersonic cruise drag, also promote the development of strong vortical flows at low-speed high-angle-of-attack conditions. These vortical flows can lead to complex, nonlinear stability and control characteristics. Providing desired flight dynamic characteristics for such configurations will place heavy reliance on the flight control system. The challenge is to develop a high-angle-of-attack flight control system that blends a number of powerful control effectors in such a way that good flying characteristics are maintained well into the stall region.

Wind-tunnel free-flight tests have been conducted in the Langley 30- by 60-Foot Tunnel to examine the high-angle-of-attack stability and control characteristics and control law design of a Supersonic Persistence Fighter (SSPF) at 1g flight conditions. The SSPF was designed as a Mach 2 cruise, highly maneuverable fighter aircraft concept. In addition to conventional control surfaces, the SSPF also incorporates deflectable wing tips (tiperons) and pitch and yaw thrust vectoring. The use of these unconventional controls blended with conventional pitch, roll, and yaw surfaces provides good stability and control characteristics over a



*Supersonic Persistence Fighter model during wind-tunnel free-flight testing.*

L-90-08317

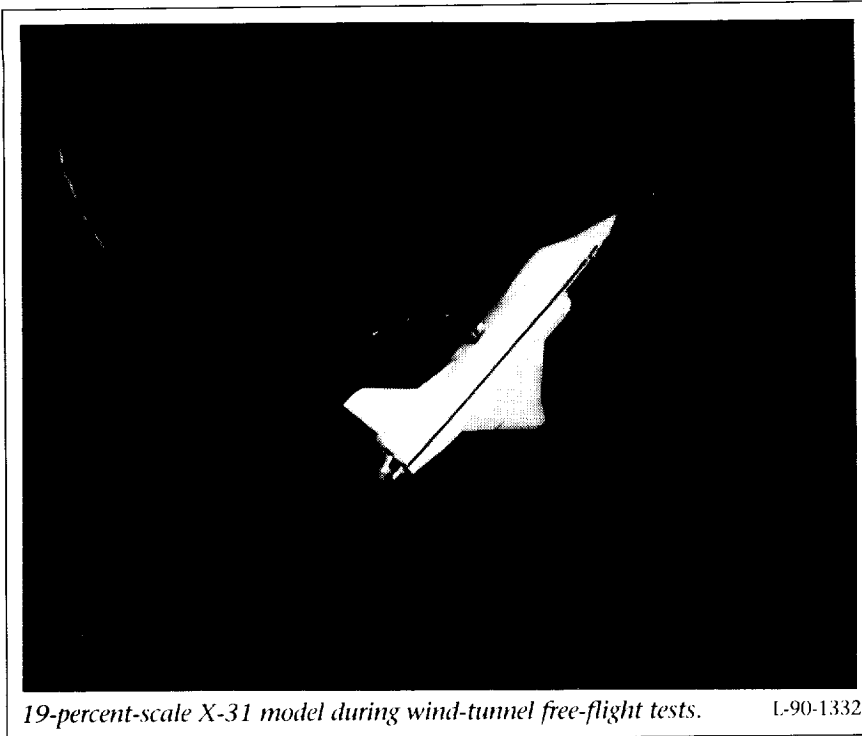
large angle-of-attack range. The free-flight test data show that proper control law design can effectively blend conventional and unconventional control devices to provide good flying characteristics well into the stall/post-stall regions. These results indicate that it is possible to achieve good high-angle-of-attack characteristics in a fighter configuration optimized for efficient supersonic cruise. (David E. Hahne, 41162)

### X-31 Wind-Tunnel Free-Flight Tests

The Defense Advanced Research Projects Agency (DARPA) is currently sponsoring an experimental aircraft program that focuses on flight demonstration of the tactical usefulness of post-stall maneuvering in air combat. The key element in the program is the Rockwell International Corporation/Messerschmitt-Bölkow-Blohm designed X-31 configuration that

incorporates an all-movable canard, a cranked delta-wing planform, and thrust vectoring to augment pitch and yaw control at high angles of attack.

In support of the development of this airplane, wind-tunnel free-flight tests have been conducted in the Langley 30- by 60-Foot Tunnel on a 19-percent dynamically scaled model of the X-31 configuration. The wind-tunnel studies addressed several flight dynamics related issues including the evaluation of static and dynamic stability and control characteristics, an assessment of the maneuverability and stability enhancements afforded by the thrust vectoring controls, and an evaluation of flight control law concepts to provide desired high- $\alpha$  flight dynamic characteristics. The results of these tests show that the basic airframe has generally good stability characteristics except for an undamped roll oscillation in the stall region which can lead to loss of control. A control system concept for alleviating this problem

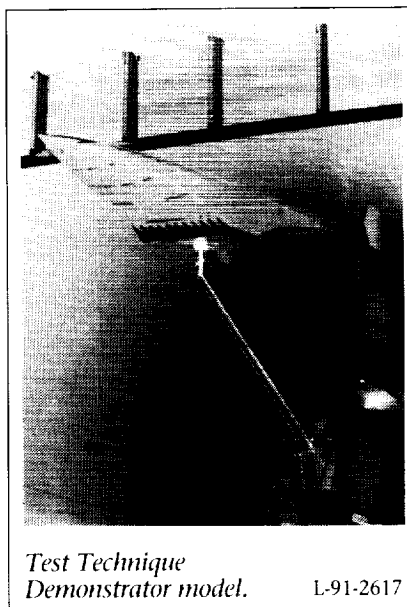


was identified. Model flights conducted above the stall showed that the thrust vectoring controls are very effective in providing the desired controllability capability. Overall, the tests indicate that with proper control system design, the X-31 can achieve the high-angle-of-attack flight dynamic characteristics required to successfully meet its mission goals.  
(Mark A. Croom, 41174)

### Stability and Control Research on Generic NASP Configuration

A series of tests have been conducted in the Langley 30- by 60-Foot Tunnel to investigate the low-speed stability and control characteristics of the National Aero-Space Plane (NASP) Test Technique Demonstrator (TTD) configuration. The studies were

conducted using a model outfitted with a high-pressure air propulsion simulator to investigate the main engine power effects on the aerodynamic characteristics. The objectives of this program were to develop and demonstrate powered



low-speed testing techniques for NASP-type configurations and to evaluate the effect of power on stability and control characteristics of a generic NASP design.

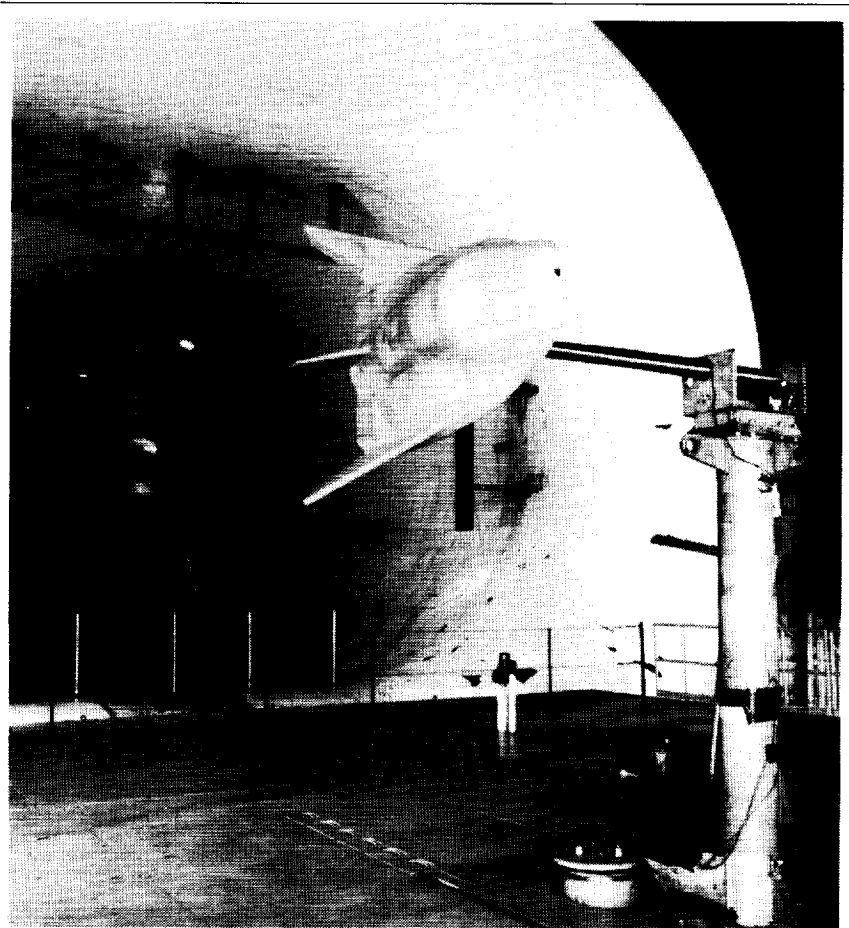
Both conventional static force testing and dynamic stability investigations utilizing a forced-oscillation technique were conducted on the TTD model. A compact bellows system was developed and validated to efficiently bring compressed air to the model for power simulation.

Data obtained during the force tests included the effects of configuration components, control effectiveness characteristics, and the effect of power. Six-component static force and moment data were obtained over a wide range of angle of attack and sideslip angles. Parametric variations included evaluation of the baseline fuselage, wing, canard, and outboard vertical tail geometries at a number of control deflections and power settings. The power data were obtained for both approach and takeoff conditions. Forced oscillation results documented the pitch, yaw, and roll damping characteristics of the complete configuration with and without power.  
(E. Richard White, 41147)

### HL-20 Static and Dynamic Wind-Tunnel Tests

The HL-20 is a lifting-body reentry vehicle concept under study at Langley Research Center to provide assured manned access to Space Station *Freedom* and crew rotation capability. Following reentry, the HL-20 is designed for

an unpowered landing on a conventional runway. The ability to perform this landing is critically dependent upon the low-speed stability and control characteristics of the vehicle. As a result, a series of tests were conducted in the Langley 30- by 60-Foot Tunnel on a 20-percent scale model of the HL-20. The wind-tunnel studies included static force tests to determine static stability and control characteristics and forced-oscillation tests to assess pitch, roll, and yaw damping. The resulting data indicate that the configuration has desirable levels of static stability and damping characteristics over the operational flight envelope and adequate control effectiveness at the design center-of-gravity location. These data have been used to develop a six-degree-of-freedom piloted simulation of the HL-20 for flying qualities evaluation and for developing preliminary guidance and control law concepts.  
(Sue B. Grafton, 41145)



*Dynamic force test of HL-20 model.*

1-89-9451

## Forebody Controls Research

A series of ground-based studies has been conducted to develop actuated forebody strake controls for future flight test demonstrations utilizing the NASA F-18 High Alpha Research Vehicle (HARV). The actuated forebody strake concept is designed to provide increased levels of yaw control at high angles of attack where conventional rudders become ineffective. The studies have included low-speed and transonic wind-tunnel tests, computational aerodynamic studies, and piloted simulation

studies. The most recent tests were conducted in the Langley 30- by 60-Foot Tunnel to develop a low-speed aerodynamic data base for the strake design that is targeted for flight demonstration on the F-18 HARV. These tests included static and dynamic force tests of the 16-percent scale model shown in the figure.

Results from the studies show that a pair of conformal actuated forebody strakes applied to the F-18 HARV can provide high levels of yaw control over wide ranges of angle of attack and sideslip. The strakes generate yawing moments by modulating the forebody vortex

flow to produce differential suction pressures on the forebody, and the level of yaw control can be accurately controlled by varying the strake deflection. Results from the wind-tunnel free-flight tests and piloted simulation studies indicate that actuated forebody strakes can significantly enhance the maneuverability of fighter aircraft by providing the crucial yaw control required at high angles of attack. The enhancements in the maneuverability provided by the strakes would be expected to result in considerable improvements in air combat effectiveness.

(Daniel G. Murri, 41160)



### Tail Buffet Research

The use of vortex flows to supplement lift has become a widely used method in the design of modern fighter aircraft. The interactions of these high-energy flows with the aircraft empennage can generate substantial levels of structural buffeting and reduce the fatigue life of horizontal and vertical tails. A research program is under way to study the effects of vortex flow fields on tail buffet, with a view toward exploring methods of reducing buffet levels while maintaining the favorable effects of vortex flows on high-angle-of-attack aerodynamic characteristics.

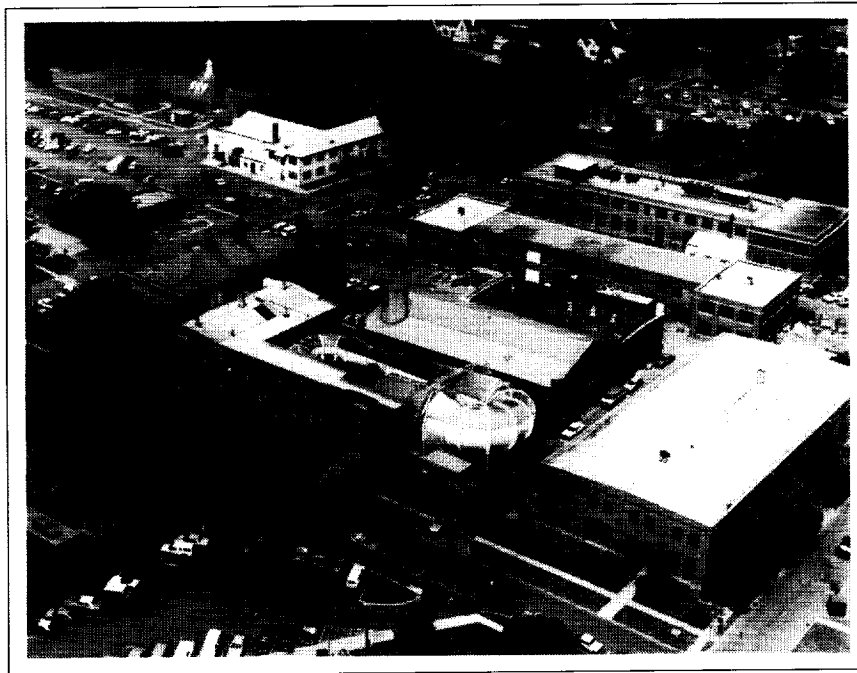
Wind-tunnel tests have been conducted in the Langley 30- by 60-Foot Tunnel using an 0.16-scale F-18 model equipped with dynamically scaled, extensively instrumented vertical tails. The tests were conducted to study the

vertical-tail flow field and dynamic response characteristics. Overall aerodynamic force and moment data for the configuration were also obtained. The investigation focused primarily on the study of airframe modifications that would alleviate

tail buffeting while also improving the aerodynamic stability characteristics at stall and post-stall flight conditions.

Results indicate that a weakening or repositioning of the main vortex flow field not only can greatly reduce tail buffeting but also can have a large impact on the aerodynamic characteristics. Several configuration concepts that provide both buffet and stability improvements have been identified. In addition, an effort to develop scaling methods for ground-to-flight data extrapolation and correlation was initiated. The ultimate goal of this program is to provide a better understanding of vortex/empennage interactions and to develop prediction and analysis tools that will allow tail buffet concerns to be effectively addressed early in the design cycle of future high-performance aircraft.  
(Gautam H. Shah, 41163)





## Low-Turbulence Pressure Tunnel

---

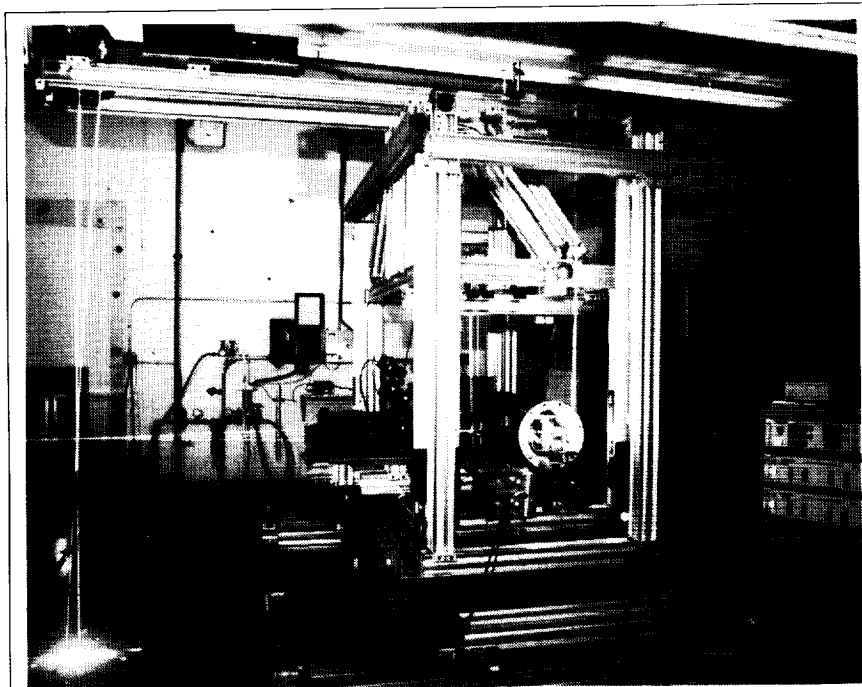
The Langley Low-Turbulence Pressure Tunnel (LTPT) is a single-return closed-circuit tunnel that can be operated at pressures from near vacuum to 10 atm. The test section is rectangular in shape (3 ft wide and 7.5 ft in height and length), and the contraction ratio is 17.6:1. The LTPT is capable of testing at Mach numbers from 0.05 to 0.50 and unit Reynolds numbers from  $0.1 \times 10^6/\text{ft}$  to  $15 \times 10^6/\text{ft}$ . The tunnel has provisions for removal of the sidewall boundary layer by means of a closed-loop suction system mounted inside the pressure chamber. This system utilizes slotted vertical sidewalls just ahead of the model test section, and the removed air is reinjected through an annular slot downstream of the test section. A flow control system allows the flow and pressure requirements to be varied as dictated by tunnel operation. This system can be used to provide boundary-layer control (BLC) for low-drag airfoil research.

A BLC system for high-lift airfoil testing is also available. This system utilizes compressed dry air and involves tangential blowing from slots located on the sidewall mounting end plates. Flowmeters can be used to monitor the amount of air blown into the tunnel. An automatically controlled vent valve is utilized to remove the air injected into the tunnel by this system. A high-lift model support and force balance system is provided to handle both single-element and multiple-element airfoils. The LTPT has been modified to add a passive suction BLC system for high-lift testing and a three-component laser Doppler velocimeter (LDV).

The measured turbulence level of the LTPT is very low due to the large contraction ratio and the many fine-mesh antiturbulence screens. The excellent flow quality of this facility makes it particularly suitable for

testing low-drag airfoils. Recent flow quality measurements in the LTPT indicate that the velocity fluctuations in the test section range from 0.025 percent at Mach 0.05 to 0.30 percent at Mach 0.20 at the highest unit Reynolds number.

The drive system is a 2000-hp direct-current motor with power supplied from a motor-generator set. The tunnel stagnation temperature is controlled by a heat exchanger, which provides both heating and cooling via steam injectors and modulated valves that control the flow volume of water through a set of coils.



Three-component laser velocimeter system.

L-90-9328

### Three-Component Laser Velocimeter Development for LTPT

Computational fluid dynamic methods have been increasingly used for the design and analysis of aircraft in recent years. The data required to validate these methods include highly detailed and accurate flow field measurements. The laser velocimeter is an excellent instrument for the acquisition of these measurements. An investigation was conducted to verify the performance of the laser-optical package of a three-component laser Doppler velocimeter (LDV) system in the LTPT.

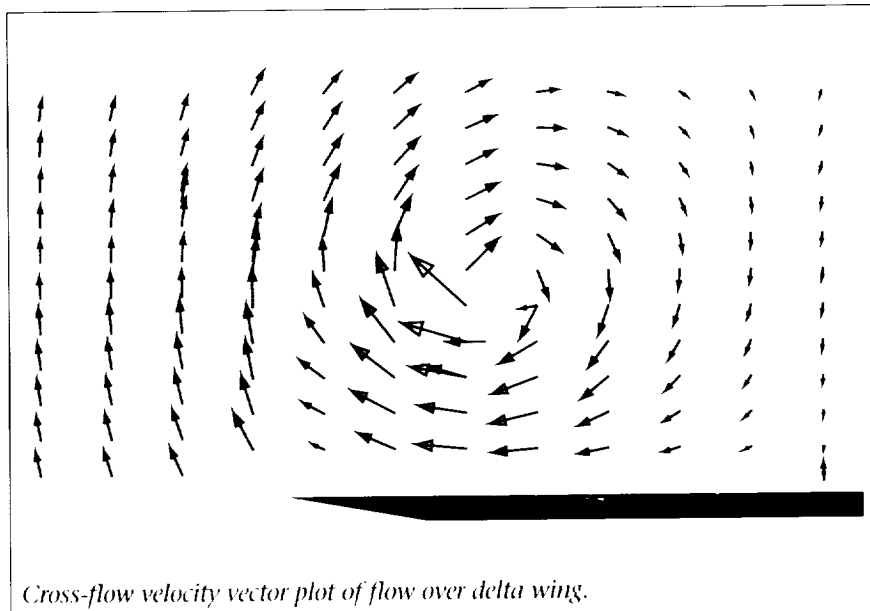
The 10-atm pressure capability of the LTPT provides an excellent facility for investigations requiring a high Reynolds number. The high-pressure environment, however, causes a change of the index-of-refraction of the air. This refractive index change

affects the alignment and performance of the optics and laser. The installed LDV system included a pressure vessel to enclose the laser and color separator

and remotely controlled optics for beam refocusing. A photograph of the system is shown in the first figure.

The LDV system was used to measure the vortical flow field over a delta wing swept  $75^\circ$  for comparison with previously acquired LDV data from the Basic Aerodynamics Research Tunnel (BART). The second figure presents a color vector plot (shown here in black and white) of the results obtained from the LTPT investigation at ambient pressure. These results show excellent agreement with the results obtained in the BART. The LDV data also were obtained at pressures up to 5 atm. Operation of the LDV system at pressures greater than 5 atm was restricted to the limitations of the traverse system electronics. The results of this test confirmed the LDV performance capability at ambient and high-pressure conditions.

(Timothy E. Hepner, 44588, and Scott O. Kjelgaard)



Cross-flow velocity vector plot of flow over delta wing.

## High-Lift Airfoil Research

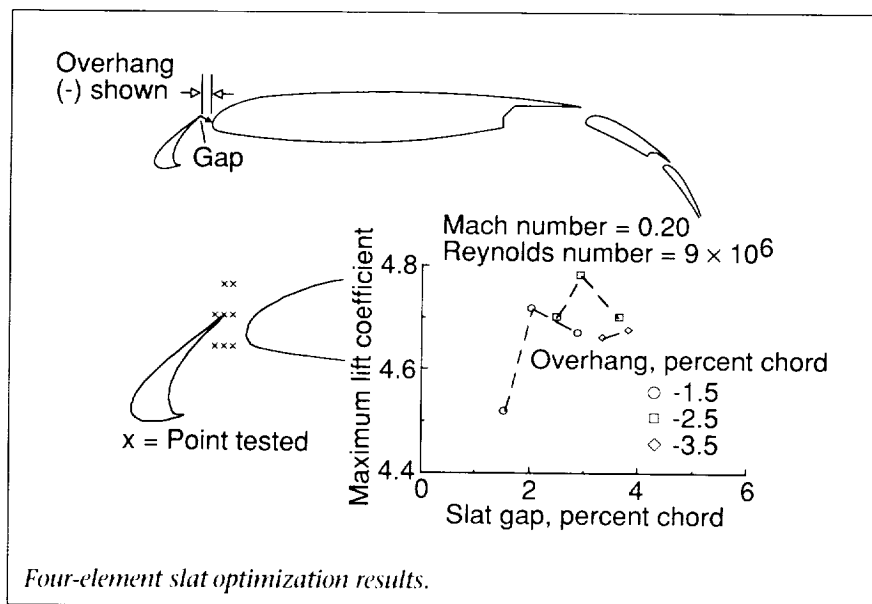
A cooperative test program in the LTPT between the Douglas Aircraft Company and Langley Research Center is under way. The objectives of this research program are to gain an understanding of the effects of increasing the Reynolds

Future tests are planned to optimize slat/flap performance for takeoff and landing three-element configurations for an advanced transport aircraft. Also, the use of multielement sensors for boundary-layer transition/separation detection is to be evaluated.

(Robert J. McGhee, 41005)

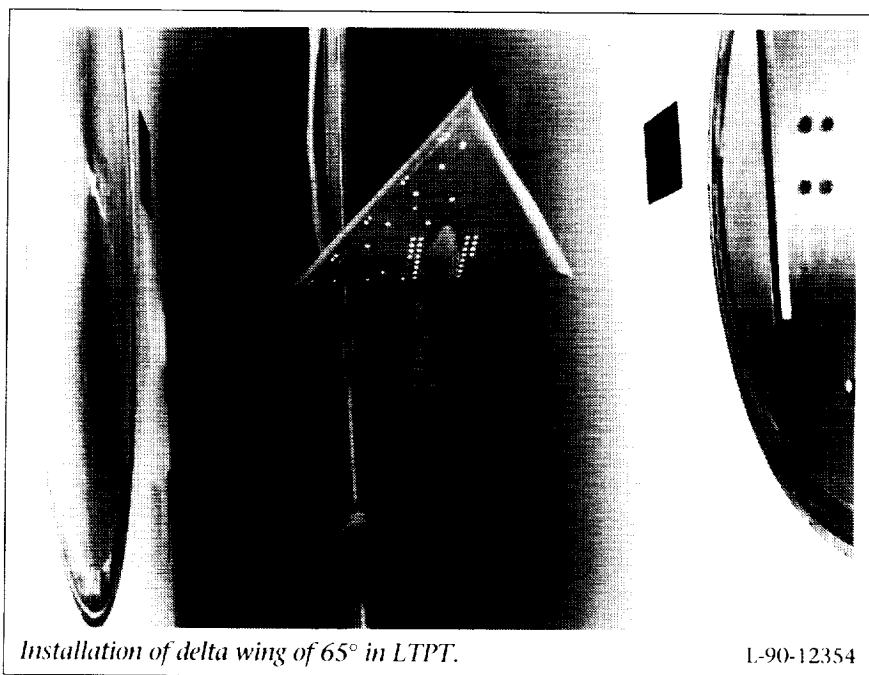
## Reynolds Number Effects on Delta Wing of 65°

A broad research program is under way to extend the experimental data base for the purpose of validating computational fluid dynamics codes. One aspect of this effort includes the experimental measurement of the surface and offbody flow around a delta wing configuration of 65°. The subject configuration, shown in the figure, was designed with a complete analytical description that maintains continuity in surface curvature through the second derivative. The model contains 183 pressure orifices and utilizes four interchangeable parts to vary leading-edge radius. The leading-edge radii have ratios of radius-to-mean-chord of 0.0030, 0.0015, 0.0005, and nominally 0 (sharp). A subsonic test was conducted in the LTPT to initiate the surface pressure measurements. The objective of the test was to explore the effect of



number up to near-flight values on the maximum lift characteristics of advanced multielement high-lift airfoil geometries and to provide detailed flow measurements to guide further development of computational methods.

Recent tests have been completed on the Douglas model using sidewall venting for tunnel sidewall boundary-layer control. Maximum lift was optimized for both four-element and three-element high-lift configurations. The figure illustrates typical results for a four-element slat optimization at a deflection angle of 30°. The sensitivity of maximum lift to slat gap and overhang is well illustrated.





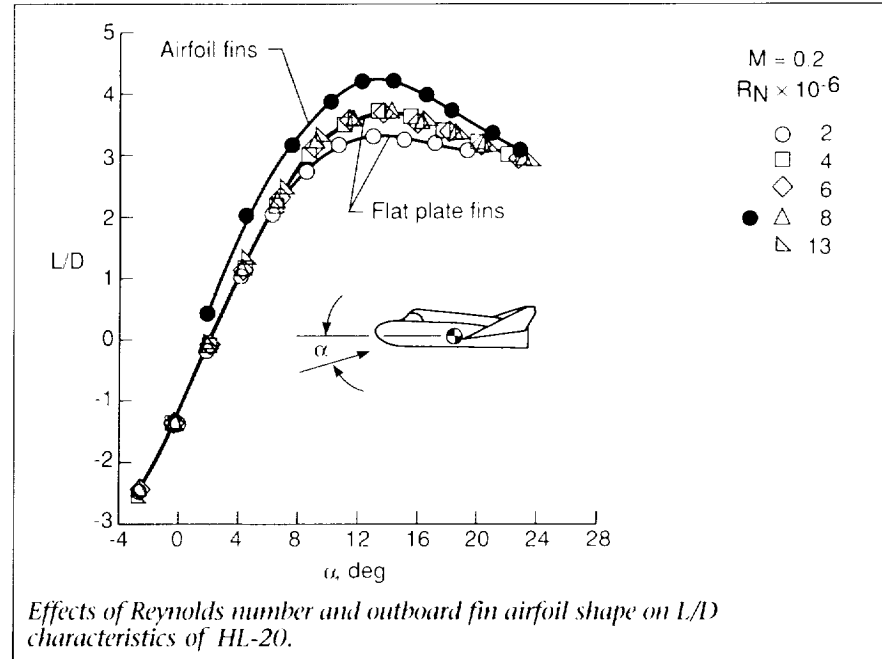
Reynolds number on the formation of leading-edge vortex flow from round leading edges.

Pressure data were obtained for the three finite leading-edge radii at a Mach number of 0.2 and Reynolds numbers of 2, 3, 4, 6, and  $8 \times 10^6$ , based on the mean aerodynamic chord. The angle of attack was varied in increments of  $1^\circ$  from  $-2^\circ$  to  $30^\circ$ . Although the model contained no force balance due to limited space, nominal forces were measured using sting-mounted strain gauges. A preliminary examination of the pressure data indicates that the expected effects from the parameter variations are well represented. Further reduction and analysis of the data are under way, and additional tests in the LTPT are being considered. These tests are part of a broader program for the delta wing which includes the testing of a second larger model over a full range of Mach and Reynolds numbers in the National Transonic Facility (NTF).

(James M. Luckring and Neal T. Frink, 42869)

### Subsonic Aerodynamics Characteristics of HL-20 Lifting-Body Configuration

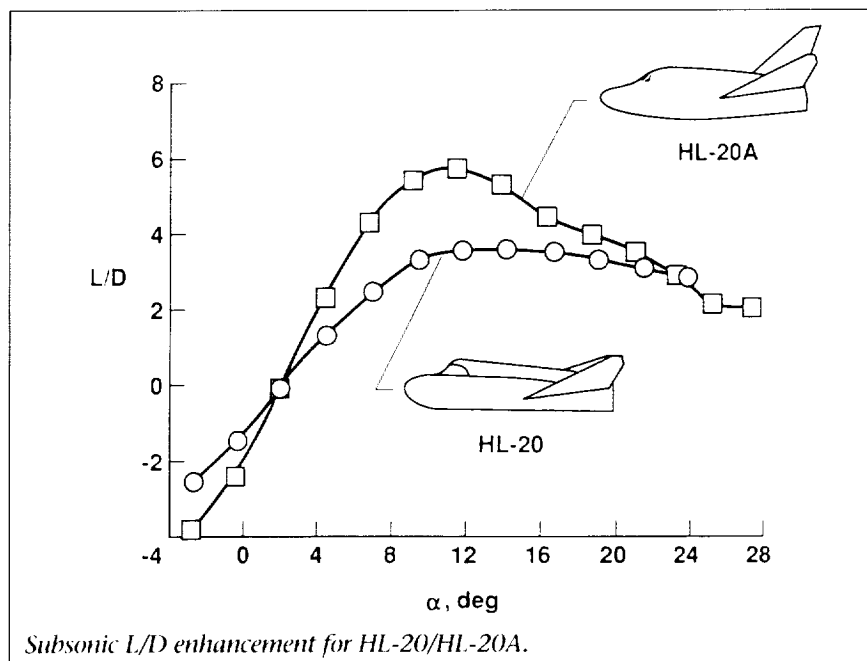
Two current NASA studies, the Assured Crew Return Capability (ACRC) Program and the Personnel Launch System (PLS) Program, employ manned spacecraft. In the ACRC plan, one or more reentry vehicles are docked at Space Station *Freedom* and used to return crew members to Earth in case of emergency. In the PLS Program, a small, man-carrying spacecraft is



used to augment the Space Shuttle capabilities in transporting crew members to and from the space station. One of the candidate configurations for both the ACRC and PLS Programs is a lifting-body vehicle designated HL-20. This vehicle is designed to have aerodynamic performance similar to the Space Shuttle. The HL-20 consists of a low-aspect-ratio body with a flat undersurface and blunt base. Center and outboard fins are mounted on the upper aft body. The outboard fins are rolled outward  $40^\circ$  from the vertical.

A series of wind-tunnel investigations are under way to define the aerodynamic and aerothermodynamic characteristics of the HL-20 across the speed range from low-subsonic to hypersonic speeds. The current investigation was conducted in the LTPT to determine the effects of Reynolds number  $R_N$  on the aerodynamic characteristics of the HL-20 model that is 0.07 scale.

The primary results of the tests are shown in the figure. Plotted are the effects of Reynolds number on subsonic lift to drag  $L/D$ . As Reynolds number is increased from  $2 \times 10^6$  per foot to  $4 \times 10^6$  per foot, the maximum value of  $L/D$  is increased from 3.2 to 3.6. This increase is probably due to reduced skin friction drag at the higher (more nearly flight) Reynolds numbers. Above a Reynolds number of  $4 \times 10^6$ , no change occurs in  $L/D$ . Also presented in the figure are the effects of replacing the original outboard fins that had a simple flat plate cross section with fins with an airfoil shape. The data indicate an increase in maximum  $L/D$  from 3.6 to 4.3. Results from this wind-tunnel study and others are being continually added to the aerodynamic data base used in flight simulator studies of the handling qualities of the HL-20. (George M. Ware and Bernard Spencer, Jr., 45246)



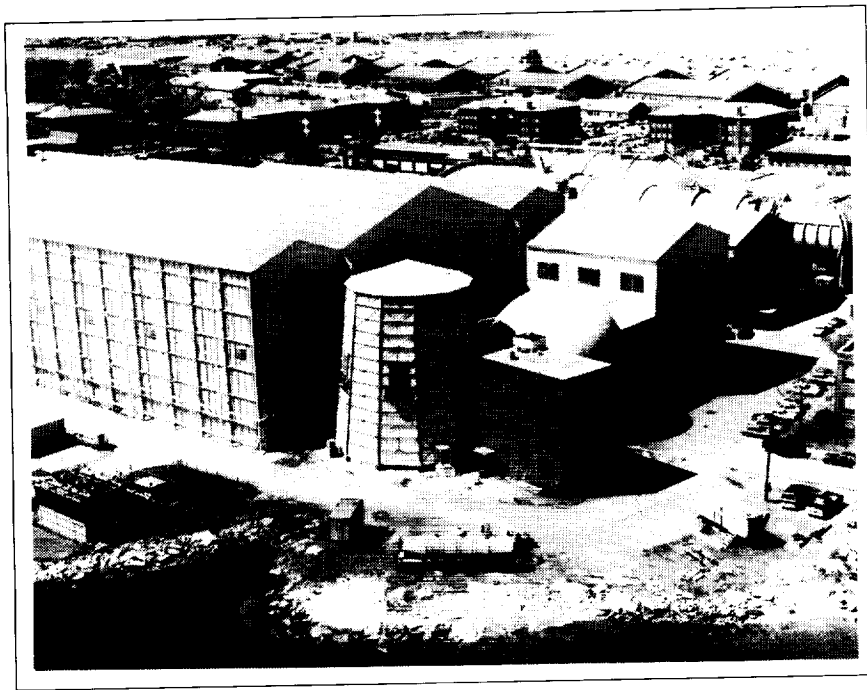
the Mach range to ensure that the modifications have no adverse effects at other speeds.

(Bernard Spencer, Jr., and George M. Ware, 45245)

### Subsonic Aerodynamics Characteristics of HL-20A Lifting-Body Configuration in LTPT

The HL-20 lifting-body shape has been suggested as the vehicle configuration for NASA's Assured Crew Return Capability and Personnel Launch System Programs. Both programs are designed around an entry vehicle with the capability of transporting a crew of 6 to 10 members from Space Station *Freedom*. The HL-20 is a small personnel carrier vehicle approximately 28 ft long with aerodynamic characteristics similar to those of the Space Shuttle. The vehicle has a low-aspect-ratio body with a flat undersurface and blunt base. Center and outboard fins are mounted on the upper aft body. The outboard fins are rolled outward 40° from the vertical. Control surfaces are mounted on the outboard fins and aft body.

An extensive wind-tunnel test program is under way to define the characteristics of the HL-20. Preliminary results of the wind-tunnel tests have shown some deficiencies. As a result, a parallel investigation has been undertaken to improve the aerodynamics through configuration modifications; the refined configuration is referred to as HL-20A. These modifications include forebody shaping to minimize drag, changes in body camber, body base area, outboard fin dihedral, and fin airfoil shape. The study reported here was conducted in the LTPT at subsonic speeds at Reynolds numbers sufficiently high to reasonably simulate flight values. The emphasis was to improve lift to drag  $L/D$  at landing. Presented in the figure is the effect on  $L/D$  of the modifications. The data show that the original HL-20 had a maximum  $L/D$  of 3.6, whereas the HL-20A has a maximum  $L/D$  of almost 6. Tests of the HL-20A are continuing over



## 20-Foot Vertical Spin Tunnel

---

*The Langley 20-Foot Vertical Spin Tunnel is the only operational spin tunnel in the Western Hemisphere and one of only two in the free world. The present facility was built in 1941 and has been essentially in continuous operation since that time. All U.S. military fighters, attack airplanes, primary trainers, bombers, and most experimental airplanes are tested in this facility. General-aviation airplanes and many foreign designs are also evaluated in this tunnel when required.*

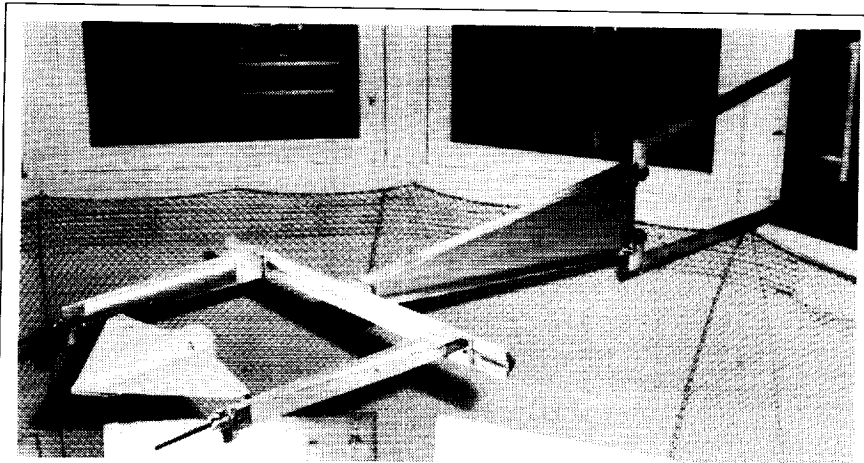
*The tunnel, which is used to conduct spin and tumbling research on aerospace vehicles, is a vertical tunnel with a closed-circuit annular return passage. The test section has 12 sides and is 20 ft across by 25 ft high. The test medium is air. Tunnel speed is variable from 0 ft/s to 90 ft/s with accelerations to 15 ft/s. The main drive motor (which is rated at 400 hp*

*for continuous runs and 1300 hp for short runs) turns a 20-ft-diameter three-bladed fixed-pitch fan.*

*Dynamically scaled models are used to investigate the spinning and tumbling characteristics of airplane configurations. Spin recovery is studied by remote actuation of the aerodynamic controls of the models to predetermined positions. Tests are recorded using high-resolution color videotape with a superimposed time code. A rotary balance apparatus supported by a swinging boom is used to conduct force and moment testing and pressure testing of models under spinning conditions, at angles of attack from  $0^\circ$  to  $\pm 90^\circ$ , and at spin rates from  $0^\circ$  to  $\pm 90$  r/min. Data are recorded in coefficient form on any standard digital medium.*

### **Tumbling Research**

Certain trends in contemporary airplane design (including such concepts as flying wings and canard and tailless configurations) and high levels of relaxed static stability have renewed research interest in the tumbling phenomenon. Tumbling, an autorotational motion about the pitch axis of an airplane, presents a potentially catastrophic loss-of-control condition. Tumbling research is directed toward exploring configuration effects and evaluating susceptibility to the phenomenon. Dynamically scaled models are used to investigate tumbling in the 20-Foot Vertical Spin Tunnel. Free-tumbling tests, analogous to free-spinning tests, are conducted with hand-launched models that are given an initial pitching rotation and permitted to tumble unrestrained in the test section.



*Research wing model mounted on free-to-pitch apparatus.*

L-90-10983

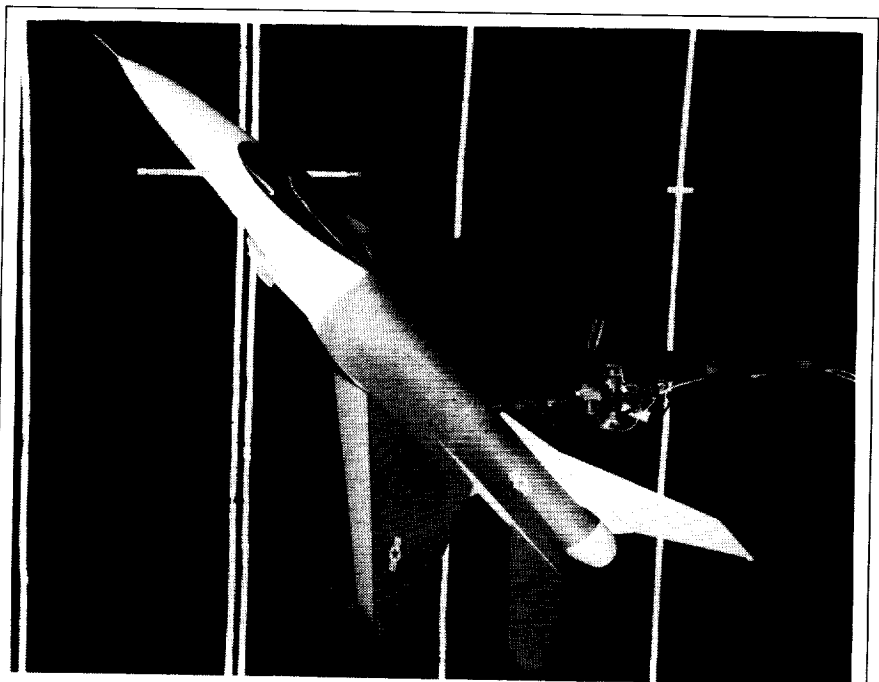
The free-to-pitch apparatus shown in the photograph has been developed to enable continuous pitching of a model about a selected axis of rotation. The effects of variations in moments of inertia, center-of-gravity location, and airspeed on autorotation can be evaluated. The leading-edge-sweep model of  $38^\circ$  mounted on the rig is one of a set of generic wing models being tested in the current research program to assess the effects of wing planform geometry on tumble susceptibility. Initial experiments have used high-resolution video data acquisition while a digital instrumentation package is being developed. Later, models will be equipped with remotely actuated controls for tumble recovery evaluations. (Daniel M. Vairo, 41190)

### Pressure Distributions in Rotational Flow

The pressure distributions over various component surfaces of an airplane undergoing rapid, sustained rotations (such as spins) are significant for analyzing the high-

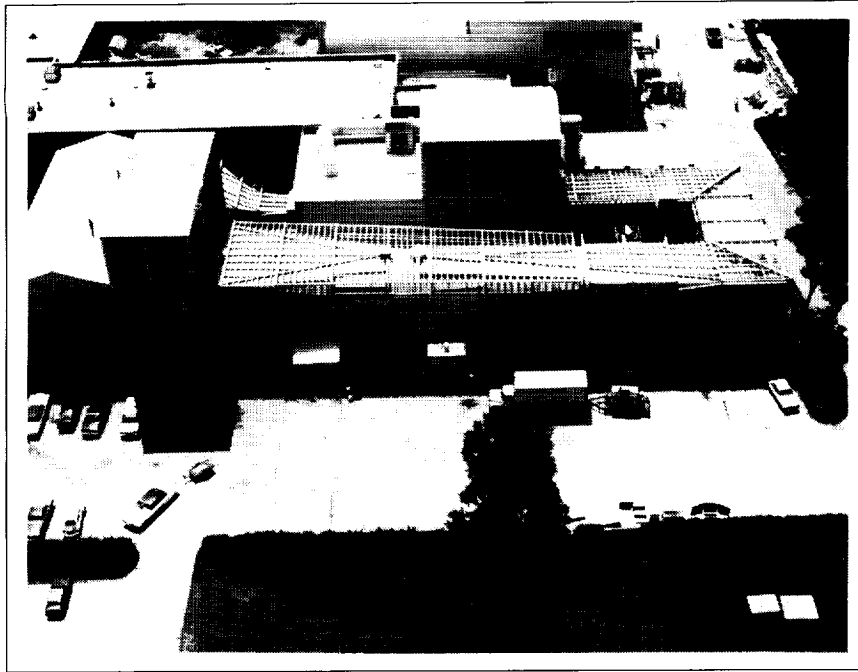
angle-of-attack flight dynamics of high-performance aircraft. The rotary balance apparatus located in the 20-Foot Vertical Spin Tunnel is used to measure aerodynamic forces and moments on airplane models in such rotational flow environments. Recently, the ability to efficiently measure surface pressures also has been incorporated into this test technique.

Using an electronically scanned pressure sensing system that permits the simultaneous sampling of over 1000 pressure ports at 2000 samples per second on a model mounted on the rotary balance, high-resolution three-dimensional pressure distributions under rotating flow conditions were obtained for critical components of a modern fighter airplane. Color computer graphic techniques were adapted to illustrate the pressure fluctuations on the surface of the model as the angle of attack, angle of sideslip, and rate of rotation were varied. A key result from these tests was the visualization of adverse interference effects between the horizontal and vertical tails, which produced prospin aerodynamic moments. The same technique was used to determine ways to alleviate the problem. (Jack N. Ralston, 41184)



*Pressure test model installed on rotary balance.*

L-81-13381



## 7- by 10-Foot High-Speed Tunnel

---

*The Langley 7- by 10-Foot High-Speed Tunnel is a closed-circuit single-return continuous-flow atmospheric tunnel with a solid-wall test section 6.6 ft high, 9.6 ft wide, and 10 ft long. The tunnel, which is fan driven and is powered by a 14 000-hp electric motor, operates over a Mach number range from 0.2 to 0.9 to produce a maximum Reynolds number of  $4 \times 10^6$ /ft. In addition to static testing of models to high angles of attack and large sideslip angles, the facility is equipped for both steady-state roll and oscillatory stability testing.*

*The facility has an important role in a wide range of basic and applied aerodynamic research, including advanced vortex lift concepts, drag reduction technology, highly maneuverable aircraft concepts, and the development of improved aerodynamic theories, such as the difficult*

*separated-flow and jet interaction effects needed for computer-aided design and analysis.*

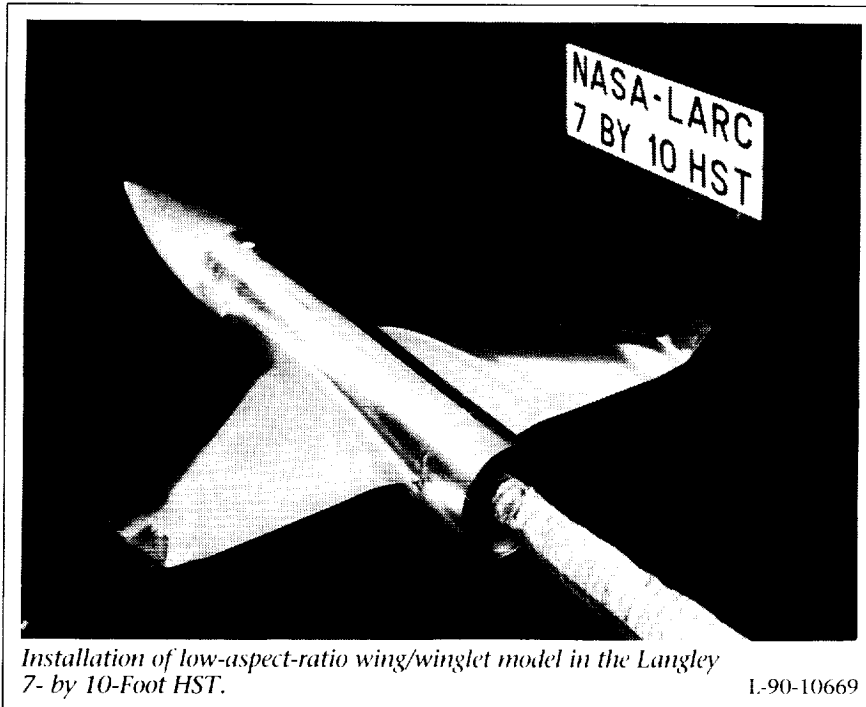
*The flow visualization capability of the facility has been upgraded through the installation of a permanent laser vapor screen system.*

### **Effect of Winglets on Induced Drag for Low-Aspect-Ratio Wing**

An experimental investigation has been conducted to evaluate the effectiveness of winglets for reducing induced drag on a low-aspect-ratio wing. The test was conducted in the Langley 7- by 10-Foot High-Speed Tunnel over a Mach number range from 0.3 to 0.85 and an angle-of-attack range from  $-2.0^\circ$  to  $10.0^\circ$ . Force data, oil-

flow pictures, and laser lightsheet videos were obtained. Two models were tested (one with winglets and one without winglets). Both models had a cropped delta planform with a leading-edge sweep of  $50^\circ$ , and these models were attached to a cylindrical body with an ogive nose. The winglet span was 15 percent of the planform semispan and extended only above the wing. The camber distribution for each model was optimized to give the minimum induced drag for that configuration at design conditions of a Mach number of 0.8 and a lift coefficient of 0.3.

The results of the experiment show the winglets to be effective in reducing induced drag. Improvements were seen in lift to drag  $L/D$  over the entire Mach number range for lift coefficients between 0.2 and



*Installation of low-aspect-ratio wing/winglet model in the Langley 7-by 10-Foot HST.*

L-90-10669

0.7, including improvements in the maximum  $L/D$ . At the design condition, an increase of 11 percent in  $L/D$  was observed. This increase is in close agreement with the percent increases predicted theoretically during the model design process. Preliminary results show the small disturbance theory used to predict the performance of the model to be in good agreement with the experimental values obtained. (Leigh Ann Smith, 42878)

Limitations on computer capabilities and geometry definition confined the CFD computation to include only the forward fuselage and wing leading-edge

extension (LEX) back to the main wing junction. Although favorable comparisons were made with test data from the forebody of the full configuration, the computations showed noticeable differences in the aft region of the LEX due to the influence of the wing. A physical model matching the actual computational configuration was devised using the front section of an existing model, which included the LEX. This portion of the model was substantially instrumented to measure surface pressures and had been used in prior comparisons with the computations. The figure shows the wind-tunnel model mounted in the facility.

The wind-tunnel test on this F/A-18 forebody/LEX model was conducted in the 7-by 10-Foot High-Speed Tunnel using a unique model support system that allows angles of attack (AOA) up to  $50^\circ$ . The model was tested extensively between AOA's of  $20^\circ$  and  $45^\circ$  at

### F-18 Forebody/LEX Test

Advanced computational fluid dynamics (CFD) codes are now being used to compute complex flows over actual aircraft. The F/A-18 aircraft configuration is one example that has been subjected to an extensive CFD program with results compared to both flight and wind-tunnel tests.



*F-18 forebody/LEX wind-tunnel test.*

L-90-11210

Mach numbers ranging from 0.075 to 0.60. Conditions in this range matched those both from the computations and in previous flight and wind-tunnel experiments. These test data are currently being compared to both CFD computations and full-configuration flight and wind-tunnel tests. (W. G. Sewall, R. M. Hall, G. E. Erickson, and D. W. Banks, 42861)

of these flows. Thus, subscale wind-tunnel testing must simulate the turbulent boundary-layer flows appropriate for flight Reynolds numbers to correctly approximate flight values of aerodynamic quantities such as pitching and yawing moments.

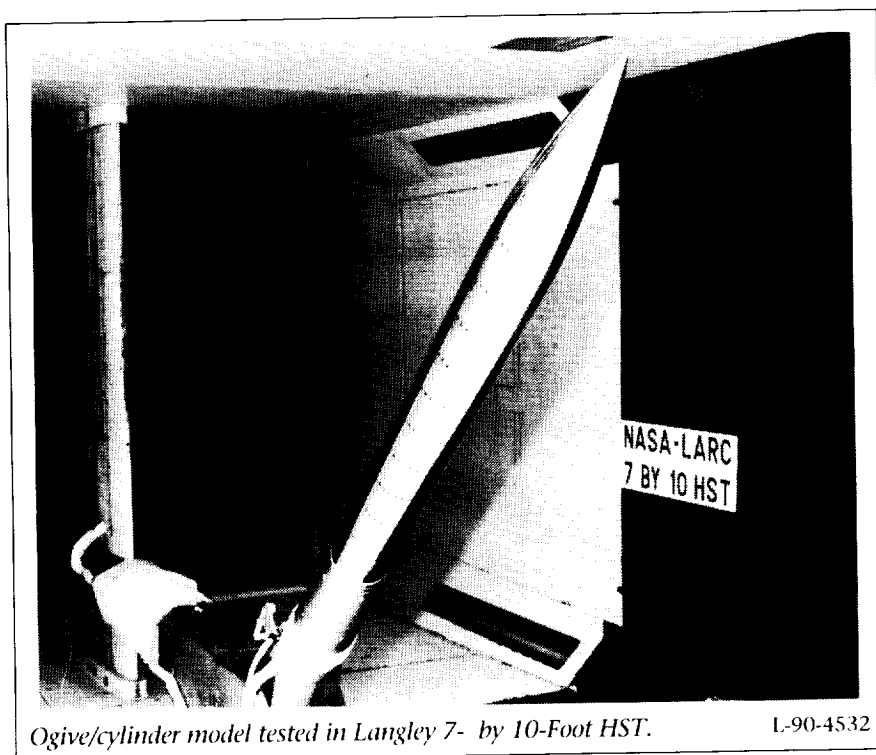
A pressure-instrumented ogive/cylinder model (shown in the figure) permitted detailed comparisons of surface pressures between a

patterns are very effective and yield results that are consistent with each other and with high Reynolds number data. Based on this work, further gritting studies with aircraft configurations have also shown results similar to full-scale flight. (Robert M. Hall, Daniel W. Banks, and William G. Sewall, 42883)

### Subsonic Control Effectiveness of HL-20 Lifting-Body Configuration

The HL-20 configuration is a low-aspect-ratio body with a flat undersurface and blunt base. Center and outboard fins are mounted on the upper aft body. The outboard fins are rolled outward from the vertical 40°. Control surfaces are mounted on the outboard fins and aft body. This shape is being considered for use as a manned carrier vehicle in two proposed U.S. space missions. The Assured Crew Return Capability Program plans to dock one or more reentry vehicles at Space Station *Freedom* for the return of crew members to Earth in case of an emergency. The Personnel Launch System Program calls for a small man-carrying spacecraft to be used to augment the Space Shuttle capabilities (primarily in transporting crew members to and from Space Station *Freedom*). The HL-20, which is designed for performance characteristics similar to those of the Space Shuttle, will have a gliding entry, aerodynamic maneuvering, and a horizontal landing.

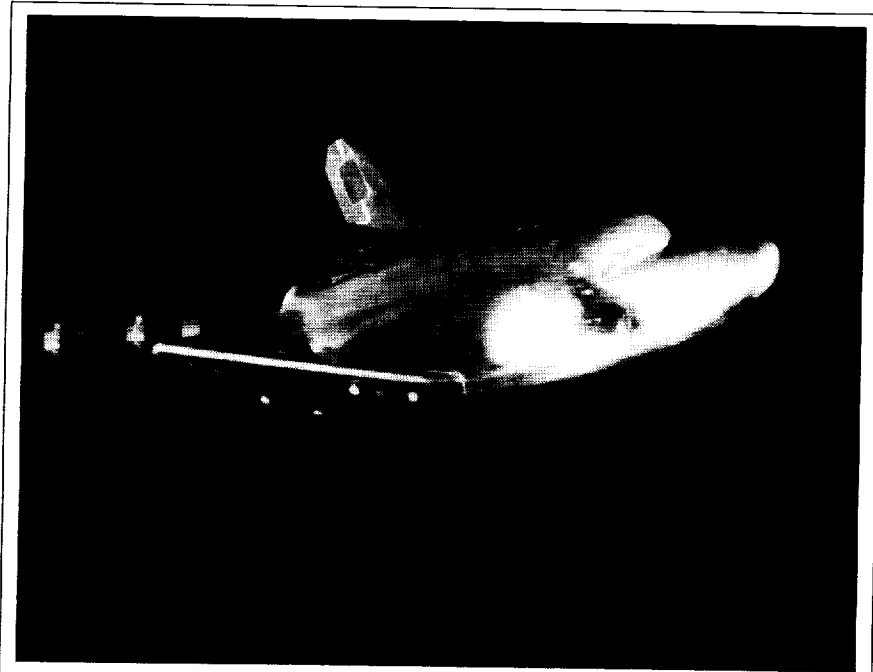
A series of wind-tunnel investigations were undertaken to define the aerodynamic and aerothermo-



### High-Alpha Gritting to Simulate Flight Reynolds Numbers

Despite extensive procedures for gritting models for low-alpha tests, comparable procedures have not been developed for high-alpha testing. The literature on aircraft forebodies and other slender shapes contains many examples of the strong Reynolds number sensitivity

baseline, no-grit case and three different grit patterns. These patterns include the traditional low-alpha nose ring, twin, longitudinal strips located 54° from the windward plane of symmetry, and "global" patterns with grit generally covering the entire surface of the model. Results demonstrate that the nose grit ring is ineffective at high alpha, but that the twin strip pattern and the "global"



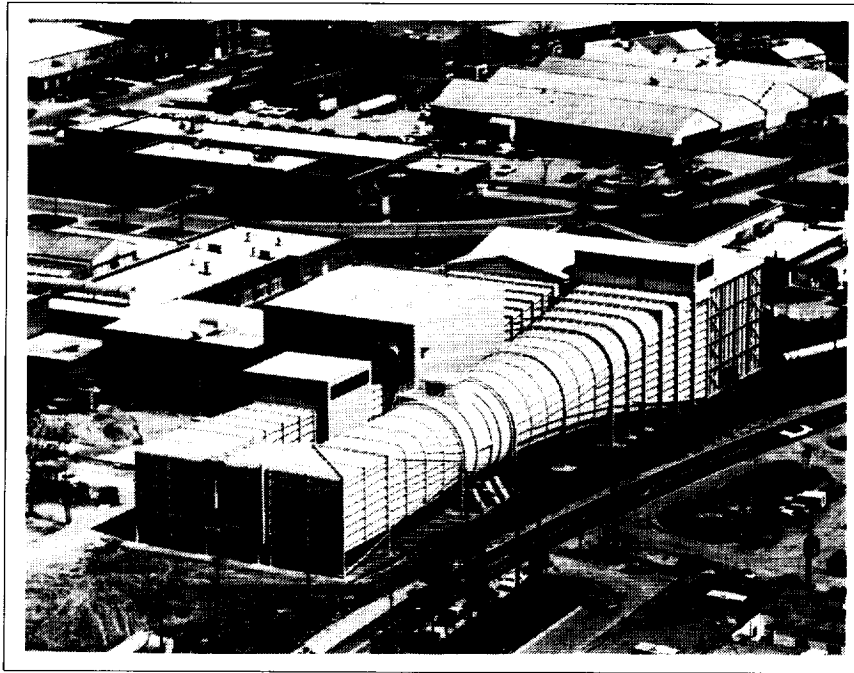
*HL-20 model mounted in Langley 7- by 10-Foot HST.*

L-91-1454

dynamic characteristics of the HL-20 across the speed range from low-subsonic to hypersonic speeds. Tests have been conducted in a number of wind tunnels at Langley Research Center and in industry. This investigation was conducted in the Langley 7- by 10-Foot High-Speed Tunnel to define, in detail, the aerodynamic control effectiveness of the lifting-body configuration. The control characteristics will be used in a man-in-the-loop flight simulation study to determine the handling qualities of the HL-20. A photograph of the model is presented in the figure.

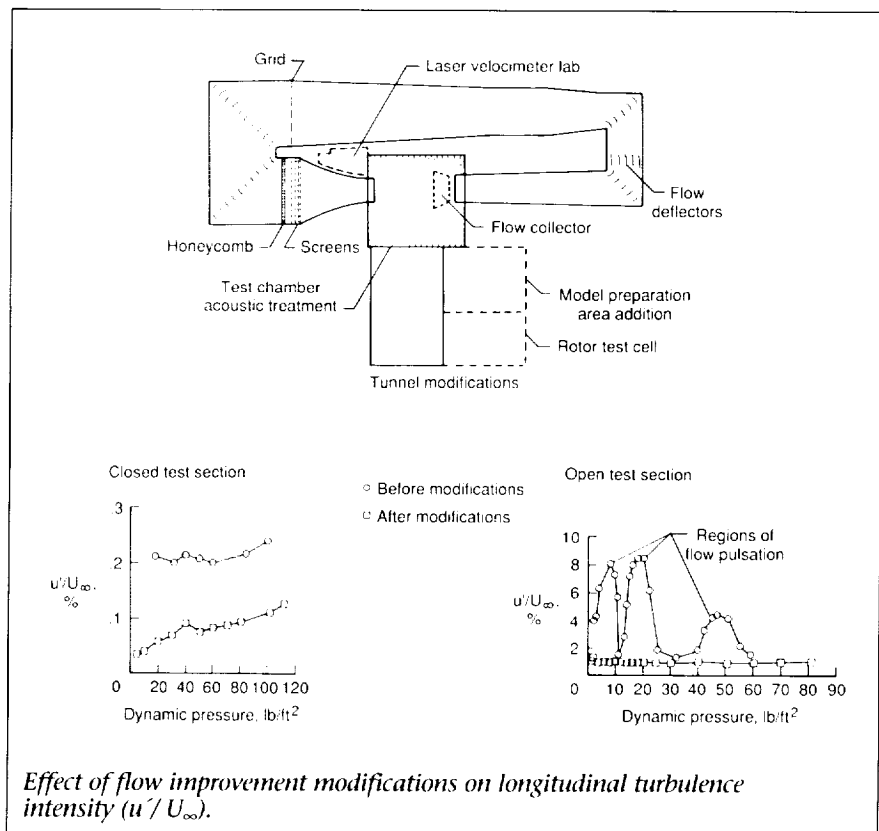
**(George M. Ware and Bernard Spencer, Jr., 45246)**





# 14- by 22-Foot Subsonic Tunnel

The Langley 14- by 22-Foot Subsonic Tunnel (formerly the 4- by 7-Meter Tunnel) is used for low-speed testing of powered and unpowered models of various fixed- and rotary-wing civil and military aircraft. The tunnel is powered by an 8000-hp electrical drive system, which can provide precise tunnel speed control from 0 ft/s to 318 ft/s with the Reynolds number per foot ranging from 0 to  $2.1 \times 10^6$ . The test section is 14.5 ft high, 21.8 ft wide, and approximately 50 ft long. The tunnel can be operated as a closed tunnel with slotted walls or as one or more open configurations when the sidewalls and ceiling are removed to allow extra testing capabilities, such as flow visualization and acoustic tests. The tunnel is equipped with a two-component laser velocimeter system. Furthermore, boundary-layer suction on the floor at the entrance to the test section and a moving-belt



ground board for operation at test section flow velocities to 111 ft/s can be installed for ground effect tests.

Langley Research Center has completed significant modifications to the Langley 14- by 22-Foot Subsonic Tunnel to improve and expand its aerodynamic and acoustic test capability. One of the more significant aerodynamic improvements was achieved through the use of flow deflectors installed downstream of the first corner of the tunnel circuit to improve the performance of the tunnel fan. The deflectors resulted in a more uniform velocity distribution into the tunnel drive system and eliminated regions of large-scale flow separation in the return leg of the tunnel circuit.

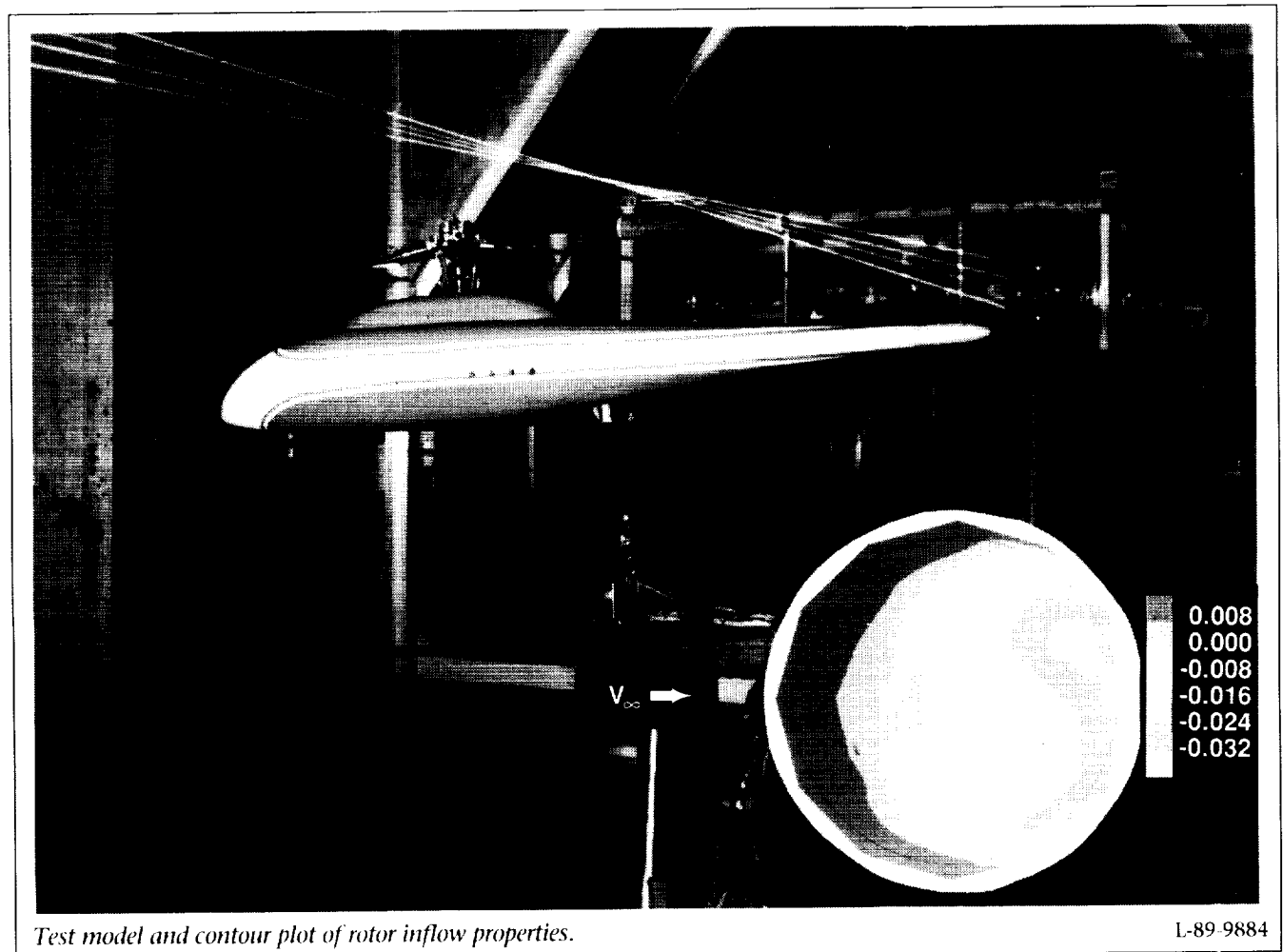
A turbulence reduction system consisting of a grid, a honeycomb, and four fine-mesh screens dramatically reduced the level of longitudinal turbulence intensity in the tunnel test section. This system provided a reduction in turbulence of 50 percent or more for the closed test section configuration. Periodic flow pulsations that occurred at several speeds in the unmodified configuration of the open test section were eliminated by the installation of a new flow collector.

Acoustic reverberations in the open test section were reduced through the use of sound-absorbing panels on the test chamber walls. A major

operational improvement was achieved through the construction of a specially designed laser velocimeter laboratory for setup and maintenance of the two-component laser velocimetry system. Finally, an addition to the model preparation area, which includes a support system and rotor test cell, provides the capability to assemble and test rotor models in hovering conditions prior to actual entry into the tunnel.

### Rotor Inflow Research

The fifth in a series of rotor inflow measurements tests was conducted in the Langley 14- by



22-Foot Subsonic Tunnel using a 2-Meter Rotor Test System and a laser velocimeter for measuring flow velocities. The purpose of this U.S. Army/NASA program is to establish an experimental data base of rotor inflow and wake velocities which can be used for the validation of computational methods that predict flow velocities near a rotor. In the most recent test, rotor inflow data were acquired for a four-bladed rotor with a generic research fuselage. The data were measured at 180 locations in a plane approximately 3 in. above the plane formed by the rotating blade tips for advance ratios (ratio of flight speed to rotor tip speed) of 0.23 and 0.30. Both average and time-dependent data were acquired for each measurement location. The predictions of various computational analyses of rotor inflow were compared to the experimental data. A photograph of the test model and a contour plot of the mean induced inflow ratio are presented in the figure.

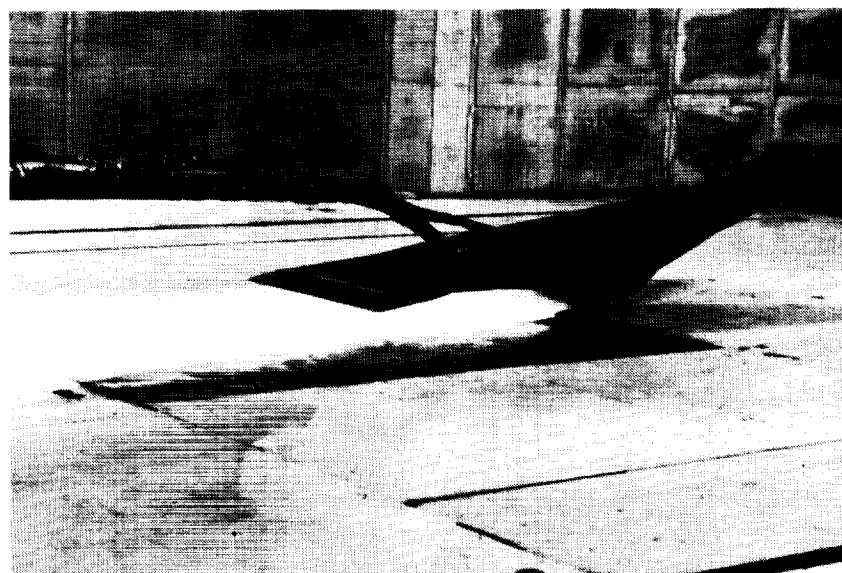
The experimental data show that as wind speed is increased, the area of upflow induced by the rotor moves progressively from the far-forward region of the rotor disk to cover the complete forward half of the disk. The induced inflow characteristics at all wind speeds are asymmetric about the longitudinal axes of the rotor, with the maximum downwash concentrated in the aft portion of the rotor disk, skewed to the advancing blade side. The computational methods show significant differences from the experimental data, thus indicating that improvements in the methods are necessary for the proper calculation of the flow conditions

affecting rotor performance.  
(Susan L. Althoff, Joe W. Elliott,  
and Danny R. Hoad, 45059)

### Powered Ground Effects Investigation of a Single-Stage-to-Orbit Vehicle

As part of the National Aerospace Plane Program, an investigation was conducted in the Langley 14- by 22-Foot Subsonic Tunnel to determine the low-speed, powered

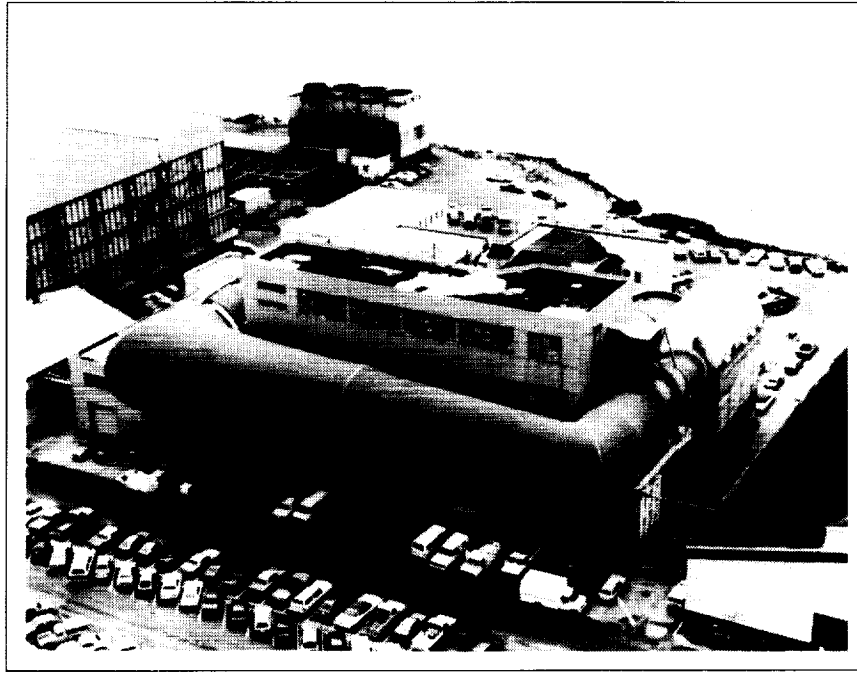
system was used to generate an inlet flow as well as provide exhaust flow for complete simulation of low-speed engine operations. Aerodynamic force and moment data have been obtained for powered and unpowered conditions both in and out of ground effect. Oil-flow visualization studies were conducted on the entire upper surface of the configuration as well as on the under-surface of the forebody in the vicinity of the inlet plane. In addition, exhaust flow visualization



*Exhaust flow visualization on single-stage-to-orbit configuration.*

ground effects of a single-stage-to-orbit vehicle. These vehicles, in which the overall configuration design is driven by high-speed constraints, are generally not well suited for low-speed operations. Thus, in order to investigate the low-speed powered aerodynamics, a 9.5-ft-long model was tested over a broad angle-of-attack, sideslip, and thrust coefficient range. An ejector-type propulsion simulation

was generated using a water injection technique in combination with a laser lightsheet. Model parameters investigated included wing and afterbody flap deflections, a large and small canard, large and small twin vertical tails, nozzle flaps on each engine unit, vortex flaps, a faired inlet, and two alternate forebody planforms.  
(G. M. Gatlin, J. W. Paulson, Jr.,  
and K. J. Kjerstad, 45065)

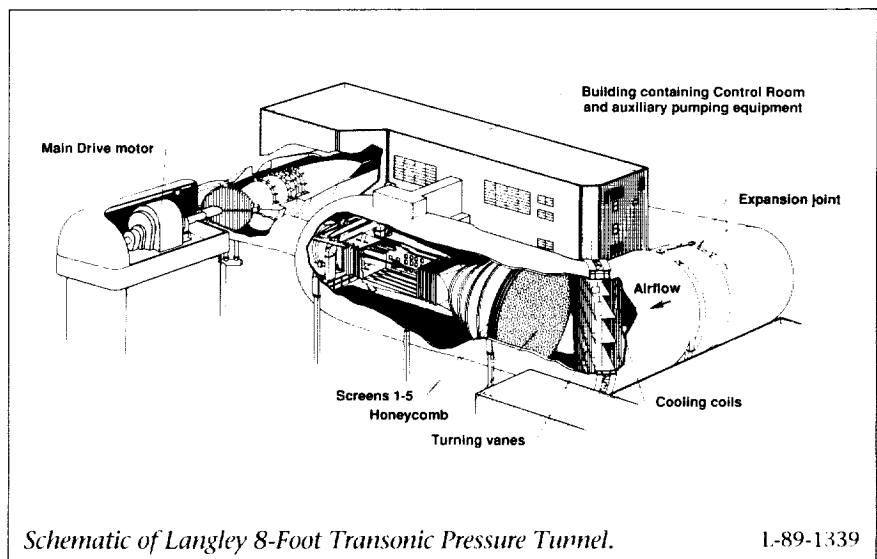


## 8-Foot Transonic Pressure Tunnel

The Langley 8-Foot Transonic Pressure Tunnel (TPT) is a variable-pressure slotted-throat wind tunnel with controls that permit independent variations of Mach number, stagnation pressure and temperature, and dew point. Air is circulated through the circuit by an axial compressor located downstream of the test section diffuser and driven by an electrical drive system. The test section is square with filleted corners and a cross-sectional area approximately equivalent to an 8-ft-diameter circle. The floor and the ceiling of the test section are axially slotted (approximately a 6.9-percent porosity in the calibrated test region) to permit continuous operation through the transonic speed range. The sidewalls are solid and fitted with windows for schlieren flow visualization. The contraction ratio of the test section is 20:1.

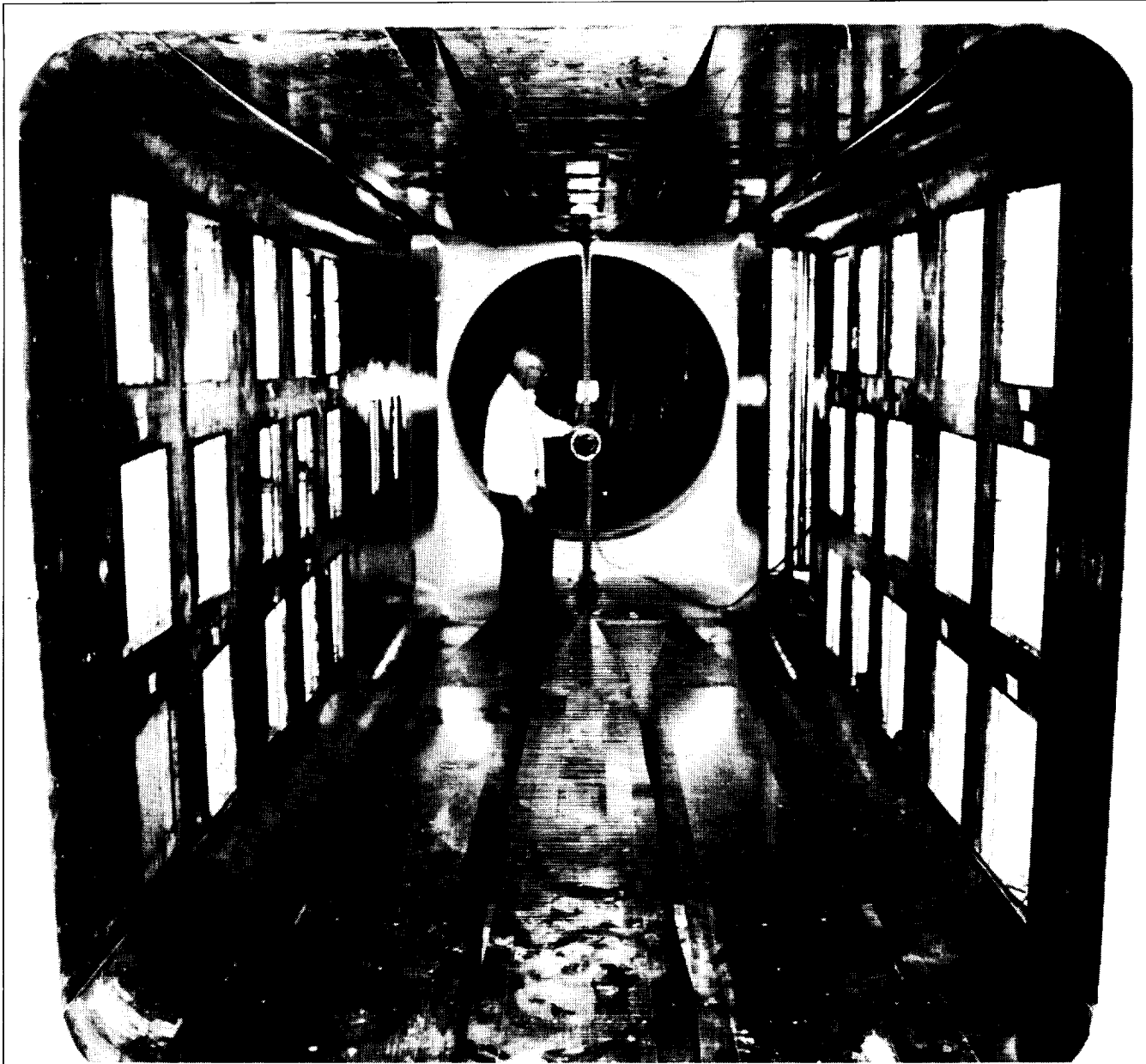
Tunnel stagnation pressure can be varied from a minimum of approximately 0.25 atm at all test Mach numbers to approximately 1.0 atm at a Mach number of 1.2 atm, approximately 1.5 atm at high subsonic Mach numbers, and approximately 2.0 atm

at Mach numbers of 0.4 or less. Temperature is controlled by water from an outside cooling tower circulating through cooling coils across the corner of the tunnel circuit upstream of the settling chamber. The tunnel air is dried until the dew point temperature



Schematic of Langley 8-Foot Transonic Pressure Tunnel.

1-89-1339



Slotted test section.

1-88-11585

is reduced enough to prevent condensation in the flow by use of dryers using silica gel desiccant.

Based upon both centerline probe and wall pressure measurements, generally uniform flow is achieved over a test section length of at least 50 in. at Mach numbers of 0.20 to 1.20. The higher the Mach number, the

shorter the region of uniform flow becomes. The tunnel is capable of achieving Mach numbers to approximately 1.3, but most testing is limited to a maximum Mach number of 1.2 because the calibrated region of the test section for  $M = 1.3$  is further downstream than for lower Mach numbers and requires that a model be located farther aft in the test section.

The 8-Foot TPT is a very versatile wind tunnel capable of supporting basic fluid dynamics research as well as a wide range of applied aerodynamic research. With the installation of screens and honeycomb in conjunction with the recently completed Laminar-Flow-Control Experiment, the quality of the flow in the test section is suitable for performing

reliable code validation experiments. The test section already is instrumented with many ceiling, floor, and sidewall pressure orifices; more orifices could be added easily if desired. In addition, fixed chokes and test section slot covers are currently being designed which would permit data to be obtained on both open and closed tunnel configurations as well as improve the flow quality in the test section by blocking upstream propagation of diffuser noise.

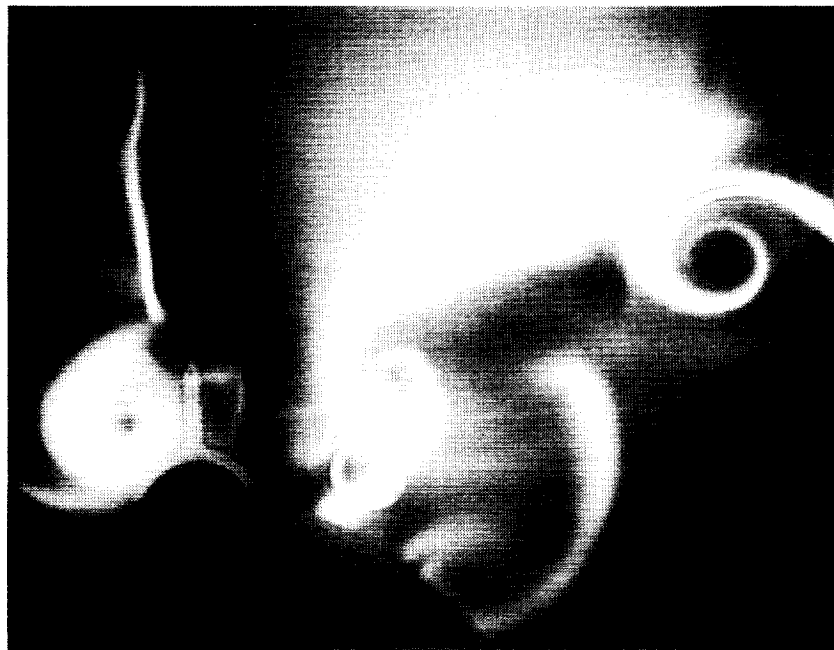
### Fiber Optic-Based Laser Vapor Screen System

Laser vapor screen flow visualization capability that features a fiber optic-based beam delivery system was established in the 8-Foot TPT. The vapor screen technique features the injection of water into the tunnel circuit to increase the relative humidity in the test section. The cross-flow patterns are visualized by illuminating the regions of condensed water vapor above the model with an intense sheet of laser light. This illumination provides a powerful diagnostic tool to assess vortex-dominated flow fields about complex aerodynamic shapes at subsonic through transonic speeds. The 8-Foot TPT flow visualization system is all-encompassing because it contains the light source (6-W argon ion laser), fiber optic beam delivery system, lightsheet-generating optics, remote controllers for all aspects of the laser and lightsheet optics, water seeding mechanism, and video observation, documentation, and editing equipment.

The use of fiber optics represents a significant advancement in the safety, reliability, and effective-

ness of the laser vapor screen technique in transonic wind tunnels and provides a means of steering high-power laser beams in a contained manner over large distances, which are typical of

transonic tunnel installations. Fiber optics eliminates the beam misalignment due to tunnel structural vibration or to variations in operating pressure and temperature that are encountered with



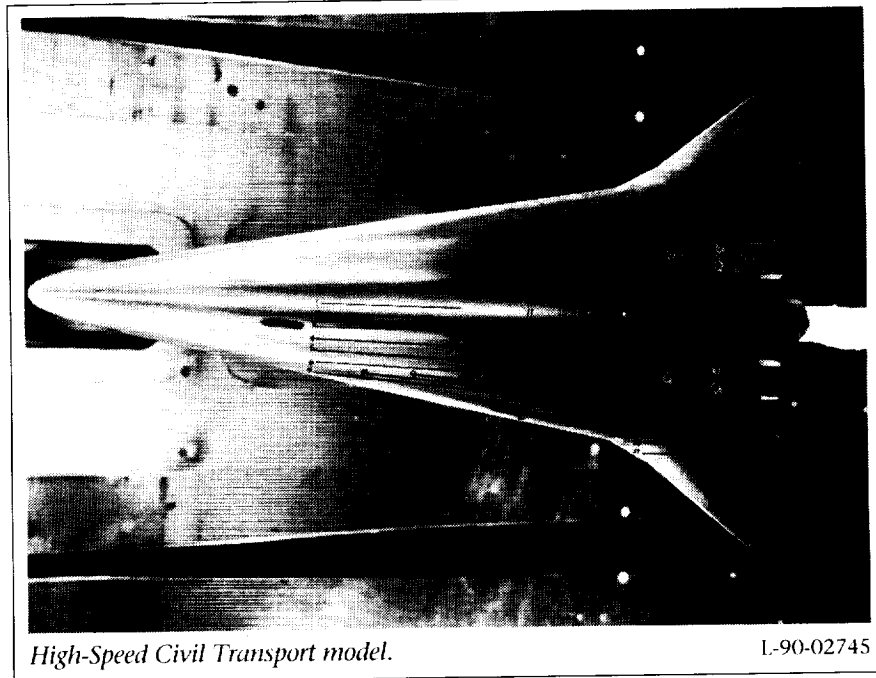
*Laser vapor screen flow visualization in 8-Foot TPT. Camera outside test section (above); camera on model support system (below).*

more conventional mirror-based beam delivery systems. The 8-Foot TPT system has been demonstrated to be a turnkey operation that maintains alignment indefinitely.

Representative results obtained on an advanced fighter model in the 8-Foot TPT are shown in the figure, which highlights the laser lightsheet and the vortex cross-flow patterns above the model. The photographs contain images captured from a video camera mounted outside the test section and from a miniature video camera mounted to the model sting support system. The fiber optic-based laser vapor screen system has been used extensively in the 8-Foot TPT on a variety of models at Mach numbers from 0.30 to 1.20. An identical system has been established in the Langley 7- by 10-Foot High-Speed Tunnel (HST) for vortex flow visualization at subsonic speeds.  
(Gary E. Erickson, 42886)

### Wind-Tunnel Investigation of Generic High-Speed Civil Transport

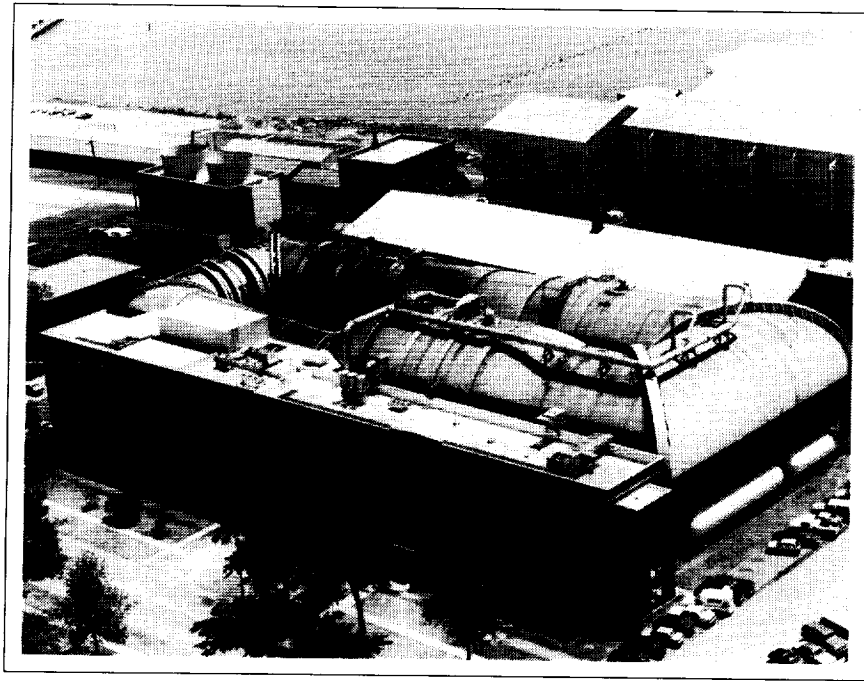
Two generic High-Speed Civil Transport models were tested in the 8-Foot TPT as part of the High-Speed Airframe Integration Research (HiSAIR) Program. The purpose of the test was to create a data base consisting of force, moment, and pressure data at transonic speeds. The data will be used to assess the ability of various computational methods to predict the aerodynamic characteristics of a High-Speed Civil Transport.



The geometry of the two models tested differs only in the wing-tip region. One has a straight wing tip, and the other has a curved wing tip (shown in the figure). The leading-edge sweep of these models is approximately  $79^\circ$  inboard and  $53^\circ$  outboard. The aspect ratio is 3.039, and the span is 18 in. Force data were taken on both models from  $M = 0.30$  to  $M = 1.19$  at angles of attack from  $-2^\circ$  to  $9^\circ$ . At  $M = 0.30$ , data were obtained up to an angle of attack of  $18^\circ$ . Sideslip data were also obtained at selected Mach numbers. Pressure data were obtained on the curved wing-tip model at the same conditions except no sideslip data were taken. Both models were tested with nacelles on and off.

Preliminary data indicate no significant difference between the straight and curved wing-tip models. A laser lightsheet flow visualization system was used on the curved wing-tip model at  $M =$

0.30 and at  $M = 0.90$ . Vortical flow was seen at  $M = 0.90$  at an angle of attack as low as  $3^\circ$ .  
(Pamela S. Phillips, 42880)



## Transonic Dynamics Tunnel

---

*Conversion of the original Langley 19-Foot Pressure Tunnel into the Transonic Dynamics Tunnel (TDT) was begun in the late 1950's to satisfy the need for a large transonic wind tunnel dedicated specifically to work on the dynamics and aeroelastic problems associated with the development of high-speed aircraft. Since the facility became operational in 1960, this tunnel has been used almost exclusively to clear new designs for safety from flutter and buffet, to evaluate solutions to aeroelastic problems, and to research aeroelastic phenomena at transonic speeds.*

*The tunnel is a slotted-throat single-return closed-circuit wind tunnel with a 16-ft by 16-ft test section. The stagnation pressure can be varied from slightly above atmospheric to near vacuum, and the Mach number can be varied from 0 to 1.2. Test section Mach number and density are both*

*continuously controllable. A 30 000-hp fan motor is used to drive the test medium at various velocities. The facility can use either air or a heavy gas (R12) as the test medium. The tunnel has a reclamation system so that the heavy gas can be purified and reused.*

*The facility is equipped with many features uniquely suited to dynamic and aeroelasticity testing. These features include a computerized data acquisition system especially designed to rapidly process large quantities of dynamic data, a system for rapidly reducing test section Mach number and dynamic pressure to protect models from damage when aeroelastic instabilities occur, a system of oscillating vanes to generate sinusoidal variations in tunnel flow angle for use in gust response studies, and special mount systems that enable simulation of airplane free-flight*

*dynamic ground motions and of launch vehicle ground wind loads.*

*The heavy gas (R12) medium is usually used during aeroelastic testing in the TDT because it has several advantages over air for dynamically scaled models. The R12 is four times heavier than air, and this allows for the design of heavier (and consequently stronger) models that still meet the mass density scaling ratios for proper modeling of full-size aircraft. Furthermore, the speed of sound in R12 is one-half that of air; this allows for lower dynamic frequency scaling ratios that benefit data acquisition and model safety and for lower tunnel power requirements during operation. Currently, the heavy gas reclamation system is being upgraded and is due to be completed in late 1991.*



## Flutter Tests of A-12 Advanced Fighter

Modern fighter aircraft must be designed so that their performance capabilities are not degraded by flutter restrictions. The objective of this program is to ensure that the U.S. Navy advanced fighter (A-12) aircraft will have the required flutter margin of safety throughout its flight envelope.

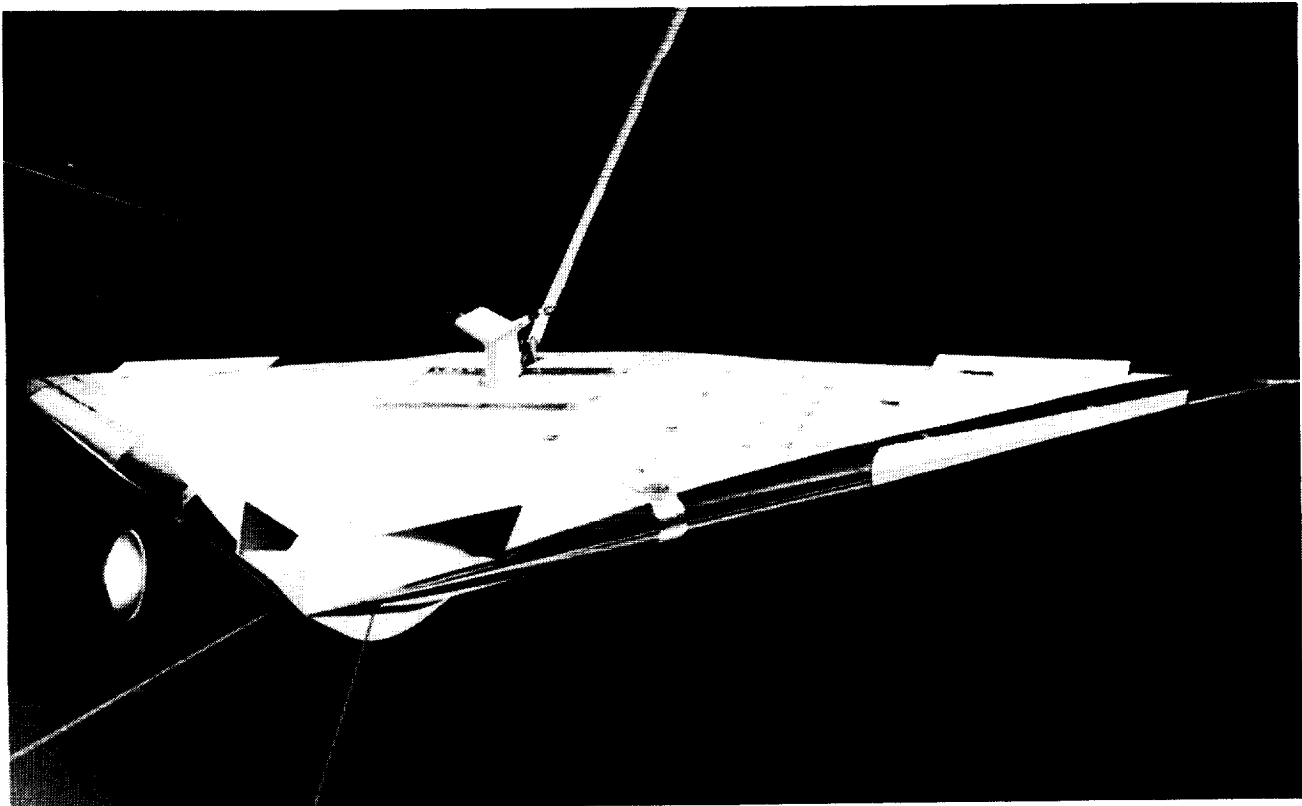
A dynamically scaled aeroelastic model of the A-12 was tested in the TDT as part of the flutter clearance program. The figure shows the model installed in the TDT on a cable mount system that has been used previously for many other models. The cable mount system is flexible enough to adequately simulate the vibrations

of the aircraft in flight. Initial testing was conducted using an overly stiff (dummy) model to determine dynamic stability of the model on the cable system. In addition, some configurations that were considered most likely to flutter were first tested on a sting mount to increase safety of the model. All tests were conducted using Freon in the TDT. These tests were jointly funded by NASA and the U.S. Navy.

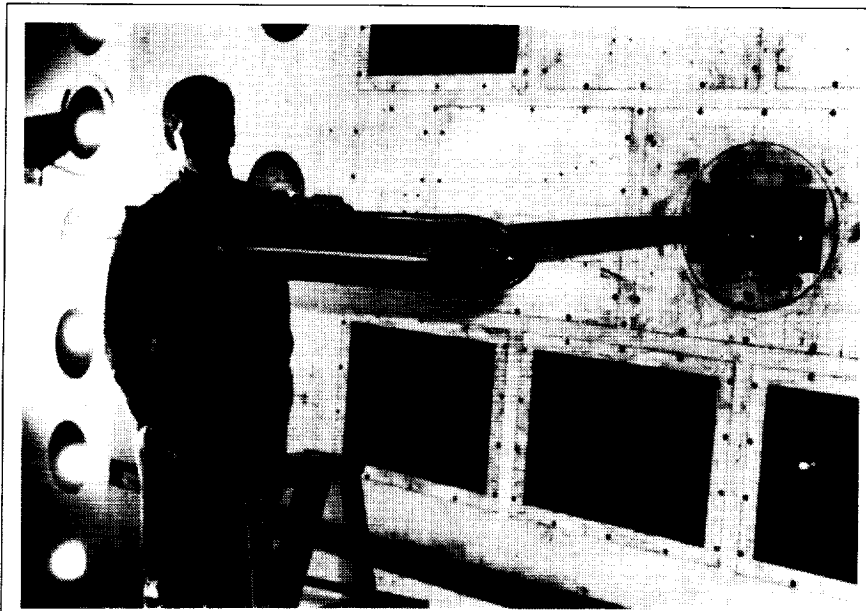
A total of 41 configurations were tested during four wind-tunnel tests in the TDT between July 1989 and August 1990. Model configurations that were tested during this time include the clean wing and the wing configured with internal and external stores. Some configurations were tested to

determine the influence on flutter of free-play effects and flexibility in the wing fold joints and wing control surfaces. Furthermore, fuel-mass effects on flutter also were determined. All configurations that were tested were shown to have the required flutter margins of safety throughout the vehicle flight envelope.

Tests such as these are very useful during the development of an advanced aircraft. After wind-tunnel tests, the design of the aircraft can proceed with greater confidence. In addition, the full-scale flight testing hours required for flutter clearance can be significantly reduced by results of such tests. (Moses G. Farmer and Maynard C. Sandford, 41263)

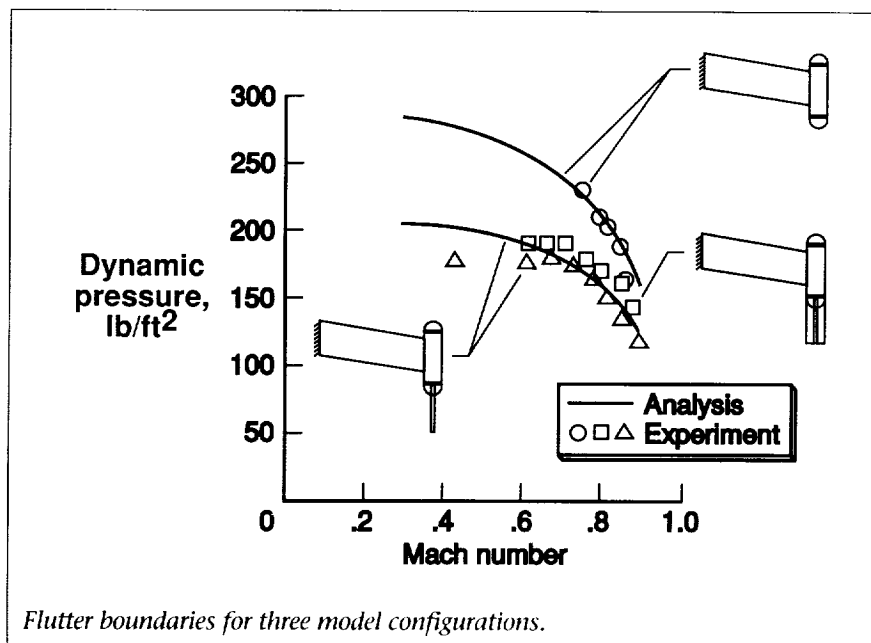


*A-12 advanced fighter flutter model.*



Trail-rotor model mounted on sidewall.

L-90-14504



Flutter boundaries for three model configurations.

### Flutter Characteristics of Trail-Rotor Model

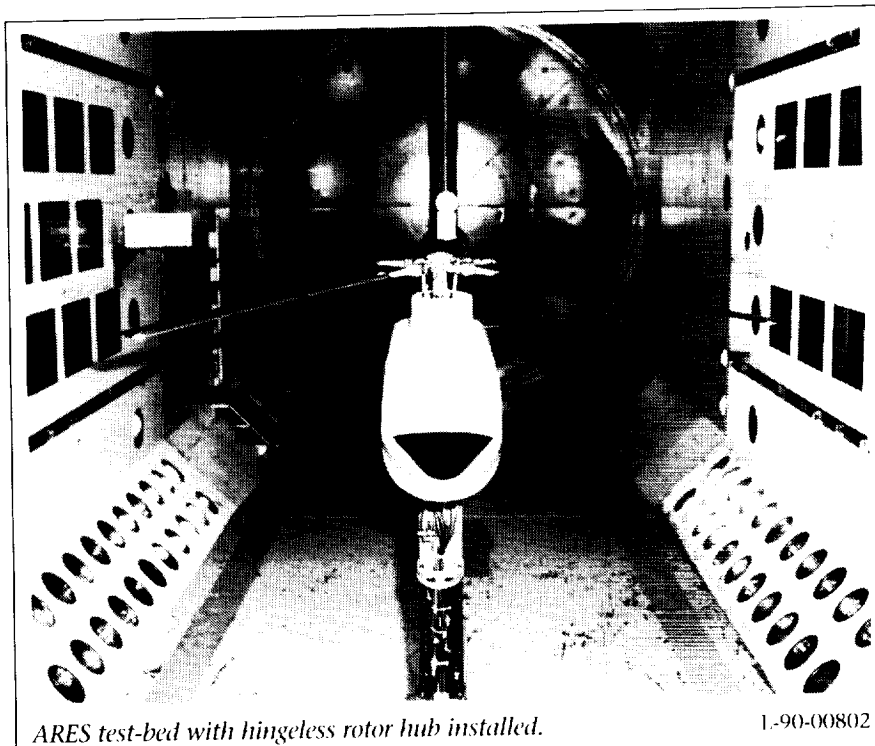
The trail-rotor vehicle is one design for a future generation high-speed rotorcraft. This vehicle uses a tilt-rotor concept that includes a fixed wing with a gear-box nacelle

and rotor blades at each wing tip. In the takeoff, landing, and hover conditions, the nacelles are in the vertical position with the blades extended. During conversion to the forward flight mode, the blades are feathered as the nacelles tilt aft and then are folded back into a fixed trailing position. Turbofan

engines located near the wing root power the vehicle. The objective of this study was to investigate the flutter behavior of a simple trail-rotor model in the forward flight mode.

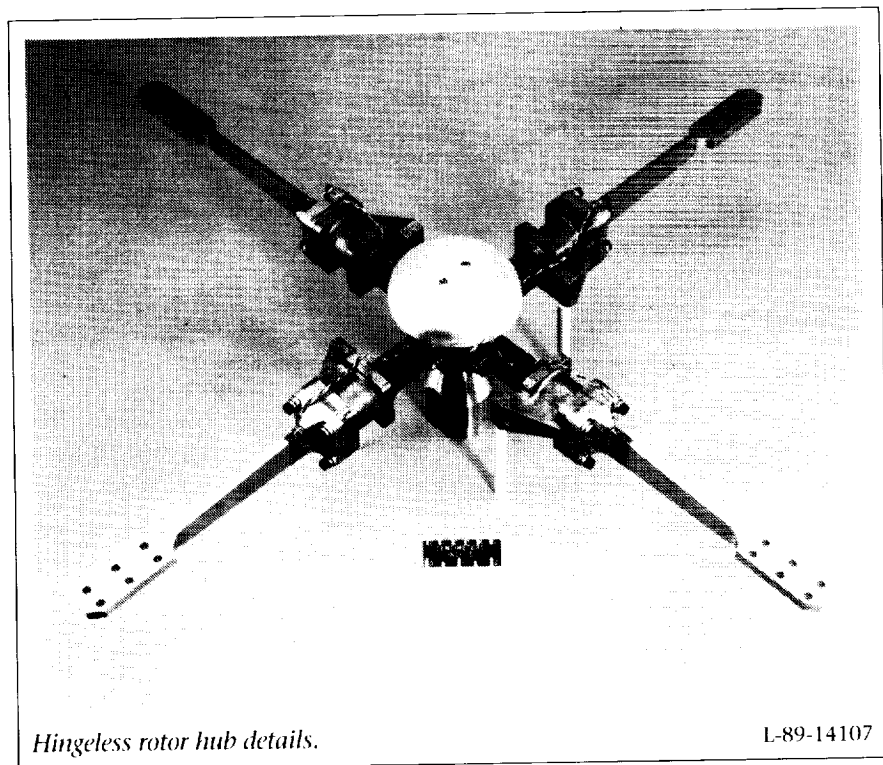
Several configurations of this trail-rotor concept were tested in the TDT. Each configuration was a wing model that was cantilever mounted to the tunnel sidewall. One configuration had only the nacelle attached at the wing tip. Two other configurations had folded blades attached to the nacelle. One set of folded blades was a baseline; the other set represented the baseline mass distribution but was streamlined to reduce the longitudinal aerodynamics of the blades. The first figure shows the model configuration with the wing, nacelle, and baseline blades mounted in the TDT. Structural finite-element models and kernel function aerodynamics were used to predict the flutter behavior.

Experimental flutter boundaries for these configurations are shown as open symbols in the second figure. (The model is stable below the flutter boundary.) The flutter boundaries for the configurations that include the blades are substantially lower than the wing/nacelle configuration. In comparing the results of the blade configurations, blade aerodynamics are seen to be slightly stabilizing. The analytical results (also shown in the second figure) accurately predict the results from the tests and indicate that these state-of-the-art tools can be used effectively during the design of such a vehicle.  
(David L. Soistmann, 41073)



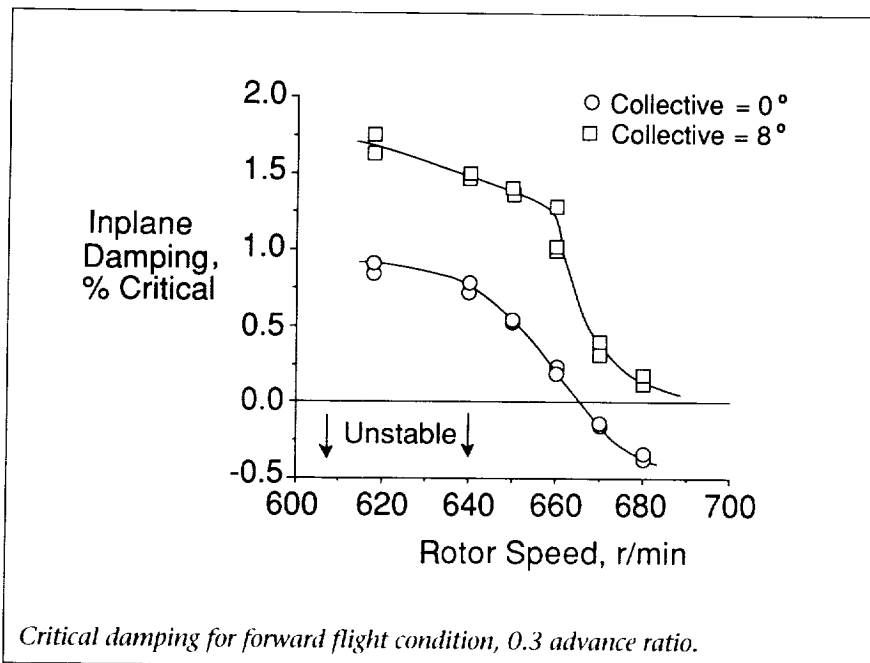
## Aeromechanical Stability of Hingeless Rotors

The Aeroelastic Research Experimental System (ARES) is a test-bed used for conducting helicopter rotor research in the TDT. One goal of the research is to develop the capability to test hingeless and bearingless rotor configurations. An important part of this capability is the development of an experimental technique for accurate measurement of the aeromechanical stability of the coupled rotor-body system. The objectives of these tests are to generate a data base for analytical correlation and to ensure safe testing of hingeless and bearingless rotors in the TDT. Photographs of both the ARES (first figure) and a hingeless rotor (second figure) are shown.



Testing of the hingeless rotor was recently completed for both hover and forward-flight conditions in the TDT. The moving-block technique was utilized to measure rotor inplane damping for determination of aeromechanical stability. Damping measurements were made for a range of parameters including rotor speed, collective pitch, and blade droop.

Testing in hover was conducted at different values of collective pitch over a range of rotor speeds. Testing in forward flight was performed over a range of advance ratios up to 0.35. Some illustrative results of inplane damping values for forward flight conditions are shown in the third figure. The data obtained show a trend of increasing damping with collective pitch. The figure also shows that inplane damping



decreases with increasing rotor speed. An unstable region is indicated in the figure. Similar results were obtained for configurations incorporating changes to blade droop.

performance and combat maneuverability. As a result, it is becoming more difficult to test on cable systems the full-span models that

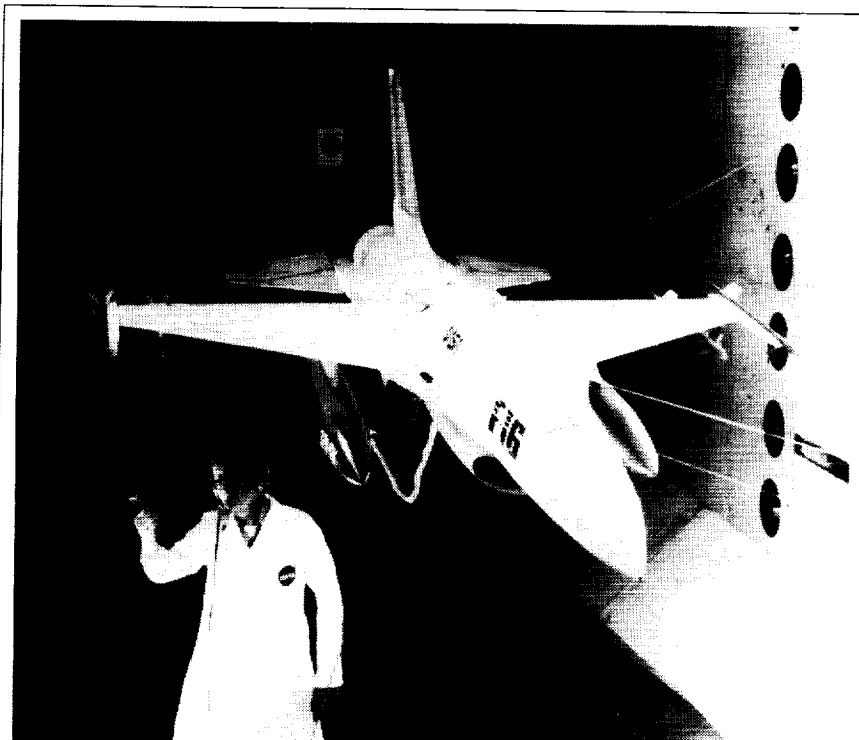
accurately scale aeroelastic characteristics. A study has been conducted in the TDT to develop and demonstrate the ability to test a statically unstable aeroelastic flying model using an onboard stability augmentation system (SAS).

A full-span aeroelastic flying model was designed and constructed to represent an advanced fighter aircraft such as shown in the first figure. Statically stable and unstable test conditions were achieved with a movable mass system within the model that allowed the center of gravity (CG) to vary over a wide range (12 percent) of mean aerodynamic chord. An onboard hydraulic system was used to actuate horizontal tail surfaces providing pitch and roll stability. Rate gyros were mounted in the model to provide pitch and roll inputs to the SAS.

This test has expanded the aeromechanical stability data base for the parametric hingeless rotor. Consistent and repeatable measurements of the rotor inplane damping were obtained. The experimental data will be used for future correlation with analytical codes. The test showed that safe testing can be accomplished even near and into the instability region. (M-Nabil H. Hamouda, Jeffrey D. Singleton, and William T. Yeager, Jr., 41266)

### Statically Unstable Model on Cable Mount System

Fighter aircraft are being designed to fly in a statically unstable manner to improve

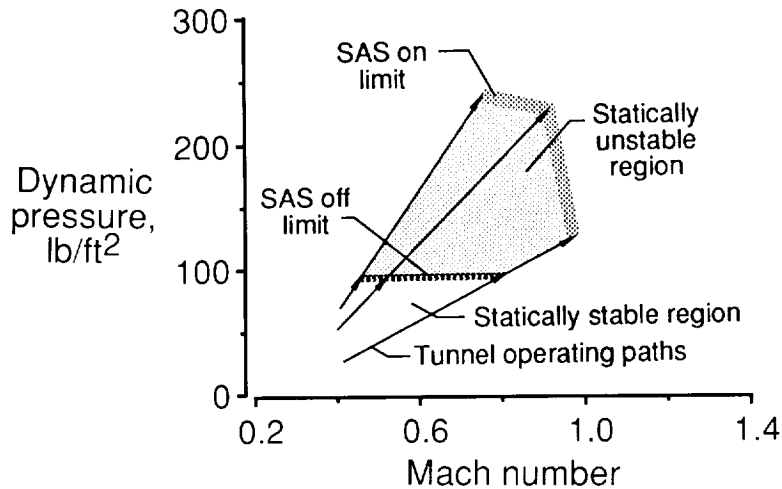


*Fighter model on cable mount system.*

## NACA 0012 Benchmark Model Test

A Benchmark Models Program has been initiated at Langley Research Center with the primary objective of obtaining data for aeroelastic computational fluid dynamics (CFD) code development, evaluation, and validation. The first model in the series is a wing with a conventional airfoil supported on a flexible mount system. This model was tested to define the conventional flutter boundary, the angle-of-attack  $\alpha$  flutter boundary, and other transonic instability boundaries with simultaneous measurements of surface pressures during flutter.

A rigid rectangular wing of panel aspect ratio 2 and an NACA 0012 airfoil were tested in the TDT on the flexible Pitch and Plunge Apparatus (PAPA). The model is shown in the first figure. This model was equipped with in situ



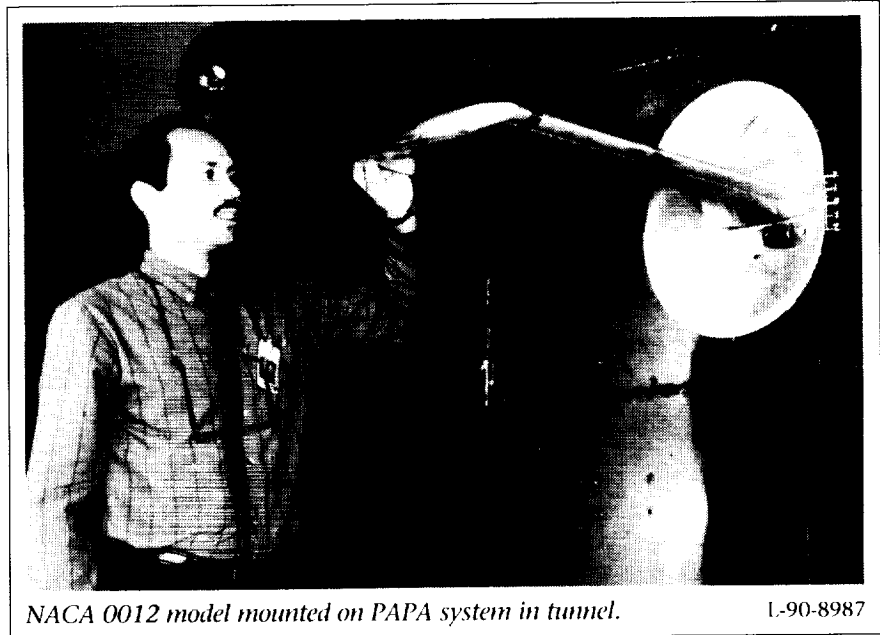
*Augmented and unaugmented model test regions.*

An analog control system was designed to command the individual horizontal tail surfaces using pilot trim inputs, horizontal tail position, and gyro feedback. Model tests were conducted in the TDT over a Mach number range of 0.6 to 1.2 using both a heavy gas (R12) and air as test mediums.

Some results of the tests are shown in the second figure. These results were acquired for the model configuration with the movable mass in its most aft position (most statically unstable). The shaded region in the figure represents the increased test envelope achieved with the use of the SAS. The dashed line indicates the test limits without the SAS. The active SAS allowed testing to a maximum dynamic pressure of 250 lb/ft².

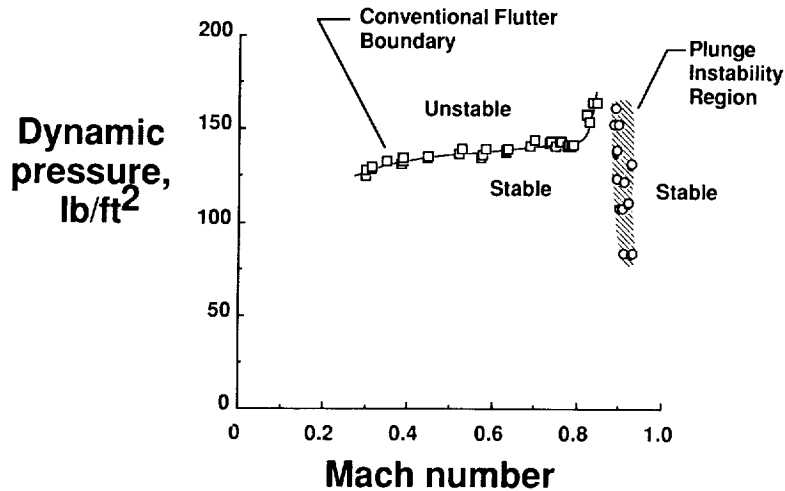
The capability to fly statically unstable aeroelastic models was demonstrated in the TDT. These tests evaluated the use of an active SAS to allow flutter testing of a

model that accurately scaled a statically unstable aircraft.  
(Michael H. Durham and Donald F. Keller, 41262)

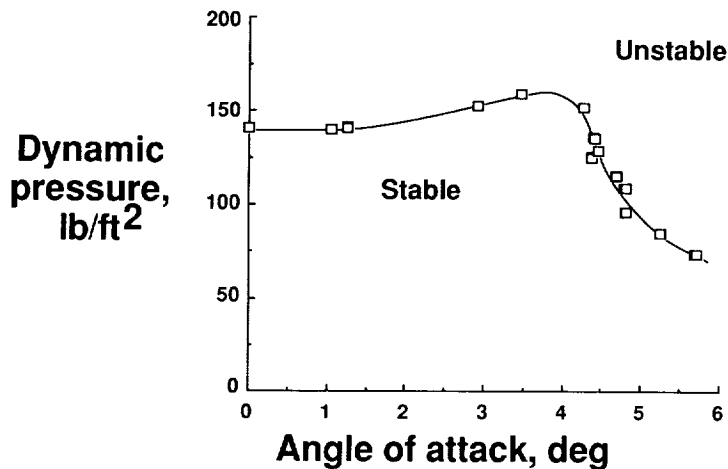


*NACA 0012 model mounted on PAPA system in tunnel.*

L-90-8987



Conventional and plunge instability boundaries at  $\alpha = 0^\circ$ .



Angle-of-attack instability boundary at Mach number of 0.78.

pressure transducers to measure wing upper and lower surface steady and unsteady pressures. The model and support system also were instrumented with accelerometers and strain-gauge bridges to measure model loads and response. Wind-on data were obtained for Mach numbers of 0.30 to 0.97.

The Mach number effects on the conventional flutter boundary (coupling of pitch and plunge modes) for the model at an angle of attack of  $0^\circ$  are shown in the second figure as a function of dynamic pressure and Mach number. A narrow instability region is also shown near a Mach number of 0.90, in which the mode of oscillation was primarily plunge

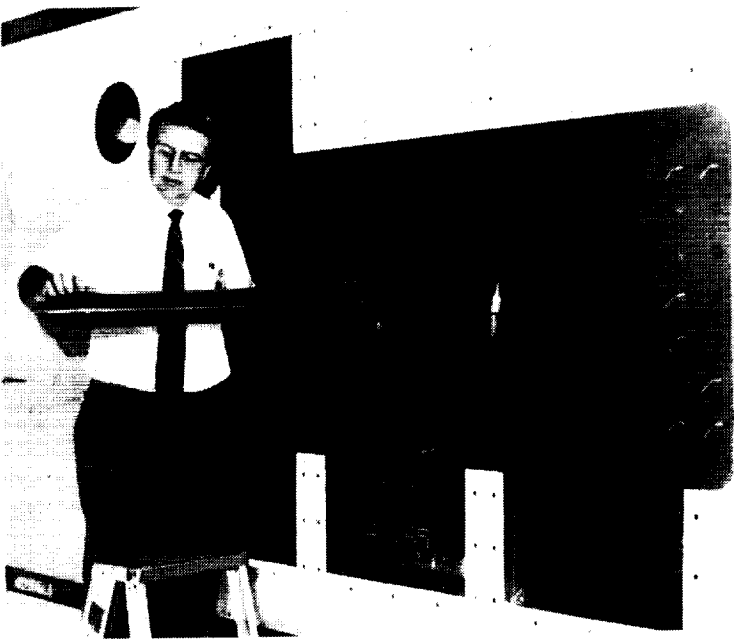
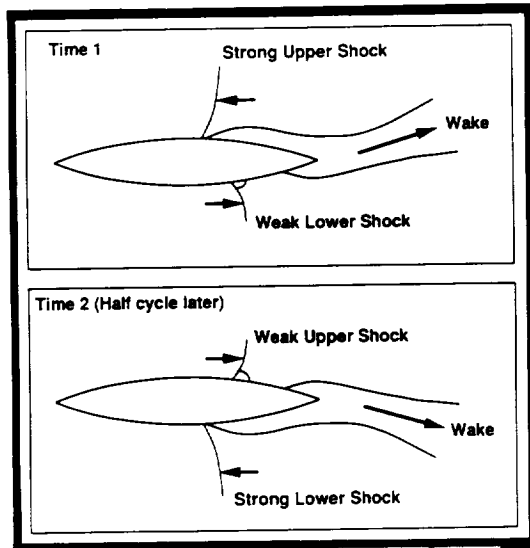
motion. Angle-of-attack effects on model flutter at a Mach number of 0.78 are shown in the third figure. At angles of attack greater than approximately  $4.3^\circ$ , the motion was primarily in the pitch mode (stall flutter). Instrumentation time history records were recorded at most instability points as well as at some subcritical test conditions.

This test provided an extensive data set defining the model structural dynamic characteristics and measured model instability boundaries along with associated steady and unsteady pressure measurements. This data set is expected to be a useful tool for the development, evaluation, and validation of modern aeroelastic CFD methods. (José A. Rivera, Jr., Bryan E. Dansberry, Moses G. Farmer, Clinton V. Eckstrom, Robert M. Bennett, and David A. Seidel, 41270)

## Transonic Shock-Induced Dynamics of Flexible Wing in TDT

Periodic transonic shock-boundary-layer oscillations are known to occur over a narrow range of Mach numbers on thick rigid circular-arc airfoils, as illustrated in the left half of the first figure. The objective of this research was to determine the dynamic response of a flexible wing under these conditions. This model is an element of the Benchmark Models Program and is an investigation intended to aid in the physical understanding of complex unsteady transonic aerodynamics.

### Sketch of Shock-Boundary-Layer Oscillation



Model Mounted in TDT

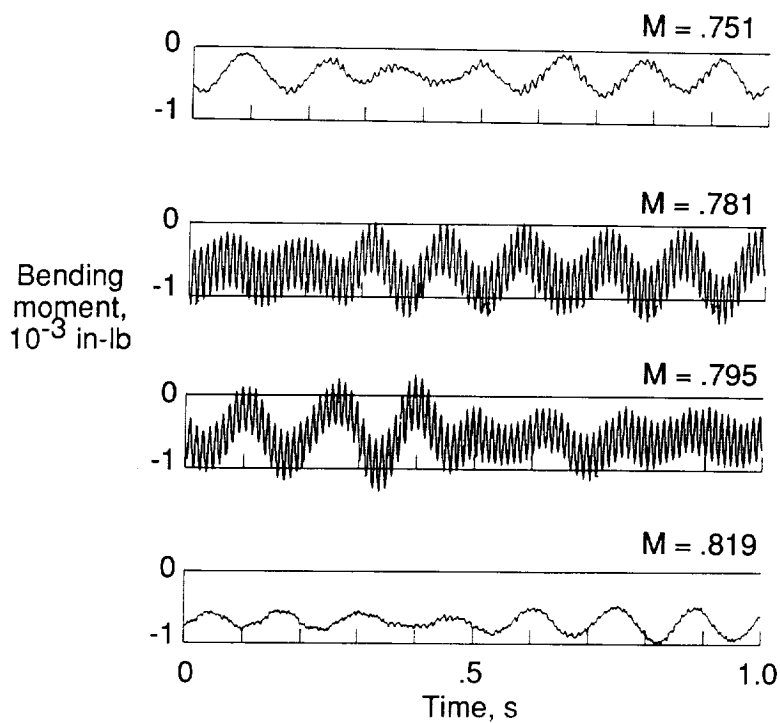
*Flexible wing with 18-percent circular-arc airfoil section.*

A simple flexible wing was designed and built at Langley Research Center and tested in the TDT to determine the shock-boundary-layer induced dynamics. The wing was rectangular in planform with an 18-in. chord and a 45-in. span. The wing consisted of an aluminum plate with balsa wood forming an 18-percent circular-arc airfoil section. The right half of the first figure shows the model mounted in the TDT. The model was instrumented with bending and torsion strain gauges at the root and accelerometers on the outer portion of the wing.

In the region of the shock-boundary-layer oscillations, an increased random buffeting level was found for the first bending mode; this level was at a much lower frequency than the frequency of the shock-boundary-layer oscillations. A limit-cycle oscillation was found for a third-bending-like mode that involved splitter plate motion and which had a natural frequency that was near the frequency of the shock-boundary-layer oscillations. These results are illustrated in the second figure. For  $M = 0.751$ , a random

amplitude buffeting response in the first bending mode is shown in the bending moment time history. At  $M = 0.781$  and  $0.795$ , the first bending buffeting response is larger, and a nearly constant amplitude high-frequency response is evident. With a further increase in Mach number to  $0.819$ , the high-frequency response disappears, and the first-mode buffeting is again of lesser magnitude.

A small spanwise strip and wishbone-type vortex generators were used to alleviate the limit



*Sample time history of bending moment response.*

cycle oscillations, but they resulted in either increased buffeting of the first mode or induced flutter.

(Robert M. Bennett, 42274, Bryan A. Dansberry, Moses G. Farmer, Clinton V. Eckstrom, and José A. Rivera, Jr.)





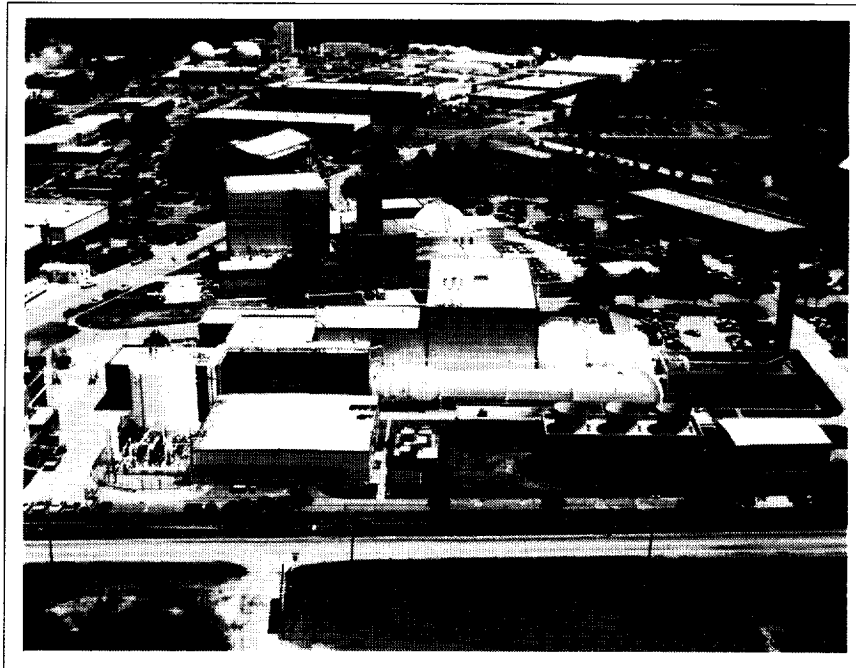
## 16-Foot Transonic Tunnel

---

*The Langley 16-Foot Transonic Tunnel is a closed-circuit single-return continuous-flow atmospheric tunnel. Speeds up to Mach 1.05 are obtained with the tunnel main-drive fans, and speeds from Mach 1.05 up to Mach 1.30 are obtained with a combination of main-drive and test section plenum suction. The slotted octagonal test section measures 15.5 ft across the flats. The tunnel is equipped with an air exchanger with adjustable intake and exit vanes to provide some temperature control. This facility has a main-drive power of 60 000 hp, and a 36 000-hp compressor provides test section plenum suction.*

*The 16-Foot Transonic Tunnel was closed to research during most of 1990 to allow completion of several major modifications. These modifications included a floor-mount system to facilitate semispan model testing and a model preparation area for model buildup and calibration.*

*The tunnel is used for force, moment, pressure, and flow visualization studies on propulsion-airframe integration models. Model mounting consists of sting, sting-strut, and fixed-strut arrangements; propulsion simulation studies are made with dry, cold, high-pressure air.*



## National Transonic Facility

---

*The National Transonic Facility (NTF) is a fan-driven, closed-circuit, continuous-flow, pressurized wind tunnel. The test section is 8.2 ft by 8.2 ft and approximately 25 ft long with a slotted-wall configuration. There are six slots each in the top and bottom walls.*

*The test gas may be dry air or nitrogen. For the elevated-temperature mode of operation (in which the test gas is normally air), heat removal is by a water-cooled heat exchanger (cooling coil) located at the upstream end of the settling chamber. For the cryogenic mode of operation, heat removal is by evaporation of liquid nitrogen, which is sprayed into the circuit upstream of the fan. By utilizing liquid nitrogen as a coolant, the tunnel design test-temperature range is variable from 150°F to -320°F. When nitrogen is injected into the circuit, venting must occur to*

*maintain a constant pressure. Thermal insulation is installed internal to the pressure shell to minimize energy consumption. The design total pressure range for the NTF is from 15 psia to 130 psia.*

*The combination of pressure and cold test gas can provide a maximum Reynolds number of  $120 \times 10^6$  at a Mach number of 1.0 based on a chord length of 9.75 in. By using the cryogenic approach to high Reynolds numbers, the NTF achieves its performance of near full-scale conditions at lower cost and at lower model loads than concepts based on ambient temperature operation. In addition, with both temperature and pressure as test variables, three types of investigations are possible; these include Reynolds number effects at constant Mach number and dynamic pressure (model deflections), model aeroelastic effects at constant Reynolds number*

*and Mach number, and Mach number effects at constant dynamic pressure and Reynolds number.*

*Flow quality was considered an important part of facility design. Four antiturbulence screens incorporated in the settling chamber and a contraction of 15:1 from the settling chamber to the nozzle throat are provided to reduce turbulence. Acoustic treatment upstream and downstream of the fan is provided to minimize fan noise effects.*

*Basic three-dimensional model support is provided by an aft-mounted sting. This sting is attached to a vertically mounted arc sector that is driven by a hydraulic cylinder to change the model pitch attitude. The arc-sector center is designed so that the model pitch center is maintained on the tunnel centerline throughout the angle-of-attack range. The arc sector*

can be pitched over a range of  $30^\circ$  with the model angle-of-attack range being set by the use of bent stings. A roll mechanism provides the interface between the arc sector and the model-sting combination; this mechanism has a roll range of  $-90^\circ$  to  $270^\circ$ . Sideslip angles are achieved by using combined roll and pitch angles.

The tunnel drive system consists of two variable-speed induction motors with a combined power output of  $3.5 \times 10^7$  W ( $4.9 \times 10^7$  W overload), a two-speed gear box, and a synchronous motor with a power output of  $3.1 \times 10^7$  W ( $4.5 \times 10^7$  W overload). The compressor consists of a fixed-pitch, single-stage fan with variable-inlet guide vanes. The drive system can be operated in either of two modes: the synchronous mode (in which the fan is operated at the constant synchronous

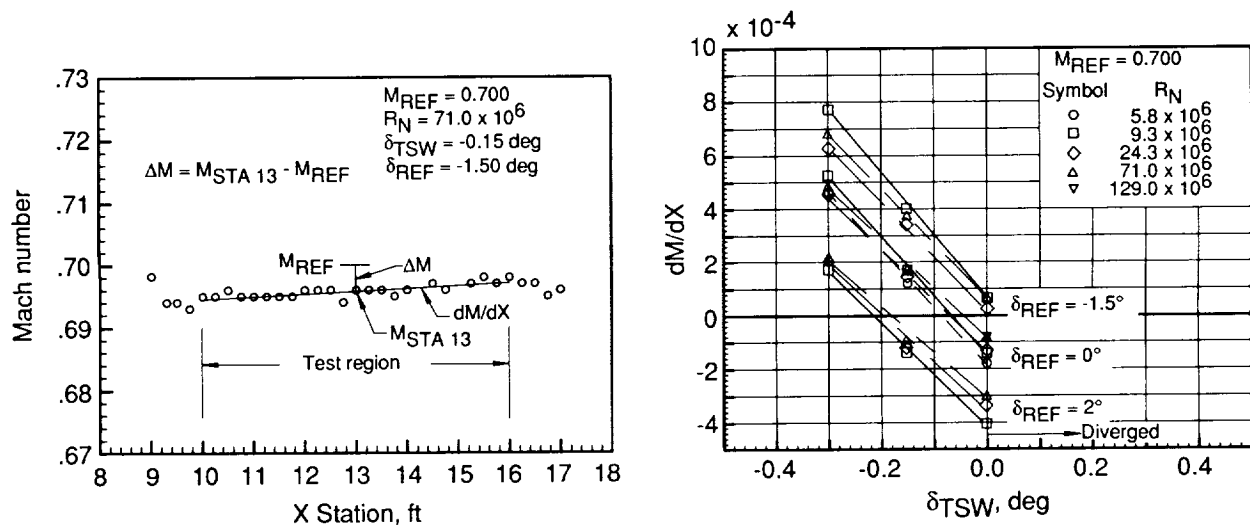
speed of 360 r/min and the inlet guide vanes are varied to achieve the desired compression ratio) and the variable fan speed mode (in which the induction motors are used to drive the fan over a range of rotational speeds (up to 600 r/min) to achieve the desired compression ratio).

### Mach Number Calibration on National Transonic Facility Test Section

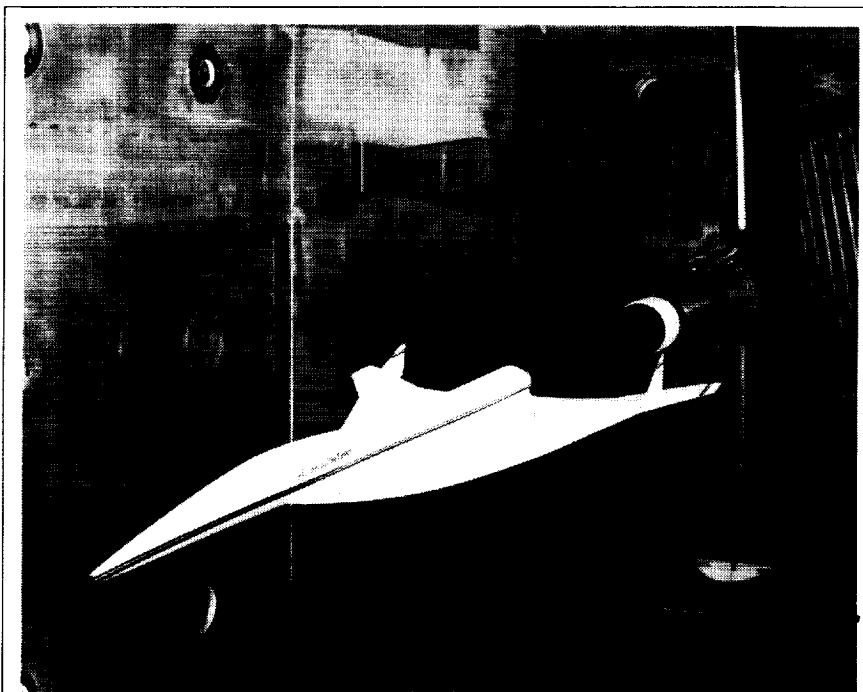
The test region of wind tunnels must be calibrated to provide precise settings of Mach number and to correct the test results for Mach gradients that exist in this region. The calibration measurements were made in the NTF with a centerline pressure probe that had multiple pressure

orifices distributed along its length. Mach number level and gradients on the centerline were determined as a function of reference test conditions (Mach and Reynolds number) and of the variable test section geometry (wall divergence  $\delta_{TSW}$  and reentry flap angle  $\delta_{REF}$ ).

Because the test section geometry was variable, one thrust of the test was to find combinations of wall and reentry flap angles that produced a Mach gradient ( $dM/dX$ ) of  $0^\circ$ . Data at  $M_{REF} = 0.7$  indicate that various combinations of the angles produced this result. Combinations with the walls diverged as much as possible would be chosen because of lower tunnel power consumption. The Mach gradients at a fixed geometry are a function of Reynolds number. This variation is not always monotonically



Mach number distributions in NTF test section.



HSCT model installed in NTF test section.

1-90-12564

*consistent, but the NTF test section geometry can be optimized as a function of Mach number and Reynolds number. Note the increased Reynolds number or viscous effects for wall combinations that produce large positive or negative Mach number gradients. These occurrences are conditions of increased flow through the slots, and they suggest viscous effects on this flow.*

**(Jerry B. Adcock and M. Susan Williams, 45135)**

### **Reynolds Number Effects on High-Speed Civil Transport at Takeoff Speeds**

This test investigated Reynolds number effects on the low-speed aerodynamic characteristics of the NTF High-Speed Civil Transport (HSCT) configuration. The figure shows the model in the NTF test

section. The model was tested without leading-edge deflection, trailing-edge flaps, or vertical stabilizers. Mach numbers ranged from 0.2 to 0.5, and Reynolds numbers ranged from  $7 \times 10^6$  to  $86 \times 10^6$ , based on the mean aerodynamic chord. Forces, moments, and tuft patterns were recorded. This model, which was sized to maximize the Reynolds number range at takeoff and landing conditions, is the largest airplane model ever tested in the NTF. This test provides a data baseline with a nearly sharp leading edge on the wing as well as a test technique experience for this type of configuration.

The data indicate that even with this nearly sharp leading edge (a leading-edge radius to mean chord ratio of 0.0009), Reynolds number effects on the lift are noticeable when the model is clean (with no tufts). The addition of

tufts for flow visualization reduced the slope of lift versus angle-of-attack curve. This effect was observed at the high Reynolds numbers of this investigation and is thought to be the result of the tufts energizing the boundary layer and delaying its separation.

The use of minitufts in a cryogenic environment was validated during this test for the duration of many test runs. A new optical disc image storage system was utilized to work with the minituft video system. Conventional cameras are not used because no way exists to change film at cryogenic conditions.

**(Pierce L. Lawing, Julio Chu, and Lewis R. Owens, 45137)**

### **Reynolds Number Effects on Commercial Transport**

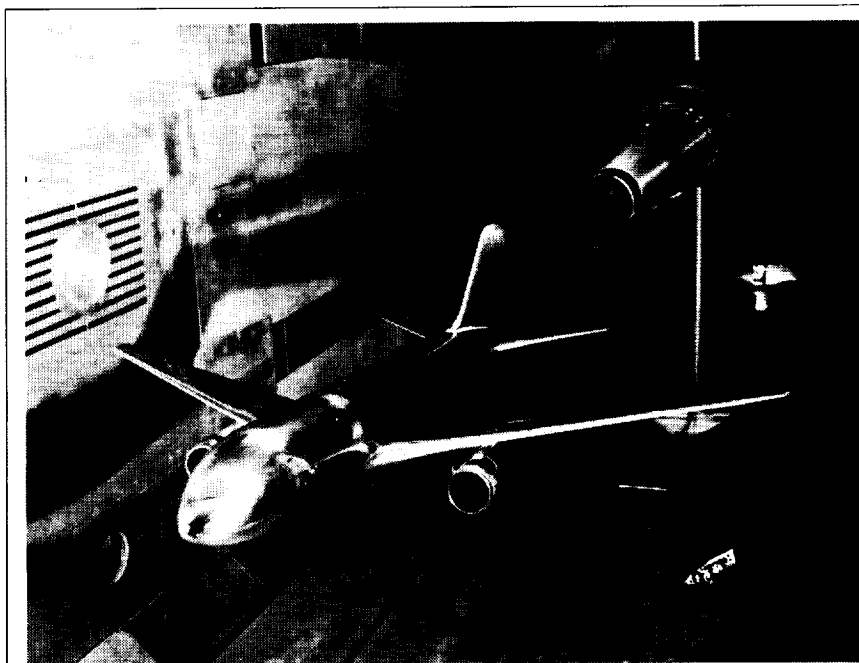
An investigation of an 0.03-scale model of the Boeing 767-200 aircraft has been conducted in the NTF to determine the Reynolds number effects on the aerodynamic characteristics of the model, to obtain data at full-scale Reynolds numbers for comparison with available flight data, and to obtain data for the development and enhancement of Reynolds number scaling techniques. The model was tested over a Mach number range from 0.40 to 0.92 and a Reynolds number range from  $7.50 \times 10^6$  to  $67.37 \times 10^6$  per foot. High Reynolds number data were obtained using cryogenic nitrogen; low Reynolds number data were taken in air. The repeatability of the data taken in both the air and nitrogen modes of operation was very good.

The data indicate that increasing the Reynolds number results in higher lift at a constant angle of attack, higher drag-divergence Mach number, increased stability, and lower drag. Physically, the boundary layer is thinner for higher Reynolds numbers, which causes an increased effective camber of the wing; this effect also increases the downwash on the horizontal tail. A model-support system buffet, primarily in the rigid-body roll mode, was experienced at the full-scale Reynolds number only ( $67.37 \times 10^6$  per foot)

ena are a function of Reynolds and Mach numbers rather than dynamic pressure. Data from independent variation of the dynamic pressure indicate significant aeroelastic effects on the wing; force, moment, and pressure data indicate an unloading and nose-down twisting of the wing-tip region with increasing dynamic pressure.

(Richard A. Wahls, 45108)

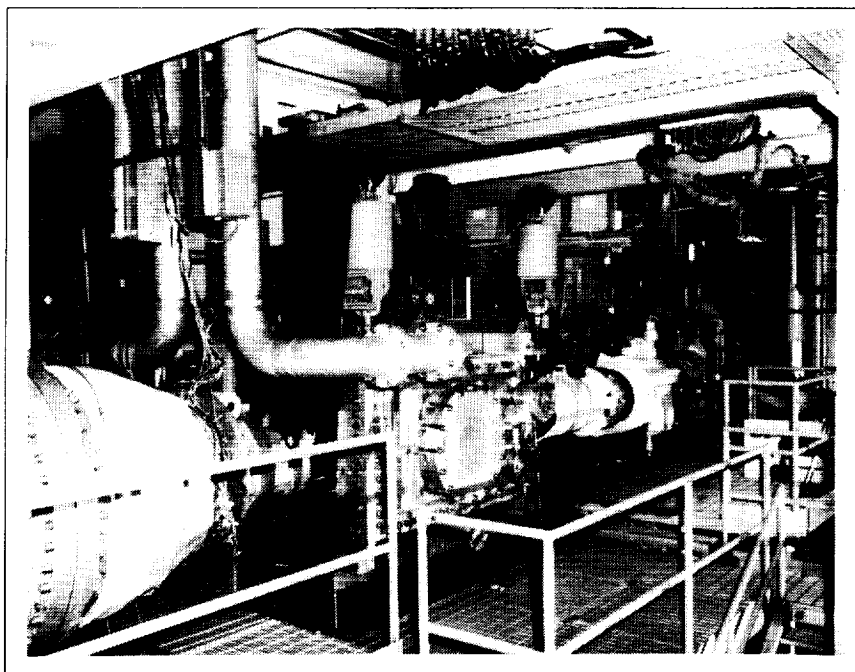
ORIGINAL PAGE  
BLACK AND WHITE PHOTOGRAPH



*Boeing 767-200 model in NTF test section.*

L-87-4167

for test Mach numbers of 0.75, 0.80, and 0.82. The buffet did not occur for any other test Reynolds numbers ( $7.50 \times 10^6$  and  $35.54 \times 10^6$  per foot) or at a Mach number of 0.86 for the full-scale Reynolds number. Buffet onset occurred above the cruise angle of attack just prior to pitch-up. These phenom-



## 0.3-Meter Transonic Cryogenic Tunnel

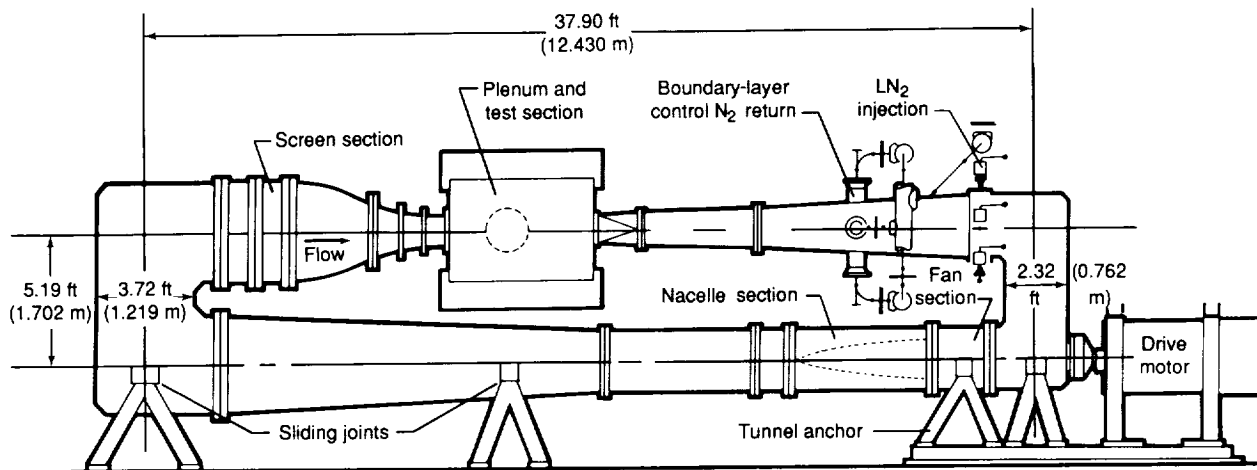
The Langley 0.3-Meter Transonic Cryogenic Tunnel (0.3-Meter TCT) is a continuously operating cryogenic pressure tunnel. The test section Mach number is continuously variable between 0.2 and approximately 1.3, with suitable adjusted test section shapes. The stagnation pressure can vary from slightly over 1 bar up to 6 bars and the stagnation temperature from 340 K down to approximately 77 K (196°C). The test gas is nitrogen. The wide ranges of pressure and temperature allow the study of approximately a 30-to-1 range in Reynolds number effects. A maximum Reynolds number of more than  $100 \times 10^6/\text{ft}$  is possible. The 0.3-Meter TCT has automatic control of Mach number, pressure, and temperature.

The tunnel was placed in operation in 1973 as a three-dimensional pilot tunnel to demonstrate the cryogenic wind-tunnel concept at transonic speeds. The successful demonstration of the cryogenic concept in the 0.3-Meter TCT played a major role in the decision to build the U.S. National Transonic Facility (NTF). Subsequently, the 0.3-Meter TCT has played a major part in the Advanced Technology Airfoil Program because the tunnel allows Reynolds number effects to be studied in two-dimensional testing. The 0.3-Meter TCT is currently involved in the evaluation of testing techniques for improving data quality (by minimizing boundary interferences) in both two- and three-dimensional testing. The combination of flight Reynolds number capability and minimal boundary interferences makes the

0.3-Meter TCT a powerful tool for aeronautical research at transonic speeds.

During more than 15 years of operation, the 0.3-Meter TCT has run with three different test sections. The original test section was octagonal with a sting-type model support system. In 1975, an 8- by 24-in. two-dimensional test section was installed with slotted top and bottom walls. In 1985, a new Adaptive-Wall Test Section (AWTS) was installed.

The AWTS is nominally square with 13 in. sides and has an effective length of 55.8 in. This unusual transonic test section has four solid walls with a flexible floor and ceiling. The complete test section is enclosed in a pressure shell that forms a 73.2-in.-long insert into the 0.3-Meter TCT



Sketch of 0.3-Meter TCT with 13-in. by 13-in. two-dimensional Adaptive-Wall Test Section installed.

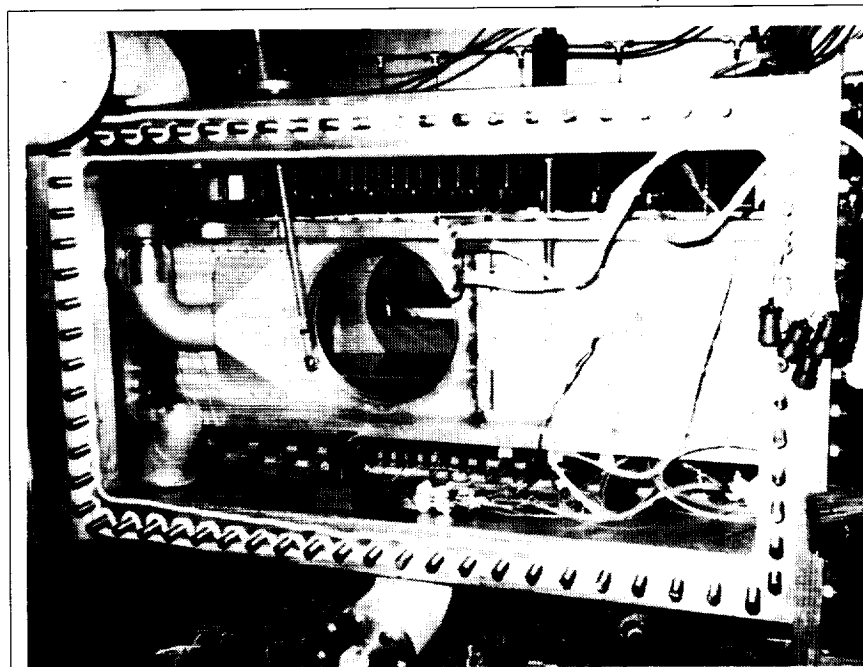
tunnel circuit. A system of 21 computer-controlled jacks supports each flexible wall. These flexible walls are made of 308 stainless steel. The AWTS has motorized model support turntables and a traversing wake survey probe, both of which are computer controlled.

For each data point, the flexible walls are adapted to shapes that drastically minimize wall interferences that would exist around the model if it were in free air. The floor and ceiling of the test section, in effect, become invisible to the model. With wall interferences minimized, the model size and therefore the Reynolds number capability of the tunnel can be increased. In addition, the removal of noisy slots in the test section gives the added benefit of much improved data quality.

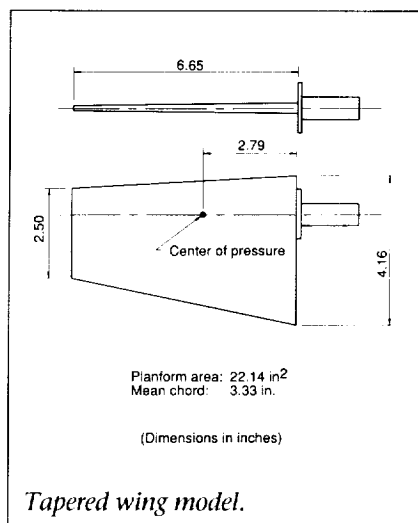
For two-dimensional testing, the AWTS has provisions for both active and passive sidewall boundary-layer control (BLC). Porous plates can be fitted into the rigid sidewalls just

upstream of the model location. The BLC system allows the investigation of another source of boundary interference.

#### ORIGINAL PAGE BLACK AND WHITE PHOTOGRAPH



View of 0.3-Meter TCT AWTS with left side of surrounding pressure shell removed.



## Half-Wing Test in Adaptive-Wall Test Section

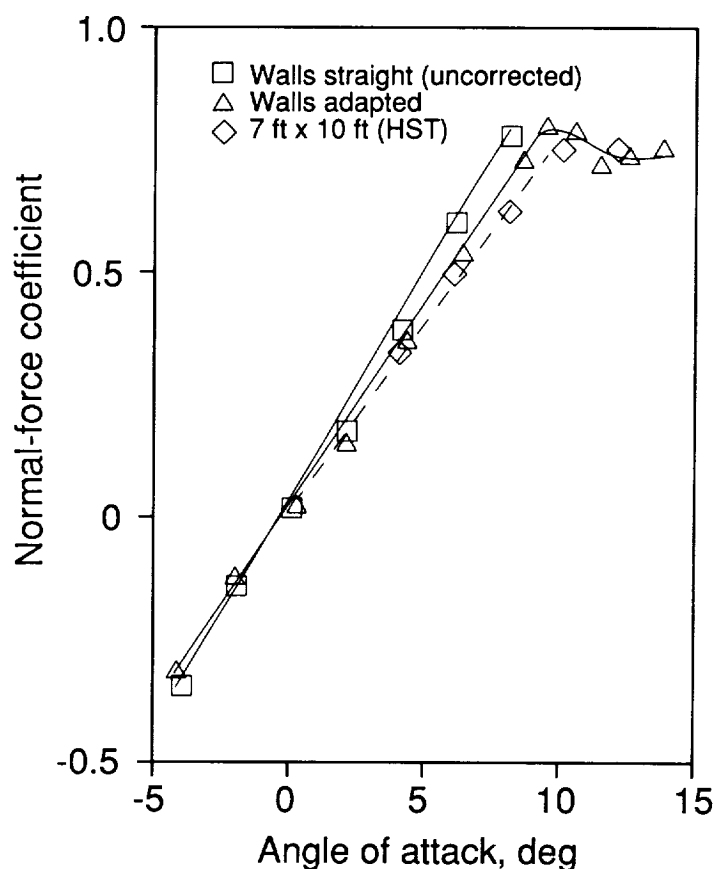
Conventional test sections with solid or ventilated walls prevent proper deflection of streamlines around the model in a wind tunnel. A solution to reducing the undesirable wall effects at the source is offered by using the adaptive-wall concept; this concept has been successfully demonstrated for minimizing two-dimensional wall interference in the 0.3-Meter TCT.

Recently, a semispan tapered wing model (shown in the first figure) mounted on one of the test section sidewalls was used to study effects of wall adaptation at high angles of attack. This study consisted of an iterative adjustment of test section top and bottom walls and a measurement of forces on the model using a strain-gauge balance. The calculation of wall interference and new wall shapes was conducted on-line. The wall interference reduced considerably after the first iteration up to moderate angles of attack. For angles higher than 8°, the test

section flow choked with the walls straight. For these conditions, wall adaptation was accomplished starting from a previously adapted contour. The wall-adjustment process was terminated when the correction to the test Mach number was less than 0.003.

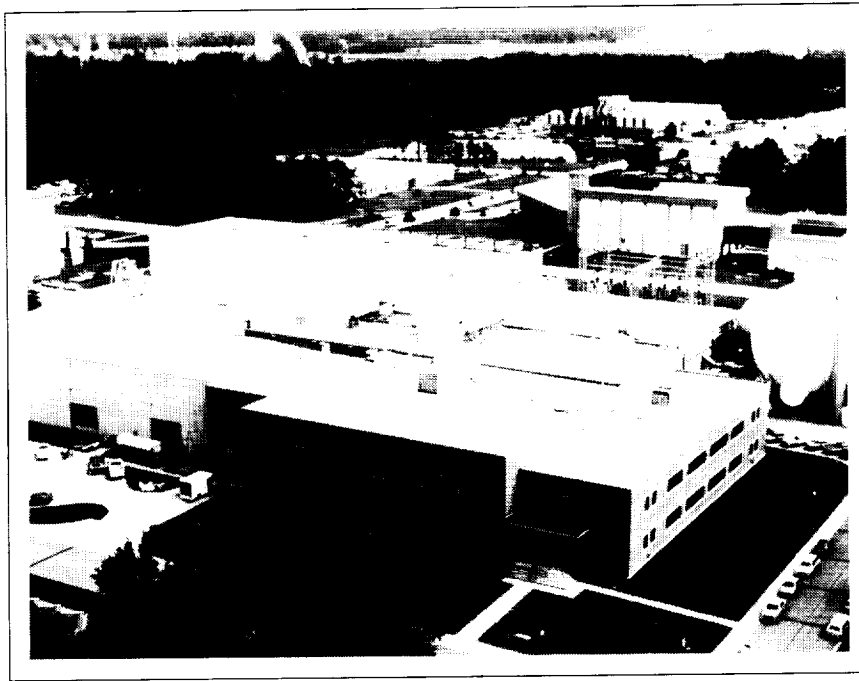
The second figure shows the measured normal-force coefficient variation with wing incidence. The normal force decreased when the walls were adapted starting from straight shapes. The adapted wall data are closer to the nearly interference-free data measured in

the Langley 7- by 10-Foot High-Speed Tunnel (HST). The data in the stall region could be obtained only by adapting the walls because the straight-wall shapes had large interference and caused choking of the test section. This study demonstrated that the 0.3-Meter TCT Adaptive-Wall Test Section can be successfully used to measure the high-lift characteristics of three-dimensional wings. Some differences at high angles are probably due to residual errors and sparse wall pressures used for computing the wall shapes. (A. V. Murthy, 45007)



Effect of wall adaptation on normal-force variation at Mach number of 0.8 and Reynolds number of  $1.4 \times 10^6$ .





## Unitary Plan Wind Tunnel

---

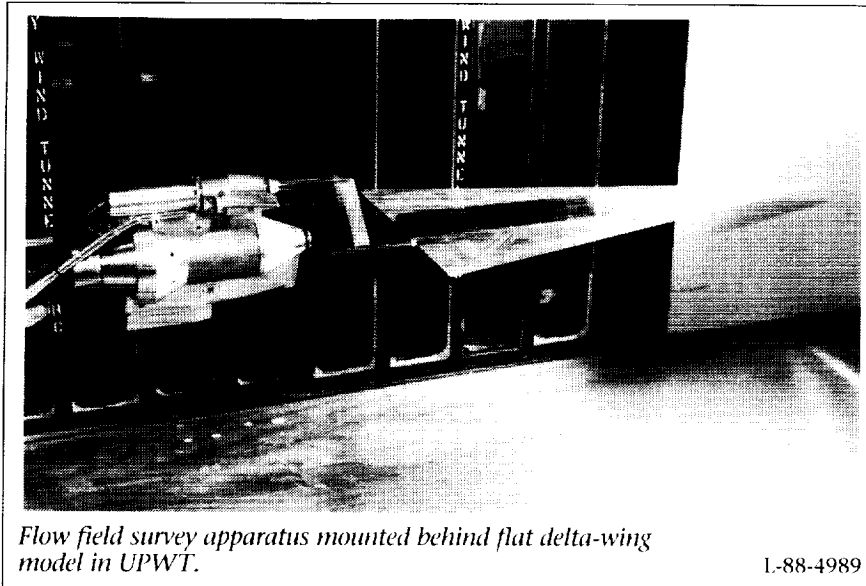
Immediately following World War II, the need for wind-tunnel equipment to develop advanced airplanes and missiles was recognized. The military and the National Advisory Committee for Aeronautics (NACA) developed a plan for a series of facilities which was approved by the United States Congress in the Unitary Wind Tunnel Plan Act of 1949. This plan included five wind-tunnel facilities, three at NACA laboratories and two at the Arnold Engineering Development Center. The Langley Unitary Plan Wind Tunnel (UPWT) was among the three built by NACA. The UPWT is a closed-circuit continuous-flow variable-density tunnel with two 4-ft by 4-ft by 7-ft test sections. The low-range test section has a design Mach number range of 1.5 to 2.9, and the high-range section Mach number varies from 2.3 to 4.6. The tunnel has sliding-block-type nozzles that allow continuous variation in

Mach number while on-line. The maximum Reynolds number per foot varies from  $6 \times 10^6$  to  $11 \times 10^6$  depending on Mach number. The tunnel is used for force and moment, pressure distribution, jet effects, dynamic stability, and heat-transfer studies. Flow visualization data, which are available in both test sections, include schlieren, oil flow, and vapor screen.

### **Flow Field Survey Apparatus for Unitary Plan Wind Tunnel**

The UPWT Flow Field Survey Apparatus is a research tool designed to acquire flow field data in the vicinity of a wind-tunnel model. The apparatus can be used over the entire Mach number range (Mach 1.5 to 4.6) of the UPWT.

A five-hole conical-shaped pressure probe was used to measure pressure data. Five miniature pressure transducers were located within 10 in. of the probe tip to permit rapid measurement response. A mechanical survey apparatus is used to position the five-hole probe in a user-selected, organized grid survey. The mechanical apparatus contains two electric motors to position two separate mechanical arms. The motor control system is a closed-loop microprocessor-based motor controller that executes instructions downloaded by a host computer. The host computer is an IBM desktop computer operating with the Quickbasic programming language. The host computer applies engineering units to the data, saves the data on a hard disc, downloads motion control programs to the microprocessor motion controller, and manages the user display. A Hewlett-Packard 9845 Draftmaster II plotter is used to generate the plots.



*Flow field survey apparatus mounted behind flat delta-wing model in UPWT.*

L-88-4989

*The figure shows the survey apparatus mounted downstream of a flat delta-wing model in the UPWT. (James E. Byrd, 45961)*

## Sonic Boom Tests

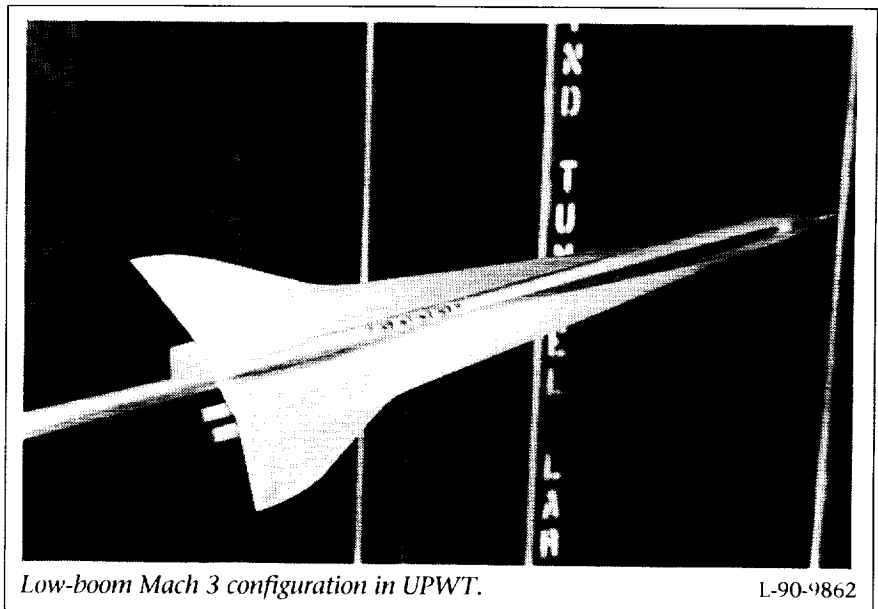
Sonic boom tests on two 12-in. cambered and twisted low-boom configurations were conducted in the UPWT. One configuration was designed to produce a flat-top ground signature at Mach 2 conditions; the second model was designed to produce a minimum shock or "ramp-type" ground signature at Mach 3 test conditions. Both models included a vertical fin and four axisymmetric flow-through nacelles. Tests were conducted at Mach 2.5 and 2.96 at a Reynolds number per foot of  $2 \times 10^6$ . Free-stream reference pressure and local pressures were measured with conical probes of  $2^\circ$ , which were connected by tubing to a differential transducer of  $1 \text{ lb/in}^2$  located outside the tunnel. Sonic boom pressure signatures were read

at axial distances of 6 in. to 18 in. from the model in an effort to evaluate the accuracy of prediction methods at these distances. To better assess flow conditions over the models, the tests also included flow visualizations using vapor screen, oil flows, and schlieren photographs.

Objectives of previous sonic boom tests in the UPWT had been

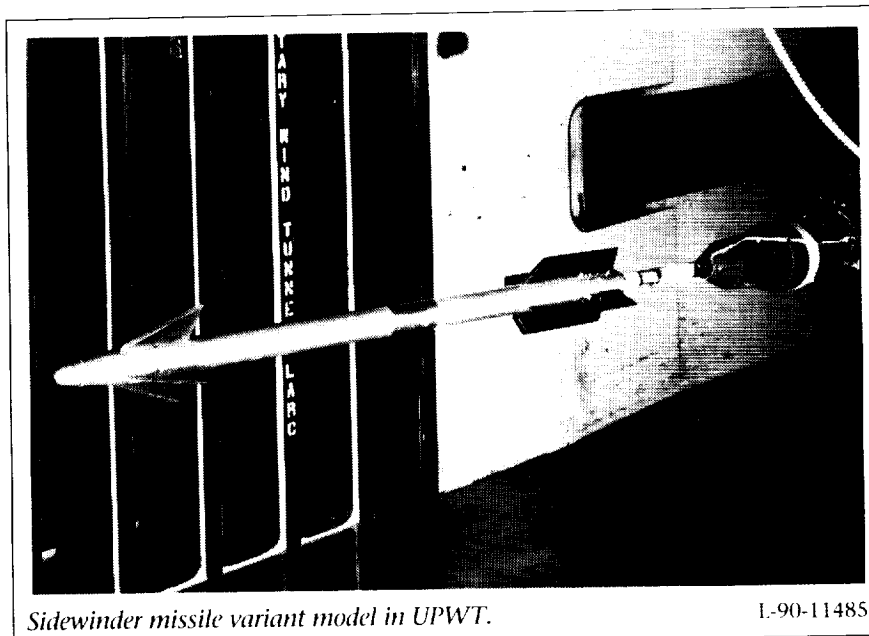
to validate sonic boom mid- and far-field theories. To accomplish those objectives, measurements had to be taken at axial distances of up to 30 body lengths away and thus restricted model size to 1 in. or 2 in. in length in this 4-ft by 4-ft test section. For those models that included nacelles, only solid needle representatives of nacelles were employed. The current tests included the largest sonic boom models ever tested in the UPWT and the first attempt to include flow-through nacelles. Initial test results indicated that flow had not been established in these small  $1/4$ -in.-diameter nacelles and that a standing shock in front of the nacelles prevented any meaningful nacelle-integration pressure data from being obtained.

Pressure results for the configurations without nacelles did, however, verify the low-boom shaping technique for the current twisted and cambered models. (R. Mack, 45988, C. Darden, K. Needleman, and D. Baize)



*Low-boom Mach 3 configuration in UPWT.*

L-90-9862



*Sidewinder missile variant model in UPWT.*

L-90-11485

### **Supersonic Aerodynamic Characteristics of Sidewinder Missile Variant Configurations**

Previous tail-span optimization studies at supersonic speeds on a modified Sidewinder missile-type airframe indicate that this configuration may be a viable design for use with advanced fighter aircraft. Performance improvements associated with the modified configurations included lower stability levels accompanied by higher trim angles of attack and reductions in zero-lift drag.

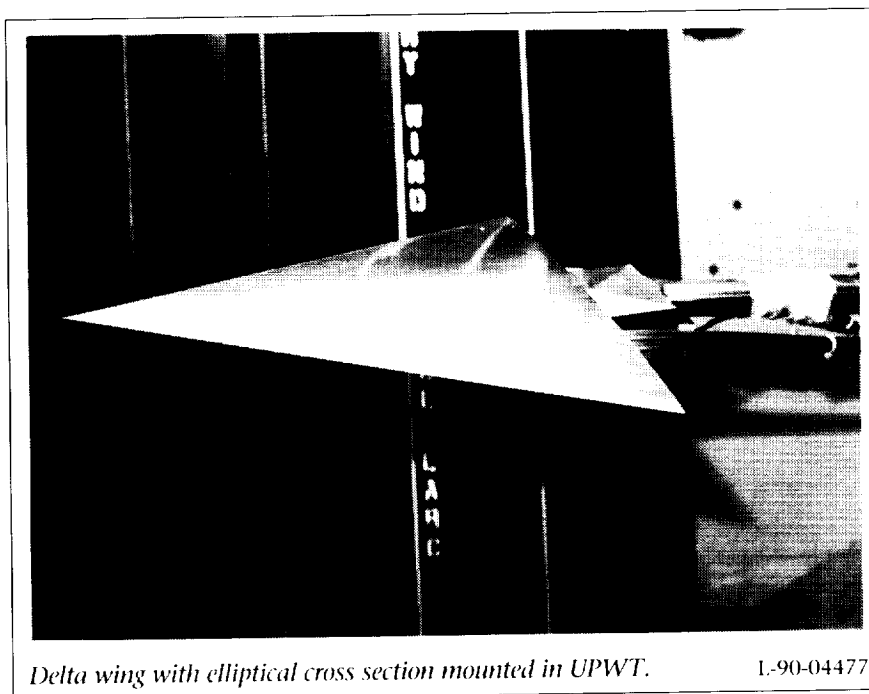
A cooperative research effort between Langley Research Center and the Naval Weapons Center, China Lake, California, was established to further investigate variations of the Sidewinder missile-type airframe. As part of this cooperative effort, models of selected U.S. Navy-designed canard-controlled missile configurations were fabricated with reduced tail-span geometries and tested in the

UPWT to determine the longitudinal and lateral-directional aerodynamic characteristics. The test Mach numbers ranged from 1.75 to 2.86 at a Reynolds number of  $2.0 \times 10^6$  per foot. Angles of attack ranged from  $-4^\circ$  to  $28^\circ$  at model roll angles from  $0^\circ$  to  $180^\circ$ .

Preliminary test results indicate that the reduced tail-span configurations exhibit favorable supersonic aerodynamic characteristics. Selected test missile configurations appear to have the potential for a single aerodynamic control system that provides canard pitch, yaw, and roll/roll-rate control.  
(A. B. Blair, 45735)

### **Incipient Leading-Edge Separation Study**

In supersonic wing design, the aerodynamicist wants control over the formation of leading-edge separation in order to optimize both separated and attached-flow conditions at the leading edge. Thus, the ability to predict and understand the effects of certain geometric parameters on the initial formation of leading-edge separation becomes important. A computational study has been conducted



*Delta wing with elliptical cross section mounted in UPWT.*

L-90-04477

to determine the effect of leading-edge radius and camber on the initial formation of leading-edge separation. The leeward side of a conical delta wing swept  $65^\circ$  was tested at Mach 1.60.

Based upon these computational results, three wind-tunnel models were designed to verify the predictions. Each model had a different cross-sectional geometry and a delta planform with a leading-edge sweep of  $65^\circ$ . The three geometries were a sharp leading edge, a rounded leading edge, and a rounded leading edge with a circular-arc camber of  $10^\circ$  imposed across the span. The models were tested in the UPWT at a Mach number of 1.60 and at Reynolds numbers of  $1 \times 10^6$ ,  $2 \times 10^6$ , and  $5 \times 10^6$  per foot. Surface pressure and flow visualization data were obtained for all three models.

Preliminary analysis of test results shows that leading-edge radius and camber are effective in delaying the onset of leading-edge separation. However, the angle of attack at which separation was observed experimentally was not well predicted.

(S. Naomi McMillin, 45581)

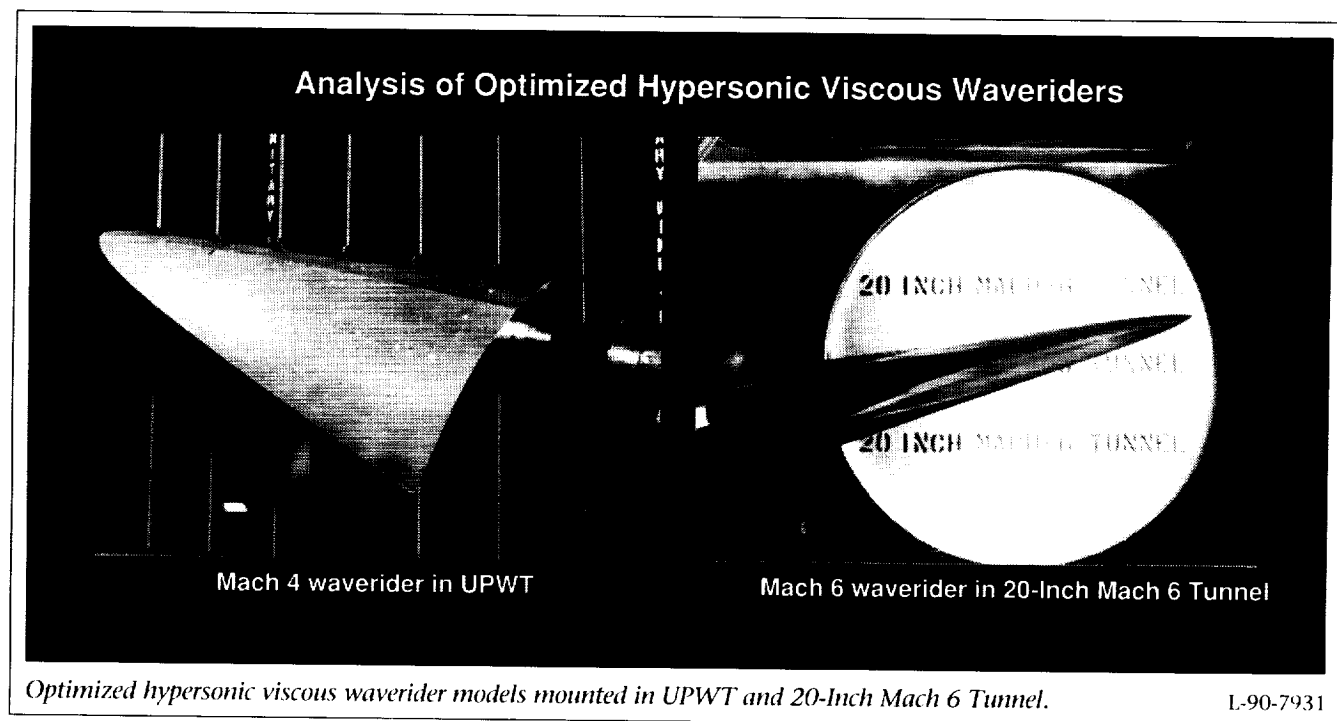
### Experimental Analysis of Optimized Waveriders

The waverider concept offers high aerodynamic performance due to the efficient containment of the high-pressure flow beneath the vehicle. However, most waverider concepts have never exhibited the expected benefits because the viscous drag effects were not accounted for in the design optimization process. A study has been conducted to analyze two waverider configurations that were

designed using a hypersonic cone-derived waverider optimization code (developed by the University of Maryland) which includes viscous drag effects for Mach numbers of 4 and 6. A reference model with the same planform and cross-sectional area distributions as the Mach 4 design but with a flat upper surface also was designed.

The Mach 4 waverider model and reference flat model were tested in the UPWT at Mach numbers of 1.5 to 4.5 and Reynolds numbers from  $1 \times 10^6$  per foot to  $4 \times 10^6$  per foot. The Mach 6 waverider model was tested in the 20-Inch Mach 6 Tunnel at Reynolds numbers of  $0.6 \times 10^6$  per foot to  $6 \times 10^6$  per foot. Force and moment, surface pressure, and flow visualization data were obtained for all three models. The photograph shows the models in each of the test facilities.

ORIGINAL PAGE  
BLACK AND WHITE PHOTOGRAPH

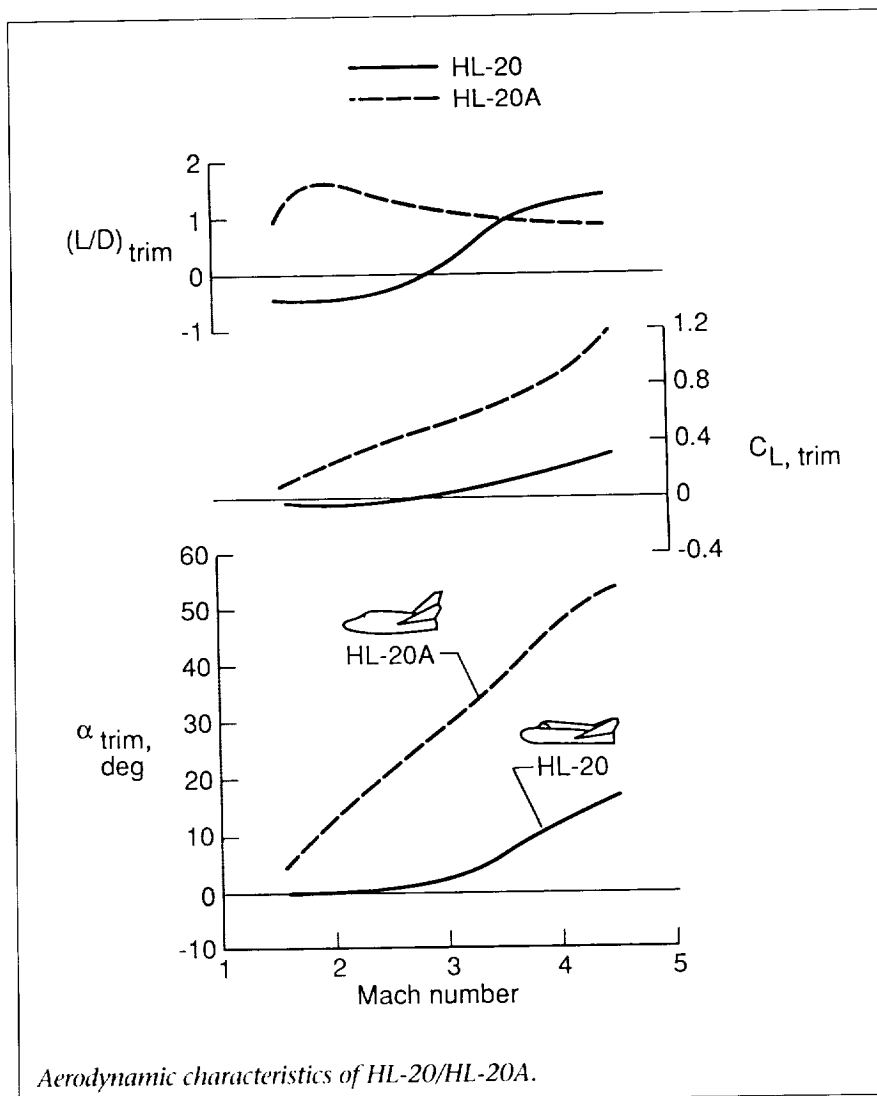


Theoretical analyses using full-potential and Euler solvers agree well with experimental data for the Mach 4 waverider at the design Mach number and angle of attack. Additional analyses will be performed to verify the performance potential of waveriders.  
(Steven X. S. Bauer, 45946)

## Supersonic Aerodynamics Characteristics of HL-20A Lifting-Body Configuration in UPWT

The HL-20 lifting-body shape has been suggested as the vehicle configuration for the NASA Assured Crew Return Capability (ACRC) and Personnel Launch System (PLS) Programs. Both programs are designed around an entry vehicle with the capability of transporting a crew of 6 to 10 members from the space station. The HL-20 is approximately 28 ft long with aerodynamic characteristics similar to those of the Space Shuttle. The vehicle has a low-aspect-ratio body with a flat undersurface and blunt base. Center and outboard fins are mounted on the upper aft body. The outboard fins are rolled outward 40° from the vertical. Control surfaces are mounted on the outboard fins and aft body.

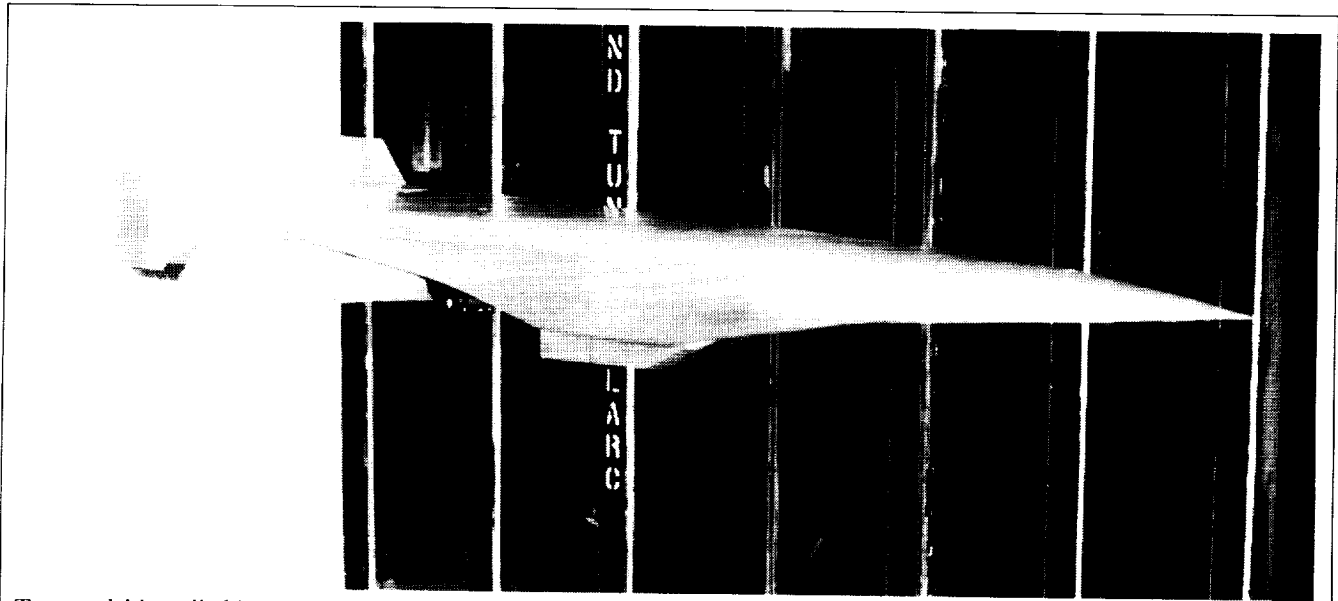
An extensive wind-tunnel test program is under way to define, in detail, the aerodynamic characteristics of the HL-20. Preliminary results of the wind-tunnel tests have shown some deficiencies. As a result, a parallel investigation has been undertaken to improve the aerodynamics through configuration modifications. The refined configuration is referred to as the



*Aerodynamic characteristics of HL-20/HL-20A.*

HL-20A. The modifications include forebody shaping to minimize drag, as well as changes in body camber, body base area, outboard fin dihedral, and fin airfoil shape. The study reported here was conducted in the UPWT at supersonic speeds. The emphasis was to improve the longitudinal trim characteristics through the Mach range from 1.5 to 3.0. In addition, it was necessary to determine if modifications made to improve performance in other speed ranges did not adversely affect supersonic characteristics. Presented in the

figure is the effect of body camber on longitudinal trim. The original HL-20 trim characteristics are presented along with those of a variation of the HL-20A featuring negative body camber. The data show that with body camber the HL-20A trims at positive angles of attack with positive values of lift and lift to drag  $L/D$ . Tests are continuing at other speed ranges to refine the HL-20A configuration.  
(Bernard Spencer, Jr., and George M. Ware, 45245)



*Test model installed in UPWT.*

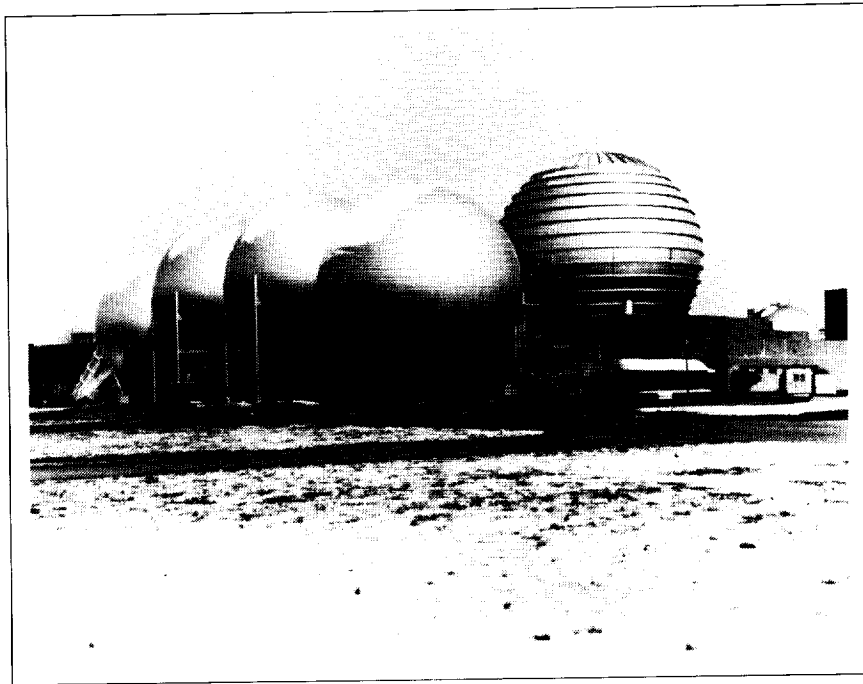
### **Supersonic Dynamic Stability Characteristics of NASP Test Technique Demonstrator Configuration**

The aerodynamic damping in pitch, yaw, and roll was obtained at supersonic speeds on the National Aero-Space Plane (NASP) Test Technique Demonstrator (TTD) configuration. These tests were conducted using the small-amplitude, forced-oscillation technique. In addition to the primary damping parameters, other stability parameters were measured. These parameters include secondary damping parameters such as the rolling moment due to yaw rate and the yawing moment due to roll rate. Other parameters include the oscillatory longitudinal-stability, oscillatory directional-stability, and rolling moment due to roll displacement.

The NASP TTD configuration was tested with and without wings, vertical tails (both inboard and

outboard), canards, nacelle, and body flap. Data were acquired for a range of supersonic Mach numbers from 1.5 to 4.5 and a range of angles of attack.

(David A. Dress, 45126, and  
Richard P. Boyden)



# Hypersonic Facilities Complex

*The Hypersonic Facilities Complex consists of several hypersonic wind tunnels located at four Langley Research Center sites. These facilities*

*are considered a complex because together they represent a major unique national resource for wind-tunnel testing. The complex currently*

*includes the Hypersonic CF<sub>4</sub> (tetrafluoromethane) tunnel (M = 6), the Mach 6 High Reynolds Number Tunnel, the 20-Inch Mach 6 Tunnel,*

## **Hypers. CF<sub>4</sub> Tunnel**

$M_{\infty} = 6$  CF<sub>4</sub>  $R_{\infty} = 0.25 - 0.55 \times 10^6$



## **M 6 High R<sub>∞</sub> Tunnel**

$M_{\infty} = 6$  AIR  $R_{\infty} = 0.8 - 42.0 \times 10^6$



## **20-Inch M 6 Tunnel**

$M_{\infty} = 6$  AIR  $R_{\infty} = 0.7 - 9.0 \times 10^6$



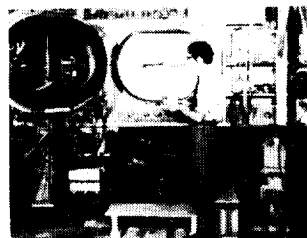
## **M 8 Var.-Dens. Tunnel**

$M_{\infty} = 8$  AIR  $R_{\infty} = 0.1 - 10.7 \times 10^6$



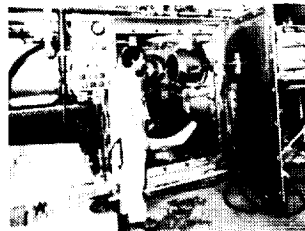
## **31-Inch M 10 Tunnel**

$M_{\infty} = 10$  AIR  $R_{\infty} = 0.4 - 2.4 \times 10^6$



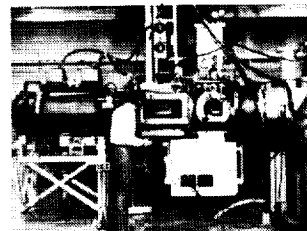
## **Hypers. Nitrogen Tunnel**

$M_{\infty} = 17$  N<sub>2</sub>  $R_{\infty} = 0.35 \times 10^6$



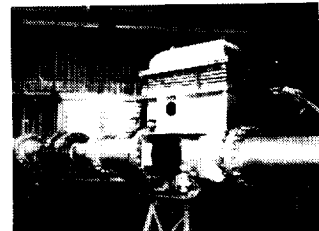
## **Mach 20 Hypers. Helium Tunnel**

$M_{\infty} = 19-21.6$  He  $R_{\infty} = 3.5 - 12.5 \times 10^6$



## **15-Inch M 6 High T<sub>0</sub> Tunnel**

$M_{\infty} = 6$  AIR  $R_{\infty} = 0.5 - 6.0 \times 10^6$

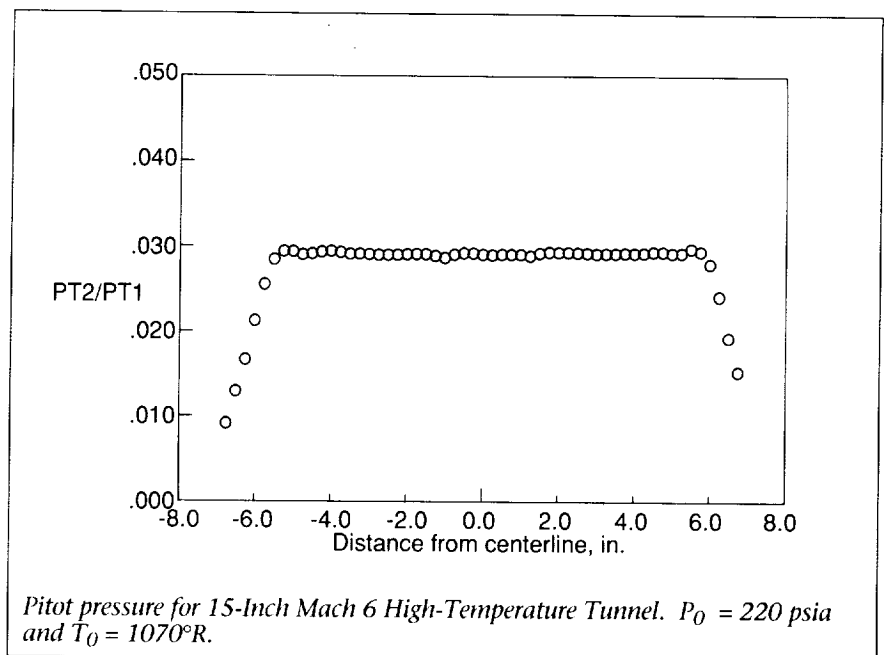


the Mach 8 Variable-Density Tunnel, the 31-Inch Mach 10 Tunnel, the Hypersonic Nitrogen Tunnel ( $M = 17$ ), the Mach 20 Hypersonic Helium Tunnel, and the 15-Inch Mach 6 High-Temperature Tunnel. These facilities are used to study the aerodynamic and aerothermodynamic phenomena associated with advanced space transportation systems, including future space transfer and Personnel Launch System vehicles; to support the development of the National Aero-Space Plane technology, lunar and Mars entry vehicles, and hypersonic missiles and transports; and to perform basic fluid mechanics studies, to establish data bases for calibration of computational fluid dynamics (CFD) codes, and to develop measurement and testing techniques. A significant amount of the current testing in these facilities is classified, thus restricting the amount and content of test results that can be reported in the open literature.

This complex of facilities provides an unparalleled capability at a single installation to study the effects of Mach number, Reynolds number, test gas, and viscous interactions on the hypersonic characteristics of aerospace vehicles. Several modifications are being made to the facilities to improve their reliability, flow quality, and capability.

### Flow Field Calibration of 15-Inch Mach 6 High-Temperature Tunnel

The 15-Inch Mach 6 High-Temperature Tunnel, formerly the Hypersonic Flow Apparatus (HFA), was originally designed for Mach 10 flow. The axisymmetric nozzle was recently modified to provide Mach 6



flow at Reynolds numbers and wall temperature ratios similar to the 31-Inch Mach 10 Tunnel. The inviscid contours for the modified nozzle were developed using an inverse method of characteristics procedure; corrections to the wall contour for viscous effects were made using a finite-difference boundary-layer code. The flow field was analyzed by a Navier-Stokes solver to verify the accuracy of the design procedure. Further, the nozzle contour was machined to a tolerance of  $\pm 0.0005$  in. in the throat region,  $\pm 0.001$  in. downstream of the inflection region, and  $\pm 0.002$  in. throughout the remainder of the nozzle. Such stringent standards help provide higher flow quality.

The tunnel is presently being calibrated; preliminary pitot surveys of the test section have revealed good flow uniformity. As shown in the figure, at a stagnation pressure  $P_0$  of 220 psia and a stagnation temperature  $T_0$  of  $1070^\circ\text{R}$ , the center 10.5 in. of the flow field has less than  $\pm 1$  percent variation in the ratio of

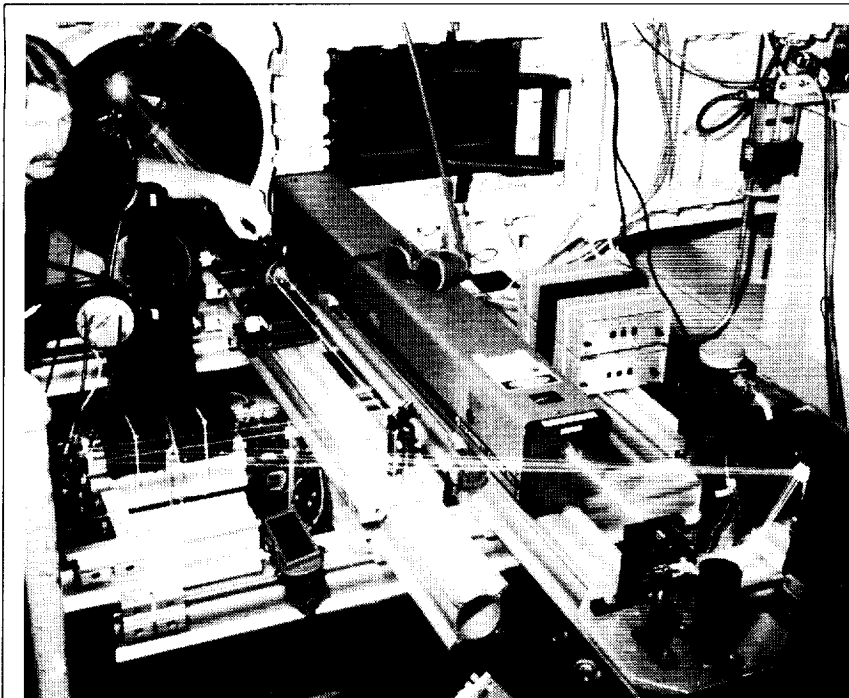
measured pitot pressure to upstream stagnation pressure. The tunnel has been run at stagnation conditions ranging from 45 psia to 350 psia total pressure and  $850^\circ\text{R}$  to  $1250^\circ\text{R}$  total temperature. Further calibrations are planned over a more extensive operating range.

(Jeffrey S. Hodge and Charles M. Hackett, 45237)

### 20-Inch Mach 6 Tunnel Laser Velocimeter Measurements

Two series of laser velocimeter tests were conducted in the 20-Inch Mach 6 Tunnel. The first test series, conducted with a laser transit anemometer (LTA), established the operational capability of a particle injection system designed for the Mach 6 facility. The injection system consisted of a solid particle fluidizing chamber and a differential pressure system. The pressure system main-



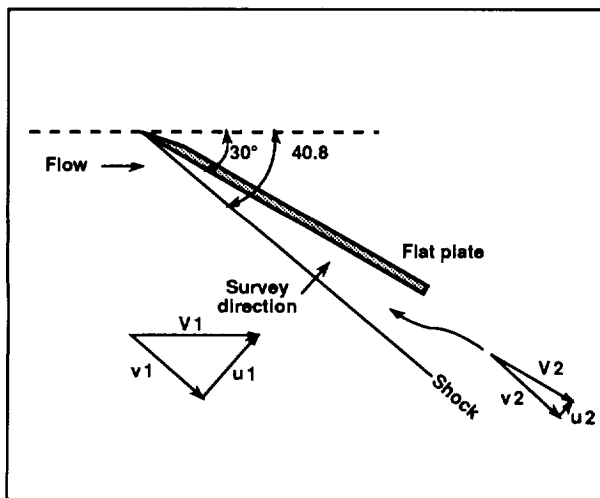


Two-dimensional LDV facility installation.

L-90-7497

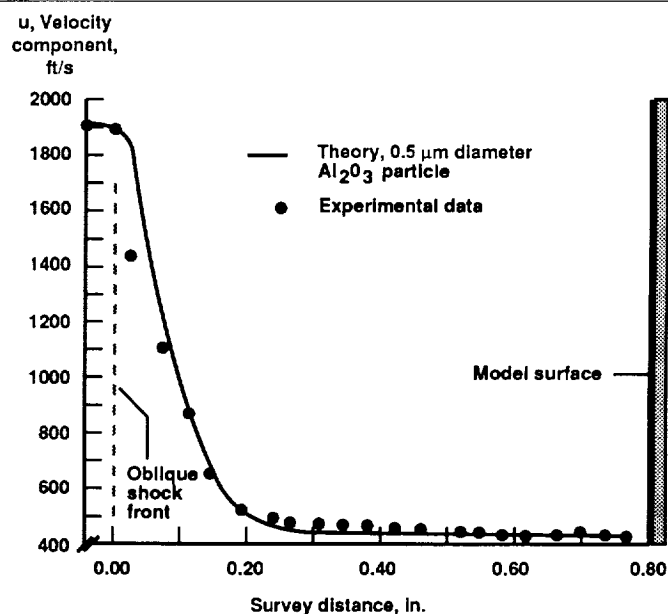
tained a small positive pressure across the fluidizing chamber, 0.5 psi to 1.0 psi above the tunnel settling chamber pressure (350 psi).

The second series of tests, conducted with a two-component laser Doppler velocimeter (LDV) system, determined the effective aerodynamic size of the particles in the tunnel test section. Velocity spatial response of the particles across an oblique shock was compared with the particle equation of motion. Alumina oxide ( $\text{Al}_2\text{O}_3$ ) particles, classified as  $0.3 \mu\text{m}$  diameter agglomerate free material, were the laser scattering media for these tests. The velocity measurements and the comparison with theory showed that the seed material responded as  $0.5 \mu\text{m}$  diameter size particles. These tests showed that Mie-scattering-based laser velocimeter



### Experimental geometry

20-Inch Mach 6/LDV system performance tests.



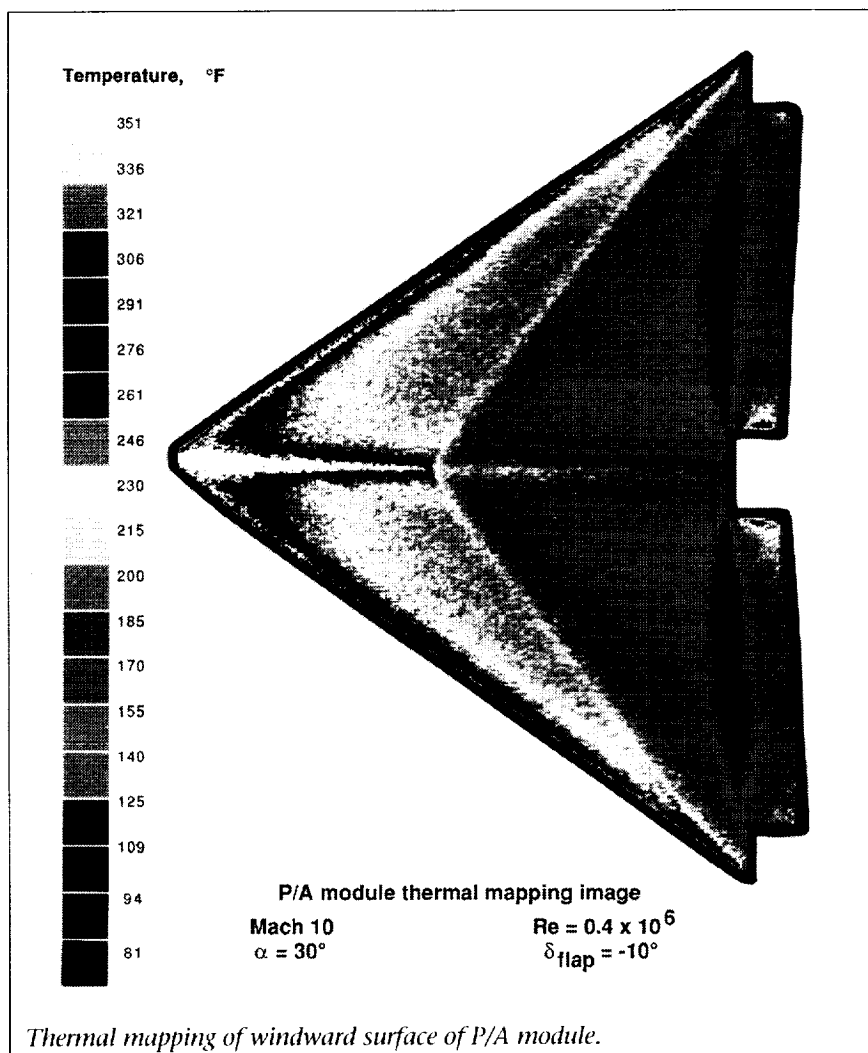
### Particle dynamic response across $40.8^\circ$ oblique shock

systems with a properly designed and operated seeding system could get useful velocity measurements in Mach 6 model flow fields. Velocity measurements upstream of the shock agree with the expected free-stream values. (William Hunter, Jr., 44594, Luther Gartrell, William Humphreys, Cecil Nichols, David Witte, and James Dillon)

### Aerothermodynamic and Aerodynamic Testing of Propulsion/Avionics Module

As part of a cooperative agreement between Martin Marietta Corporation Manned Space Systems and Langley Research Center, thermal mapping patterns were determined on a wedge-shaped propulsion/avionics (P/A) module. The wedge-shaped entry vehicle is a proposed reusable carrier for the high-cost propulsion and avionics components of a rocket booster package. Tests were performed in the 31-Inch Mach 10 Tunnel over a Reynolds number range of  $0.25 \times 10^6$  to  $1.3 \times 10^6$  and from angles of attack of  $0^\circ$  to  $35^\circ$ .

Thermal mapping images were obtained using a two-color phosphor thermography technique. In this method, ceramic models are coated with phosphor materials that radiate in the visible spectrum according to their temperatures when excited by ultraviolet light. A video camera and data acquisition system record, digitize, and store images during a tunnel run. The images are later retrieved for surface temperature analysis. Results from tests in the 31-Inch



Mach 10 Tunnel are shown in the figure as surface temperature distributions on the windward side of the model. High surface temperatures are noted on the body nose, leading edges, and windward surface chines. High temperatures reveal the reattachment regions at the trailing edges of the flaps, and the cooler zones at the base of the flaps indicate flow separation.

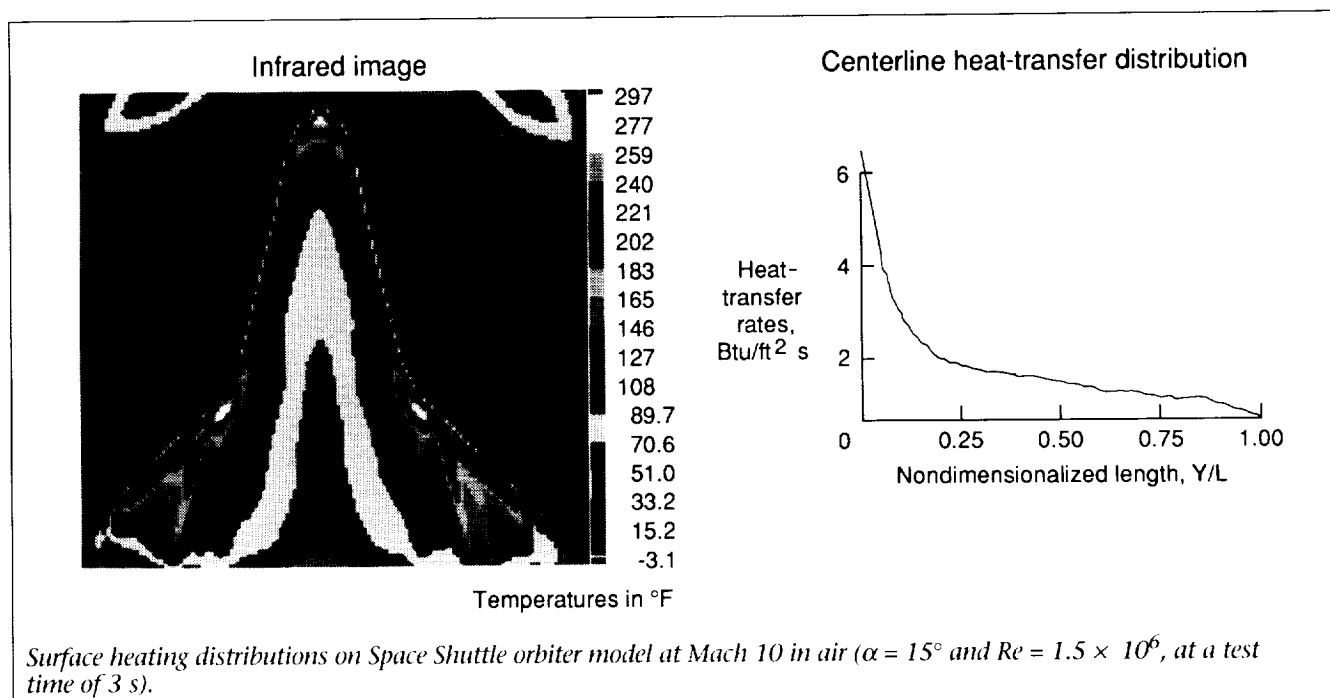
Further aerodynamic tests to obtain force and moment data are planned for the Hypersonic Facilities Complex. Extensive testing across the hypersonic speed

range will establish aerothermodynamic data and complement the aerodynamic data already available for the P/A module.

(Charles M. Hackett, 47661)

### Evaluation of Infrared Thermography for Hypersonic Heat-Transfer Measurements

Infrared thermography (IRT) techniques were evaluated for providing nonintrusive global heat-transfer rate measurements on



wind-tunnel models in hypersonic flow. Because of recent advances in infrared technology and image processing, a program was initiated to compare IRT with other techniques for providing surface temperature/heat-transfer measurements on various aerodynamic geometries at hypersonic speeds. A commercial infrared imaging system with an 8- $\mu$ m to 12- $\mu$ m wavelength bandpass and a video rate of 6.25 frames per second was utilized. A PC-based image processing system capable of real-time digitization, processing, and display of data was used. A zinc selenide window, optimized for 98 percent transmission of the 8- $\mu$ m to 12- $\mu$ m range, was utilized for optical access to the wind-tunnel test section. The spectral emittance of wind-tunnel model material was measured using spectrophotometric techniques.

A series of tests were conducted on a Space Shuttle orbiter model in

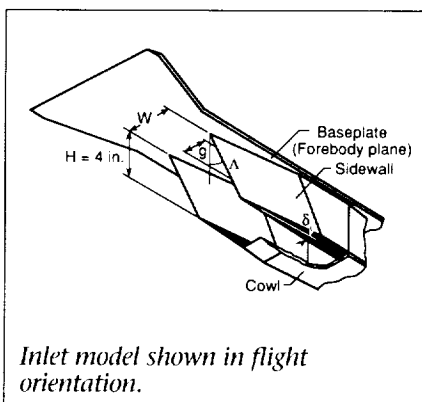
the 31-Inch Mach 10 Tunnel for model angles of attack  $\alpha$  of  $0^\circ$ ,  $15^\circ$ , and  $30^\circ$  and Reynolds numbers  $Re$  of  $0.2 \times 10^6$  and  $1.5 \times 10^6$  based on model length. The infrared images provided real-time qualitative heating patterns such as effects of shock/shock interaction on the model. The time variation of measured surface temperature distributions was used for calculating heat-transfer rates based on the one-dimensional semi-infinite heat-transfer principle.

This IRT thermographic measurement capability has been developed and applied in three hypersonic wind tunnels, the 31-Inch Mach 10 Tunnel, the 20-Inch Mach 6 Tunnel, and the Mach 20 Hypersonic Helium Tunnel. Initial test results demonstrate a capability for providing nonintrusive heat-transfer measurements in hypersonic facilities using IRT. (Kamran Daryabeigi, 44745, and Gregory M. Buck)

## Wind-Tunnel Blockage Tests of Scramjet Inlet at Mach 10

Careful design of primary engine components such as the inlet is necessary to exploit effectively the potential of propulsion-airframe integration for hypersonic air-breathing vehicles such as the National Aero-Space Plane (X-30). Based on the results of a computational parametric study, a model of a generic three-dimensional sidewall compression scramjet inlet has been designed for testing in the 31-Inch Mach 10 Tunnel at Langley Research Center. In order to increase the instrumentation density in interaction regions for a highly instrumented model, making the model as large as possible is desirable. When the cross-sectional area of the model becomes large relative to the inviscid core size of the tunnel, the effects of blockage must be consid-

ered. In order to assess these effects, a blockage model (an inexpensive, much less densely instrumented version of the configuration) was fabricated for preliminary testing. Because it was desirable to determine the effect of the model on the performance of the wind tunnel and also to determine the ability of the inlet to start, the model was instrumented with 32 static pressure orifices distributed on the forebody plane and sidewalls; 17 static pressure orifices on the tunnel wall and three pitot probes on the model were used to monitor the tunnel performance. The wind-tunnel blockage aspects of the effects of contraction ratio (sidewall proximity), cowl location, Reynolds number, and angle of attack were investigated.



A complex swept shock structure was observed to develop inside the inlet. Inviscidly the swept shocks impart a downward component to the flow, which (for the cowl aft configurations) leads to high flow spillage, a quality that helps the inlet start at low Mach numbers. The primary effect of moving the cowl forward was to capture the flow that otherwise would have spilled out ahead of the cowl. Increasing the contraction

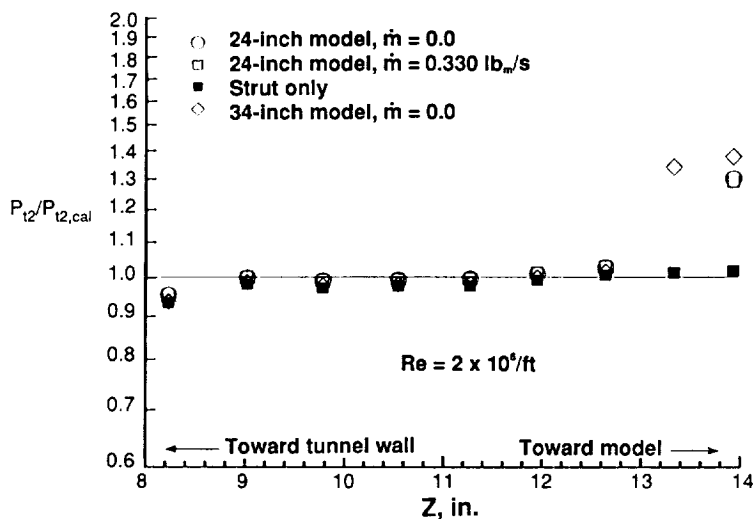
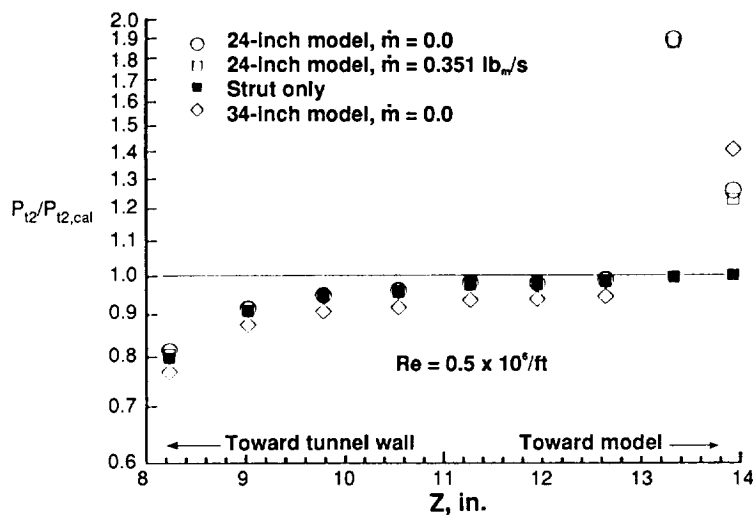
ratio (moving the sidewalls closer together) increased the number of internal shock reflections and hence incrementally increased the sidewall pressure distribution. Decreasing the Reynolds number tended to increase the overall compression of the inlet via stronger shocks and stronger shock/boundary-layer interactions. The present configuration was the largest inlet model tested in the 31-Inch Mach 10 Tunnel to date. (The maximum cross-sectional area of the model exceeded 30 percent of the tunnel inviscid core.) For each of the configurations tested, the tunnel remained started following model injection. Based on pitot and tunnel sidewall pressure distributions, no evidence of tunnel blockage due to the presence or orientation of the model was noted. Furthermore, the inlet appeared to start and remain started, based on the pressures measured with the static pressure orifices distributed on the baseplate and sidewalls. Since the completion of these tests, a highly instrumented version (256 channels of pressure data) of the configuration has been designed and fabricated to better resolve the internal shock/boundary-layer interactions and their effects on the global performance of the inlet. A concurrent computational fluid dynamics effort is also under way to provide a more detailed accounting of the internal flow physics and a comparison with experimentally obtained surface static pressures and entrance and exit plane pitot profiles.

(Scott D. Holland and Charles G. Miller, 45221)

## Tests of Large Slender Bodies in 31-Inch Mach 10 Tunnel

Two large models of a hypersonic cruise configuration have been tested in the 31-Inch Mach 10 Tunnel in air at an angle of attack of  $0^\circ$ . The goal was to evaluate the potential for wind-tunnel blockage with large slender-body models with and without simulated scramjet propulsion. The models were 24 in. and 34 in. in length, and they were tested over a Reynolds number range of  $0.25 \times 10^6/\text{ft}$  to  $2.0 \times 10^6/\text{ft}$ . The 24-in. model, which was made from aluminum, had the capability of simulating scramjet propulsion by ejecting a cold gas at rates up to  $0.5 \text{ lb}_m/\text{s}$ , and the large model was an uninstrumented wood version without simulated propulsion capability. At low Reynolds number, the tunnel area blockage ratios (model and strut area to inviscid test core area) were 42 percent for the 24-in. model and 55 percent for the 34-in. model. At high Reynolds numbers, the corresponding blockage ratios were 21 percent and 28 percent.

Previous studies in this tunnel have used tunnel unchoked/choked criteria to determine the presence of blockage. Blockage in the present study was assessed using total pressures measured with pitot probes mounted on the model support strut and static pressures measured on the wind-tunnel wall. The figure presents the total pressure measured with pitot probes attached to the model support strut  $P_{t2}$  divided by the total pressure from previous wind-tunnel calibrations  $P_{t2,cal}$  as a



Evaluation of wind-tunnel blockage generated by slender-body models in 31-Inch Mach 10 Tunnel.

function of distance from the tunnel floor. Data are presented for both models with and without propulsion simulation at Reynolds numbers of  $0.5 \times 10^6/ft$  and  $2.0 \times 10^6/ft$ . No significant deviations between the calibration and present results were observed for the  $2.0 \times 10^6/ft$  Reynolds number or at lesser Reynolds numbers with

the 24-in. model and maximum blowing; however, significant deviations from the calibration appeared with the 34-in. blockage and the resultant invalidation of the tunnel calibration for these conditions. Interestingly, the decrease in  $P_{12}$  is indicative of the flow expanding to a higher Mach number, which is contradictory to

the traditionally observed choking typical of wind-tunnel blockage. (Joel L. Everhart, 45253)

## Aerothermodynamic Measurement and Prediction for Modified Orbiter at Mach 6 and 10 in Air

For many years, Langley Research Center has been involved in examining new initiatives in Earth-to-orbit space transportation concepts. These concepts will fulfill a variety of anticipated mission needs. Current examples are programs such as the Assured Crew Return Vehicle (ACRV), a vehicle designed to return crew members from Space Station *Freedom*; the Personnel Launch System (PLS), a personnel carrier to low Earth orbit; and the Advanced Manned Launch System, the next U.S. manned space transportation system. All these programs will benefit from knowledge gained as a result of the comprehensive data base established for the Space Shuttle program. Therefore, it is important that computational, experimental, and flight data bases be brought together in an effort to gain an accurate knowledge of flow field phenomena associated with the current space transportation system. These data bases should include improvements to current computational fluid dynamic techniques and to ground-to-flight extrapolation techniques that would be applied to the next space transportation system.

This study augments the well-established comprehensive data



*Modified Space Shuttle orbiter configuration installed in 20-Inch Mach 6 Tunnel.*

L-89-8530

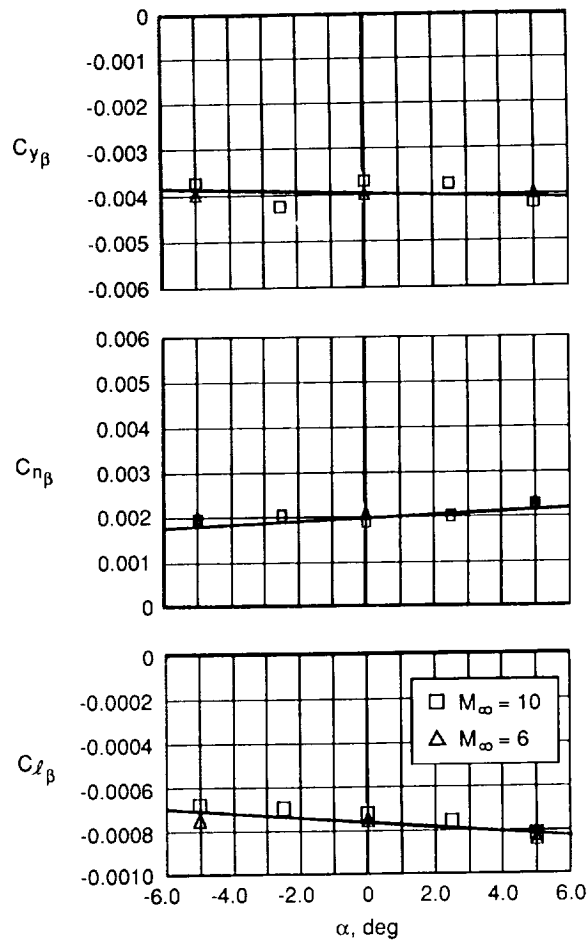
base for the Space Shuttle orbiter while providing additional information concerning the complex three-dimensional windward surface flow field of an orbiter-like configuration. Areas of interest include laminar and transitional heating phenomena and shock/shock interaction phenomena on windward surface heating distributions. For this study, detailed spanwise heat-transfer distributions are measured at Mach 6 and 10 in air over the windward surface of a winged lifting entry vehicle or "modified orbiter" configuration. Data were obtained for a range of angles of attack  $\alpha$  from  $0^\circ$  to  $40^\circ$ . The free-stream Reynolds number based on model length was varied from  $4.2 \times 10^5$  to  $6.0 \times 10^6$ , corresponding to laminar, transitional, and turbulent boundary layers at Mach 6.

Results indicate, as expected, a significant increase in measured heat-transfer rate with increasing angle of attack for both longitudinal and spanwise directions. For  $\alpha \leq 10^\circ$ , an order of magnitude increase of 2 was noted between heat-transfer rates measured at the centerline and the wing leading edge; this measured difference decreased with increasing  $\alpha$ . By increasing the free-stream Reynolds number, laminar flow over the windward surface became turbulent, and measured heating rates for the turbulent flow cases were approximately five times the laminar-flow cases. Spanwise distributions indicate that boundary-layer transition occurs in regions or pockets (that is, for a particular longitudinal station, the flow may be characterized as laminar and transitional combinations before becoming completely

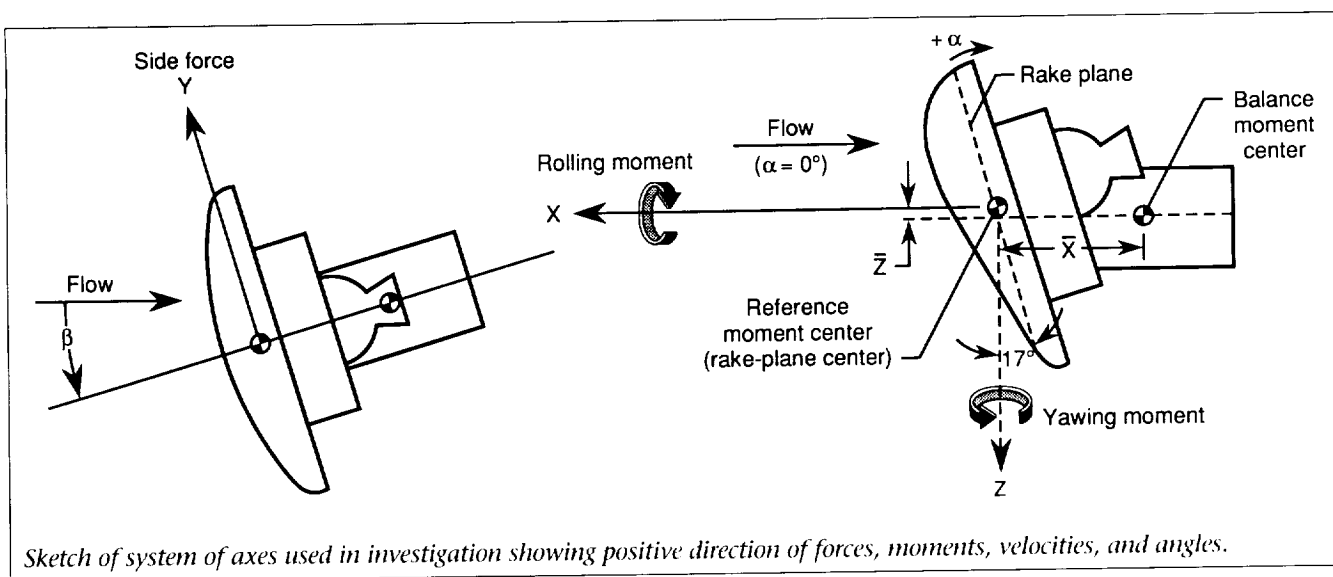
turbulent). A local enhancement in heating over the wing was observed in spanwise distributions; this heating enhancement is the result of bow shock and wing shock interaction. Preliminary heat-transfer rates predicted with the AA3DBL and LAURA codes were generally in good agreement with measurements for both longitudinal and spanwise distributions. (J. R. Micol, 45250)

## Lateral-Directional Stability Characteristics of AFE Vehicle Configuration

As part of an extensive experimental program to develop an aerodynamic and aerothermodynamic data base for the Aeroassist Flight Experiment (AFE) configuration, a test series has been conducted in hypersonic wind tunnels to determine the lateral-directional stability characteristics. These data are of particular significance for this vehicle because trajectory variations are to be accomplished through roll control.



Experimental lateral-directional stability characteristics of AFE vehicle. ( $C_{y\beta}$ ,  $C_{n\beta}$ , and  $C_{l\beta}$  are side-force, yaw, and roll lateral and directional stability parameters, respectively.)



Sketch of system of axes used in investigation showing positive direction of forces, moments, velocities, and angles.

Furthermore, relevant computational fluid dynamics computer programs have not yet matured to the point of considering the effect of sideslip.

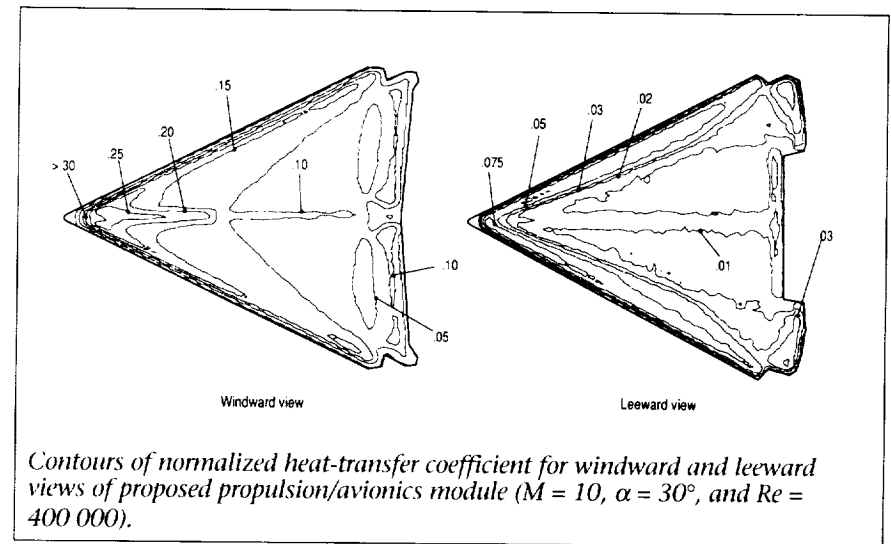
Two model sizes (a 2.2-percent scale and a 1.5-percent scale) were tested in air at Mach 6 and at Mach 10, respectively. Tests were conducted with unit free-stream Reynolds numbers of  $0.63 \times 10^6/\text{ft}$  and  $2.0 \times 10^6/\text{ft}$  at Mach 6, and  $1.0 \times 10^6/\text{ft}$  at Mach 10. The tests were conducted over ranges in angle of attack from  $-5^\circ$  to  $5^\circ$  and angle of sideslip from  $-4.5^\circ$  to  $4.5^\circ$ .

The experimental test results revealed no significant effect of the changes in Mach number, Reynolds number, or model size included in this study. For this investigation, forces and moments are based on a reference moment center located at the center of the rake plane as shown in the bottom figure. The axis system is the same as that of the original elliptic cone. As illustrated by the stability derivatives presented in the top figure, the configuration remained laterally and directionally stable over the tested range of angle of attack.

(John R. Micol and William L. Wells, 45221)

## Thermal Mapping Data Obtained With Thermographic Phosphors

Digital thermal mapping images that were experimentally obtained on a proposed atmospheric entry vehicle were analyzed, filtered, and examined using



the Image Processing Laboratory (IPL) Precision Visuals Workstation Analysis and Visualization Environment (PV-WAVE) software. Experiments were performed on ceramic models of the configuration in the 31-Inch Mach 10 Tunnel using a two-color, relative intensity, thermographic phosphor technique. The models were coated with phosphors that radiate in the visible spectrum according to their temperature when excited by ultraviolet light. The model was photographed at 15 frames per second by a three-color charged-coupled device (CCD) camera, and the resulting images were digitized and stored on computer disc.

The 512 by 512 pixel images were transferred to the IPL Sun for further visualization, analysis, and enhancement using PV-WAVE. Surface temperature maps were examined using PV-WAVE as a data visualization tool. Data reduction incorporated calculation of heat-transfer coefficients over the body using one-dimensional semi-infinite slab heat conduction theory and taking advantage of the efficient large array manipulation

capability of the software. The semiquantitative heat-transfer characteristics of the configuration were examined with line plots, two-dimensional contour plots, and color images to determine the effects of angle of attack, sideslip angle, Reynolds number, and control surface geometry. Comparisons between sequences of heat-transfer maps at different times during a wind-tunnel run enabled an estimate of the accuracy of the one-dimensional assumption to be made and compared with theoretical predictions.

As part of a cooperative agreement between Martin Marietta Manned Space Systems and Langley Research Center, thermal mapping patterns were used to investigate the hypersonic entry environment that the actual vehicle might encounter. The wind-tunnel data were compared to engineering code predictions with favorable results. The wedge-shaped entry vehicle is a proposed reusable carrier for the high-cost propulsion and avionics components of a rocket booster package. Results from tests in the 31-Inch



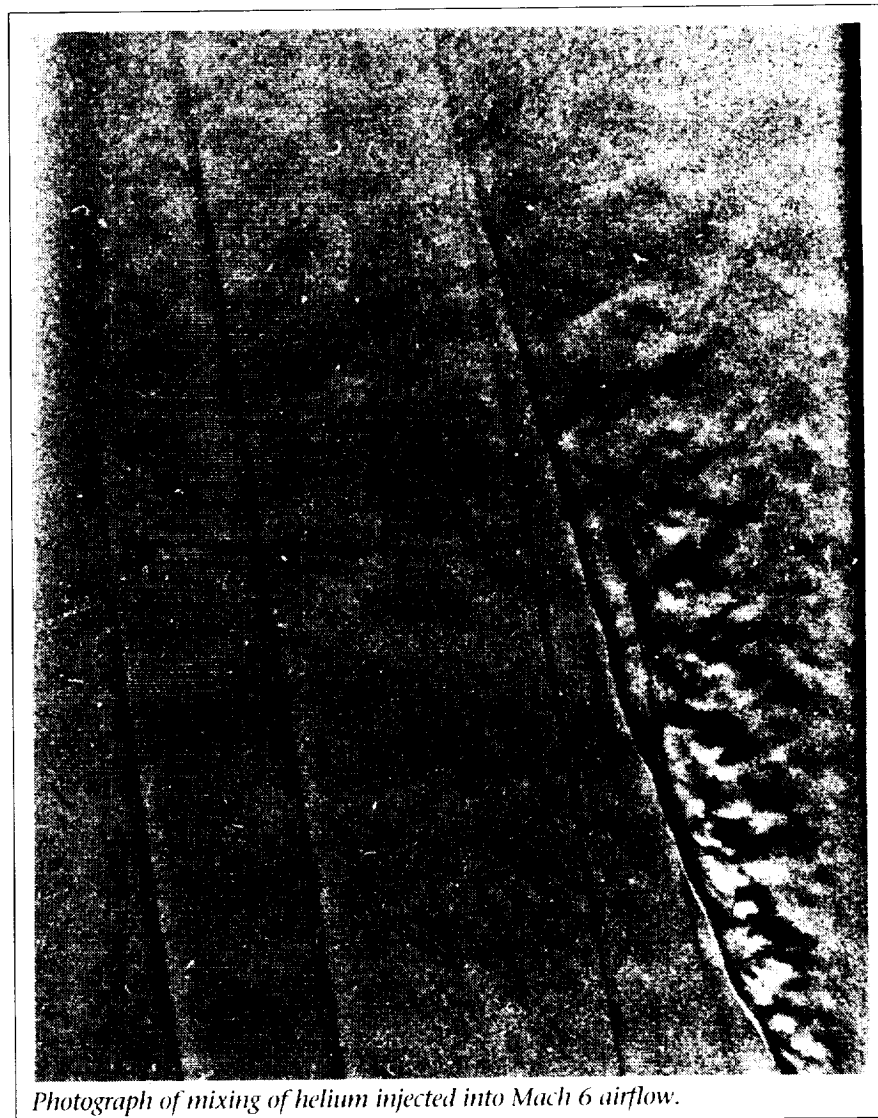
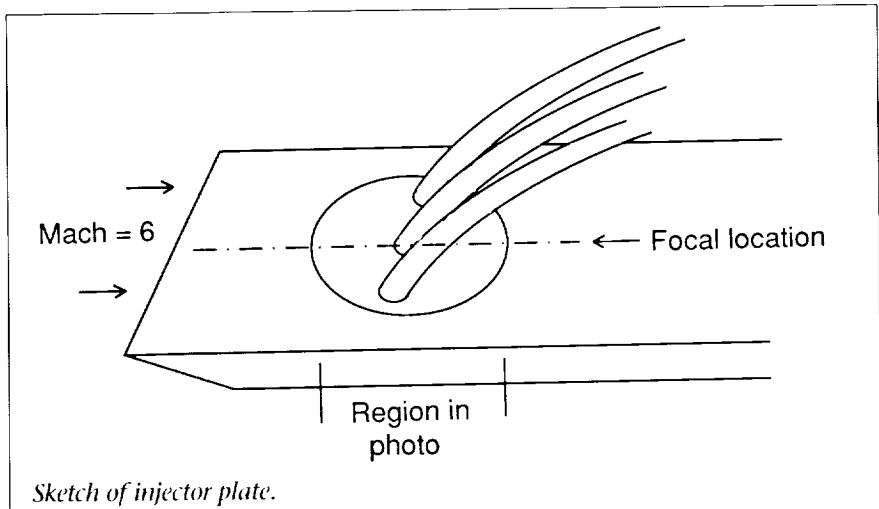
Mach 10 Tunnel are shown in the figure as distributions of surface heat-transfer coefficient normalized by the stagnation point heat-transfer coefficient on a sphere of radius equal to that of the model nose. High heat-transfer rates are noted on the body nose, leading edges, and windward surface chines. Also evident are the reattachment regions at the trailing edges of the flaps, while the cooler zones at the base of the flaps indicate flow separation. The leeward surface exhibits relatively lower heating rates, except for reattachment of a vortex along the centerline of the body and impingement of a separated shear layer on the outboard corner of the flap.

(Charles M. Hackett, 47661)

### Application of Focusing Schlieren Photograph for Flow Visualization

An improved, large-field focusing schlieren system has been developed to examine complex flow fields in high-speed flow facilities. A series of photographs of two-dimensional slices of the three-dimensional flow field allows detail to be seen in each separate longitudinal location rather than showing the entire integrated flow field in a single picture (as in conventional schlieren or shadow-graph techniques).

Focusing schlieren pictures were obtained in the Mach 6 High Reynolds Number Tunnel during a study of the mixing rate of injected helium in a high-speed air stream. This research was part of a combus-



tor study for the National Aerospace Plane Program. The injector plate, shown in the sketch in the first figure, had three injectors across the tunnel which injected helium at nearly the same velocity as the free-stream airflow. Because each jet produced a complex three-dimensional mixing region and there were three side-by-side jets, examination of the narrow slices of the flow was necessary to properly understand the details of the mixing.

The focusing schlieren photograph shows a narrow slice of the flow field in the center of the middle jet. Shock waves from the leading edge of the model and from the interaction of the jet and free stream are easily seen in the second figure. Additional shocks from joints in the model are also seen above the jet. The bow shock

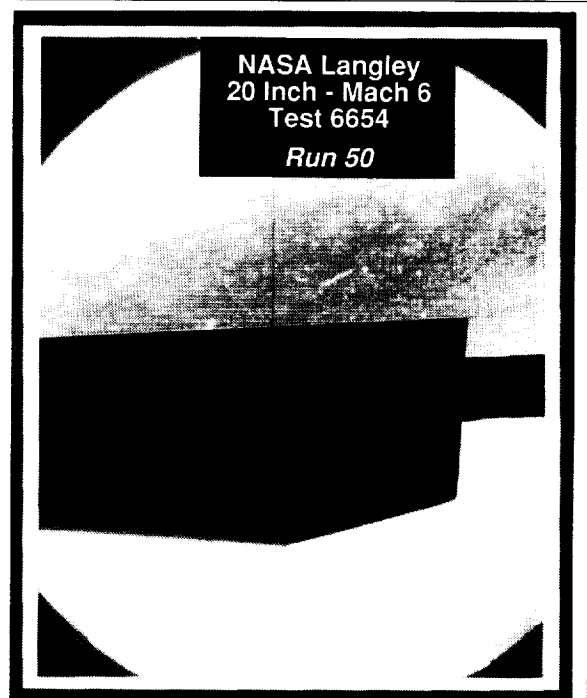
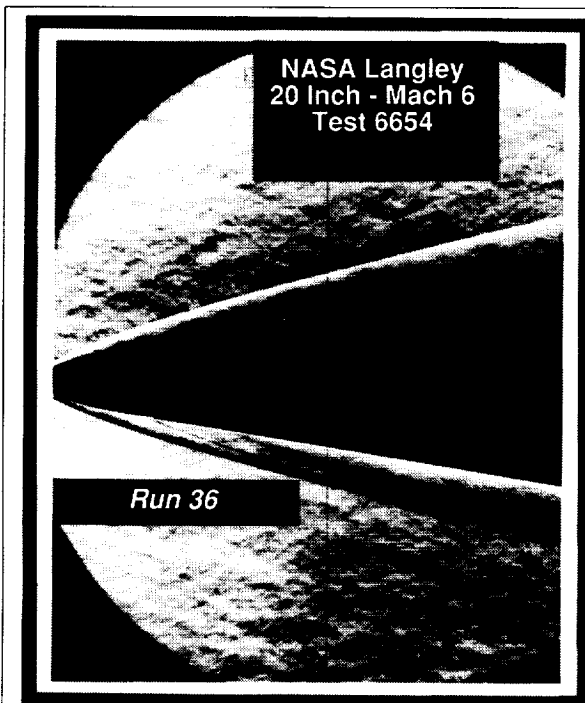
from the jet is "kinked" due to the reflection of shocks from large flow structures in the jet. These structures of unmixed flow are traveling at sufficiently less than the local stream velocity to produce local shock waves. This type of detail would not have been seen without the focusing schlieren photograph. (Leonard M. Weinstein, 45543)

### Thermal Effects on Flow-Through Balance Used in Hypersonic Scramjet Exhaust Flow Simulation Studies

A wind-tunnel test was conducted on a "powered" hypersonic, air-breathing cruise missile configuration (HAPCM-50) utilizing a flow-through electrical strain-gauge

balance designed to provide a passage for the injection of substitute noncombusting gas to simulate the scramjet exhaust. Geometric constraints prevent the use of watercooling for flow-through balances in small-scale models, and temperature sensitivity of this balance is a major concern. The test was conducted in the 20-Inch Mach 6 Tunnel on a set of configurations both with and without simulant gas injection to assess the thermal effects on a flow-through noncooled balance.

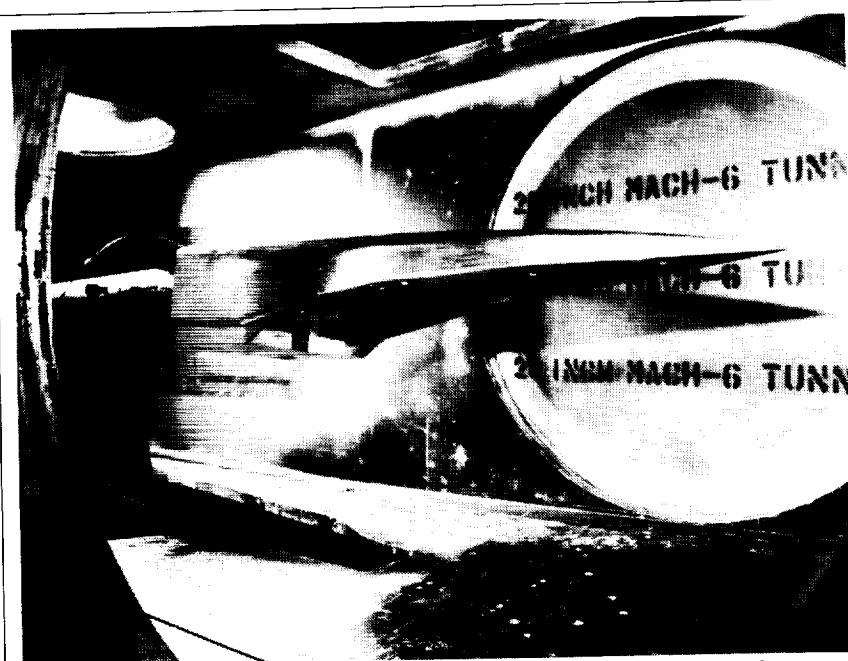
The body alone was initially used to assess aerodynamic heating effects due to the high-temperature tunnel flow environment. Subsequent tests were conducted on a configuration incorporating a body, inlet-fairing, scramjet, and nozzle with exhaust flow simulation. All force and moment



HAPCM-50 schlieren photograph under "powered" test conditions. Free-stream Mach number is 6, free-stream Reynolds number is  $4.0 \times 10^6/\text{ft}$ , angle of attack is  $0^\circ$ , plenum jet total pressure is 29 psi, and plenum jet total temperature is  $87^\circ\text{F}$ . Air exhaust jet was used.

balance components were unaffected by the balance thermal effects from the injection gases and the high-temperature tunnel flow, except the axial force that was significantly affected by balance heating. For example, in some cases, once the simulant gas was turned on, an increase in the jet total temperature was followed by temperature increases of up to 56°F at various points on the balance, and an axial force shift of almost 1 lb occurred due to the balance thermal effects.

(Lawrence D. Huebner, 45583,  
William J. Monta, and Marc W.  
Kniskern)



*Installed TTD forebody-inlet model with two-module, flow-through inlet.*

### Testing of Metric Forebody-Inlet Test Technique Demonstrator Model

The Test Technique Demonstrator (TTD) model is a generic model that is being used by researchers at Langley Research Center to develop the test techniques necessary for conducting hypersonic wind-tunnel investigations of the National Aero-Space Plane (NASP) concepts. One part of this research effort is focused on developing the techniques for obtaining the total force and moment values for hypersonic "powered" models. Testing actual burning scramjet models in small hypersonic wind tunnels is impractical, and alternate means must be developed for "powered" test investigations. One method of conducting "powered" model tests is to cover the inlet with a fairing and use a substitute gas to simulate the scramjet exhaust. This method

requires that the effects of the modified inlet be separated. The powered TTD force accounting effort was conducted in two separate wind-tunnel tests. The first test provided force and moment data on a metric forebody-inlet model; the other test provided force and moment data on a powered TTD model with metric afterbody in the presence of a simulated scramjet exhaust.

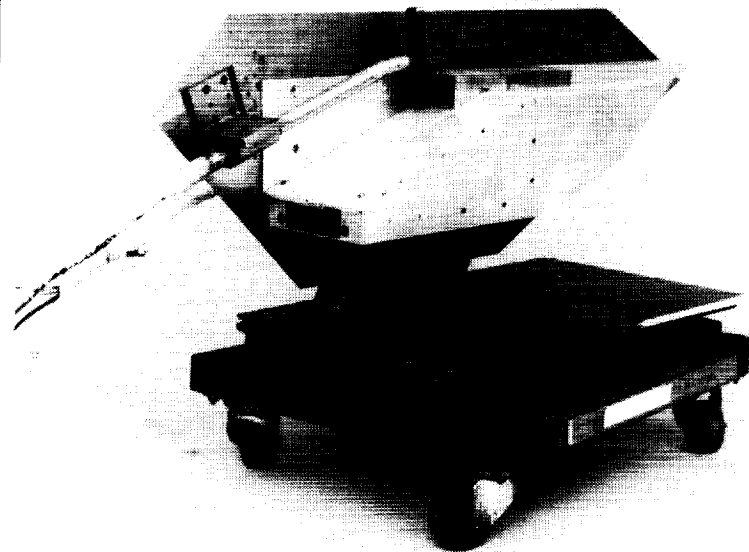
The tests were conducted in the 20-Inch Mach 6 Tunnel. Force and moment data were obtained on five component-buildup configurations of the metric model at four Reynolds numbers and two sideslip conditions. In addition, flow field total and static pressures were obtained at the inlet entrance and exit planes at two Reynolds numbers. These data will be used to estimate internal inlet drag, as well as for comparison with computational predictions.

The test, along with the powered TTD metric aftbody test, provided the necessary force and moment components to develop and verify a force accounting procedure for metric model parts of a powered NASP-like vehicle and to analyze its external aerodynamic performance.

(Lawrence D. Huebner, 45583)

### Pitot-Rake Survey of Simulated Scramjet Exhaust Flow Field of 2-D Nozzle Model

Previous studies to examine the requirements for adequate experimental wind-tunnel simulation of scramjet exhaust flows showed that several cold substitute gas mixtures are suitable and that combustor exit Mach number, ratio of specific heats, and ratio of combustor exit to free-stream-static



*Two-dimensional semispan scramjet nozzle wind-tunnel mode with flow-survey pitot rake installed.*

L-90-15018

pressures are important simulation parameters. A simulant gas mixing apparatus for the 20-Inch Mach 6 Tunnel was designed and constructed.

A recent effort in support of the NASP Program utilized the substitute-gas mixing apparatus in a test program to measure surface pressures on a two-dimensional (2-D) scramjet nozzle model. In addition, the exhaust gas flow field on the model was surveyed, with and without a flow fence, for a simulant gas mixture of 50 percent argon and 50 percent Freon-12, and for dry air.

The wind-tunnel model shown in the figure was designed to simulate the external nozzle of a hypersonic air-breathing vehicle with the scramjet exhausting onto the afterbody. A pitot-pressure rake was used to survey the exhaust flow field, and the flat, inclined ramp surface was instrumented to

measure surface pressures. Tests were made at a free-stream Mach number of 6 for two combustor exit pressure ratios. Oil-flow photographs were taken with the rake removed for each configuration. The experimental results will be employed in scramjet-exhaust code validation studies.

(William J. Monta, 45588)

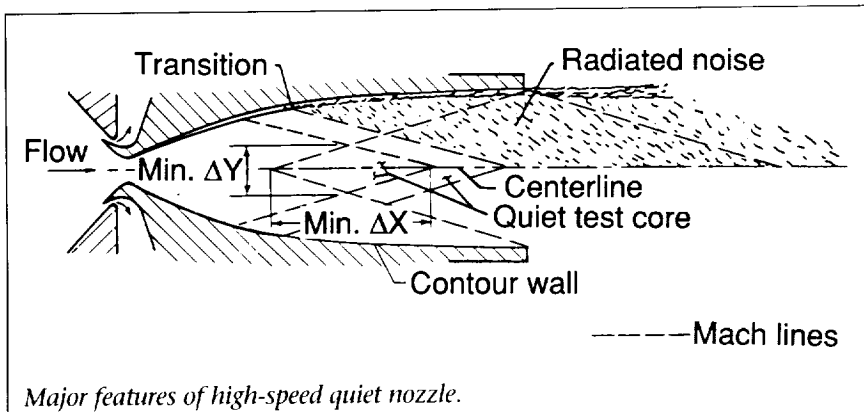
### **Advanced Mach 6 Axisymmetric Quiet Nozzle in Nozzle Test Chamber**

Wind tunnels with stream disturbance levels comparable to free-flight conditions are required to advance boundary-layer stability and transition research. The high stream disturbance levels in conventional wind tunnels cause premature boundary-layer transition on test models. Many sources

of these disturbances exist, but at higher Mach numbers ( $M > 2.5$ ), the primary source is the eddy-Mach-wave radiation from the turbulent boundary layer on the nozzle wall.

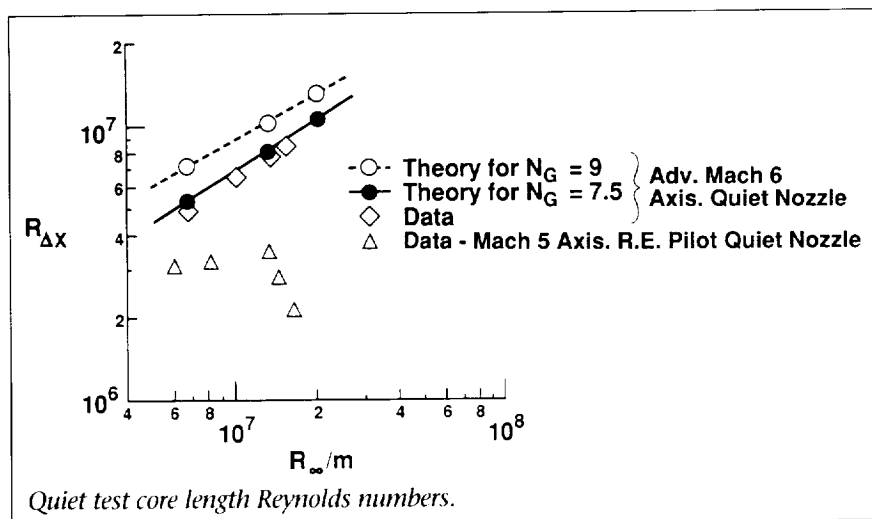
In order to develop a high-speed quiet tunnel, the instability mechanisms involved must be understood. Previous investigations indicated that transition in the wall boundary layers of nozzles for Mach numbers from 3 to 5 was caused by the Görtler instability mechanism in the concave curvature regions rather than by the Tollmien-Schlichting waves. Based on this finding, a new concept for quiet nozzle design was proposed. The new concept was to insert a straight wall, radial-flow section upstream of the inflection point of the contoured nozzle wall. The initiation of the Görtler instability was then delayed until the beginning of the concave nozzle wall, and the resulting slower expansion and larger radii of curvature reduced the growth rate of Görtler vortices. To verify this new design concept in the hypersonic speed range, the Advanced Mach 6 Axisymmetric Quiet Nozzle was built and tested in the Nozzle Test Chamber.

Preliminary experimental results indicated that the quiet test core length Reynolds numbers  $R_{AX}$ , based on the measured length of the quiet test core  $\Delta X$  (see the first figure), for this new nozzle are much higher than those for the Mach 5 Axisymmetric, Rapid Expansion (R.E.) Pilot Quiet Nozzle and also in agreement with the trend of theoretical predictions by the  $e^N$  method (see the second figure). This improved perfor-



sonic wind-tunnel models require the use of a specialized test technique because the direct approach of operating a burning scramjet engine is impractical. A non-combustion "powered" test technique was investigated using the Test Technique Demonstrator (TTD) model.

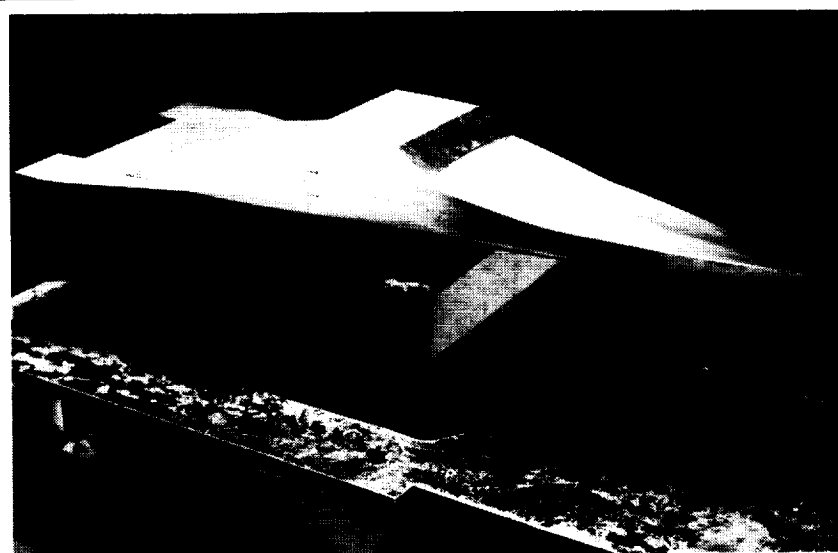
A gas mixture was used to simulate the exhaust flow exiting from a hydrogen-fueled scramjet engine. The forces and moments exerted on the model aftbody, which serves as an external scramjet nozzle, were measured using a six-component strain-gauge balance. Schlieren photographs of the exhaust plume were also obtained. The tests were conducted at Mach 6 at a free-stream Reynolds number of  $1 \times 10^6$  per foot for angles of attack of  $0^\circ$ ,  $2^\circ$ , and  $4^\circ$ . The model was configured and tested with various wing incidence angles and elevon deflection angles to examine the trim characteristics with simulated exhaust.



mance verifies that the new design concept of the advanced quiet nozzle is feasible in the hypersonic speed range. With further improvement of the nozzle finish, especially in the critical throat region, the nozzle performance can be expected to approach the design conditions in the high Reynolds number range.  
(Fang-Jenq Chen, 45732)

## Mach 6 Powered Testing of Test Technique Demonstrator

Powered aerodynamic performance tests on small-scale hyper-



Installed TTD powered metric aftbody model mounted inverted in 20-Inch Mach 6 Tunnel.

One of the primary interests of this test was to determine the effects of the strut mounting and the closed inlet on the aftbody forces/moments. Tests were conducted with the model mounted right-side-up, with and without a dummy strut attached to the forebody upper surface to assess the strut interference effect. Three different closed inlet (faired) configurations were also tested to assess their influence on the measured aftbody forces/moments. (David W. Witte, 45589)

### Shock Interaction Heating in Generic Hypersonic Engine Inlet

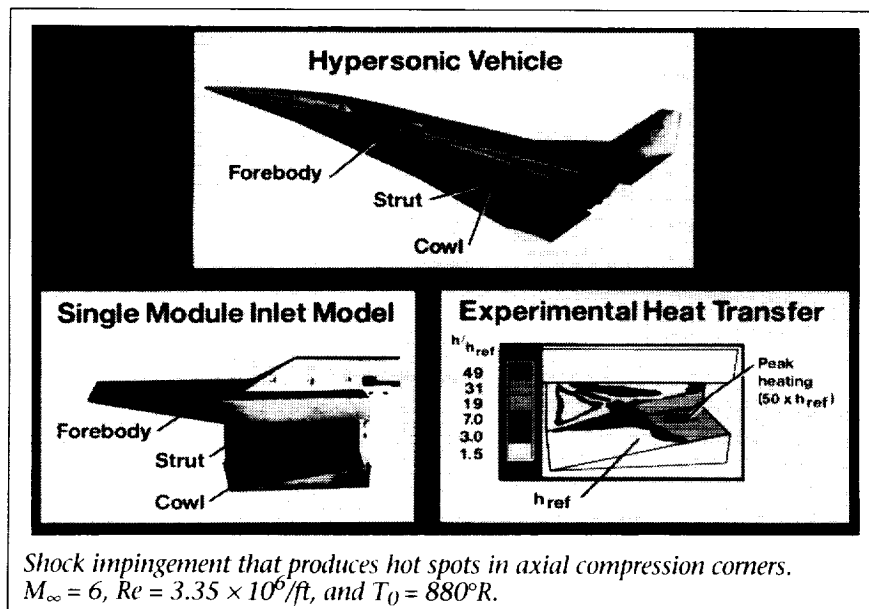
An experimental investigation was conducted in the 20-Inch Mach 6 Tunnel to determine the aerodynamic heating rate distribution in an axial-compression corner with shock impingement. Such flows would exist within the inlet of a hypersonic air-breathing

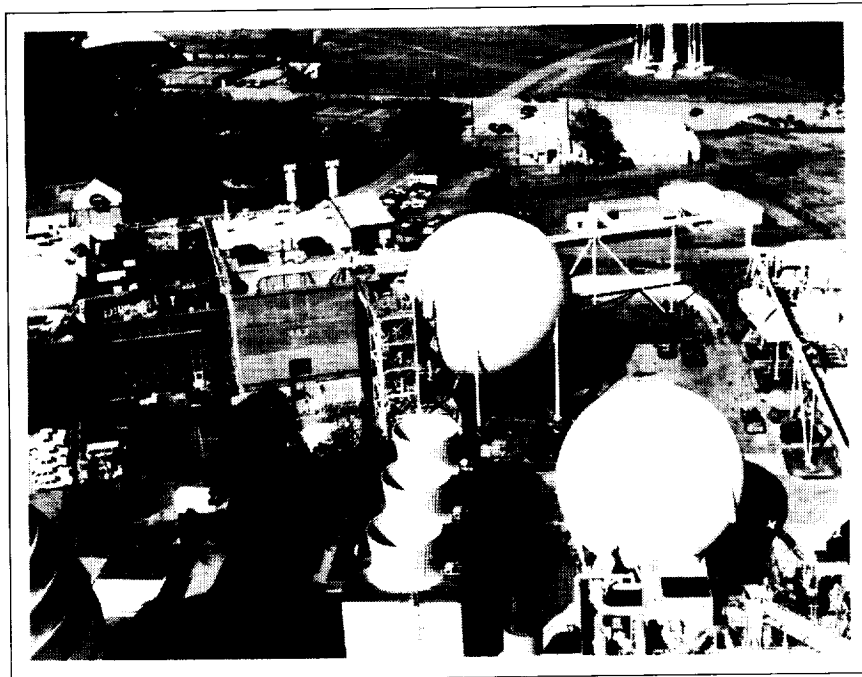
engine. At hypersonic speeds, the shock impingement will subject the cowl-strut compression corner to localized severe heat-transfer rates and large temperature gradients affecting the component. The thermal load data will be useful in the design of corner seals and thermal protection systems for the engine inlet of the National Aero-Space Plane (NASP).

The experimental model configuration (shown in the figure), which simulated a single module of a generic hypersonic engine inlet, consisted of a cowl, strut, and a forebody. The cowl and strut intersected at right angles producing the axial-compression corner, and the forebody generated the impinging shock. Tests have been performed using phase-change paint, infrared imagery, and oil-flow visualization techniques to obtain the heating pattern and associated flow structure in the compression corner region. The test free-stream unit Reynolds numbers were  $1.68 \times 10^6/\text{ft}$  and  $3.35 \times 10^6/\text{ft}$ .

The heating rate contours obtained from the phase-change paint are shown in the figure. Two patches of peak heating of approximately 50 times the undisturbed reference laminar heating level  $h_{\text{ref}}$  occurred in the compression corner region. This peak heating level is approximately 1.5 times that in the neighborhood region. The two heating peaks appear to be associated with a corner vortex system and flow reattachment downstream of the shock impingement region. More details can be found in AIAA Paper Number 91-0527.

(S. Venkateswaran, David W. Witte, and L. Roane Hunt, 41370)





## Scramjet Test Complex

---

The Scramjet Test Complex consists of four test facilities and a diagnostics laboratory that are dedicated to supersonic combustion ramjet (scramjet) engine research. The complex is a unique national resource that offers a complete spectrum of subscale scramjet test capabilities over a simulated flight Mach number range from Mach 3.4 to 8. These capabilities include inlet and combustor component studies and tests of complete, hydrogen-fueled, component-integration engine models. The current complex includes the Mach 4 Blowdown Tunnel, the Direct-Connect Supersonic Combustion Test Facility (DCSCTF), the Combustion-Heated Scramjet Test Facility (CHSTF), the Arc-Heated Scramjet Test Facility (AHSTF), and the Nonintrusive Diagnostics Laboratory (NDL). These facilities and the 8-Foot High-Temperature Tunnel (8-Foot HTT), a facility in the Aerothermal Loads

Complex which will be on-line in late 1992 as a scramjet test facility, comprise a Scramjet Test Complex unequaled in the Western World in the capability to investigate engine flow fields, scale effects, and engine/airframe integration.

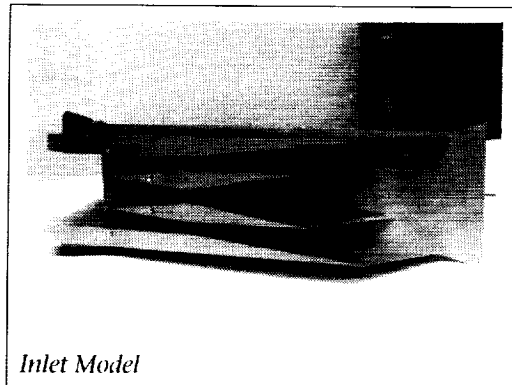
A research program to develop technology for hydrogen-fueled, airframe-integrated scramjet propulsion systems has been in progress for several years in the current Scramjet Test Complex. This effort continues in support of the National Aero-Space Plane Program and the NASA Generic Hypersonics Program.

Small-scale tests of potential scramjet inlet designs are conducted in air in the 9-in. by 9-in. Mach 4 Blowdown Tunnel to demonstrate performance near the ramjet/scramjet takeover Mach number. Larger scale inlet tests are conducted in air or

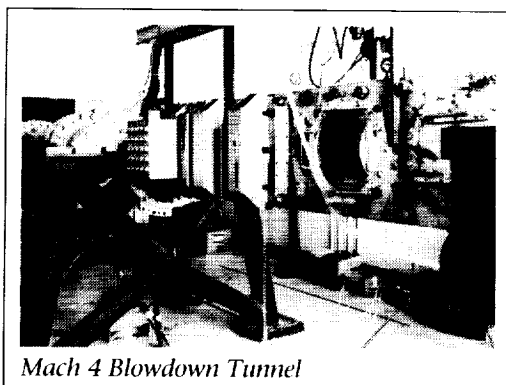
nitrogen from Mach 1.6 to 10 in various other Langley Research Center aerodynamic wind tunnels. In addition, tests in helium at Mach 18 and 22 are used to study high hypersonic inlet flow phenomena and to validate computational fluid dynamics (CFD) codes.

Small-scale combustor tests are conducted in the DCSCTF. The feature that separates this propulsion facility, the CHSTF, and the AHSTF from aerodynamic wind tunnels is their capability to produce true-velocity, true-temperature, and true-pressure flow for flight simulation. Either portions of combustors or complete combustors are tested in the DCSCTF to provide basic research data on supersonic fuel/air mixing, ignition, and combustion processes. The hot test gas is supplied to the combustor models by a hydrogen/air/oxygen combustion heater that

## Small-Scale Inlet Tests

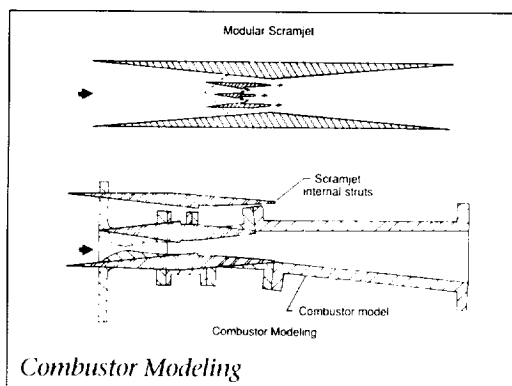


*Inlet Model*

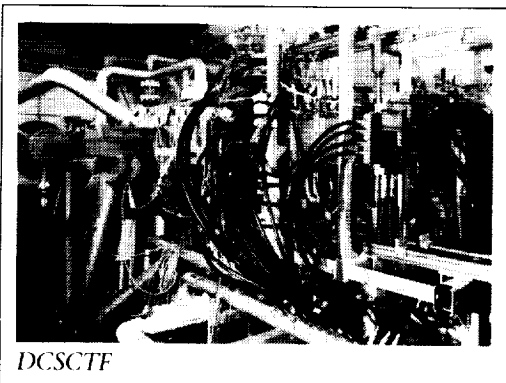


*Mach 4 Blowdown Tunnel*

## Small-Scale Combustor Tests

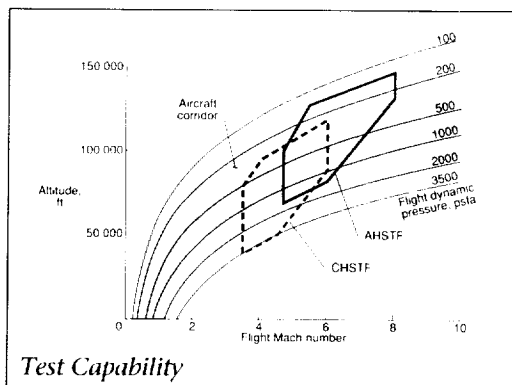


*Combustor Modeling*

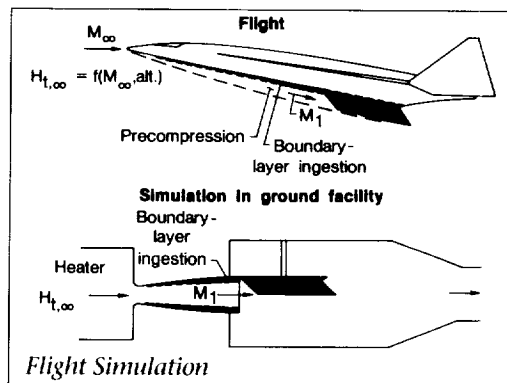


*DCSCF*

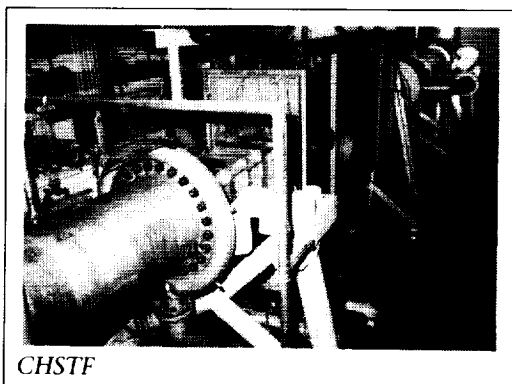
## Engine Model Tests



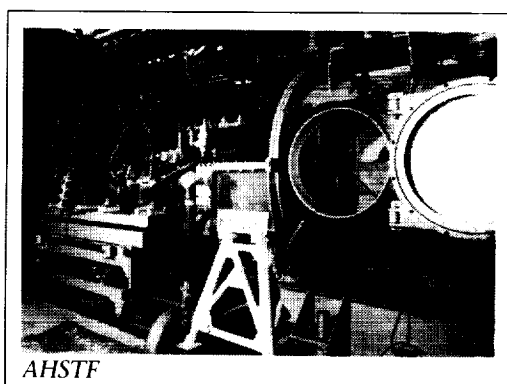
*Test Capability*



*Flight Simulation*



*CHSTF*



*AHSTF*



*maintains 21-percent free oxygen by volume to simulate air with total enthalpy levels ranging up to Mach 8 flight speeds (i.e., total temperatures up to 5000°R). Various facility nozzles produce the desired combustor entrance flow conditions.*

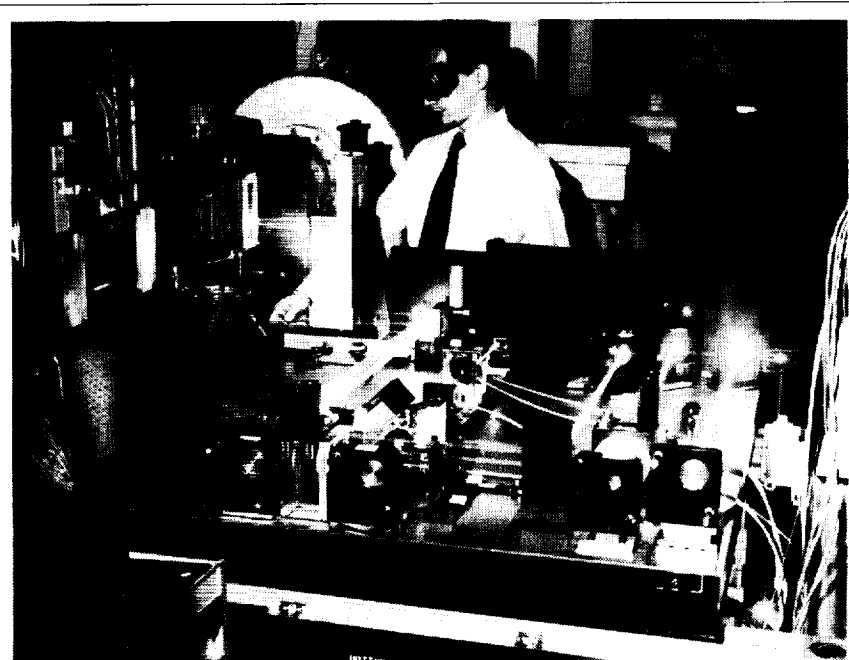
*Designs from the individual component tests are assembled to form component integration engines, and tests then are conducted to understand any interactions between the various engine components and to determine the overall engine performance. These component integration tests are conducted in the two engine test facilities, the CHSTF and the AHSTF. The CHSTF uses a hydrogen/air/oxygen combustion heater to duplicate Mach 3.4 to 6 flight total enthalpies. Mach 3.4 and 4.7 contoured nozzles with 13-in. square exits are attached to the heater to yield free-jet flows for subscale scramjet tests; these tests duplicate the flow conditions that would enter the scramjet module in flight. The test gas can either be exhausted to the atmosphere with the aid of an air ejector or to a 70-ft-diameter vacuum sphere that is evacuated using a three-stage steam ejector. The AHSTF uses an electric-arc heater to produce air total enthalpy levels corresponding to flight speeds up to Mach 8. Mach 4.7 and 6 contoured nozzles with 11-in. square exits are attached to the heater to yield free-jet flows for subscale scramjet tests. The test gas is exhausted into a 100-ft-diameter vacuum sphere that is evacuated using a three-stage steam ejector. The scramjet model size in both of these facilities is approximately 6 in. by 8 in. in frontal area by 6 ft in length.*

*An oxygen replenishment system and new Mach 4 and 5 facility nozzles (to complement an existing*

*Mach 7 nozzle) have been added to the 8-Foot HTT, which is a part of the Aerothermal Loads Complex. The test gas in the 8-Foot HTT will be heated by methane/air/oxygen combustion when the facility is used for scramjet tests. This facility, which is currently being prepared for operation, is capable of testing much larger scale models than either the CHSTF or the AHSTF. Injectable models up to 12 ft in length can include single or multiple engines (of the size tested in the subscale facilities) mounted on aircraft-type forebody/aft end structures with full scramjet nozzle expansion or large-scale single scramjets with frontal areas of approximately 20 in. by 28 in. Tests can be conducted at total enthalpy levels duplicating Mach 4, 5, and 7 flight.*

*The NDL provides space for the development of various optical diagnostic techniques for supersonic*

*reacting flow. This facility contains laboratory-scale combustion devices used for fundamental combustion studies. Devices include an electronically heated furnace and three hydrogen-air combustion devices (a subsonic diffusion burner, a supersonic diffusion burner, and a premixed flat flame burner) which provide an air temperature range from 540°R to 4000°R and a speed range from air at rest to Mach 2. This laboratory has been used to develop the hardened Coherent Antistokes Raman Spectroscopy (CARS) system, shown installed in the DCSCFT, which is now being used to nonintrusively measure combustor temperature profiles. The laboratory also has been used to demonstrate the application of ultraviolet Raman scattering to simultaneously measure temperature and O<sub>2</sub>, N<sub>2</sub>, H<sub>2</sub>, H<sub>2</sub>O, and OH mole fractions, and it is currently being used to develop laser-induced fluorescence of OH in supersonic reacting flow.*



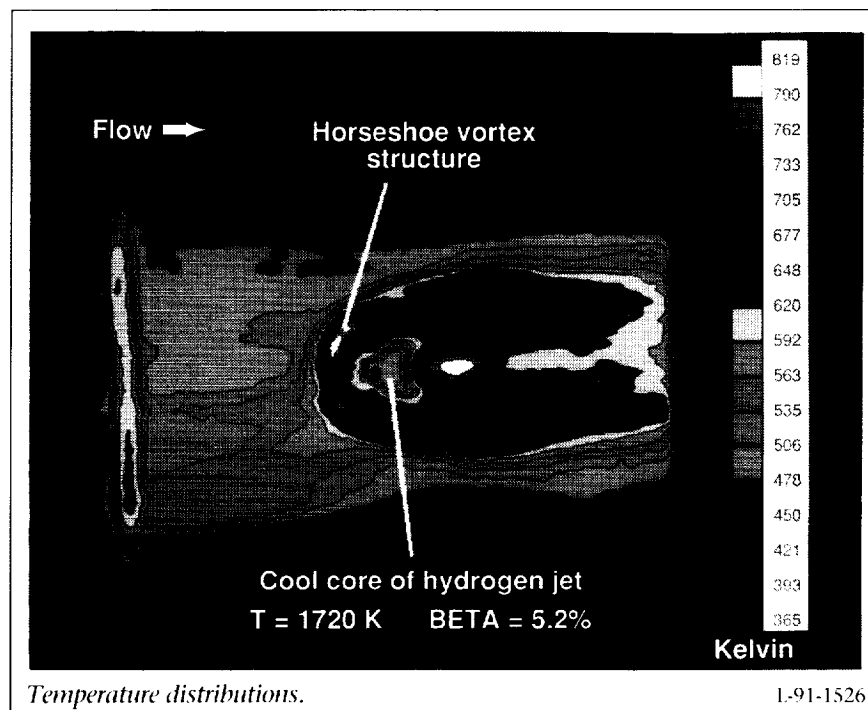
*Hardened CARS optical system developed in NDL and installed in DCSCFT.*

1-90-05774

## Transpiration Cooling in Vicinity of Fuel Injectors

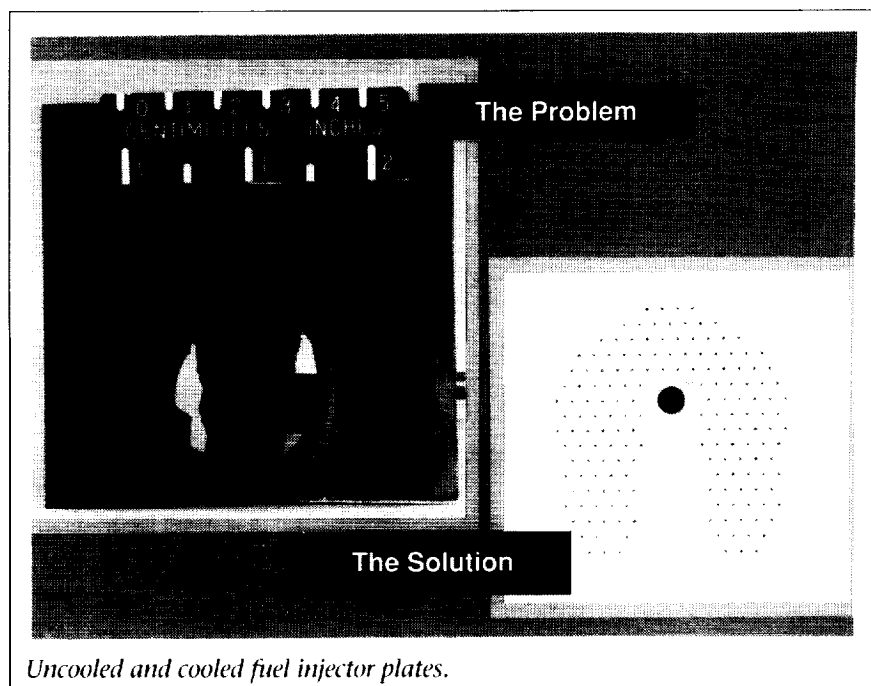
The objectives of this research were to determine the effect of film cooling on local heat transfer in the vicinity of a transverse fuel jet and to assess the effect of the cooling flow on flame holding in a scramjet combustor. The tests were conducted using the vitiated heater in the DCSCF. Based on the heating pattern (entitled "the problem" in the first figure), a series of small (0.012 in.) diameter holes were laser drilled in the high heating rate area of an injector block (entitled "the solution" in the first figure).

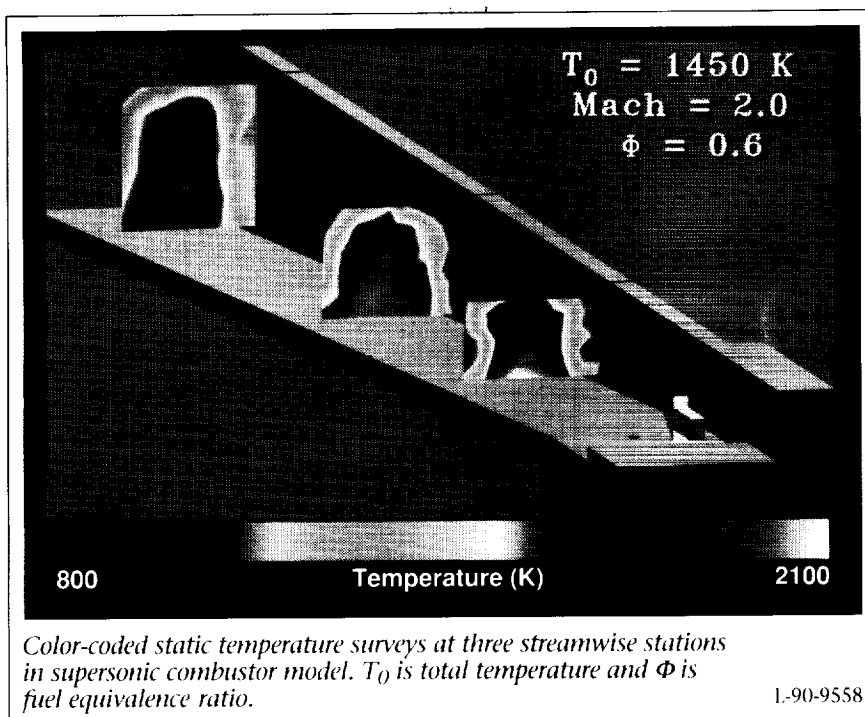
Transpiration cooling hydrogen was supplied to the holes, and a protective film was established. An infrared (IR) thermal imaging camera was used to estimate the surface temperature during simulated scramjet combustion tests with fuel injection from the 0.25-



in.-diameter fuel orifice. A typical thermal image with 5.2 percent of the fuel being used to cool the block is shown in the second figure. Based on the thermal

images, the transpiration cooling was effective in reducing the high local heating due to the shock and boundary-layer interaction and the reacting vortical flow near the wall. The calculated combustion efficiency was slightly lower with increased coolant flow, and the flame-holding characteristics for the supersonic combustor were also sensitive to the blowing rate. This work was a first attempt to document the local heating patterns and to explore the fuel cooling rates required to reduce local heat transfer associated with transverse hydrogen fuel injection. Hydrogen was used as the coolant to avoid having an additional system that would add to vehicle weight. (G. Burton Northam, 46248, Carl Byington, and Diego Capriotti)





## Static Temperature Surveys in Scramjet Combustor

Detailed measurements of the internal flow fields are required to optimize the performance of supersonic combustion ramjet (scramjet) engines. Static temperature surveys were made in a scramjet combustor model in the DCSCTF at Langley Research Center. The free-stream flow was heated by hydrogen/air combustion and accelerated to Mach 2 to simulate combustor inlet conditions for a scramjet at a flight Mach number of approximately 5. Hydrogen fuel was injected into the flow through a circular port in the wall. The port, drilled perpendicular to the wall, was six injector diameters downstream of a rearward facing step.

The CARS system was used to measure the temperature at discrete points in this reacting supersonic

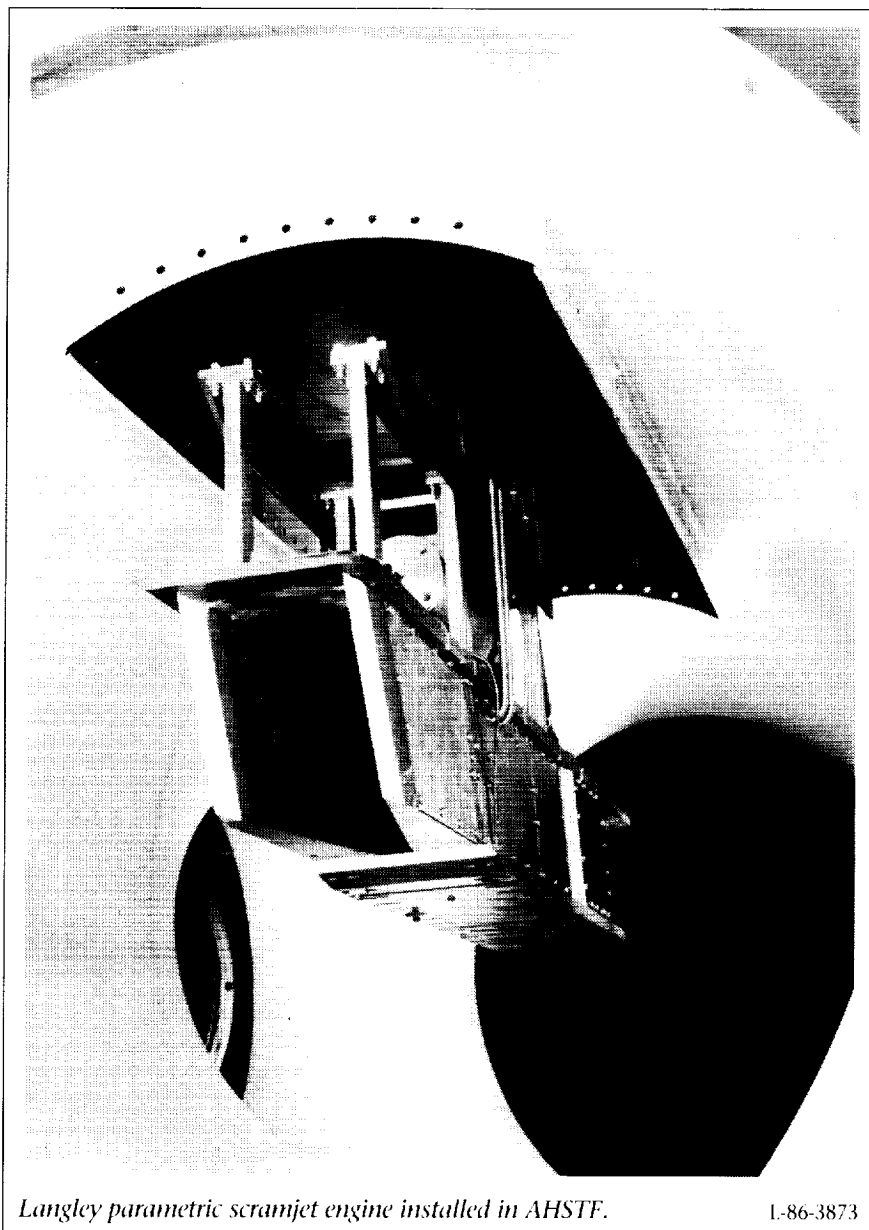
flow. This system is a laser technique that can be used to non-intrusively measure the temperature and density of major gas species. In these tests, only the temperature of the dominant species, nitrogen, was measured. Both mean temperatures and the fluctuating temperatures due to fluid turbulence were measured. Fluctuating temperatures provide insight into the supersonic mixing and combustion process. Optical access to cross-stream planes was provided at three streamwise locations: 39, 90, and 167 injector port diameters downstream of the injector. Mean static temperature cross sections at these three data stations are shown in the figure. Note that the mean static temperatures in this combustor may exceed 2000 K in some locations. (M. W. Smith, 46261, O. Jarrett, A. D. Cutler, and R. R. Antcliff)

## Subscale Scramjet Engine Tests

Research on National Aero-Space Plane (NASP) scramjet engine concepts continued in 1990 in the Langley Research Center CHSTF and AHSTF. Approximately 200 tests were conducted on Rocketdyne and Pratt & Whitney engines during the year.

In February 1990, Rocketdyne completed an 8-month engine test program in the CHSTF; this test included a simulated flight Mach number range from 3.5 to 5.5. Hydrogen-fueled engine performance was assessed in terms of fuel injector/combustor design, combustor-inlet interaction, and mode of operation. This engine was moved to the AHSTF in July 1990 for a 3-week test program to evaluate combustor design changes at Mach 7 and 8. These tests were followed by Mach 6 to 8 tests of a new Rocketdyne scramjet configuration, which was tested in the AHSTF in August 1990. Design, fabrication, and testing of this engine were accomplished in only 3 1/2 months.

In March 1990, Pratt & Whitney completed Mach 4.7 to 7 tests of their scramjet concept in the AHSTF in a test program that had spanned 11 months. Hydrogen-fueled engine performance was assessed for various engine configurations, and issues such as fuel-air mixing, flame-holding, and combustor-inlet interaction were addressed. This engine then was moved to the CHSTF in which Mach 4 inlet tests were conducted during a 1-month test program in June 1990.



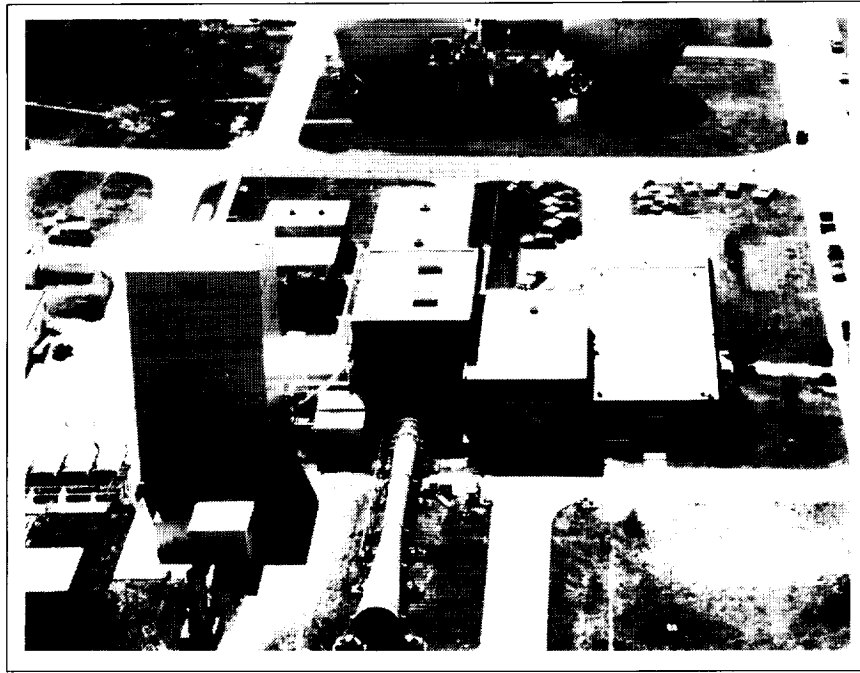
*Langley parametric scramjet engine installed in AHSTF.*

L-86-3873

operation. Additional engine tests are planned in the Langley subscale facilities under the sponsorship of the NASP Program and of the NASA Generic Hypersonics Program. (R. Wayne Guy, Earl H. Andrews, Jr., Randall T. Volland, James M. Eggers, Kenneth E. Rock, and Richard G. Irby, 46272)

The tests described here added considerably to the Nation's data base on hydrogen-fueled, airframe-integrated scramjet engines. More than 2000 scramjet-related tests have been conducted in Langley facilities since 1976. The test pace has quickened immensely during the NASP Program with approximately 1000 NASP scramjet tests occurring between mid-1988 and September 1990. This rise repre-

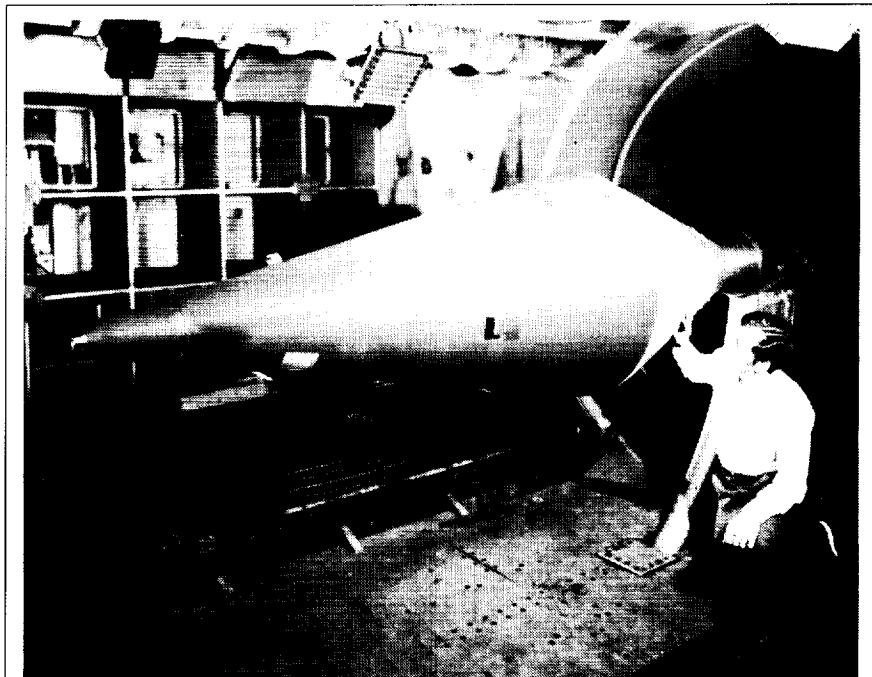
sents an increase in average tests per year from 100 between 1976 and 1988 to 500 between 1988 and 1990. The engine tests have provided a vast amount of data involving very different engine design details and operational methods. These data are currently being used by government and industry researchers to study the parametrics associated with all aspects of scramjet design and



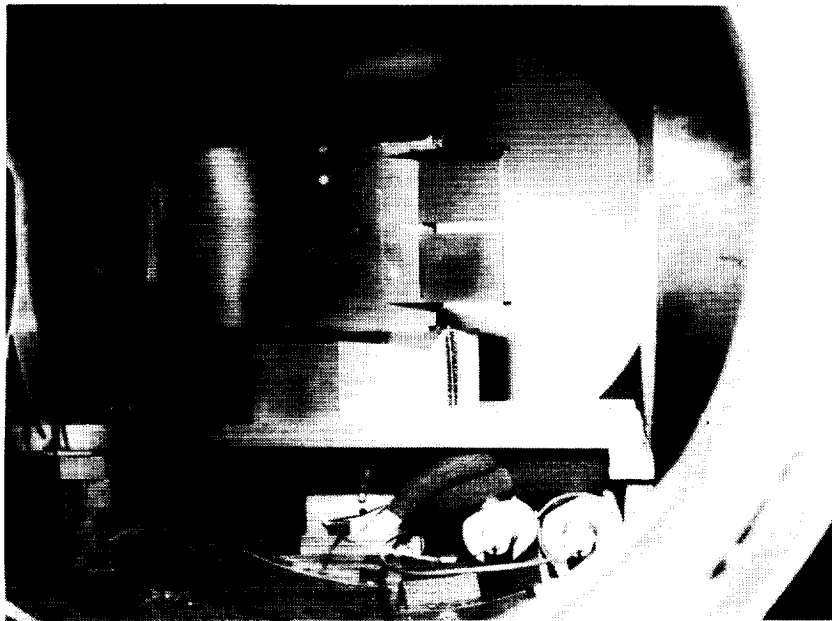
## Aerothermal Loads Complex

*The Aerothermal Loads Complex consists of four facilities that are used to carry out research in aerothermal loads and high-temperature structures and thermal protection systems.*

*The 8-Foot High-Temperature Tunnel (8-Foot HTT) is a Mach 7 blowdown-type facility in which methane is burned in air under pressure and the resulting combustion products are used as the test medium with a maximum stagnation temperature of approximately 3800°R in order to reach the required energy level for flight simulation. The nozzle is an axisymmetrical conical contoured design with an exit diameter of 8 ft. Model mounting is semispan or sting with insertion after the tunnel is started. A single-stage air ejector is used as a downstream pump to permit low-pressure (high-altitude) simulation. The Reynolds number ranges*



*8-Foot High-Temperature Tunnel,  $M = 7$ ,  $R_n = 0.3 - 2.2 \times 10^6$ , and  $H = 700 - 1000$  Btu/lb.*



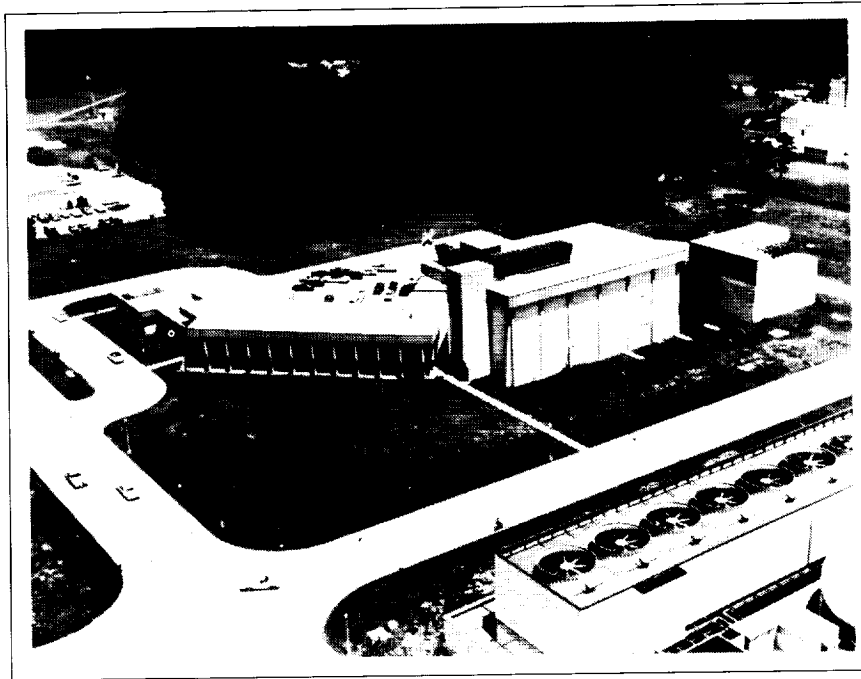
7-Inch High-Temperature Tunnel,  $M = 7$ ,  $R_n = 0.3 - 2.2 \times 10^6$ , and  $H = 700-1000$  Btu/lb.

from  $0.3$  to  $2.2 \times 10^6$ /ft with a nominal Mach number of  $7$ , and the run time ranges from  $20$  s to  $180$  s. The tunnel is used for studying detailed thermal-load flow phenomena as well as for evaluating the performance of high-speed and entry vehicle structural components. A major effort is under way to provide alternate Mach number capability as well as  $O_2$  enrichment for the test medium. This is being done primarily to allow models that have hypersonic air-breathing propulsion applications to be tested. After checkout over the next year, this facility will become a premiere tunnel in the world for testing scramjet engines.

The 7-Inch High-Temperature Tunnel (7-Inch HTT) is a 1/12-scale version of the 8-Foot HTT with basically the same capabilities as the larger tunnel. It is used primarily as an aid in the design of larger models for the 8-Foot HTT and for aerothermal loads tests on subscale

models. The 7-Inch HTT is currently being used to evaluate various new systems for the planned modifications of the 8-Foot HTT.

The 20-MW and 5-MW Aerothermal Arc Tunnels are used to test models in an environment that simulates the flight reentry envelope for high-speed vehicles such as the Space Shuttle. The amount of energy available to the test medium in these facilities is  $9$  MW and  $2$  MW, respectively. The 20-MW tunnel has a dc arc heater, and the 5-MW tunnel has a three-phase ac arc heater. Test conditions (such as temperature, flow rate, and enthalpy) vary greatly because a variety of nozzles and throats are available. Model sizes can range from  $3$  in. in diameter to  $1$ -ft by  $2$ -ft panels. These facilities are currently on standby status.



## Acoustics Research Laboratory

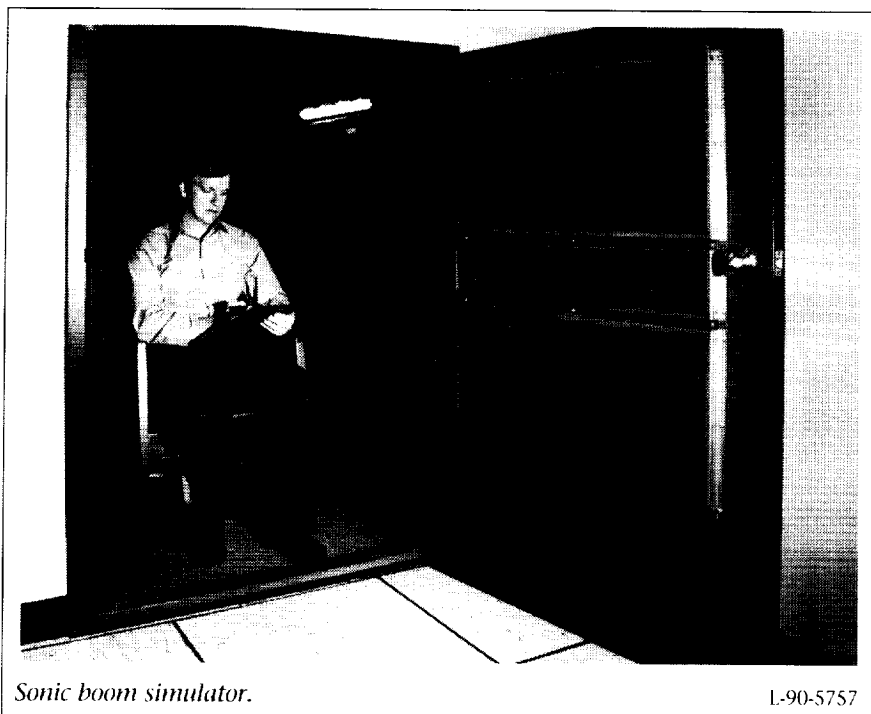
---

*The Langley Acoustics Research Laboratory (ARL) provides the principal focus for acoustics research at Langley Research Center. The ARL consists of the anechoic quiet-flow facility, the reverberation chamber, the transmission loss apparatus, and the human-response-to-noise laboratories. The anechoic quiet-flow facility has a test chamber treated with sound-absorbing wedges and is equipped with a low-turbulence, low-noise test flow to allow aeroacoustic studies of aircraft components and models. The test flow, which is provided by either horizontal high-pressure or vertical low-pressure air systems, varies in Mach number up to 0.5. The reverberation chamber, which is used to diffuse the sound generated by a noise source, provides a means to measure the total acoustic power spectrum of the source. The transmission loss apparatus has a source and a receiving room, which are joined by a connect-*

*ing wall. A test specimen such as an aircraft fuselage panel is mounted in the connecting wall for sound transmission loss studies. The human-response laboratories consist of the exterior effects room, anechoic listening room, Space Station Freedom/aircraft acoustic simulator, and sonic boom simulator.*

*Four laboratory companions of the ARL are the Anechoic Noise Facility, the Jet Noise Laboratory, the Thermal Acoustic Fatigue Apparatus (TAFA), and the Flow Impedance Facility. The Anechoic Noise Facility is equipped with a very-high-pressure air supply used primarily for simulating nozzle exhaust flow. The Jet Noise Laboratory has two coaxial supersonic jets for studying turbulence evolution in the two interacting shear flows that are typical of high-speed aircraft engines. Hot supersonic jets with temperatures corresponding to*

*those associated with afterburners can also be simulated in the Jet Noise Laboratory. The TAFA provides the capability to subject flat structural panels to high-level acoustic pressures and high-temperature radiant heating to 2000°F. The Flow Impedance Facility provides the means to measure acoustic impedance of liner materials in a grazing flow/grazing impedance configuration up to a flow speed of Mach number 0.7.*



Sonic boom simulator.

L-90-5757

### **Simulation of Sonic Booms**

A new man-rated sonic boom simulator has been brought to full operational readiness and is being used to study human subjective reactions to simulated sonic booms under controlled conditions. The simulator consists of a computer-controlled, loudspeaker-driven airtight booth that can produce user-specified sonic boom signatures with a high degree of accuracy. An exterior view of the simulator showing the door-mounted loudspeaker array is shown in the figure.

The simulator is currently being used to conduct experiments, using volunteer test subjects, to determine subjective loudness and acceptability characteristics of a wide range of potential boom signatures that have been shaped, by careful design of the aircraft, to minimize the loudness of the boom on the ground. The objective

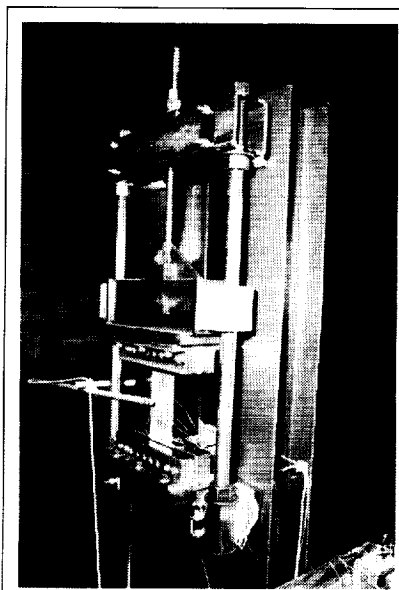
of these tests is to define sonic boom signatures that will be both acceptable to the public and achievable in the design of the aircraft.

Subjective tests conducted to date in the simulator have assessed the effects of various boom parameters (such as rise time and overpressure) on subjective loudness. Results have indicated that boom shaping offers a promising method for minimizing loudness of sonic booms and increasing the potential for public acceptance of booms heard on the ground. These results have important implications relative to the goal of designing commercial supersonic aircraft that will be permitted to fly over land at supersonic speeds.

(Jack D. Leatherwood, 43591)

### **Fatigue Crack Growth of Acoustic/Mechanical Loads in Aircraft Structures**

Numerous investigations have been conducted of fatigue crack growth in aircraft structures resulting from low-cycle, high-stress cabin pressurizations. This behavior has been successfully modeled using linear elastic fracture mechanics principles. The addition of acoustic loading, having a high-frequency content but low stress level, has been shown to dramatically increase this fatigue crack growth rate; however, little effort has been spent to model the effects of the combined loading. This aspect of fatigue analysis will become increasingly important for planned supersonic and hypersonic aircraft. Therefore, an acoustic/mechanical load apparatus has been constructed and is being used in the Anechoic Noise Facility in support of the effort to model this behavior.



Acoustic/mechanical load apparatus in Anechoic Noise Facility.

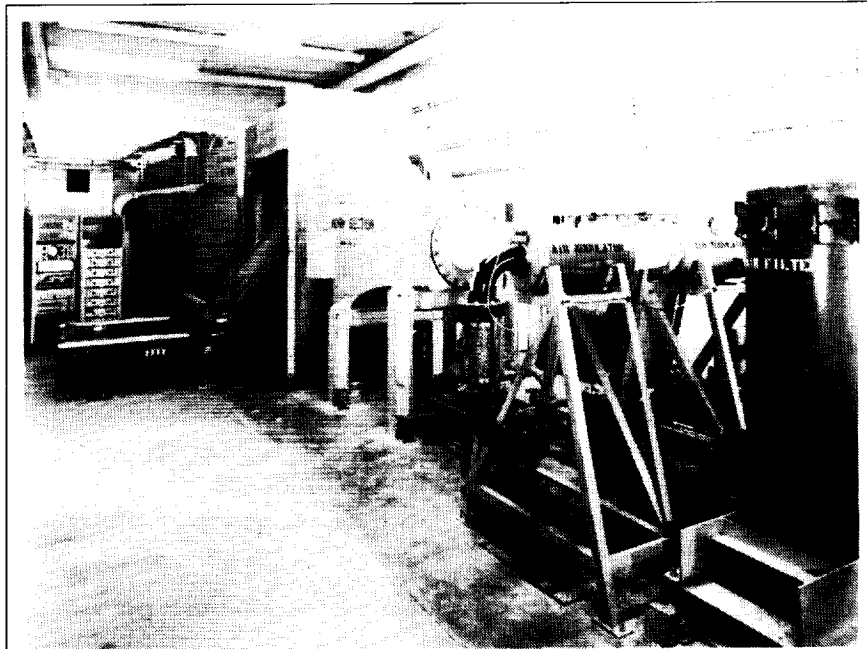
L-90-15390



The figure illustrates the apparatus mounted in the Anechoic Noise Facility. A 4-in. by 8-in. panel containing a 1-in. center crack is shown clamped in the grips. Mechanical tensile loads to 10 kips can be applied, and a loudspeaker on one side of the panel (not shown) can provide an acoustic excitation to 126 dB overall sound pressure level. In the first series of tests, the vibration response of panels containing 0-in., 1-in., 2-in., and 3-in. center cracks and subject to tensile loads to 10 ksi compared favorably with that predicted by a finite-element analysis. These tests also provided the data necessary to determine the damping. The current series of tests are aimed at collecting fatigue crack growth data for precracked panels subjected to a 10-ksi tensile load and narrowband random acoustic excitation about the fundamental vibration mode. These data then will be used in conjunction with a dynamic stress intensity factor analysis to form a frequency-dependent crack growth law. (Stephen A. Rizzi, 43599)

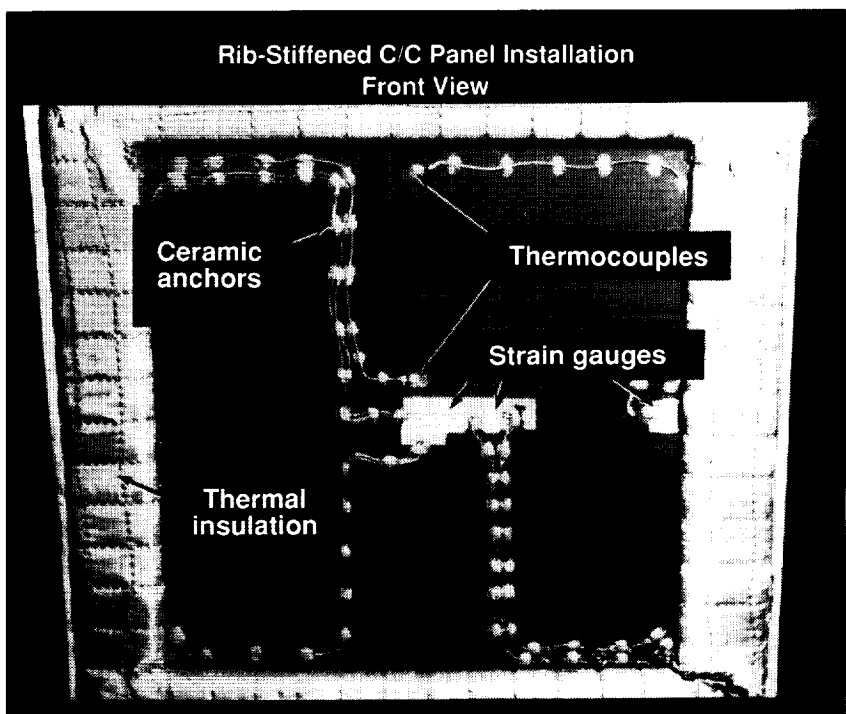
### High-Temperature Sonic Fatigue Testing

The flight envelope of hypersonic aircraft, such as the National Aero-Space Plane, poses significant challenges to the structural response and sonic fatigue test community. Many critical structural components of such aircraft may experience severe combined acoustic and thermal loads and must be tested to assure their performance and survival within these environments. These tests require facilities capable of generating the thermoacoustic loads expected in flight, as well as improved methods for



Thermal Acoustic Fatigue Apparatus (TAFA).

1-87-2448



Carbon-carbon panel mounted in TAFA showing strain-gauge and thermocouple installations.

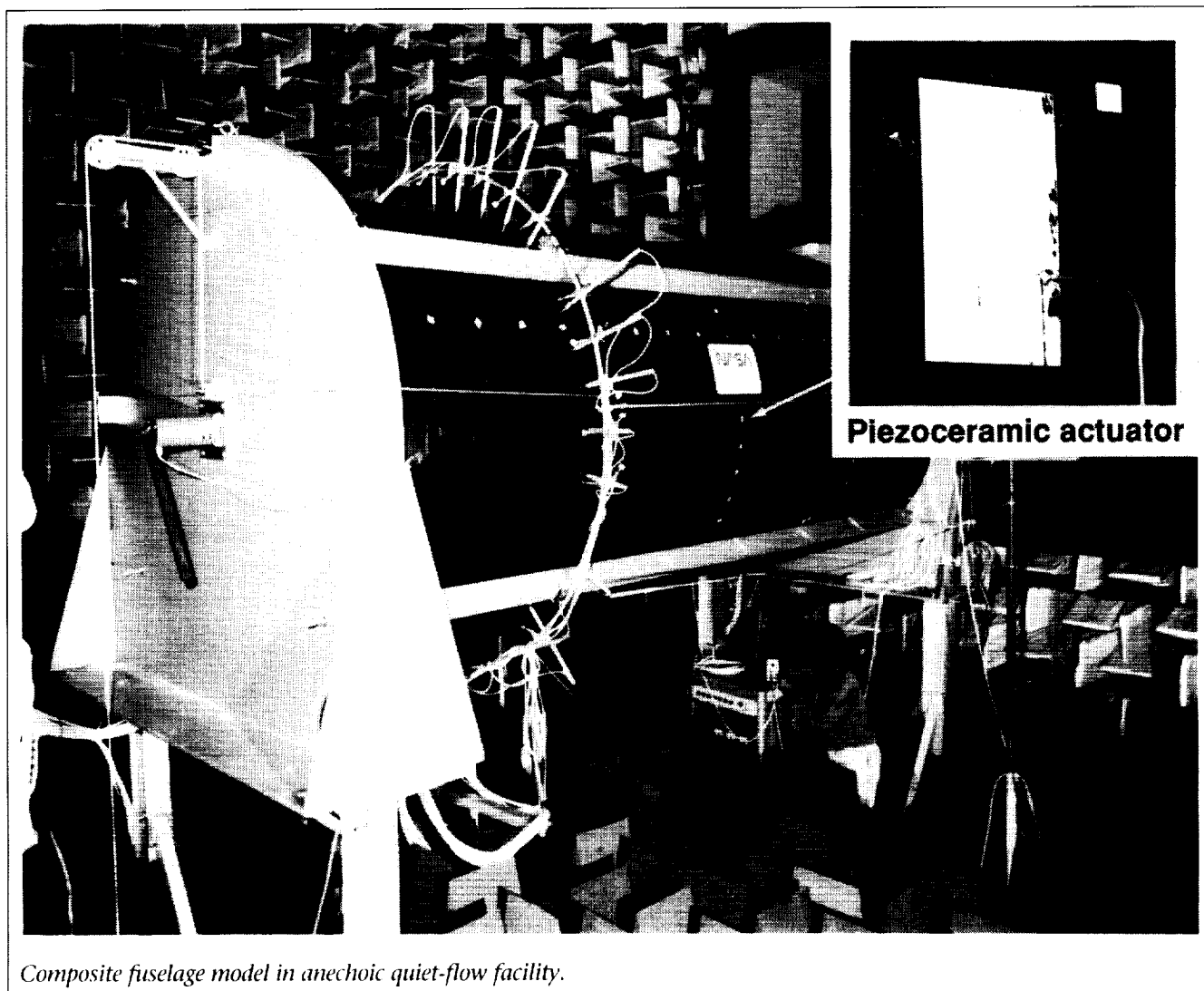
measuring structural response at elevated temperature. A facility for conducting such tests is shown in the first figure. This facility, called the Thermal Acoustic Fatigue Apparatus (TAFA), can generate acoustic levels up to 168 dB. A recent upgrade has increased heating capacity to 40 Btu/ft-s such that temperatures to 2000°F can be achieved on small (approximately 12-in. by 12-in.) structural panels.

Recent tests in the facility have investigated the sonic fatigue of carbon-carbon panels at both ambient

and elevated temperatures. The second figure, which shows the front view of a rib-stiffened carbon-carbon panel mounted in the facility for testing, illustrates the high-temperature thermal and strain measurement sensors. Results obtained from sonic fatigue tests of four carbon-carbon panels indicated that fatigue life at elevated temperature significantly exceeded fatigue life at ambient temperature. The failure mode of each panel was determined, and these data are being used to assist in the design of improved carbon-carbon structures. (Jack D. Leatherwood, 43591)

### Active Control of Interior Noise in Large-Scale Fuselage Using Piezoceramic Actuators

Recent flight evaluations of active control for interior noise control by the aircraft industry have demonstrated significant noise reductions for turboprop-powered aircraft. Reductions of 10 dB to 15 dB in sound pressure level (SPL) have been attained over the first several harmonics of the blade passage frequency. However,



utilizing interior acoustic sources, this control was obtained using up to 32 acoustic sources variously distributed throughout the aircraft interior. These numbers are required due to the spatial mismatch between the structurally induced primary acoustic field and the acoustic field produced by the interior noise sources.

In an effort to reduce the numbers of required actuators and to provide additional spatial control, ongoing work in cooperation with Virginia Polytechnic Institute and State University at Langley Research Center has demonstrated the effectiveness of using force inputs directly applied to the structure for interior noise control. The interior acoustic response is sensed using microphones and is reduced using distributions of up to four piezoceramic actuators bonded directly to the skin. These actuators provide a direct force input to the structure by expanding and contracting their planar surface when a voltage is applied to conducting upper and lower surfaces. One such actuator is shown bonded to the surface of a composite cylinder in the inset of the figure. The fuselage model shown in the figure is a graphite filament wound composite fuselage with a 5.5-ft diameter and a 12-ft length. The 0.067-in.-thick shell wall is stiffened by 12 ring frames and 22 axial stringers. A floor is installed in the interior space on a framework secured to the ring frames at four locations. Using as few as two actuators and four microphone error sensors, up to a 12 dB average reduction in SPL has been attained at frequencies corresponding to an acoustic cavity

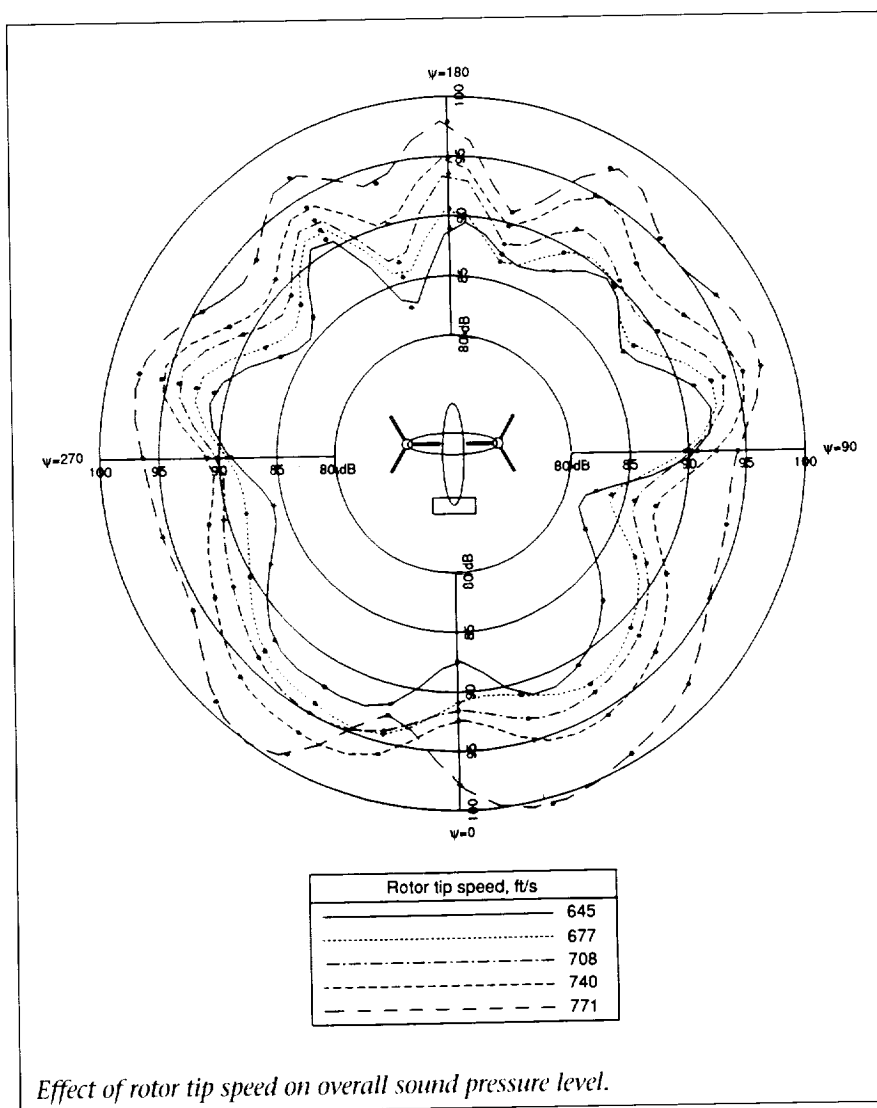
resonance. This reduction, which has been found to be nearly uniform throughout the interior space, was attained with a negligible addition of weight and at minimal cost.

(Richard J. Silcox, 43590)

## Near Inplane Tilt-Rotor Noise

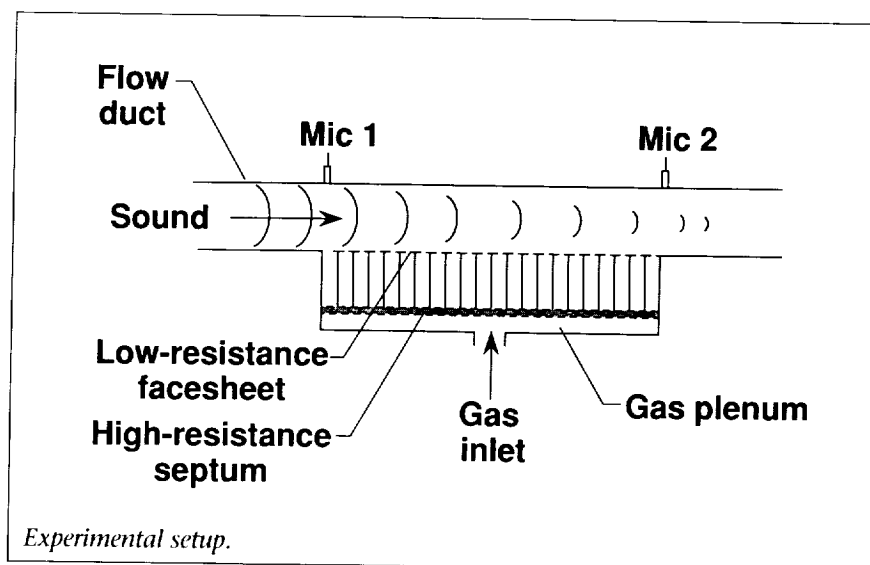
A flight experiment was conducted, in cooperation with the Ames Research Center, to obtain a

high-confidence, accurate data base of far-field hover acoustics for the XV-15 tilt-rotor aircraft with Advanced Technology Blades. The experiment, conducted in December 1990 at the Naval Air Station (NAS), Moffett Field, Mountain View, California, consisted of a hovering aircraft centered over a 500-ft radius semicircular array of 12 ground plane microphones. Each point was repeated for two aircraft headings to provide a full 360° acoustic coverage. The resulting data base provides valuable data for studies of tip



speed, gross weight effects, and acoustic directivity characteristics about the aircraft from near in-plane to approximately 45° below the rotor tip path plane. In addition, these data, which will be compared with similar data obtained in September 1988 for a tilt-rotor aircraft with standard metal blades, will be used for systems noise characterization studies.

The figure presents the overall sound pressure level (OASPL, dB) about the aircraft for a range of rotor tip speeds. The aircraft gear height was 2 ft above ground level, and the source-to-microphone distance was 500 ft; these conditions provided near inplane acoustic measurements. In general, the OASPL is maximum at azimuth angles  $\Psi$  of 30° and 330°. Previous research has shown that a "fountain flow" is created due to the blockage of the wing and is recirculated up and back through the rotors. The locations of maximum OASPL are believed to be due to the rotors interacting with this recirculated flow and directing the noise. As expected, the OASPL increases with rotor tip speed and is probably related to thickness noise. The acoustic signature is not symmetric about the aircraft longitudinal axis and has a scalloped shape in the forward quadrants ( $\Psi = 90^\circ$  to  $270^\circ$ ). Preliminary analyses indicate that this effect is due to observer-perceived phase differences between the two rotor systems. Analytical efforts are under way to evaluate this hypothesis. (David A. Conner, 45276, and Ken Rutledge)



### Duct Liner In Situ Tuning With Gas Percolation

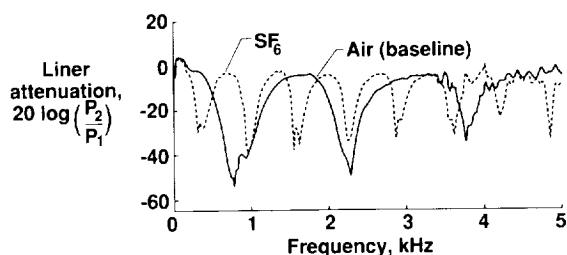
Adaptive control offers one way to improve acoustic liner efficiency for advanced ducted propellers. The acoustic properties of conventional resonant liners for acoustic suppression are fixed by the liner structure that typically consists of porous facesheets bonded to partitioned backing cavities. The airtight backing cavities are usually provided by hexagonal honeycomb cells bonded to a backing plate to provide a rigid, reflecting surface. A disadvantage of such liners is the inability to adjust their acoustic impedance in situ to attain optimum attenuation for different engine operating conditions such as takeoff versus landing. One concept for achieving in situ, adaptive control of liner properties is to change the sound speed in the backing cavities by partial replacement of the air by alternate gases.

To demonstrate the viability of this concept, a test liner consisting of a low-resistance facesheet with

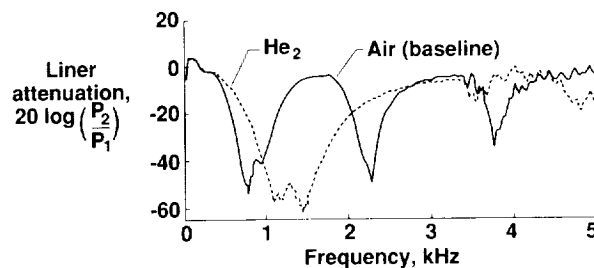
honeycomb partitioned backing cavities was mounted in a flow duct as shown in the first figure. The termination for the backing cavities was a porous but still highly reflective septum. The septum allowed gas from the pressurized plenum to percolate into the backing cavities and through the facesheet. Attenuations were measured for grazing incidence sound via two microphones as indicated. Baseline tests were conducted with air-filled cavities. The test was then repeated with cavities filled with sulfur hexafluoride or helium. The results are shown in the second figure.

Because of its low sound speed (40 percent of that for air), the attenuation maxima for sulfur hexafluoride shifted to lower frequencies by approximately 40 percent. In contrast, when the backing cavity gas was helium (with sound speed three times that of air), the attenuation spectrum peaks were shifted to higher frequency by approximately a factor of 3.

### Sulfur hexafluoride filled backing cavities



### Helium-filled backing cavities



*Effect of backing cavity gas replacement on liner attenuation.*

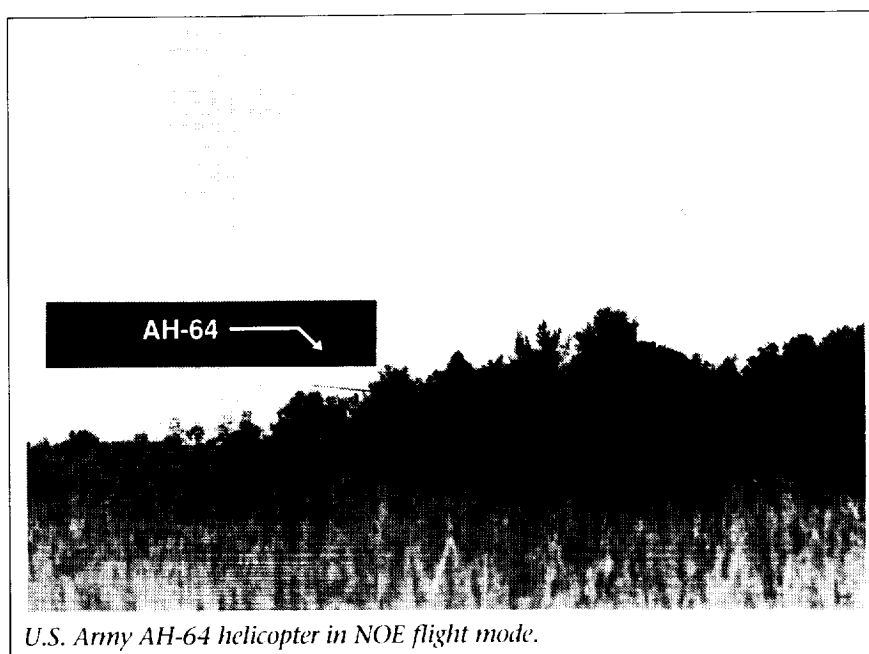
This result suggests that duct liner properties can be altered in situ to improve attenuating efficiency.

(Tony L. Parrott, 45273)

## Noise Propagation for Unique Helicopter Operational Characteristics

A long-range acoustic propagation test program was conducted at Fort A. P. Hill using two U.S. Army helicopters of different weight classes. The program goals included identification of rotorcraft propagation characteristics over a heavily forested environment in level flight, as well as Nap-of-Earth (NOE) flight conditions. The first figure shows an AH-64 helicopter in an NOE flight profile.

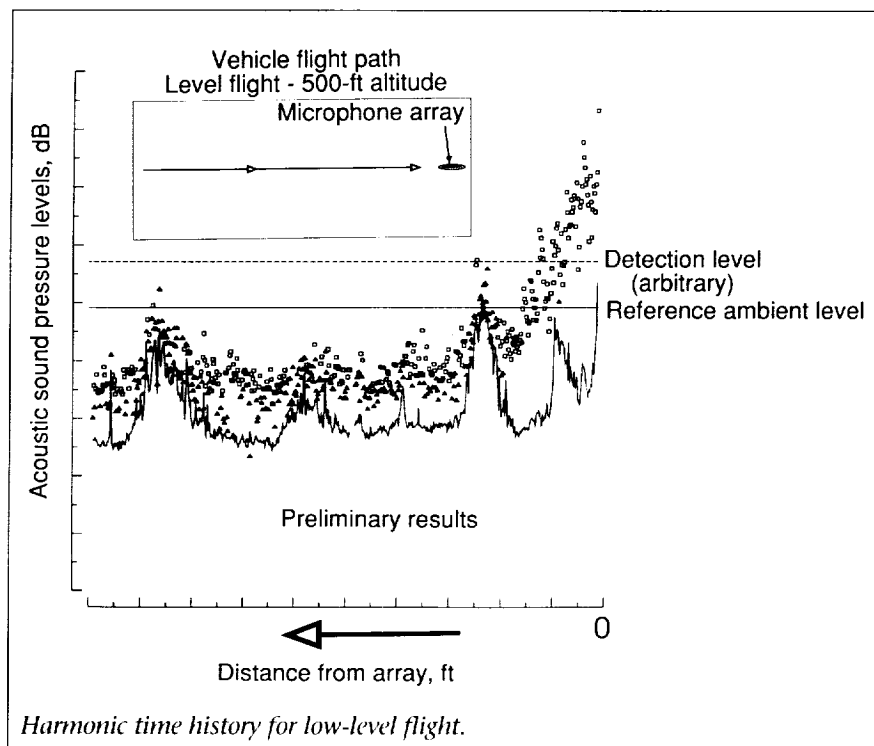
The results of these tests are used in contrasting the helicopter flight condition with the long-range propagation/detection characteristics. An analysis technique referred to as a "harmogram" was used in the data reduction procedure and is shown in the second and third figures. The



acoustic data records were analyzed to define the amplitude of a particular rotor harmonic level and the associated broadband level adjacent to the frequency of interest during the vehicle approach. These data are for the level flight case in the second figure and the NOE flight in the third figure. The harmonic amplitudes are shown as symbols, and the broadband levels are displayed as a solid line. Examples of a reference ambient level and an arbitrary

detection level are shown. The vehicle is considered to be detectable when the harmonic level exceeds the defined detection level.

In the level flight case (second figure), the detection characteristics are a function of distance from the array. For this flight condition, the particular harmonic level remained below the ambient condition until the vehicle was near the array. However, the NOE flight condition (third figure)

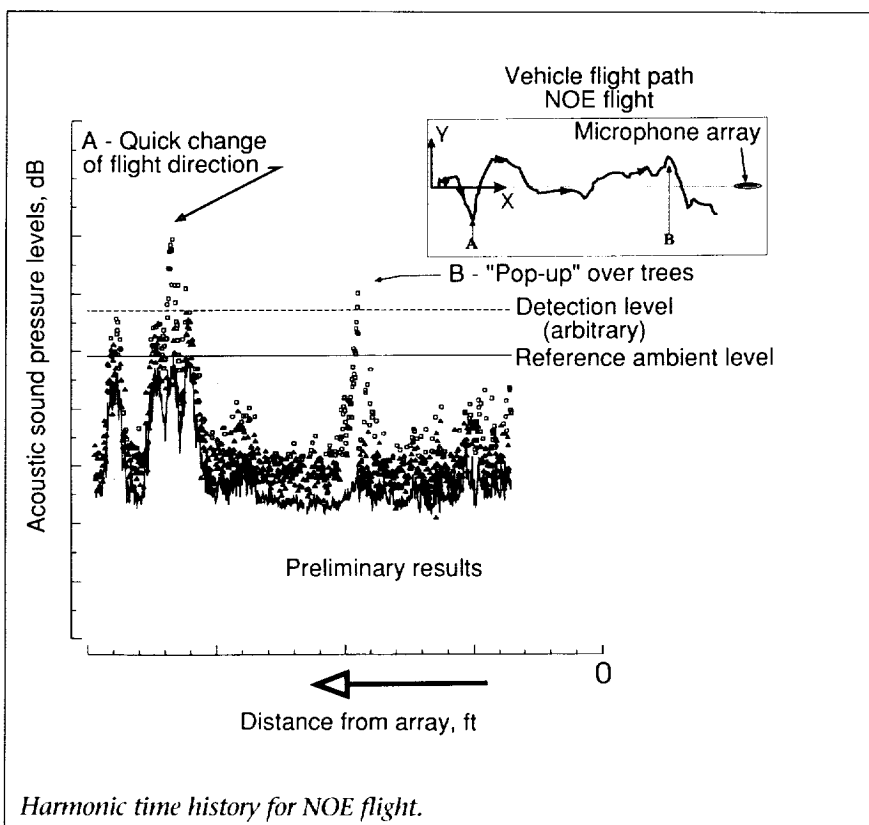


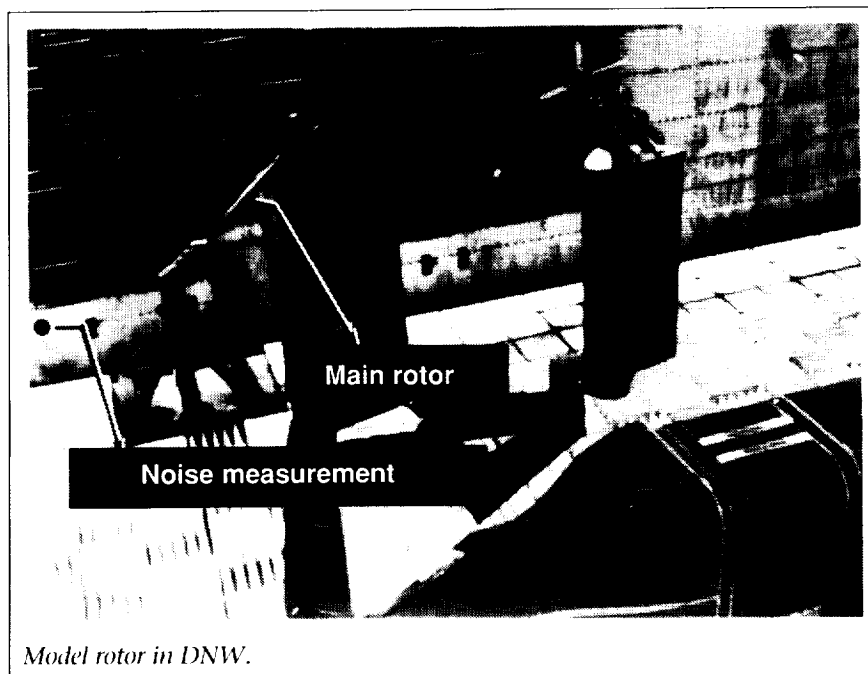
shows how the operational conditions affect the long-range detection results. The NOE flight path is provided as a sketch in the third figure, and two points A and B are identified. The results show the effect on the received signal because of these maneuvers. Maneuver A was a rapid change in helicopter direction, and it resulted in a detectable acoustic signature. Maneuver B was a rapid change or "pop-up" over obstructing trees, and it also resulted in an acoustic signature that was detectable. (Arnold W. Mueller, 45277, and Charles D. Smith)

## BVI Noise Prediction Validation

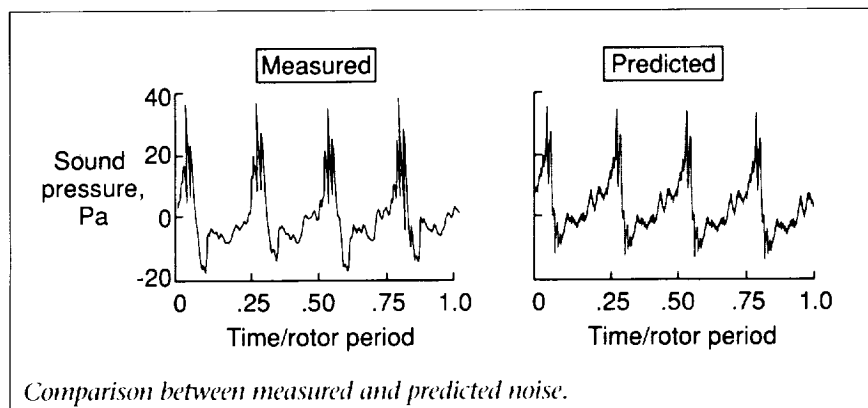
Blade-vortex interaction (BVI) noise, which is a highly impulsive helicopter noise source that occurs when rotor blades strike, or pass very close to, tip vortices previously shed into the wake of the rotor, occurs most often when the rotor is in descent.

Far-field noise and blade pressure data obtained from a model rotor test were employed to validate the Langley Research Center developed rotor noise prediction code WOPWOP for BVI noise. Research was conducted as part of a cooperative effort between the Army Aeroflightdynamics Directorate, United Technologies Research Center, Sikorsky Aircraft, and NASA Ames and Langley Research Centers. The test was performed in the Duits-Nederlandse Windtunnel (DNW), which is a large acoustic wind tunnel in the Netherlands. The





Model rotor in DNW.



Comparison between measured and predicted noise.

model rotor was a 1/6-scale, four-bladed, swept-tip design (as shown in the first figure). The rotor blades were instrumented with 176 pressure transducers on both the upper and lower surfaces. The blade pressure dynamic response was sufficiently high to capture BVI events. Noise predictions were made using the measured blade pressures as input into the WOPWOP code.

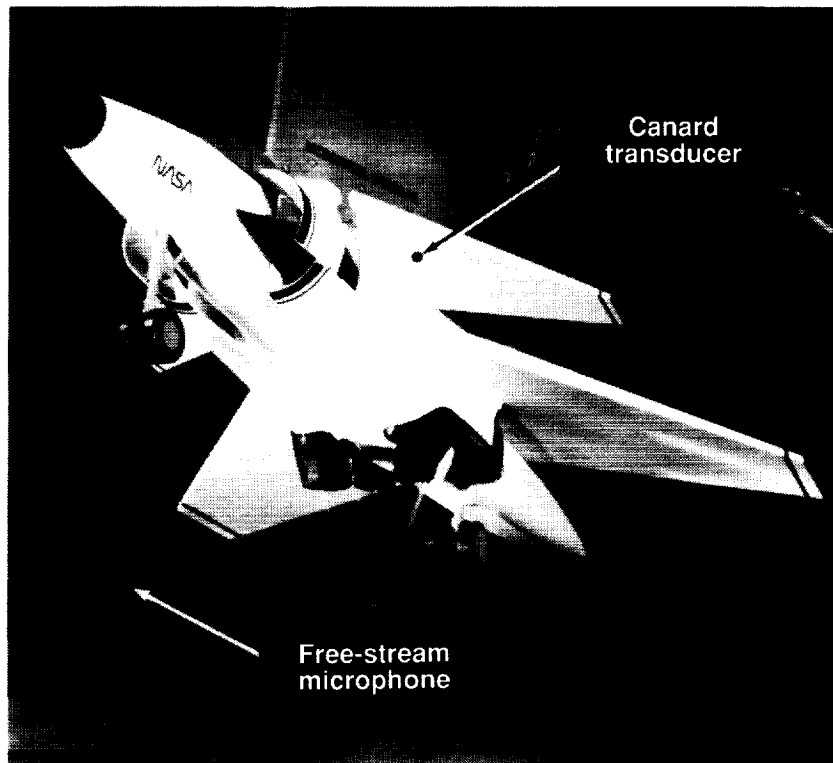
Measured and predicted acoustic time histories have been compared for a number of rotor operating conditions and measurement locations. A comparison for a case dominated by BVI noise is presented in the second figure. The major features of the measured data are well reproduced by prediction in both shape and magnitude; the amplitude of the predicted major peaks is bracketed by the blade-to-blade variability in the measured peaks.

The results show that the rotor noise prediction code predicts BVI noise when given accurate high-resolution blade pressure data as input. This fact is significant because noise predictions made with predicted air loads are not in good agreement with measured noise data. Better air load prediction capability is needed in order to improve this situation.  
(Casey L. Burley, 43659)

## ASTOVL Acoustic Loads

Advanced short takeoff and vertical landing (ASTOVL) aircraft use thrust vectoring to redirect the exhaust flow into the ground, thus providing lift in takeoffs and landings. Interactions between the high-velocity, high-temperature jets and the ground as well as the mutual interactions between the jets make the prediction of the noise of the aircraft very difficult. Presently, direct experimentation is the best way to understand this complicated flow field.

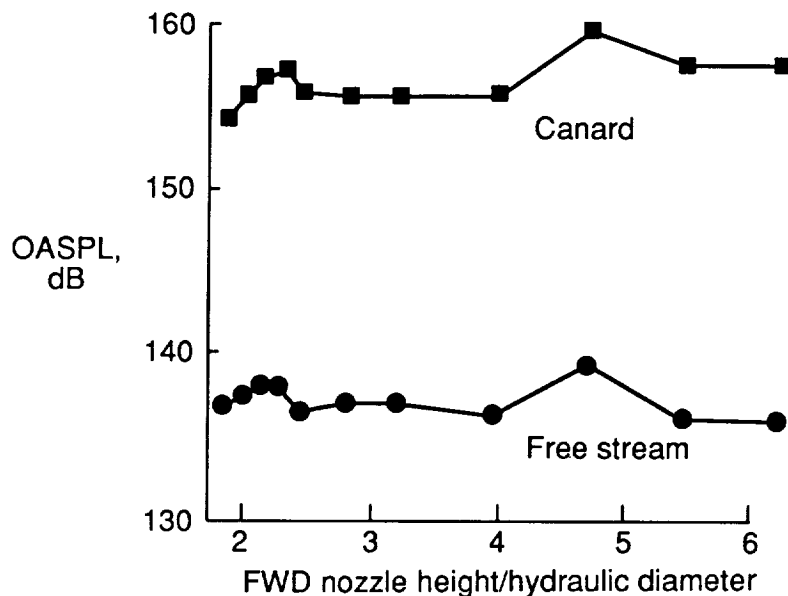
The near-field acoustics and aeroacoustic airframe loading of an ASTOVL aircraft were tested in the NASA Lewis 9- by 15-Foot Low-Speed Wind Tunnel. The testing was done using a 9.2-percent scale model of the McDonnell Douglas Corporation designed 279-3C aircraft. The objectives of the testing were to characterize ASTOVL acoustics when the aircraft is in ground effect (takeoffs and landings) and to determine the effect of jet exit temperature up to 1000°F.



ASTOVL model in NASA Lewis 9- by 15-Foot Low-Speed Wind Tunnel.

The first figure shows the model installed in the wind tunnel. Acoustic data were obtained from a linear array of five free-stream microphones, located parallel to the model centerline. The fluctuating loads on the model were measured with eight dynamic pressure transducers located on the underside of the canard, wing, and aft fuselage. The placement of the inboard canard transducer and a location of one of the free-stream microphones are illustrated in the first figure.

The data shown in the second figure illustrate the effect of the normalized nozzle height on the overall sound pressure level, as measured on the canard and in the free stream, for a jet temperature of 750°F. As shown by the data, very high levels up to 160 dB were observed on the model and up to 140 dB in the free stream. Levels of these magnitudes may lead to structural failure.



Acoustic loads and free-stream noise.

No satisfactory model exists that can predict the acoustics of multiple heated, noncircular jets operating in ground effect in an off-design condition. The data that were acquired in this test will be valuable in understanding both the fundamental physics of jet-impingement and the configuration issues involved in ASTOVL aircraft acoustics.  
(L. Kerry Mitchell, 43625)



## Supersonic Elliptic Nozzle Acoustics

The sound field generated by a supersonic elliptic nozzle was acquired to evaluate noise reduction potential relative to both round convergent and convergent-divergent nozzles. This study is associated with the development of a high-performance suppressor for commercial supersonic aircraft applications. The elliptic nozzle was designed with an exit aspect ratio of 2 to produce a shock-free plume at a Mach number of 1.52. The objective of this study was to determine if compressible turbulent mixing of the free jet shear layer could be enhanced by the non-axisymmetric distortion brought on by the elliptic shape. Of special interest was whether this enhanced turbulent mixing would lead to significant noise reduction.

The figure shows a far-field noise comparison among the three nozzles as a function of polar angle (angle from the inlet axis). The round convergent nozzle contained shocks and hence displayed the greatest noise levels at all angles.

The round convergent-divergent nozzle was designed to be shock free and therefore was approximately 10 dB quieter at forward angles. The elliptic jet, also designed to be shock free, produced the lowest noise radiation of all, especially along the direction of the major axis. Measurements of the centerline velocity decay and radial momentum thickness growth of the three jets suggested that enhanced mixing of the elliptic configuration was the cause for the noise reduction, as hypothesized. (John M. Seiner, 46276, and Michael K. Ponton)

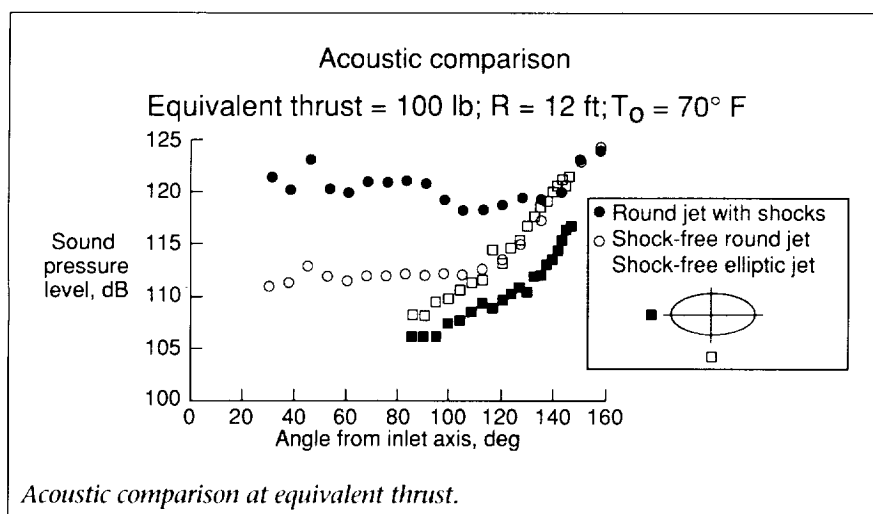
## Rotor Noise Reduction Using Higher Harmonic Control

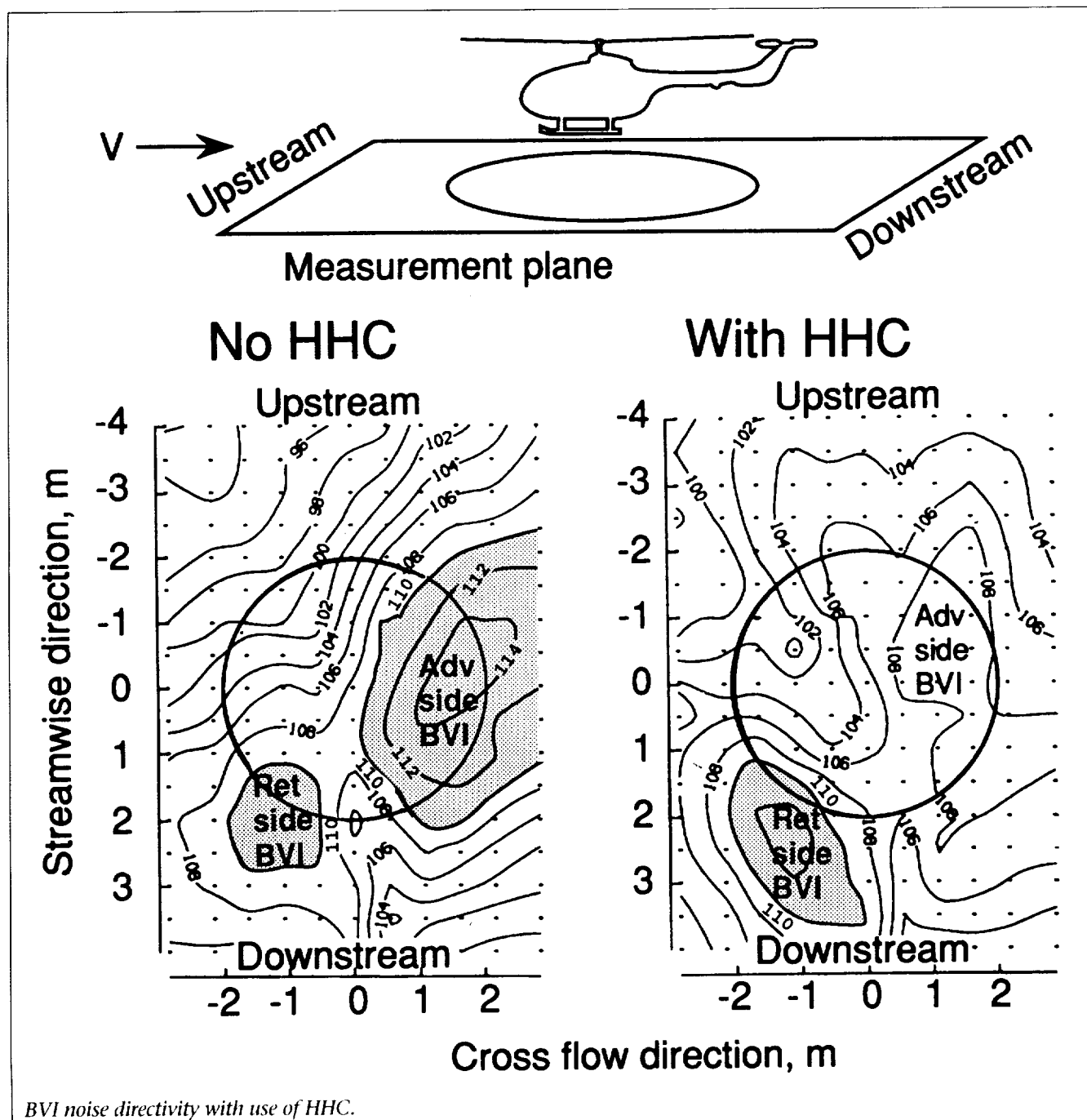
Impulsive blade-vortex interaction (BVI) noise is due to aerodynamic interaction of the rotor blades with previously shed blade tip vortices. A previous rotor noise study performed at Langley Research Center proved that higher harmonic control (HHC) of blade pitch could be used to reduce this

noise. Conceptually the noise is reduced because of increases in blade-vortex miss distances, as well as decreases in vortex strengths and mean lift at BVI locations.

The present study was undertaken to obtain for the first time a detailed noise directivity of BVI noise, while employing HHC on a 40-percent aeroelastically scaled BO-105 rotor. The test, conducted in the German/Dutch Wind Tunnel (DNW, Duits-Nederlandse Windtunnel/Deutsch Niederländischer Windkanal), was a cooperative effort among Langley Research Center, the German Aerospace Establishment, Deutsche Forschungsanstalt für Luft- und Raumfahrt (DLR), and the European helicopter companies MBB (Messerschmitt-Bölkow-Blohm) and Aérospatiale. The noise was determined over a large measurement plane underneath the rotor by the use of a traversing in-flow microphone array. Noise and vibration measurements were made for a range of matched rotor operating conditions in which prescribed higher harmonic pitch was superimposed on normal (baseline) collective and cyclic trim pitch.

Presented in the figure are noise contour plots over the measurement plane for a particular flight descent condition that is considered typical for full-scale helicopters. On the left, a baseline case is shown in which no HHC is used. The levels given are mid-frequency values, and they represent the BVI noise contributions to the total noise. Indicated on the plot are the locations of the advancing side BVI directivity lobe and the retreating side BVI lobe.



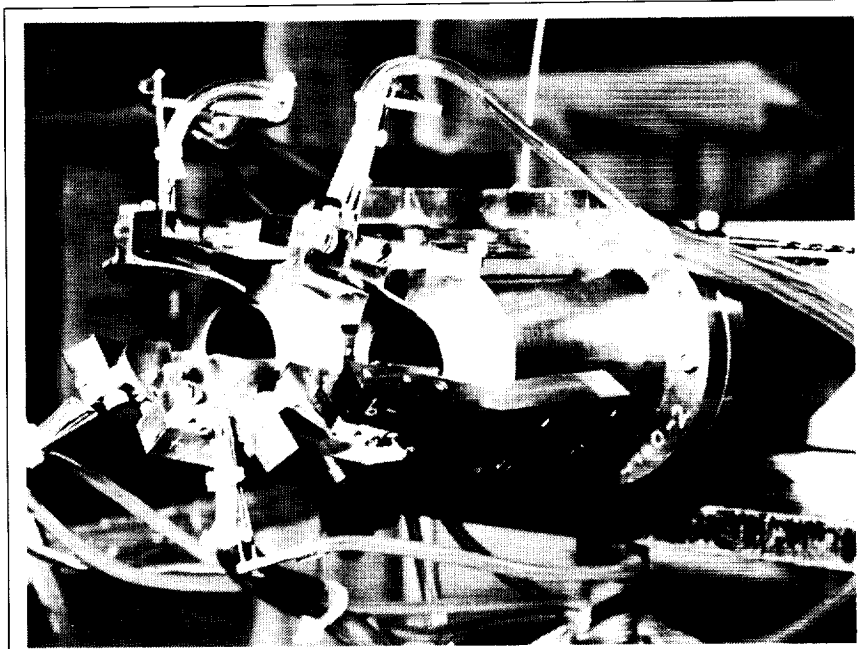


The plot to the right is the noise contour for an HHC pitch schedule (4/rev at 1.2° amplitude and 32° control phase) which causes a significant 6-dB reduction in the advancing side lobe levels, although the retreating side increases somewhat. The relative levels and

directivity can be modified by changing the control phase.

An interesting, as well as challenging, feature of the present data is the apparent strong role that rotor aeroelasticity plays in the BVI noise results. The earlier Langley

tests with relatively rigid blades found similar noise reductions but with different HHC amplitudes and phases.  
(Thomas F. Brooks and Earl R. Booth, Jr., 43634)



F-18 HARV model exhaust nozzles and vanes.

L-90-10585

## F-18 HARV Aeroacoustic Loads

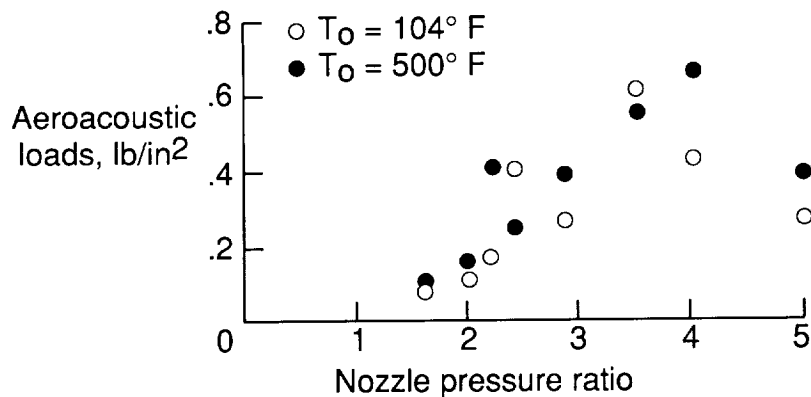
A model scale study of the aft-end aeroacoustic environment of the F-18 HARV (High-Alpha Research Vehicle) was conducted to determine dynamic loads on thrust vectoring vanes and in the near acoustic field of the vehicle. An F-18 HARV aircraft, located at

NASA/Dryden Flight Research Facility, is currently being flight tested to evaluate capabilities for achieving full vector authority using thrust vectoring. The present study was initiated to study potential problems associated with the supersonic twin-plume resonance mechanism.

The first figure shows the 7.39-percent aft-end model with three

turning vanes per nozzle attached to the nozzle afterbody. The center of each vane was instrumented with a flush-mounted water-cooled dynamic pressure sensor (with an outside diameter of 0.25 in.). These sensors permitted testing the model to high temperature. Aeroacoustic loads were obtained for vane angles ranging from  $-10^\circ$  (fully stowed) to  $20^\circ$  (full vectoring). The jet total pressure and temperatures were varied from subcritical to a nozzle pressure ratio of 5 and temperatures from ambient to  $750^\circ$ .

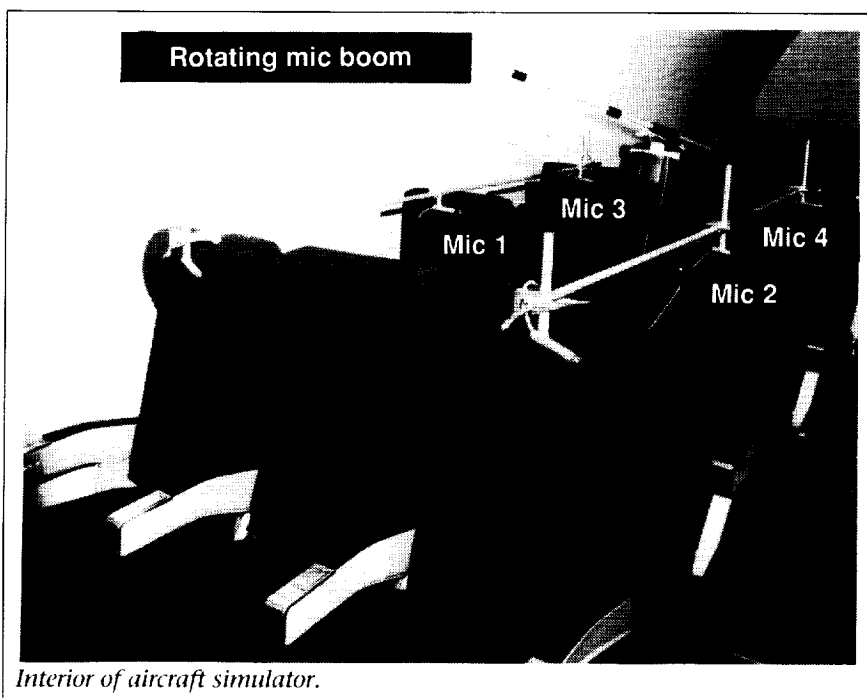
The second figure shows the overall dynamic pressure levels in  $\text{lb/in}^2$  for the upper vane set at  $0^\circ$ . At this setting, the vanes are not in the jet flow. The level is shown to increase with nozzle pressure ratio (NPR) reaching a maximum of  $0.7 \text{ lb/in}^2$ . The peak level is nearly independent of jet temperature  $T_0$ , but it does occur at a higher NPR with higher temperature. The peak level of  $0.7 \text{ lb/in}^2$  is of concern because previous research on the aft-end aeroacoustic of the F-15 and B-1B aircraft produced structural failures with much lower loads. Associated narrowband spectra show that the aeroacoustic loads (for vanes retracted from the flow) are dominated by jet shock and plume resonance mechanisms. (John M. Seiner and Bernard J. Jansen, 46276)



Aeroacoustic loads at vane angle of  $0^\circ$ .

## Active Sound Attenuation Across Double-Wall Fuselage Structure

Interior noise levels that are unacceptable for passengers and crew in the aircraft cabin need to



be controlled with a minimum weight penalty. Active noise control has been demonstrated to attenuate interior sound pressure levels substantially, thus limiting the need for heavy noise control treatment materials to be added to the interior aircraft fuselage walls. In the current study, active noise control was applied to the space between the exterior and interior cabin walls, thus yielding considerable local and global sound attenuation. In contrast to the more conventional active noise control approach, which attenuates the sound after it has entered the cabin, the current technique controls the sound before it enters the cabin. Thus, less control equipment is required, and the control equipment does not occupy space in the cabin.

This study was conducted in an aircraft fuselage mock-up (shown in the figure) which is 24 ft long with a double wall consisting

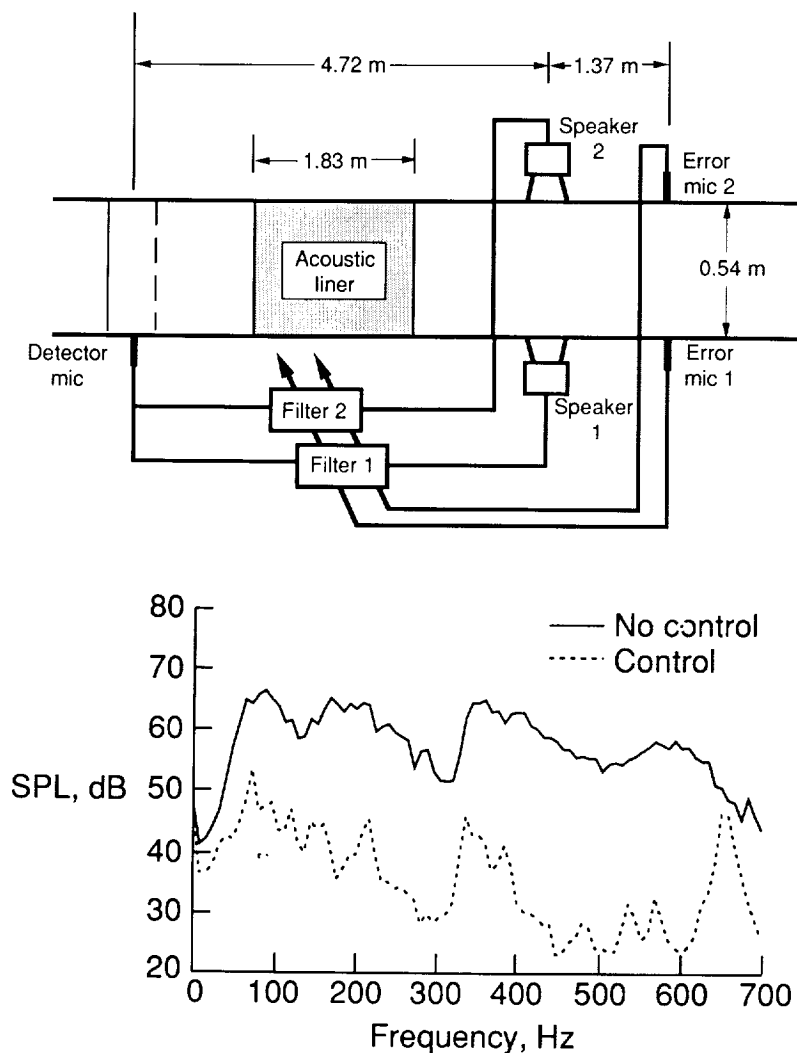
of an exterior surface of 0.75-in.-thick plywood and an interior surface of 0.25-in.-thick Masonite. The interior has the shape and the size of a Boeing 707 aircraft. The structure is reinforced with plywood ribs and stringers. A source loudspeaker is located outside the aircraft fuselage, and control speakers are mounted on the outer wall radiating into the space between the inner and outer wall. Microphones were placed at the right rear location of potential occupants of three window and three aisle seats. An additional microphone was mounted on a rotating boom to measure global interior sound pressure levels. A sinusoidal tone, arbitrarily chosen at 100 Hz, was fed into the source loudspeaker. Measured transfer functions between each of the four control loudspeakers within the double wall and the interior microphones were used in a least-mean-square adaptive algorithm to actively attenuate the interior

sound pressure levels at the fixed microphone locations. This attenuation ranged from 10 dB to 20 dB, depending on location. Measurements by the rotating boom microphone indicated that at least a 3-dB attenuation was obtained except very close to the aircraft double wall. More global attenuation was obtained when the wavelength of the sound was longer relative to the distances between the control speakers in the double wall and the microphones in the cabin.

(Ferdinand W. Grosveld and Kevin P. Shepherd, 43586)

### Active Control of Multimodal Random Sound in Ducts

The problem of controlling random noise in ducts is an important application problem that has also taken the role of a benchmark in the development of active control systems. As an indicator of control system development, this problem requires the inclusion of feedforward and feedback elements as well as the development of a broadband controller. In the past, systems have been developed that provide significant attenuations (i.e., 20 dB or greater), but with the restriction that only plane waves exist in the frequency range of interest. By extending the control to multimode propagation, this work extends the usefulness of this technology to a broader frequency range, eliminates the necessity of redundant passive techniques, and will provide in many flow systems a lower lifetime operating cost due to lower losses.



*Schematic of duct system and performance of controller.*

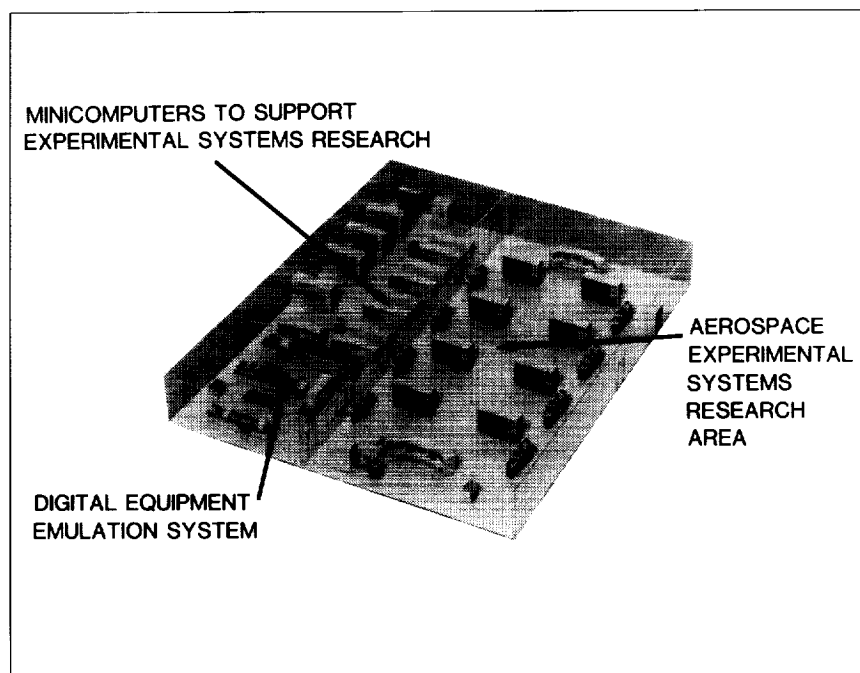
For the duct shown in the figure, the frequency below which only plane waves propagate is 325 Hz. The control system transducers consisted of a single detector microphone, two loudspeakers mounted on opposite sides of the duct, and similarly mounted error microphones. The controller was implemented as two digital filters whose design was derived from transfer functions measured between the various

transducers. These filters operate on the detector microphone signal and drive the two loudspeakers such that the outputs of the error microphones are minimized.

The plot of the overall control of sound pressure level (SPL) shows the uncontrolled SPL spectra at one of the error microphones (as indicated by the solid line). The peak at 325 Hz is due to the cut-on of the (1,0) mode. Below this

frequency, the plane wave dominates the spectra. Above 325 Hz, the pressure spectra are made up of a combination of the plane wave and the (1,0) mode. The reduced SPL as a function of frequency because of the control system is shown by the dashed line in this same plot. An overall reduction of 20 dB was recorded at both error microphones over the frequency range from 50 Hz to 600 Hz. Reductions of 19.1 dB for the plane and 22.6 dB for the (1,0) mode were recorded.

(Richard J. Silcox, 43590)



## Avionics Integration Research Laboratory (AIRLAB)

*The United States leads the world in the development, design, and production of commercial and military aerospace vehicles. To maintain this leadership role throughout the 1990's and beyond will require the incorporation of the latest advances of digital systems theory and electronics technology into fully integrated aerospace electronic systems. Such efforts will entail the discovery, design, and assessment of systems that can dramatically improve performance, lower production and maintenance costs, and at the same time provide a high, measurable level of safety for passengers and flight crews.*

*AIRLAB has been established at the Langley Research Center to address these issues and to serve as a focal point for U.S. Government, industry,*

*and university research personnel to identify and develop methods for systematically validating and evaluating highly reliable, fully integrated digital control and guidance systems for aerospace vehicles.*

*The increasing complexity of electronic systems entails multiple processors and dynamic configurations. These developments allow for greater operational flexibility for both normal and faulty conditions, thus impacting and compounding the validation process. Whereas a typical reliability requirement for current electronics systems is a probability of failure of less than  $10^{-6}$  at 60 min, the requirement for flight-critical electronic controls is for a probability of failure of less than  $10^{-9}$  at 10 hr. Obviously, a new validation process is*

*essential if this significant increase in reliability (four orders of magnitude) is to be achieved and believed.*

*Validation research in AIRLAB encompasses analytical methods, simulations, and emulations. Analytical studies are conducted to improve the utility and accuracy of advanced reliability models and to evaluate new modeling concepts. Simulation and emulation methods are used to determine latent fault contributions to electronic system reliability and hence aircraft safety. Experimental testing of physical systems is conducted to uncover the latent interface problems of new technologies and to verify analytical methods.*

*AIRLAB is a 7600-ft<sup>2</sup> environmentally controlled structure located*

in the high-bay area of Building 1220. AIRLAB houses a number of micro-computer and minicomputer resources and several special fault-tolerant research hardware test specimens dedicated to the support of validation research. The minicomputer resources consist of eight Digital Equipment Corporation VAX 11/750 computers, one VAX 11/780 computer, five MicroVAX II computers, two VAXstation 3200's, eight Sun workstations, eight IBM-PC compatibles, and seven Macintosh PC's. These resources are used to control experiments (such as fault insertions and performance monitoring); retrieve, reduce, and display engineering data; develop and validate simulations; and develop and validate analytical reliability and performance estimation tools. Also included in AIRLAB are a Lightning Upset test bed and three advanced fault-tolerant computer systems; the Fault-Tolerant Multiprocessor (FTMP); the Fault-Tolerant Processor (FTP); and the Verifiable Integrated Processor for Enhanced Reliability (VIPER). These systems are designed to explore fault-tolerant techniques for future flight-critical aerospace applications and to serve as research test beds for validation studies in AIRLAB.

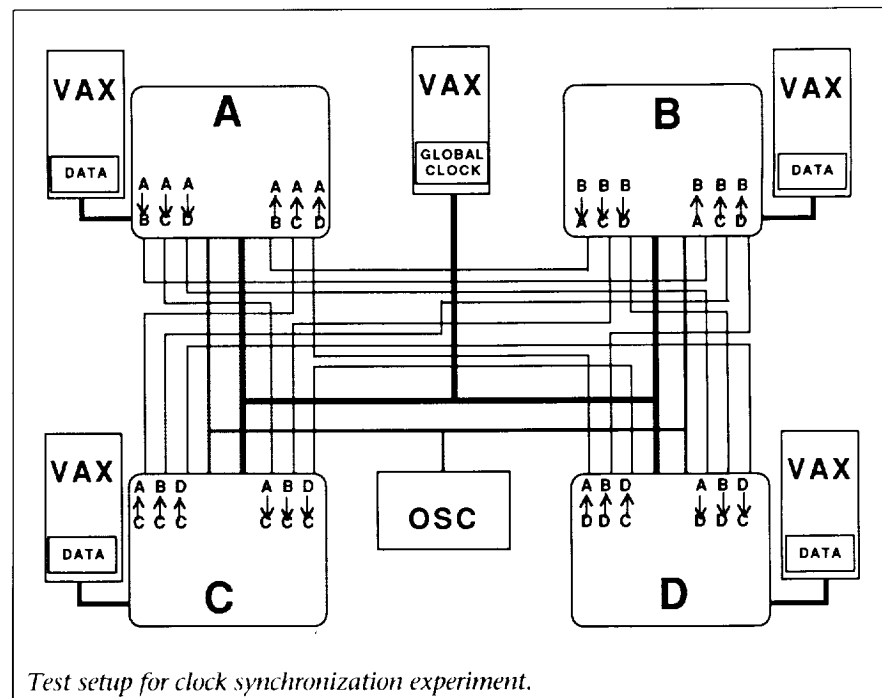
## Validation of Formally Verified Clock Synchronization Theory

A direct method of controlling the interaction between cooperating processes on different computers is to assume a global time base and then order the tasks on the computers according to time. In this way, data dependencies can be resolved across the system without

a large communication overhead. Establishing this global time base is not as straightforward as one would expect. A time base of a computer is derived from the same kind of crystal oscillators that are used in common wristwatches. And, as is well known, crystal oscillators are very accurate; most have frequencies within 10 parts per million of specification. However, what is accurate to a human's perception of time can be divergent to a computer's perception. Computers complete entire tasks within a thousandth of a second and thus require that the global time base be accurate to within milliseconds. Crystal clocks can drift fractions of a second within a few minutes. Cooperating processes on different computers cannot rely on crystal clock accuracy alone to coordinate their actions. In the case of life-critical real-time systems, the method by which clock synchronization is obtained must be highly reliable as well.

Several clock synchronization theories have been developed in response to the requirement for a reliable global time base. One of the first theories was created in the early 1980's for the Software Implemented Fault-Tolerant Computer (SIFT), which was then a central part of AIRLAB. The theory describes several parameters, a clock synchronization algorithm, and a formula for the upper limit on the time differences between the clocks in the system which compute the algorithm.

This test was devised to validate the clock theory by comparing the sensitivity of the predicted time difference upper limit to measured values. As was learned while testing SIFT and other fault-tolerant computers in AIRLAB, unless explicit means are taken to provide observability and control, much will be hidden and inaccessible to the researcher. With this in mind, custom circuitry was



---

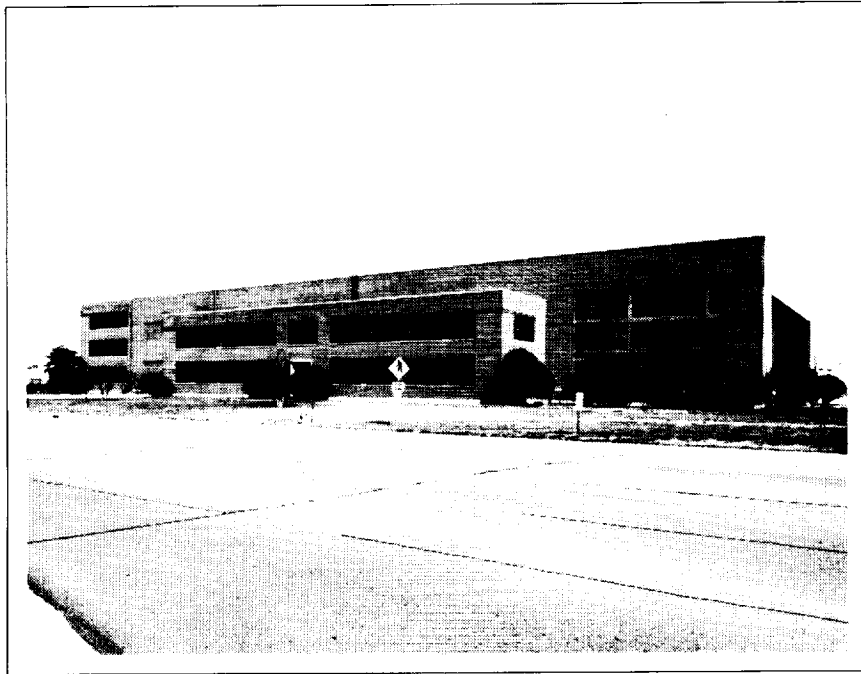
developed which provides access to and control of the internals of the synchronization algorithm. The synchronization circuitry was installed in four computers. Five other computers were used to control the experiment and provide data acquisition (see the figure).

The results have shown that the theory did predict an upper limit to the time difference, but that this limit was higher than that which occurred in practice. The exact amount of the discrepancy depends on the details of each implementation, but errors of 20 percent were observed. Corrections were made to the theory, and a new formula derived.

**(Daniel L. Palumbo, 46185)**

---





## Aerospace Controls Research Laboratory

*The purpose of the Aerospace Controls Research Laboratory (ACRL) is to conduct research and testing of spacecraft control systems. The ACRL is equipped with modern microcomputer facilities for simulations, data acquisition, and real-time control system testing. Both control law testing using structural test articles and advanced control system component development are supported by the laboratory. The ACRL provides the controls community with facilities on which the performance of competing control laws may be compared.*

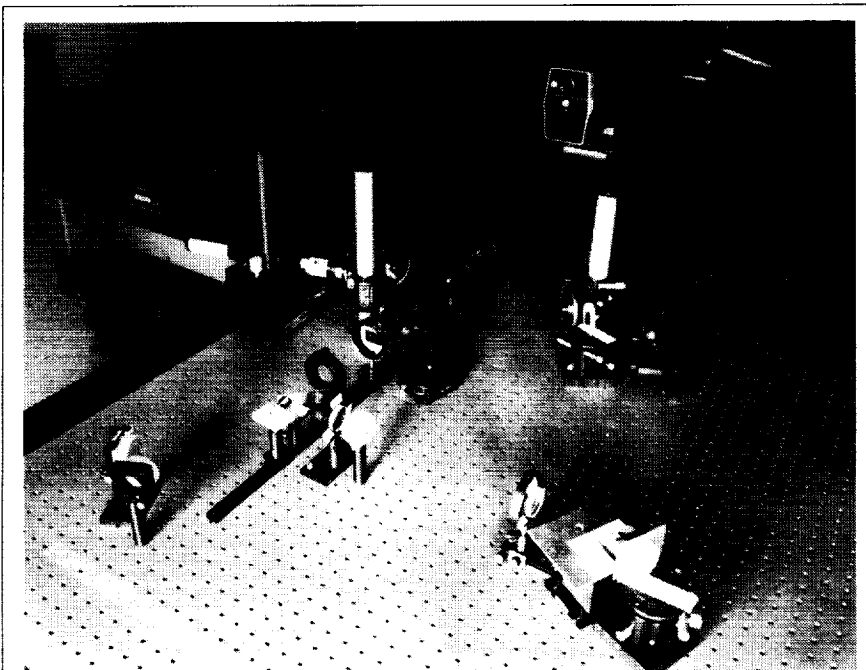
*One structural test article is currently available. The Spacecraft Control Laboratory Experiment (SCOLE) allows testing of control laws for a complete spacecraft. The test article mimics the Space Shuttle with a*

*large flexible offset-feed antenna attached to the payload bay. Reaction jets, control moment gyros, and torque wheels, along with accelerometers and rate sensors, permit real-time control law implementation on SCOLE (see the first figure).*

*The advanced sensor and actuator facility supports research in control system components for space systems. Component development currently focuses on optical sensing and computing devices. Two different photogrammetric position tracking systems and an optical holographic image storage device are being developed. The facility (shown in the second figure) includes equipment for performing experiments in optics, two stable tables, optical mounts, lenses, mirrors, polarizers, beam splitters,*



*Spacecraft Control Laboratory Experiment. L-87-7321*



*Advanced sensor and actuator facility.*

L-89-325

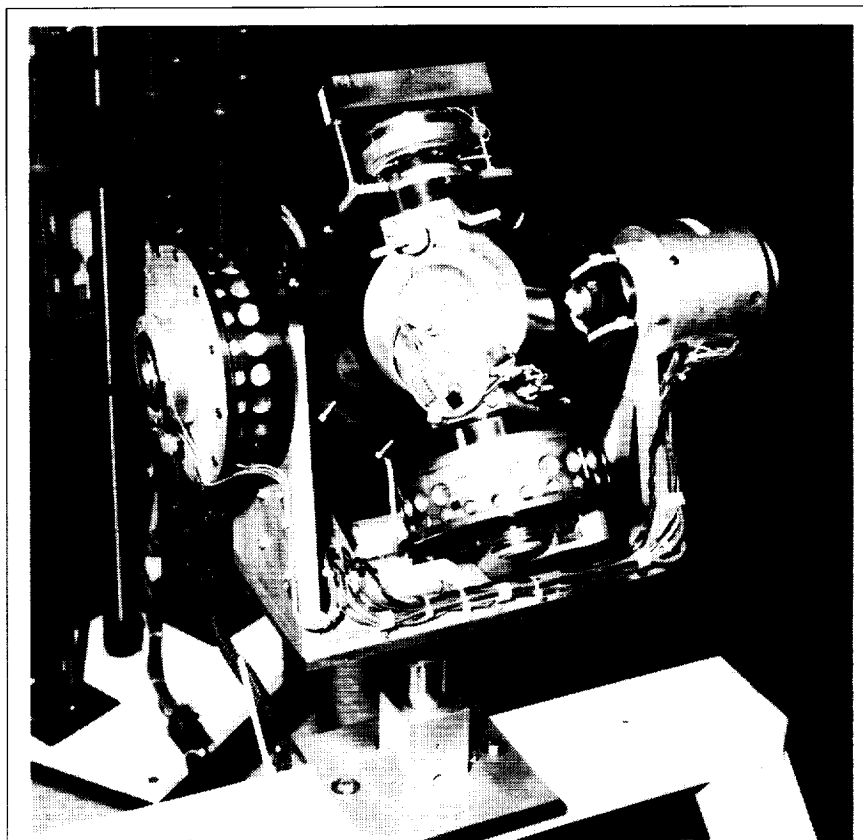
*photomultiplier tubes, a 5-mW HeNe laser and a 35-mW HeNe laser, a precision rotary stage, and laser beam steering systems.*

### **Control Moment Gyro Steering Law Testing on SCOLE**

Momentum storage devices such as control moment gyros (CMG's) are normally used to provide accurate attitude control torques for missions in which environmental contamination or reaction control system fuel requirements are excessive. A CMG device provides attitude control torque by the precession of its high constant-speed spinning flywheel. If large momentum and torque ranges with low electrical power are required, the CMG system becomes an obvious choice. The CMG's prove effective as an attitude

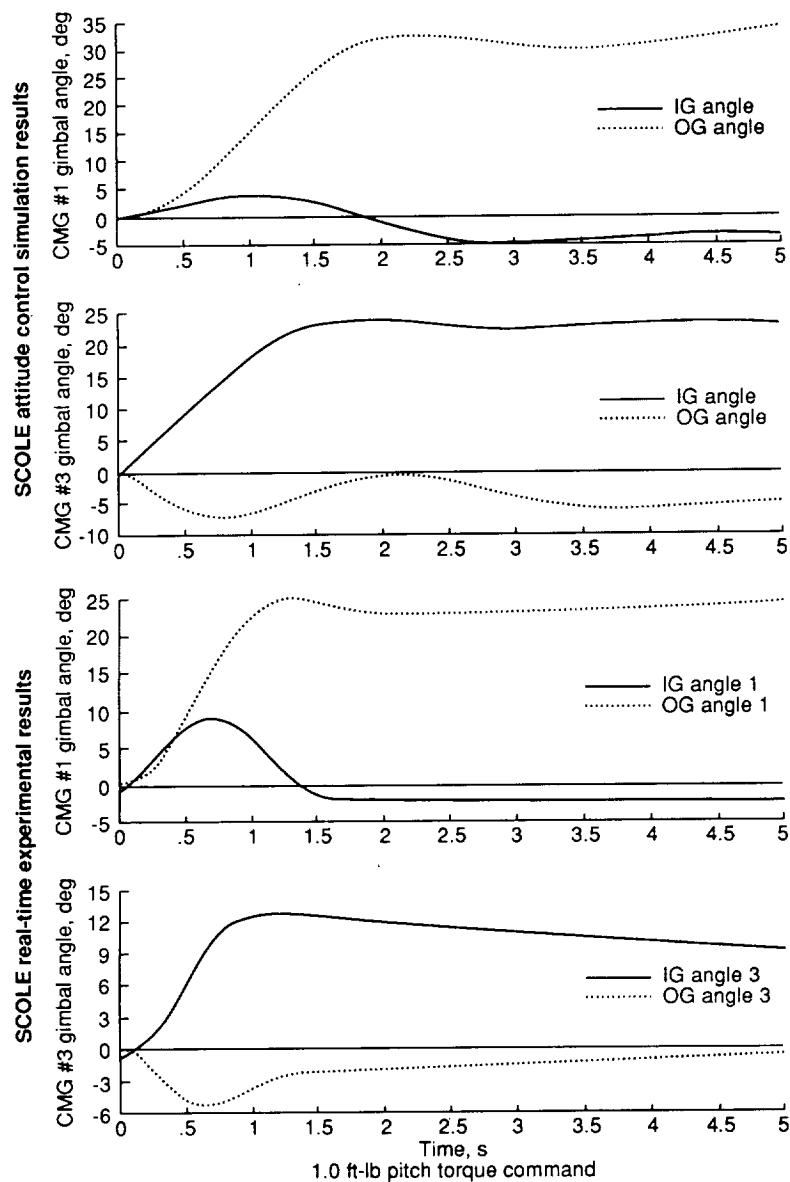
control system only as long as they can store momentum; therefore, maximizing the total momentum storage capability of the system is necessary.

Space vehicle attitude control utilizing CMG actuation involves the generation of vehicle torque gyroscopically by the slewing of the CMG gimbals. The CMG steering law algorithms determine the gimbal rate commands necessary to achieve the desired vehicle maneuver control torques. The SCOLE apparatus is equipped with a pair of double-gimbaled CMG's (DGCWG's) used to implement a no-crosscoupling steering law derived from the Skylab-A attitude control flight system. The steering law development was preceded by



*Sting-balance-mounted CMG: hardware characterization test.*

L-90-05468



Simulation versus real-time test results. (IG designates inner gimbal and OG designates outer gimbal.)

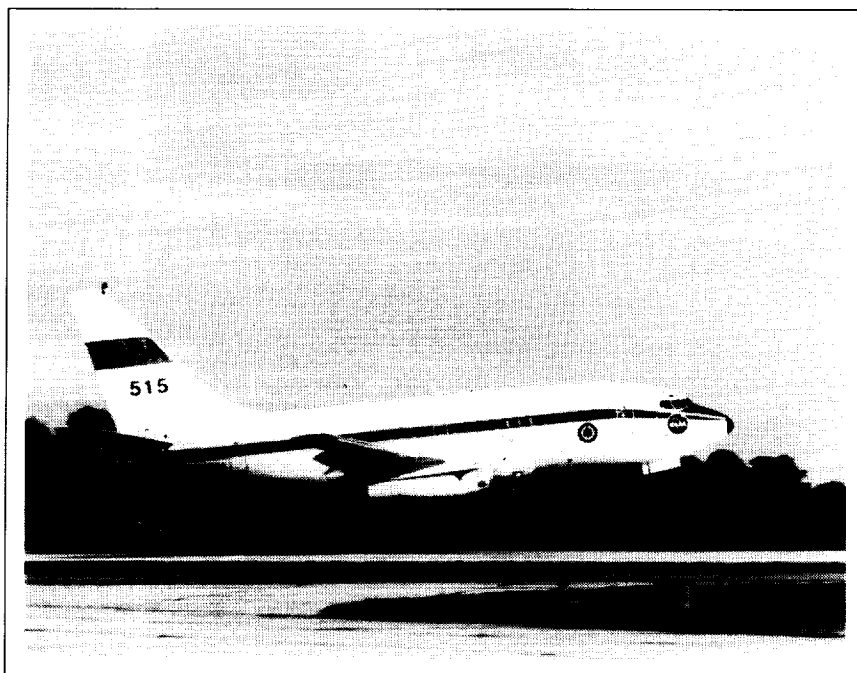
hardware characterization of the DGCWG's (shown in the first figure) and design of digital gimbal rate controllers. Nutational resonance and dynamic crosscoupling, which contributed to gimbal rate loop instability, were

identified using recursive least-squares system identification techniques on sampled test data. Appropriate compensation networks were designed and verified via simulation and hardware-in-the-loop testing. The rate control-

lers, steering law algorithms, and a digital proportional integral (PI) controller were integrated into a real-time program and implemented on the SCOLE using the onboard sensor system to provide full three-axis control of the Space Shuttle model.

Preliminary closed-loop testing results (shown in the four graphs of the second figure) revealed close agreement between test output and computer simulation. Differences can be attributed to errors in the modeling of the actual hardware dynamics and to nonlinear friction in gimbal bearings. Future testing is planned to improve compensation for instabilities incurred by variation in rotor speed. A closed-loop maneuver test is planned for the SCOLE not only to validate the effectiveness of the CMG steering law but also to incorporate the CMG actuators in a global control law.

(J. Shenhar, 46617, M. G. Maras, and R. C. Montgomery)



## Transport Systems Research Vehicle (TSRV) and TSRV Simulator

---

*The Transport Systems Research Vehicle (TSRV) and TSRV Simulator are primary research tools used by the Advanced Transport Operating Systems (ATOPS) Program. The goal of the ATOPS Program is to increase the operational capability of modern aircraft and foster their integration into the evolving National Airspace System.*

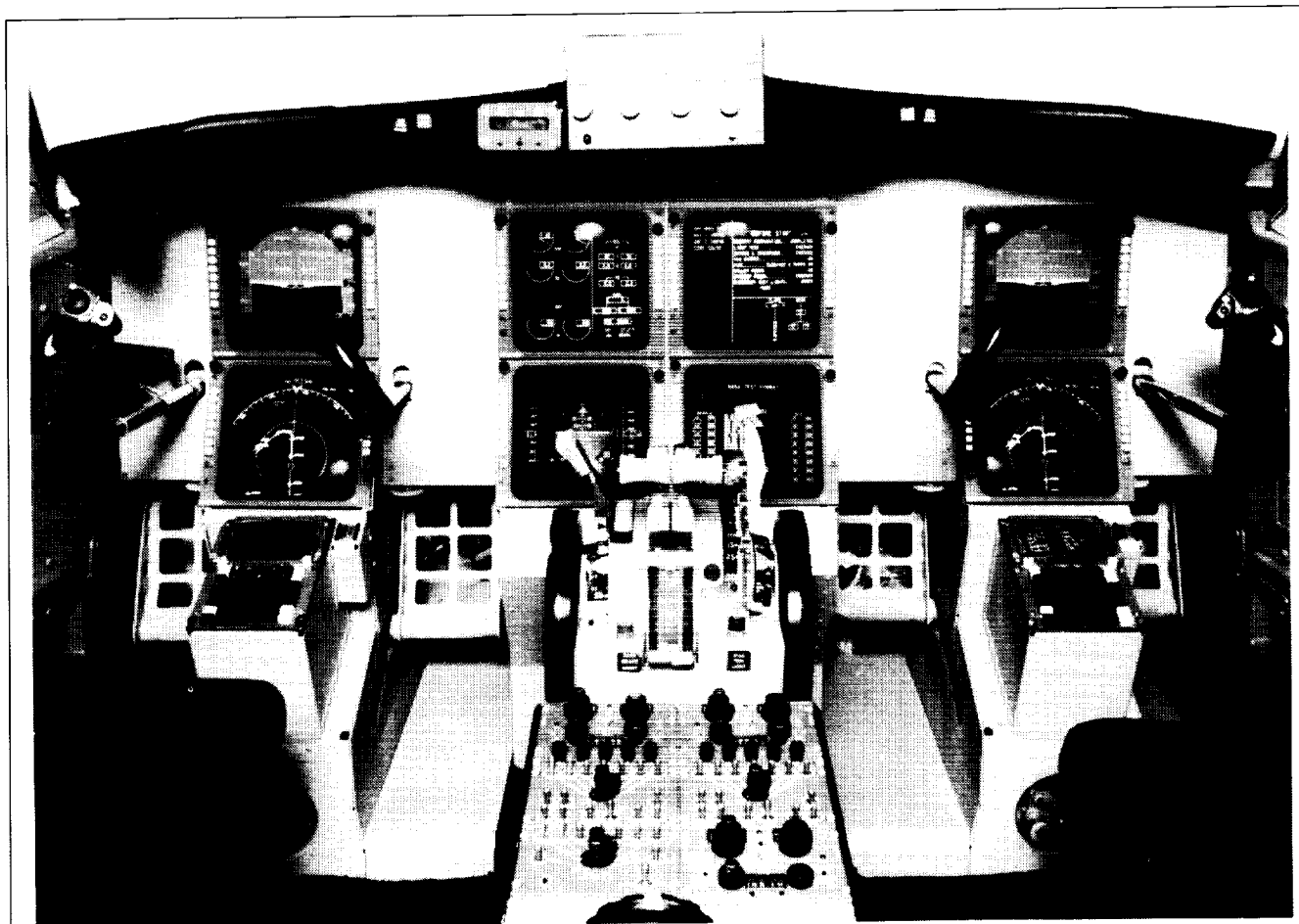
*The TSRV has two flight decks: a conventional Boeing 737 flight deck provides operational support and safety backup, and the fully operational research flight deck, positioned in the aircraft cabin, provides the capability to explore innovations in display formats, contents, and in-aircraft operations.*

*The "all-glass" research flight deck presents information to the crew via eight 8-in.-square electronic displays representative of the technology to become available in commercial transports in the 1990's. The state-of-the-art color displays are driven by new, onboard computers and, most importantly, specially developed computer software. These new technologies make it possible to more clearly display information presented only partially or in scattered locations on existing electromechanical and first-generation electronic displays in today's aircraft.*

*In addition to video concepts for primary flight and navigation displays in front of both the pilot and copilot, center panel displays provide the capability to monitor engine and*

*system status and to manage aircraft systems operation. The center panel displays will permit research on how additional information can be displayed and used to improve situational awareness, air traffic control communications, flight management options, and traffic awareness.*

*The TSRV Simulator provides the means for ground-based simulation in support of the ATOPS research program. The Simulator, which has recently been modified to duplicate the upgraded aft flight deck located in the TSRV, allows proposed concepts in such areas as guidance and control algorithms, new display techniques, operational procedures, and man/machine interfaces to be thoroughly evaluated. Four out-the-window*



New TSRV aft cockpit configuration.

1-87-3645

*display systems (driven by an Evans and Sutherland CT-6 Computer-Generated Imagery system) allow realistic real-world scenes to be presented to the crew. The system is capable of daytime, nighttime, and all ranges of weather effects. Promising simulation research results become the subjects of actual flight test research.*

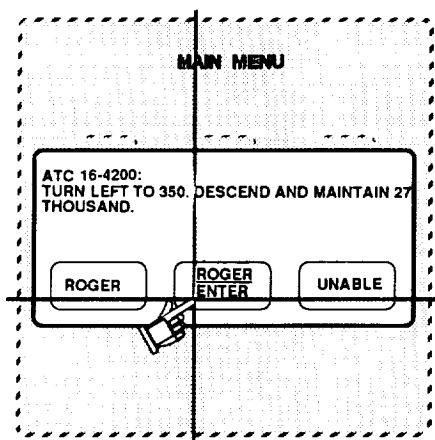
### **Flight Tests Using Data Link for Air Traffic Control and Weather Information Exchange**

Message exchange for air traffic control (ATC) purposes via data

link offers the potential benefits of increasing airspace system safety and efficiency by reducing communications errors and relieving the overloaded ATC radio frequencies that hamper efficient message exchanges during peak traffic periods in many busy terminal areas. The objective of the first data link flight test conducted in the TSRV B-737 airplane was to evaluate the use of data link as the primary communications source for ATC strategic and tactical clearances, for weather information, and for company messages during a typical commercial airline flight from takeoff to landing. A user friendly data link system

interface, incorporating a menu selection with an overlapping windows format concept (see the figure) was designed and implemented in the TSRV airplane. A flight test was conducted using 7 airline pilot crews, each flying 3 different flight paths, each approximately 250 miles long. One of these paths was a baseline flight in which normal voice communications were used. The other two paths were flown using data link as the primary communications source with voice radio as a backup source. Data collected during these tests included video recordings of the flight displays and the actions of the crew in the cockpit, audio

### Data link menu/window format concept



### ATC/airplane communication confusion, errors, & repeats

	VOICE	DATA LINK
<b>CONFUSION</b>	<b>5</b>	<b>0</b>
DIDN'T KNOW IF CLEARED TO LAND	1	--
WENT TO WRONG WAYPOINT	1	--
DIDN'T KNOW HEADING FOR VECTOR	1	--
DIDN'T KNOW ALTITUDE ASSIGNMENT	1	--
<b>ERRORS</b>	<b>7</b>	<b>4</b>
WENT TO WRONG WAYPOINT	1	--
FREQ SEL / RADIO OPS INCORRECT	2	3
MISSED CROSSING ALTITUDE	1	--
CLEARANCE READ BACK INCORRECT	3	--
DIDN'T CONTACT ATC	--	1
<b>REPEATS</b>	<b>46</b>	<b>6</b>
MISSED ALL/PART OF CALL	34	2
DUE TO ERRORS OR CONFUSION	12	4

*Data link display format and results of flight test conducted in TSRV B-737 airplane.*

recordings of all radio communications, and all data link message transmissions.

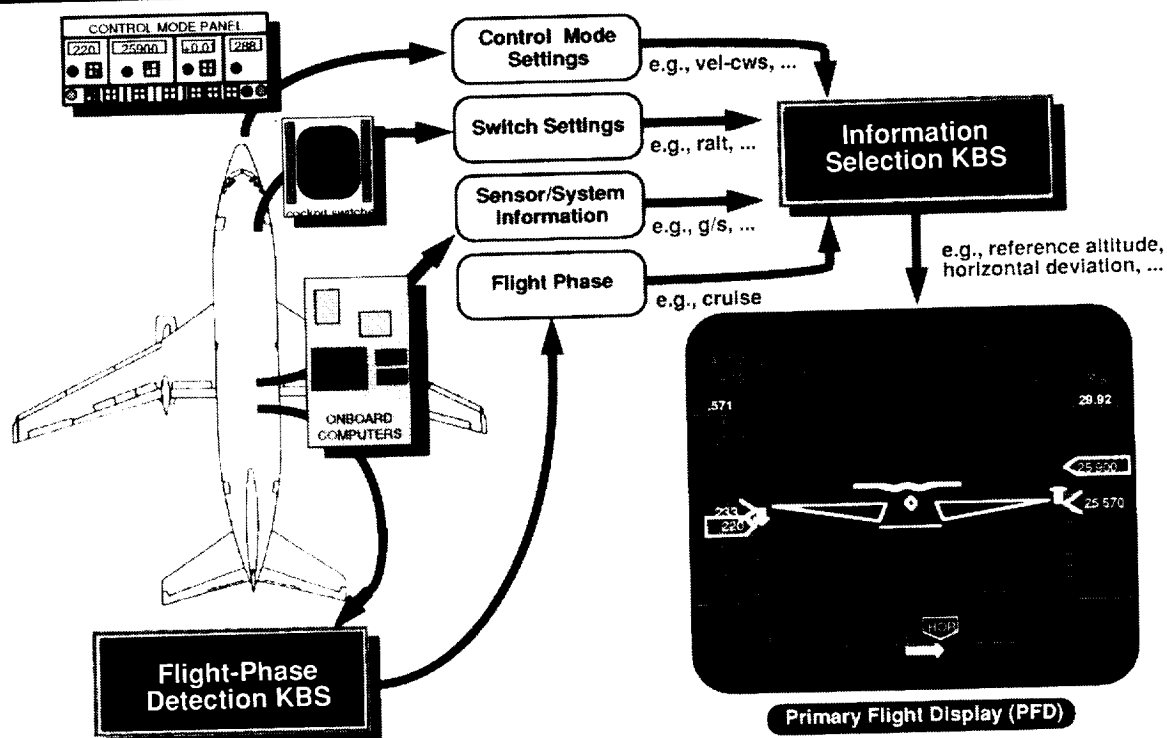
Analysis of the data shows an almost total elimination of confusion, errors, and voice communications repeats (see the figure) with the flights conducted with data link as the primary communications device. The majority of the test crews believed that data link, in general, would reduce the work load and mistakes of the nonflying pilots. All the test crews indicated that the menu/window format concept was very user friendly and required little training to use. (Charles E. Knox and Charles H. Scanlon, 42038)

### Knowledge-Based Flight Display Information Management

The amount of information already in today's civil transport cockpit, the difficulties experienced in managing the large amount of information, and the trend to increase the amount of information in future cockpits have made information management a primary concern. Therefore, an overall research objective has been established to develop concepts that will help flight crews manage the extensive amount of available information. As an initial step toward this overall objective, managing information on the primary flight display (PFD) is being explored using a task-tailoring approach. This task-tailored approach requires complex logic that led to difficult-to-manage software when traditional programming techniques were used. As a

result, a knowledge-based system (KBS) approach was chosen over the traditional programming approach; this choice was based on an earlier study that found KBS architectures were easier to manage in complex applications. The objective of this particular study was to test in flight the KBS's, collectively called the Task-Tailored Flight Information Manager (TTFIM), to validate their implementation and integration.

The TTFIM consists of two KBS's, one for information selection and the other for flight phase detection (as shown in the figure). The TTFIM was validated onboard the TSRV aircraft in two stages. The first stage of flight tests tested the KBS that selected the display information to be presented. For these initial flights, the flight engineer manually entered the flight phase. The second KBS, for flight phase detection, was then flight tested with a flight test



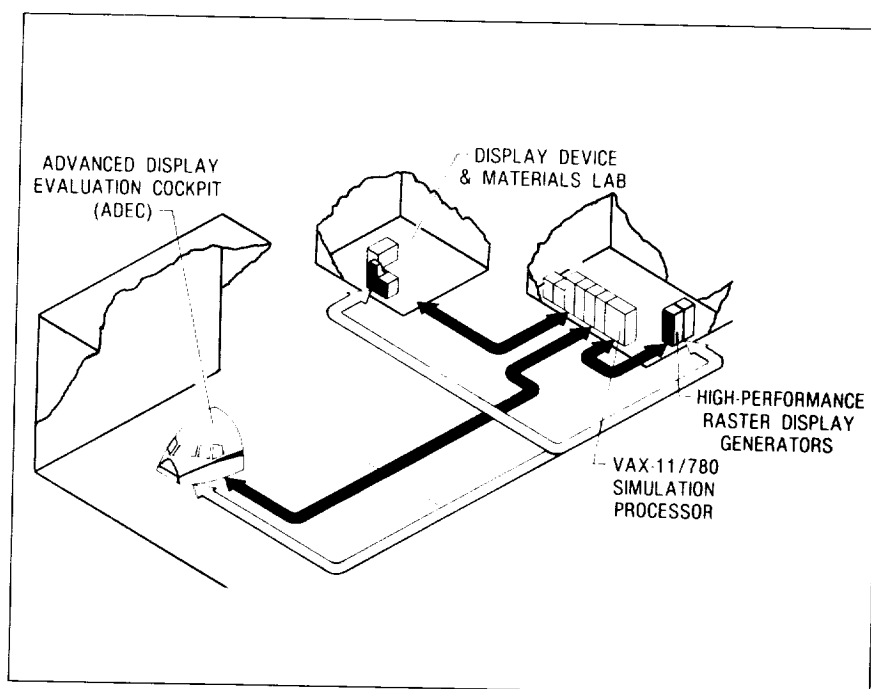
**Flight Validated:**

- Flight-phase detection logic
- Feasibility of using KBS concept for this real-time civil-transport application
- Software engineering advantages (designer and programmer productivity) of KBS approach in operational environment

*Task-Tailored Flight Information Manager (TTFIM).*

envelope consisting of multiple repetitions of each flight phase represented in the KBS and with multiple transitions between the flight phases. The flight tests successfully validated the KBS concept for PFD information management. Correct presentation of information on the PFD during all flight tests validated the implementation of the information selection KBS and the integration of the two KBS's with each other and with the existing TSRV systems. As expected, the KBS for information selection was not as

computationally fast as its equivalent traditional system when selecting some information, but this lack of speed did not interfere with cockpit operations.  
(Wendell R. Ricks, 46733)



## Crew Station Systems Research Laboratory

The trend in modern cockpits has been to replace electromechanical instruments with electronic control and display devices. The NASA Crew Station Electronics Technology research program is at the forefront of this trend with research and development activities in the areas of advanced display media, display generation, and cockpit controls/displays/flight subsystems integration. Specific areas of current interest are high-performance stereo pictorial primary flight display graphics; information management techniques; large-screen full-color display media; wide-screen, panoramic display concepts; virtual, panoramic, real-world displays; and image sensor fusion techniques.

The Crew Station Systems Research Laboratory (CSSRL) serves as a primary testing facility for the concepts and devices emerging from this research program. The laboratory provides a unique civil capability to conduct iterative development and pilot/vehicle experimental evaluation research for advanced cockpit technologies in a highly realistic flight simulation environment. The CSSRL also provides a lighting research facility that represents the full range of ambient and solar lighting conditions to be encountered by an aircraft cockpit and allows for the determination of not only the lighting characterizations of cockpit displays but also the determination of pilot/vehicle performance effects under realistic lighting conditions.

Major elements of the CSSRL are the Advanced Display Evaluation Cockpit (ADEC), which is a reconfigurable research cab; the Aircraft Cockpit Ambient Lighting and Solar Simulator (ACALSS), which provides real-world ambient and solar lighting conditions to the ADEC cockpit; and two separate general-purpose digital processors, one of which handles system input/output and vehicle math model simulation, while the other acts as host processor and preprocessor for two graphics generators. Other major elements include three high-performance raster graphics display generators (one of which has its own host co-processor), which provide sophisticated graphics formats to the display devices (cathode-ray tubes, flat panels, and helmet-mounted displays); a fiber



optic link to the central computing facility, which can provide high-fidelity simulation math models for research requiring more complex vehicles; and a Display Device and Materials Laboratory, which provides facilities for flat-panel materials/device technology developments and photometric bench evaluations.

### **Ambient Lighting Simulator Experiment for High-Brightness TFEL Display**

Advanced flat-panel display technologies offer advantages over cathode-ray tube (CRT) displays in form/fit, power, and weight and are under consideration for use in next-generation transports. Under certain external lighting conditions, however, the pilot's ability to obtain useful information from these displays may be severely limited by display washout. Standard thin-film electroluminescent (TFEL) displays are often susceptible to these washout conditions, and high-brightness augmentation techniques have attempted to alleviate the problem. The goal of this effort was to determine the washout performance of a high-brightness TFEL panel, a spin-off of NASA/U.S. Army sponsored research, in comparison to other competing display technologies.

Langley Research Center has developed the Aircraft Cockpit Ambient Lighting and Solar Simulator (ACALSS), which simulates a full range of adverse lighting conditions, in order to study display readability effects in a cockpit simulator (see the first



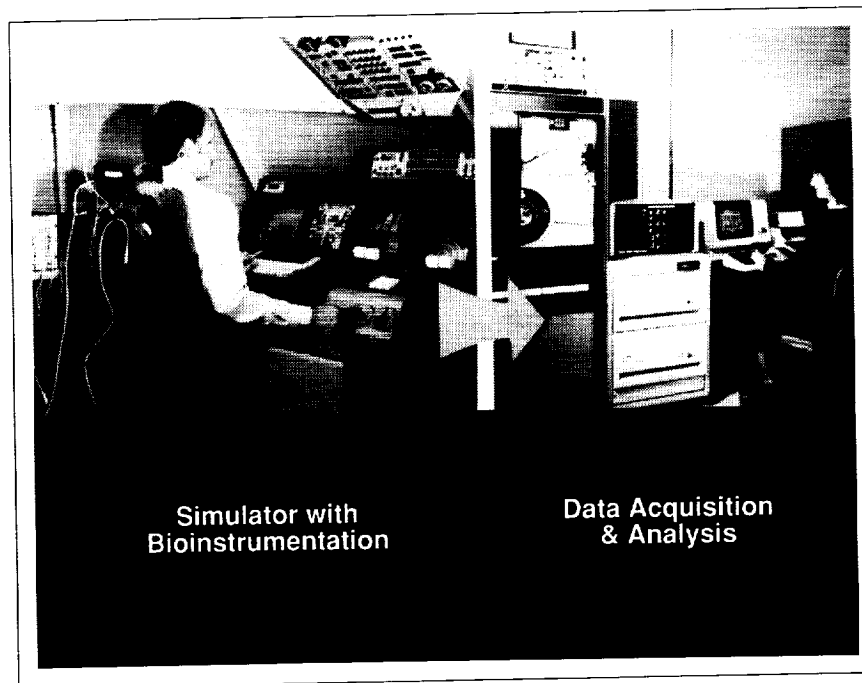
*Simulator used to study adverse lighting effects upon display media.*

figure). The ACALSS was used to determine the external brightness levels at which subjects lose the ability to maintain aircraft states when using three competing display technologies for information input. The display technologies examined were a standard monochrome TFEL panel, a laboratory-class monochrome CRT, and a high-brightness TFEL panel. Six subjects controlled a simulated transport aircraft using speed, heading, altitude, and attitude information presented in a primary flight display (PFD) format. The experiment determined the washout levels of each display for a "shafted sun" lighting condition (i.e., direct sunlight on the display surface through the side window) by measuring the subject/vehicle performance errors from constant speed, heading, and altitude conditions (in turbulence) at incremental brightness levels.

The standard monochrome TFEL display began to wash out after the 2000-ft-cd level of illumi-

nation. The monochrome CRT display began to wash out after the 5500-ft-cd level, and no performance decrements were found for the high-brightness monochrome TFEL display levels up to 13 000 ft-cd.

(Vernon M. Batson, James B. Robertson, and Russell V. Parrish, 46649)



## Human Engineering Methods Laboratory

---

*The Human Engineering Methods (HEM) Laboratory has been established to develop measurement technology to assess the effects of advanced crew station concepts on the crew's ability to function without mental overload, excessive stress, or fatigue. The laboratory provides the capability for measurement of behavioral and psychophysiological response of the flight deck crew.*

*The facility comprises state-of-the-art bioinstrumentation as well as computer-based physiological data acquisition, analysis and display, and experiment control capability. Software has been developed which enables the demonstration of work load effects on the steady-state evoked brain response and transient evoked response signals as well as the monitoring of electrocardiographic*

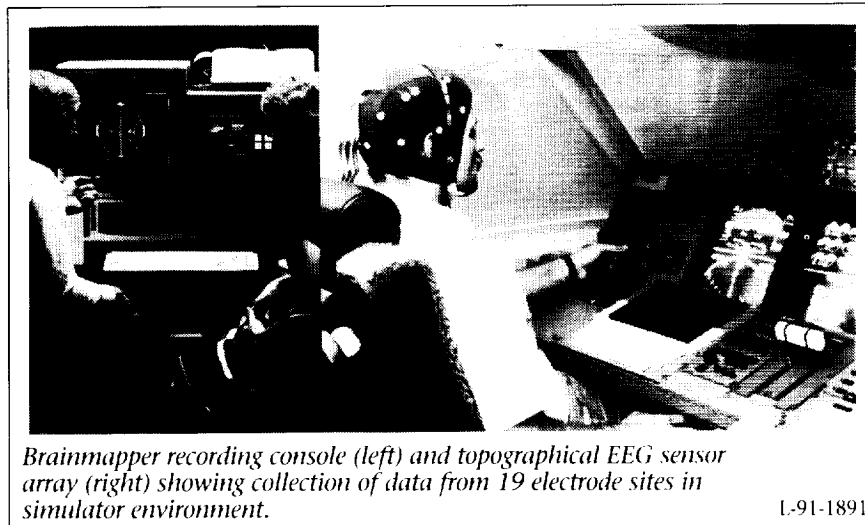
*(EKG), electromyographic (EMG), skin temperature, respiration, and electrodermal activity.*

*The Langley Research Center developed oculometer capability has been integrated with the other physiological measurement techniques. Subjective rating and secondary task methods for assessing mental work load also have been implemented. A computer-based criterion task battery is available for preliminary testing (with human subjects) of work load techniques that are being validated prior to evaluation and application in the simulators. Satellite physiological signal conditioning and behavioral response capture stations are located at the simulator sites to provide human response measurement support for flight management and operations research.*

### **Brainmap Analysis Identifies States of Awareness for System Monitoring Tasks**

---

Analysis of the Aviation Safety Reporting System (ASRS) data base reveals that flight crew members often relate their mistakes to their experience of certain states of awareness. These crew members, whose responsibility it is to monitor and manage the progress of highly complex systems, lapse into states that are incompatible with the demands of that task. These states can be characterized as hazardous. As automated systems become more capable, conditions that induce hazardous states are more likely. The objective of this research is to determine the



Brainmapper recording console (left) and topographical EEG sensor array (right) showing collection of data from 19 electrode sites in simulator environment.

L-91-1891

physiological correlates of hazardous and effective states experienced during a monitoring task.

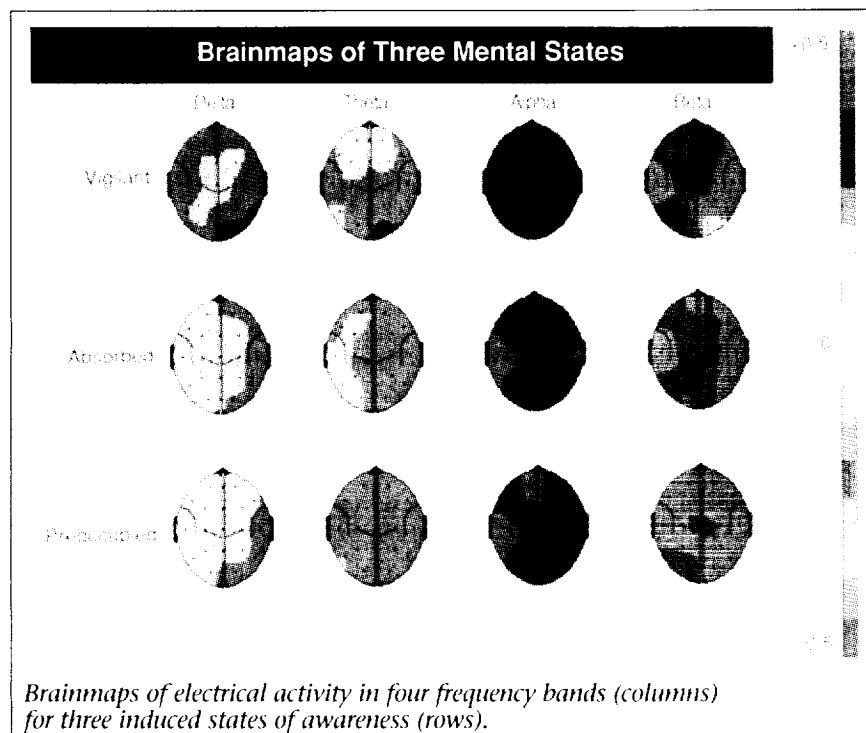
Prerecorded instructions guided individuals, in a console-monitoring setting, through exercises designed to induce target mental states. Directions to experience three target states

(vigilant, absorbed, or preoccupied) were alternated with 5-min periods during which individuals directed their awareness as instructed, and topographical electroencephalographic (EEG) data were recorded from 19 electrode sites (see the first figure). For each individual, data from the first (test) session were used to derive state discriminant

functions. Data from a second (retest) data collection session were classified using the discriminant functions derived from the test set of data.

The brainmaps shown in the second figure reveal that certain electrode sites exhibit activity in the Alpha and Beta frequency bands which is different across the three states. Across six individual cases, discriminant functions have correctly assigned better than 90 percent of the initial data and averaged better than a 60-percent correct identification of retest data. The state identification procedure, then, represents a technology for objectively indexing mental-state experiences within individuals to be used to subsequently identify these states when they occur in these same individuals under operational conditions. This technology provides the capability for evaluating the design of flight management aids, including automation and information transfer technologies, based on their capacity to promote effective performance states.

(Alan T. Pope and Edward H. Bogart, 46642)



Brainmaps of electrical activity in four frequency bands (columns) for three induced states of awareness (rows).

### Multi-Attribute Task (MAT) Battery for Pilot Strategic Behavior

The definition and measurement of strategic behavior in a complex environment is crucial to understanding pilot performance, work load, and complacency. Strategic behavior is defined as the action (or inaction) that an operator takes in order to change the

task structure, sequence of responding, or allocation of mental resources with the purpose of dealing with unexpected change in the environment, achieving a more manageable work load, and/or achieving one's goal safely and efficiently. The objective of this effort was the development of a real-time, interactive MAT Battery to facilitate studies on strategic behavior, work load, and complacency.

A flexible MAT Battery was developed, utilizing desktop computer technology, for broad application in laboratory environments. The design incorporates tasks analogous to activities that crew members perform in flight, while providing a high degree of experimenter control of task activities, automatic collection of behavioral response data, and freedom to use nonpilot test subjects. Features not found in existing computer-based tasks

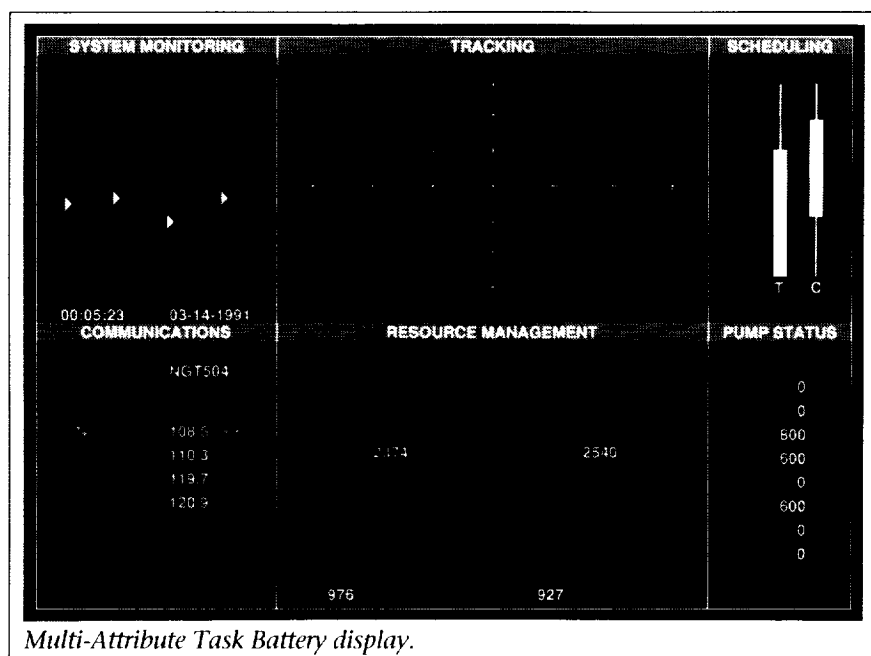
include an auditory communication task (to simulate ATC communications) and a resource management task permitting many strategies for maintaining target performance. In addition, the MAT Battery was designed so that the task can be paused and onscreen work load rating scales presented to the subject.

The MAT Battery display, shown in the first figure, presents up to four different tasks to the operator and allows the operator many different strategies for achieving good performance, including the use of automation. In an initial study, which served to validate the effectiveness of task-activity-level manipulation and to demonstrate the readiness of the MAT Battery, 92-min test sessions were employed with task activity levels patterned after a flight profile (high-low-high). Timing signals sent from the MAT Battery permitted simultaneous recording of

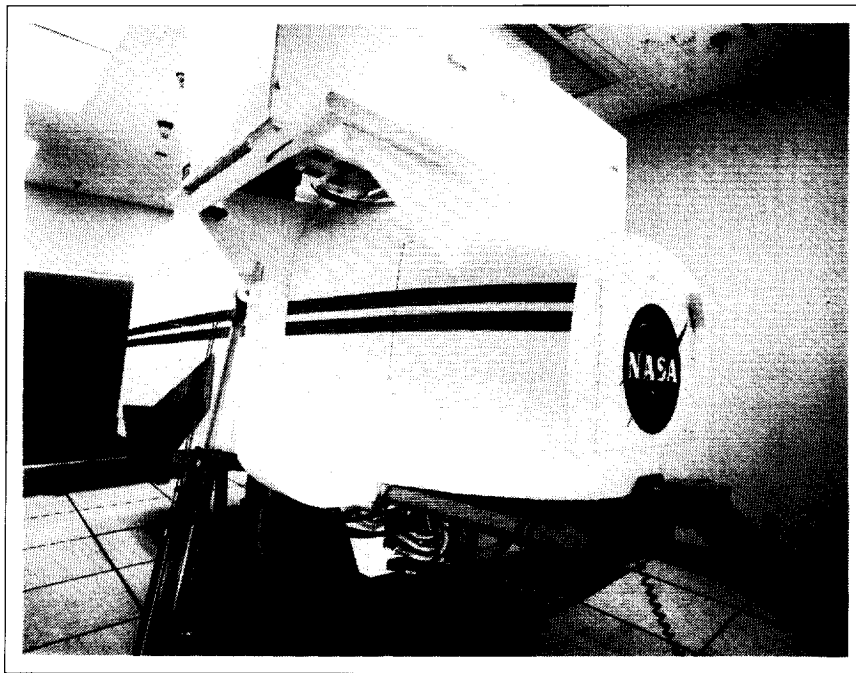
topographic EEG, eye movement/lookpoint, pupil diameter, heart rate and heart rate variability, and subjective work load ratings.

Enthusiastic requests to use the MAT Battery have been received from other government laboratories and universities involved in strategic behavior, work load, and complacency research.

(J. Raymond Comstock, Jr., and Ruth J. Arnegard, 46643)



Multi-Attribute Task Battery display.



# General Aviation Simulator

---

*The General Aviation Simulator (GAS) consists of a general-aviation aircraft cockpit mounted on a three-degree-of-freedom motion platform. The cockpit is a reproduction of a twin-engine propeller-driven general-aviation aircraft with a full complement of instruments, controls, and switches, including radio navigation equipment. Programmable control force feel is provided by a "through-the-panel" two-axis controller that can be removed and replaced with a two-axis side-stick controller that can be mounted on the pilot's left-hand, center, or right-hand position. A variable-force-feel system also is provided for the rudder pedals. The pilot's instrument panel can be configured with various combinations of cathode-ray tube (CRT) displays and conventional instruments to represent aircraft such as the Cessna 172, Cherokee 180, and Cessna 402B.*

*A collimated-image visual system provides a 60° field-of-view out-the-window color display. The visual system accepts inputs from a Computer-Generated Image (CGI) system. A Calligraphic/Raster Display System (CRDS) is used to generate the heads-down displays and for mixing with the CGI for the heads-up display. The simulator is flown in real time with a CDC CYBER 175 computer to simulate aircraft dynamics.*

*Research has been conducted to improve the ride quality of general-aviation (GA) aircraft by developing gust alleviation control laws to reduce the aircraft response to turbulence while still maintaining generally good flying characteristics. Research studies that are in progress are the GA Easy Fly, a program to investigate ways of making general-aviation airplanes easier to fly, especially for low-time or*

*nonpilots, and a piloted simulation study to address handling qualities issues of advanced commuter-type turboprop configurations.*

## Easy-to-Fly General-Aviation Airplane Concept

---

Two advanced systems for general-aviation novice pilots have been developed and studied over the past few years. The first system is a fly-by-wire automatic control system (Ez-Fly), and the second is a head-up pictorial display (Highway in the Sky or HITS). Refinements have been incorporated into both systems to further reduce the time required for a first-time novice to learn how to successfully fly a complete mission. The Ez-Fly control system was improved by



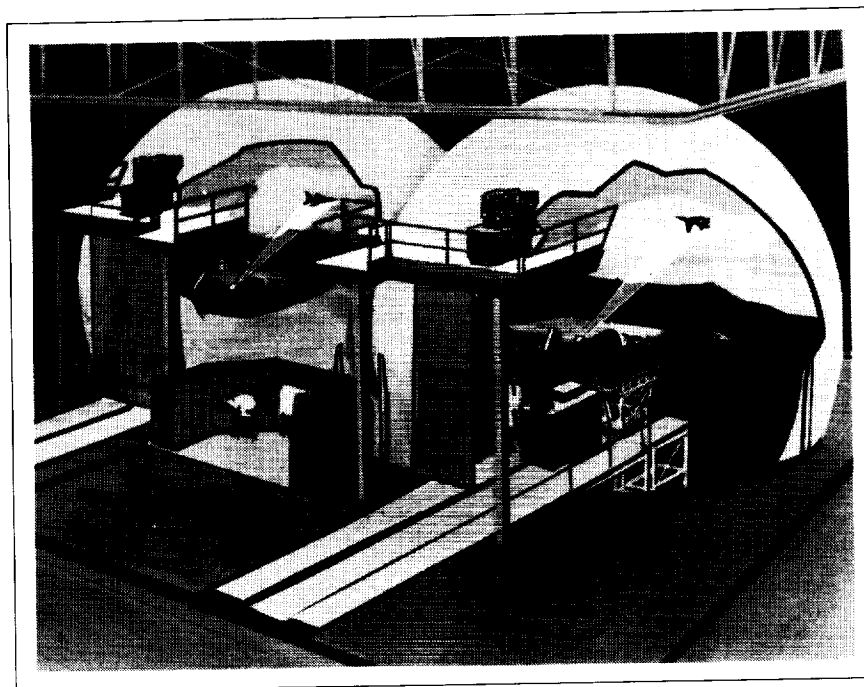
*Cockpit of General Aviation Simulator used to study advanced systems.*

1-90-1378

adding an automatic control-force trim feature. This feature was added so that the pilot no longer has to manually trim the longitudinal control forces to zero after making a large control input. Control force trim, which has no analog in automobile driving, had proved to be difficult for the novice pilot. Failure to keep the control forces trimmed to near-zero values resulted in degraded vertical speed control in many instances. Another improvement to the Ez-Fly control system was an automatic reduction in the gain of the longitudinal wheel during a final approach, in which precise control was needed.

The HITS display was also improved. Color was added to the display to help differentiate the features. In addition, boxes or hoops were added to the basic highway representation. The tops

of the hoops gave the pilot better cues for determining the desired altitude, and the sides of the hoops provided better lateral displacement cues. Supplementary flight director arrows also were studied. Although pursuit-type flight directors are ordinarily preferred by untrained subjects, the wide range of gains required in a complete mission made this addition to HITS impractical. In addition, the effect of the hoops was to reduce the need for any flight director arrows. The normal compensatory flight director arrows remain useful for rotation during takeoffs and for the flare maneuver during landings. (Eric C. Stewart, 43939)



# Differential Maneuvering Simulator

The Langley Differential Maneuvering Simulator (DMS) provides a means of simulating two piloted aircraft operating in a differential mode with a realistic cockpit environment and a wide-angle external visual scene for each of the two pilots. The system consists of two identical fixed-based cockpits and projection systems, each based in a 40-ft-diameter projection sphere. Each projection system consists of two terrain projectors to provide a realistic terrain scene and a system for target image generation and projection. The terrain scene driven by a Computer-Generated Image (CGI) system provides reference in all six degrees of freedom in a manner that allows unrestricted aircraft motions. The resulting sky/Earth scene provides full translational and rotational cues. The internal visual scene also provides continuous rotational and bounded (300 ft to

45 000 ft) translational reference to one or two other (target) vehicles in six degrees of freedom.

The target image presented to each pilot represents aircraft being flown by the other pilot in this two-aircraft simulator. This dual simulator can be tied to a third dome and can provide three aircraft interactions when required. Each cockpit provides three color displays with a 6.5-in. square viewing area and a wide-angle head-up display. Kinesthetic cues in the form of a g-suit pressurization system, helmet loader system, g-seat system, cockpit buffet, and programmable control forces are provided to the pilots consistent with the motions of their aircraft. Other controls include a side arm controller, dual throttles, and a rotorcraft collective. Research applications include studies of high-angle-of-attack flight control

laws, evaluation of evasive maneuvers for various aircraft and rotorcraft, and evaluations of the effect of parameter changes on the performance of several baseline aircraft.

## One-Versus-Two Air Combat Study

Many recent investigations have shown that the use of enhanced high-angle-of-attack maneuvering improves effectiveness during close-in one-versus-one air combat. The studies have outlined some of the maneuvers that provide advantages as well as quantified the agility enhancements needed. This capability can be achieved through the use of multiaxis thrust-vectoring or advanced aerodynamic controls.



*View of DMS cockpit and visual display.*

L-90-5139

Studies are now under way to determine the extent to which one-versus-one air combat advantages obtained from enhanced high-angle-of-attack agility carry over to close-in engagements against two opponents.

The current investigation involves piloted simulation studies using a recently developed capability that combines the DMS and the General-Purpose Fighter Simulator (GPFS). The GPFS is a single-dome facility that has been linked with the DMS to allow simulation of piloted one-versus-two engage-

ments. A full-envelope simulation model of an F-18 airplane incorporating multiaxis thrust vectoring is being used to represent the enhanced maneuvering airplane while a model of the baseline F-18 is used as the two opponent airplanes. Early results confirm that high-angle-of-attack agility advantages persist in the one-versus-two air combat environment. Continuing studies will evaluate the necessary flight dynamics requirements and further quantify the advantages.  
(Keith D. Hoffler, 41144)

### **Velocity-Vector Display in High-Alpha Air Combat Situations**

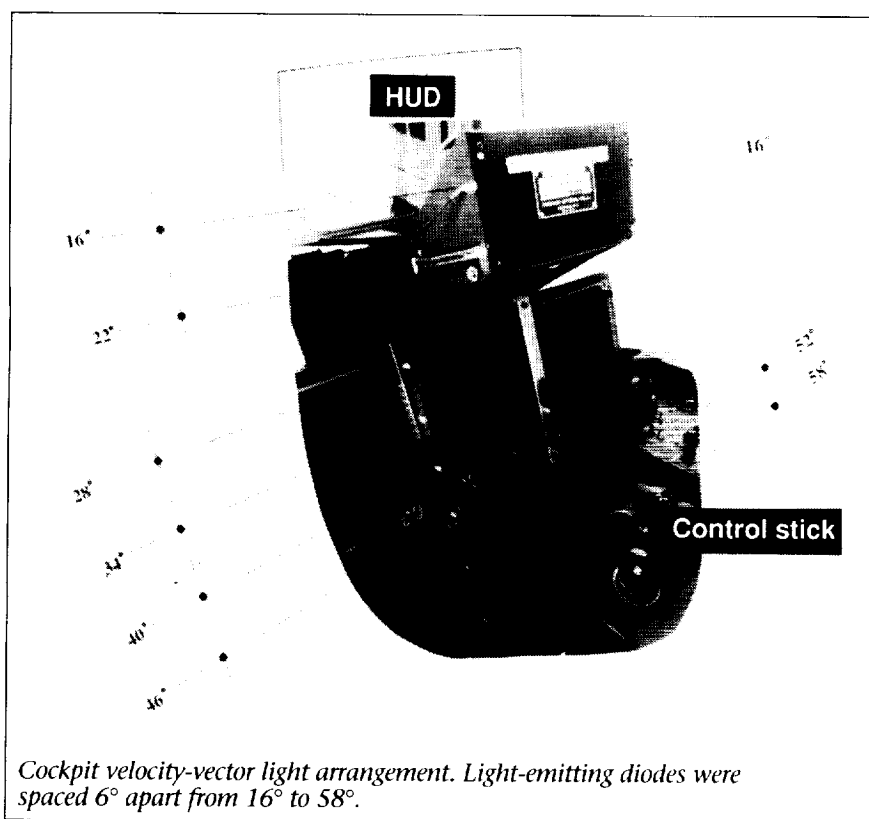
Recent developments in high-alpha controls have accentuated the perceived need of pilots to know conformally where the aircraft's velocity vector is at all times. In order to determine if the location of the velocity vector was needed during high-alpha maneuvering in an air combat situation, a simulation experiment was performed in the DMS using a modified F-18 model that employed

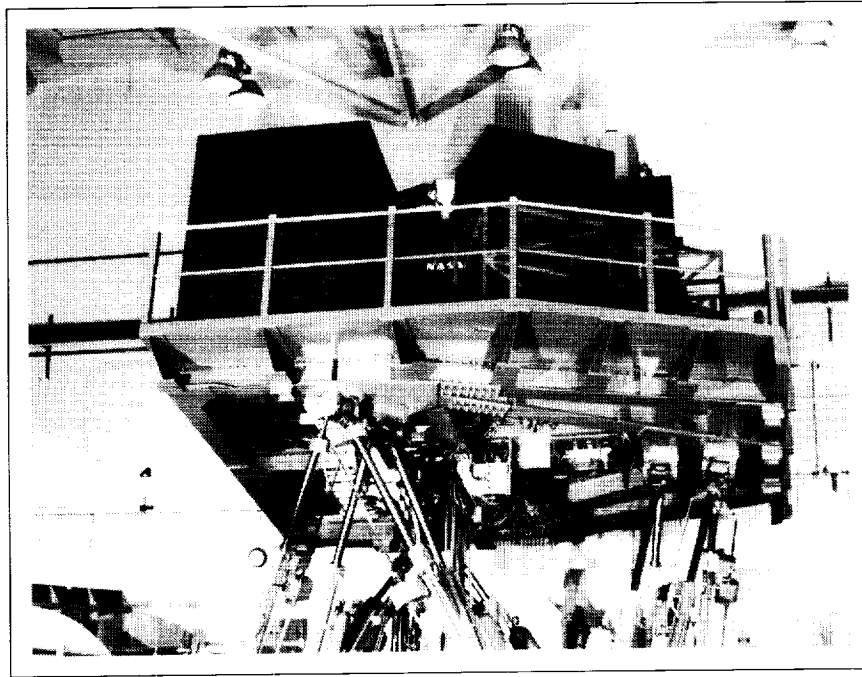


thrust vectoring for control. The conformal (aligned with the real-world) velocity-vector display was implemented as a string of lights (shown in the figure) in the vertical plane of the aircraft. The concept used was that a straight line drawn between the pilot's eye and the illuminated light would form a vector parallel to the aircraft's velocity vector. Two vertical rows of lights to the left and right of the HUD were used to prevent complete occlusion by the center control stick. The lights closest to the position of the velocity vector were illuminated and flashed at a 5-Hz rate. The experimental portion of the study required the test subjects to fly a simulated air-to-air engagement against an intelligent and equally capable opponent.

The results are based on subjective questionnaire responses by four pilots who had varying degrees of air-combat experience. The most important task for the air-combat pilots is to track their opponents visually and never lose sight of them. However, because of the large off-angles between the two aircraft and the human field-of-view limitations, the test subjects cannot see the lights during the majority of the engagement without looking away from the opponent. From this, all four pilots concluded that the velocity-vector lights were of no benefit during the air-to-air engagement. Further, they felt that the velocity-vector information was not needed for this task. The results are significant in that they are completely contrary to the information needs that have been perceived by the pilots

and display designers. However, other tasks may exist besides air combat which may benefit from this type of information display. (James R. Burley II and Denise R. Jones, 42008)





## Visual Motion Simulator

---

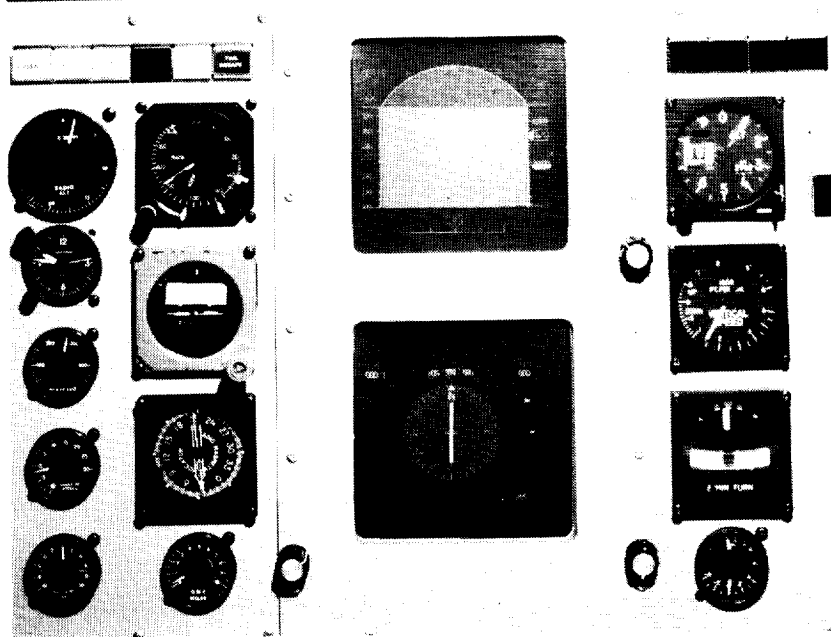
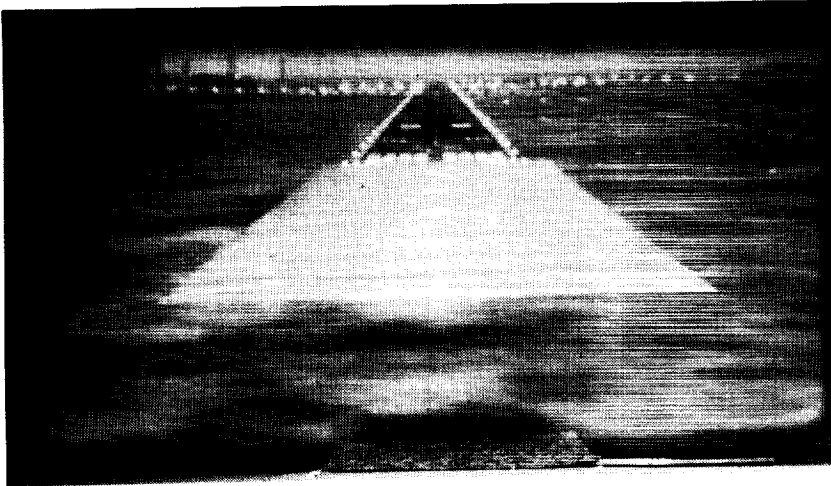
*The Visual Motion Simulator (VMS) is a general-purpose simulator consisting of a two-person cockpit mounted on a six-degree-of-freedom synergistic motion base. Three collimated visual displays, compatible with the Computer-Generated Image (CGI) system, provide out-the-window scenes for the left seat front and side windows and for the right seat front window. Three electronic displays mounted on the left side instrument panel provide for displays generated by a graphics computer. A programmable hydraulic controlled two-axis side stick and rudder pedals provide for roll, pitch, and yaw controls in the left seat. A second programmable hydraulic-control loading system for the right seat provides roll and pitch controls for either a fighter-type control stick or a helicopter cyclic controller. Right-side rudder control is an extension of the left-side rudder control system. A*

*friction-type collective control is provided for both the left and the right seats. An observer's seat was installed in 1986 to allow a third person to be in the cockpit during motion operation.*

*A realistic center control stand was installed in 1983 which, in addition to providing transport-type control features, provides auto-throttle capability for both the forward and reverse thrust modes. Motion cues are provided in the simulator by the relative extension or retraction of the six hydraulic actuators of the motion base. Washout techniques are used to return the motion base to the neutral point once the onset motion cues have been commanded.*

*Research applications have included studies for transport, fighter, and helicopter aircraft including the National Aero-Space Plane (NASP),*

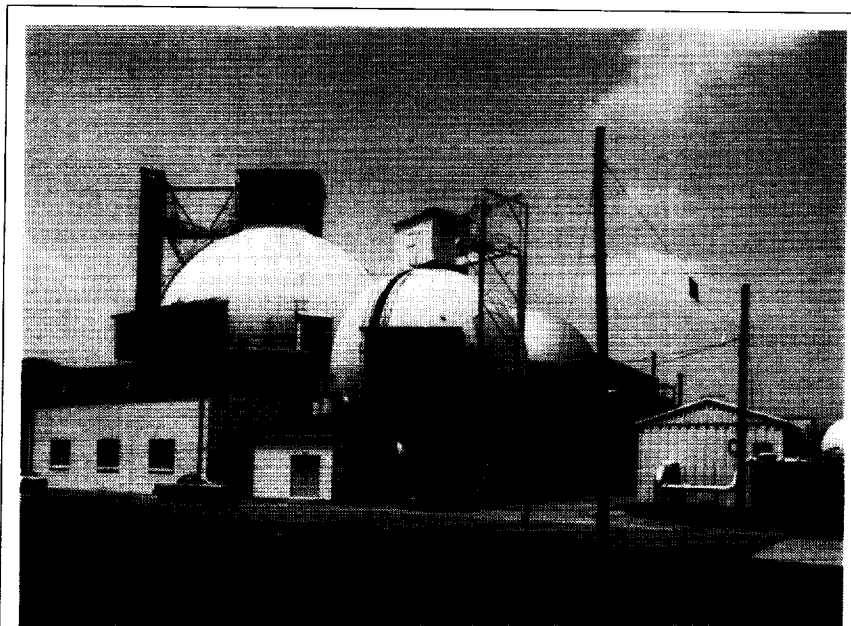
*Personnel Launch System (PLS), and High-Speed Civil Transport (HSCT). These studies addressed phenomena associated with wake vortices, high-speed turnoffs, microwave landing systems, energy management, noise abatement, multibody transports, maneuvering stability flight characteristics, wind shear recovery guidance, vortex flaps, and stereographic displays. Numerous simulation technology studies also have been conducted to evaluate the generation and usefulness of motion cues.*



*Cockpit display.*

1-90-13684

ORIGINAL PAGE  
BLACK AND WHITE PHOTOGRAPH



60-ft-diameter Space Simulation Sphere.

## Space Simulation and Environmental Test Complex

---

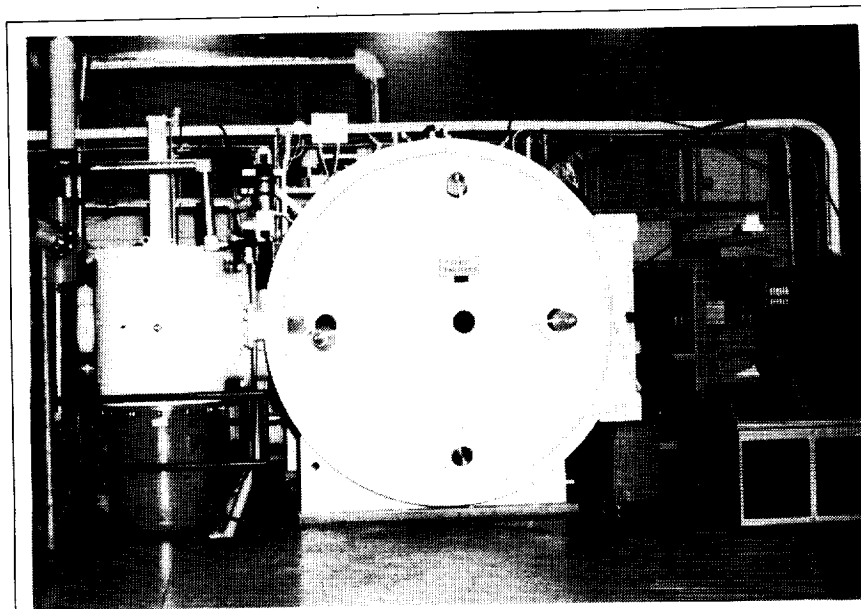
The 60-ft-diameter Space Simulation Sphere (Building 1295) can simulate an altitude of 320 000 ft ( $2 \times 10^{-4}$  mm Hg). This vacuum level is attainable in 7 hours with a three-stage pumping system. The carbon steel sphere is accessible through a personnel door, a 12-ft-diameter specimen door, and a 4-ft maintenance door at the top. A 2-ton hoist located at the top enhances specimen handling inside the sphere. Sight ports are located both at the top and at the equator. Two closed-circuit television cameras, a videocassette recorder, and an oscillograph are available. Firing circuitry and a programmer are available for the use of pyrotechnics, and a system of flood lights is installed in the sphere to facilitate high-speed photography. The sphere is used primarily for dynamic testing of

aerospace components and models at a near-space environment.

Thermal-vacuum testing has long been a prerequisite to the active deployment of space experiments. A series of experiments, which optically sense characteristics of the Earth's atmosphere from outer space, necessitated the creation of an ultra-high-cleanliness thermal facility. The optical components of these experiments would be severely degraded by contamination by oils or other vaporous materials commonly found in thermal chambers and vacuum pumping systems. Langley Research Center upgraded the 8- by 15-Foot Thermal-Vacuum Chamber (in Building 1250) by repeated vacuum bakeout and solvent wipedown. Two 35-in. cryogenic pumps were installed,

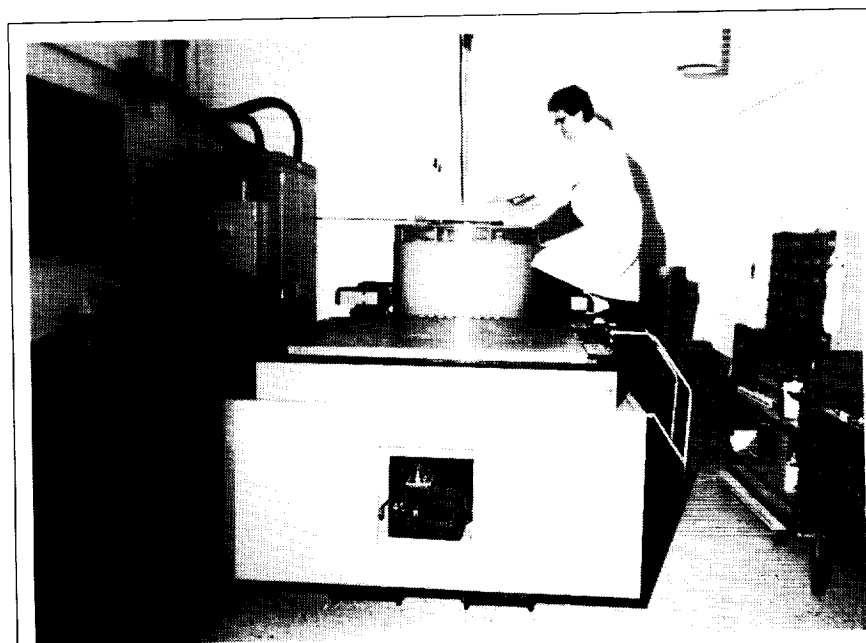
and cold traps were inserted in the roughing pump lines to eliminate back contamination from the pumps. The chamber is capable of  $-300^{\circ}\text{F}$  to  $1000^{\circ}\text{F}$  temperatures and has glass ports for solar illumination simulation.

A 5- by 5-Foot Thermal-Vacuum Chamber (also in Building 1250) augments the thermal testing capability. The smaller stainless-steel chamber is used for subsystem and component testing. A completely enclosed liquid-nitrogen cryopanel with sight ports that have externally adjustable irises can cool the ambient temperature to  $-300^{\circ}\text{F}$ . Removable heater banks are used for precise temperature control and high ambient temperature applications. The chamber uses a  $570 \text{ ft}^3/\text{min}$  roughing



8- by 15-Foot Thermal-Vacuum Chamber.

1-82-9672



Unholtz-Dickie T-1000 shaker.

1-85-10833

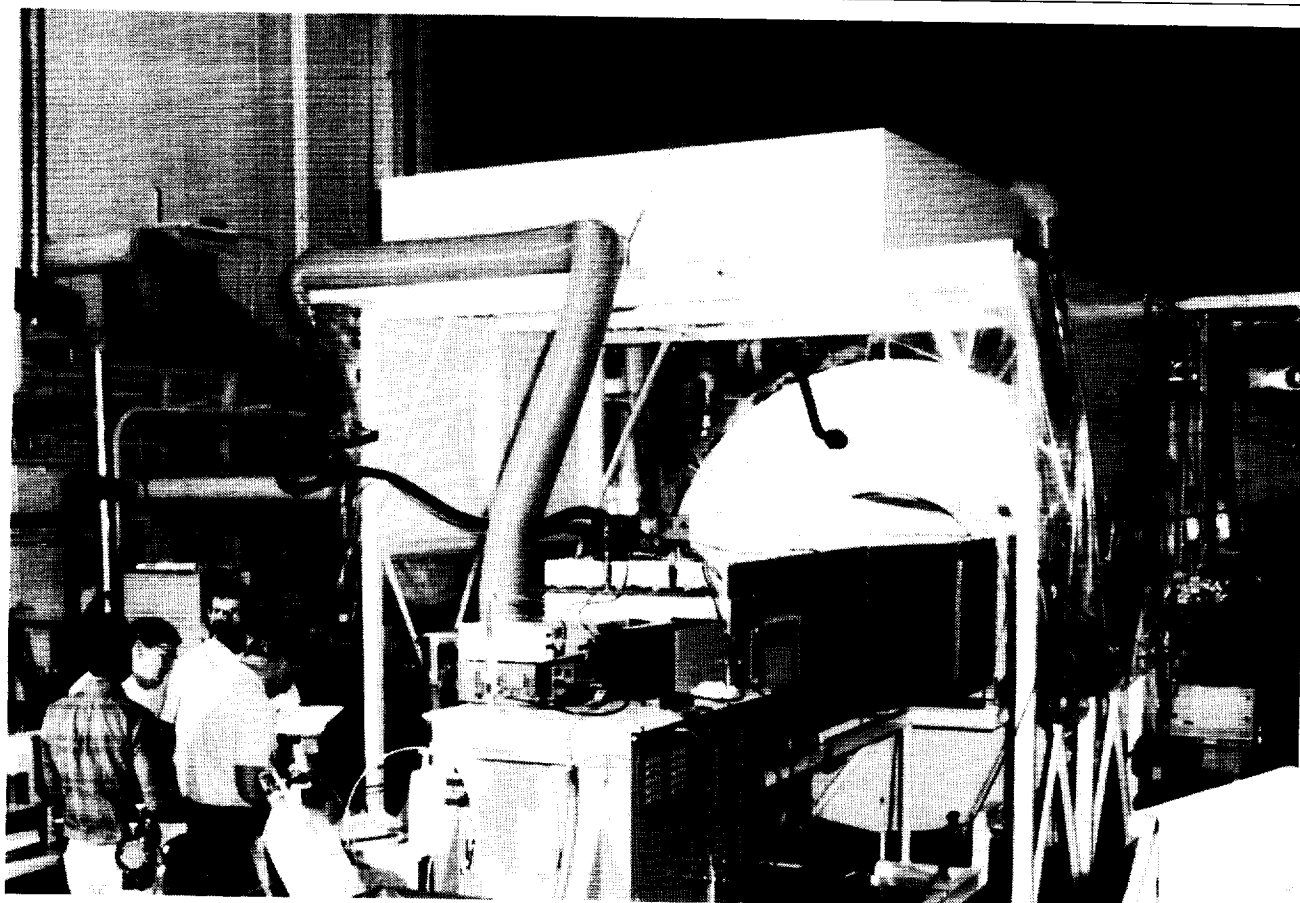
pump and a 32-in. diffusion pump to reach its capacity of  $1 \times 10^{-7}$  torr. The pumping capability is high relative to the chamber volume; therefore, the  $1 \times 10^{-7}$  torr level can be attained in 1.5 hours.

Structural integrity of aerospace hardware is essential for both performance and safety. The Engineering Vibration Test Facility in Building 1250 is used to perform environmental vibration tests on aerospace flight systems and components to demonstrate that the flight equipment will

maintain structural integrity when exposed to a mission environment. The facility includes two shaker units and centralized equipment for control, data acquisition, and signal processing. One unit is an Unholtz-Dickie T-1000 shaker with a 24 000-lbf peak force and a 1-in. armature stroke. The second shaker, a recent addition, is an Unholtz-Dickie T-4000 unit with a 40 000-lbf peak force and a 1-in. stroke (1.75-in. stroke for shock testing). The vibration control room houses a GenRad 2514 vibration control system for shaker control and signal processing plus signal conditioning and analog data recording equipment for 12 channels of data. Through auxiliary equipment, the data capacity can be expanded. Tests are conducted with great care given to equipment, test article, and personnel safety. Closed-circuit television coverage is used to safely monitor the test article during all tests.

### Gas Response Test for HALOE Instrument Verification

The Gas Response Test Apparatus, as designed, fabricated, and implemented for the calibration of the Haloe Occultation Experiment (HALOE) instrument, had to safely manage and precisely control several atmospheric gases, most of which are toxic and highly reactive. The HALOE is one of the Upper Atmosphere Research Satellite (UARS) instruments and is designed to radiometrically measure the concentrations of hydrogen fluoride, hydrogen chloride, nitric oxide, methane, nitrogen dioxide, carbon dioxide, water vapor, and ozone.



*HALOE Gas Response Test Apparatus.*

L-89-03980

The principle of the test program was to beam a Sun-simulator light source through transparent test cells in the test chamber (the cubic structure in the foreground) and into the cylindrical vacuum chamber that housed the HALOE Instrument at  $1 \times 10^{-5}$  torr for testing at 10°C, 20°C, or 30°C levels. The transparent test cells were cleaned, purged, and incrementally pressurized with test gases at controlled concentrations and pressures.

The test gas plumbing system required highly specialized materials and valves, as well as exacting assembly and verification techniques to assure absolute integrity.

A high flow rate venting system surrounded the cells as a final safety assurance.

The HALOE response measurements during an extended 7-week, 118-test point sequence agreed very well with prediction models for all gases except hydrogen fluoride (HF). The consistently lower results obtained with HF are believed to be related to the high reactivity of this gas.

(Alfred G. Beswick, 41624)

## Acceptance Testing of Aeroassist Flight Experiment Pressure Distribution/Air Data System Transducers

The thermal acceptance testing of the Aeroassist Flight Experiment (AFE) Pressure Distribution/Air Data System (PD/ADS) required the development of a novel thermal control system to provide conductive, rather than radiative heating inputs, which are normally applied

in spacecraft system evaluations. The PD/ADS, an array of pressure orifices and pressure transducers positioned across the blunt-body face of the AFE vehicle, will be subjected to thermal extremes during the AFE aerobraking trajectory through the atmosphere of the Earth.

The PD/ADS pressure transducer acceptance testing utilized contact strip heaters and liquid nitrogen cooling coils (sandwiched

between two plates within the vacuum chamber as shown) to repeatedly cycle up to eight transducers between temperature extremes of 0°F to 200°F with controlled ramp rates and dwell times. Because of the high efficiency of the conductive heat transfer, temperature changes occurred too rapidly for manual control. This necessitated the development of an automated feedback, personal computer-driven control system that ultimately exceeded the testing goals for accuracy and responsiveness.

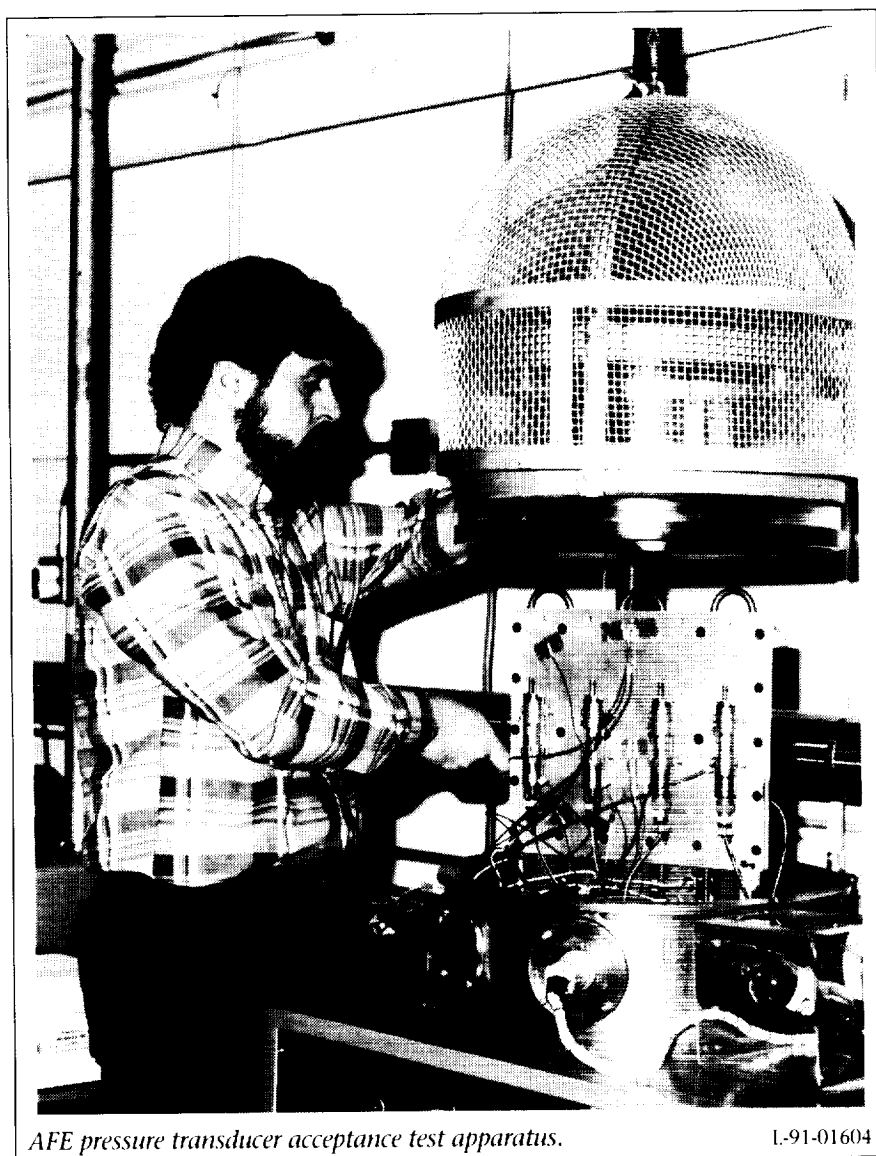
The results of this test series not only proved the capability of the transducers to withstand the rigorous thermal cycles, but it also provided information on the stability of these transducers through the rapid thermal transients necessary for system calibration.

(Craig S. Cleckner, 47048)

## LITE Load Path Verification Test

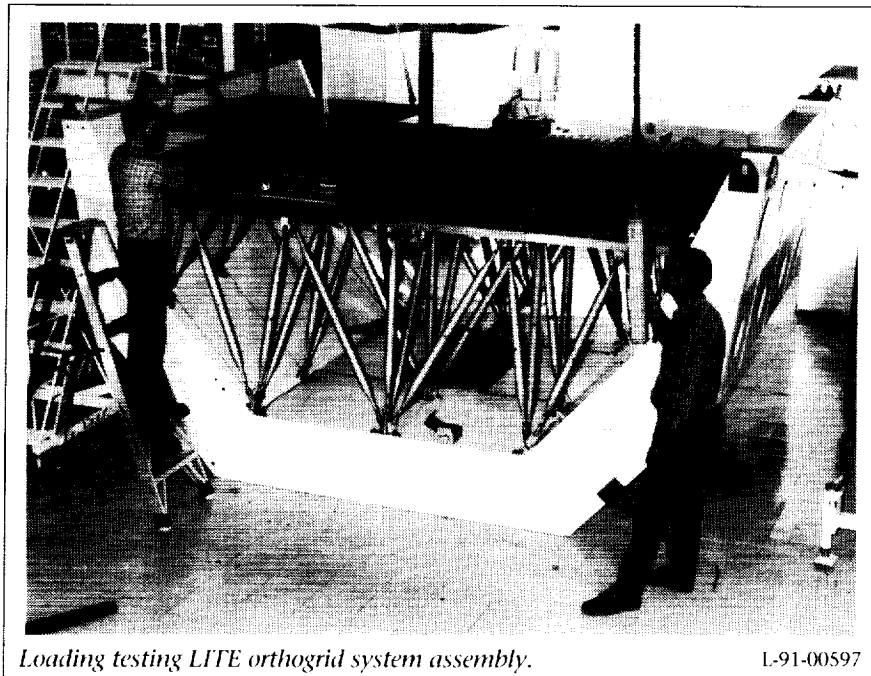
The Lidar In-space Technology Experiment (LITE) will fly on STS-62 in late 1993. In order to satisfy the payload verification requirements of the National Space Transportation System (NSTS) 14046B document, *Payload Verification Requirements*, the experiment platform (the orthogrid system assembly) was statically load tested to verify the math model of the structure.

The figure shows the LITE flight orthogrid, struts, and hardpoints mounted on a



AFE pressure transducer acceptance test apparatus.

L-91-01604



Loading testing LIFE orthogrid system assembly.

L-91-00597

nonflight pallet simulator. One quadrant of the orthogrid is being loaded to 6000 lb using seven stacked steel plates. All 52 struts in the assembly were strain gauged and monitored to determine how the load from the plates was distributed. In addition to the Z-axis orientation shown, the assembly was also tested in the X-axis and Y-axis by rotating the entire structure with cranes.

The math model successfully predicted the correct load paths through the struts in all orientations.  
(John Teter, 47163)

### Laser Doppler Velocimeter Measurements of Solar-Simulated Laser

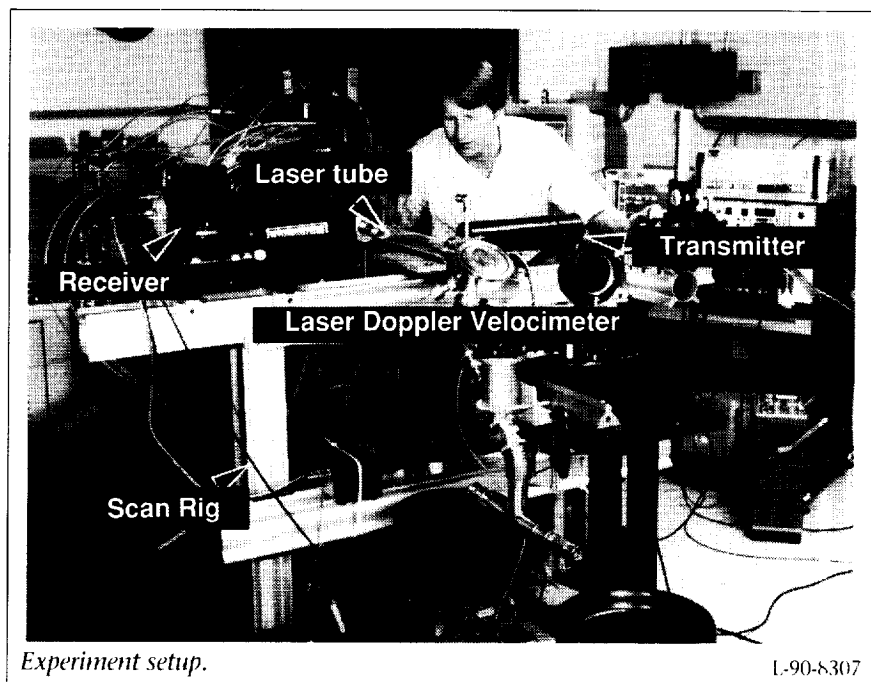
A series of flow velocity measurements were conducted in

the solar simulator pumped laser laboratory of the High-Energy Science Branch using a laser Doppler velocimeter (shown in the first figure). The purposes of these tests were to provide flow velocity

data for calibrating a mass flow instrumentation system and for analyzing the flow characteristics of a perfluoroalkyl iodide ( $n\text{-C}_3\text{F}_7\text{I}$ ) vapor inside various laser tubes.

The laser Doppler velocimeter (LDV) used in these tests was a single component system that was configured to operate in the forward-scatter mode. The LDV system utilized F/1.6 transmitting and receiving optics, a 15-mW HeNe laser, and 2.27X beam expanders. The LDV spatial and the velocity resolutions were 0.1 mm/s and 1 mm/s, respectively.

Flow velocity measurements were made in the 20-mm- and 36-mm-diameter laser tubes, under nonlasing test conditions. The operating conditions were at pressures of 5 torr and 10 torr for the 36-mm and the 20-mm-diameter laser tubes, respectively. The iodide vapor flow field was seeded with 0.3  $\mu\text{m}$  aluminum



Experiment setup.

L-90-8307



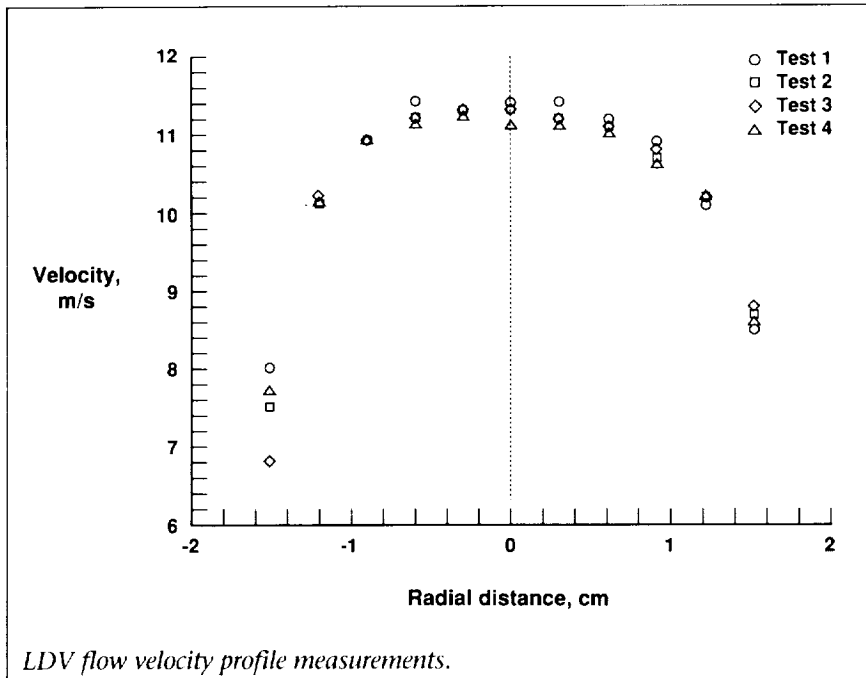
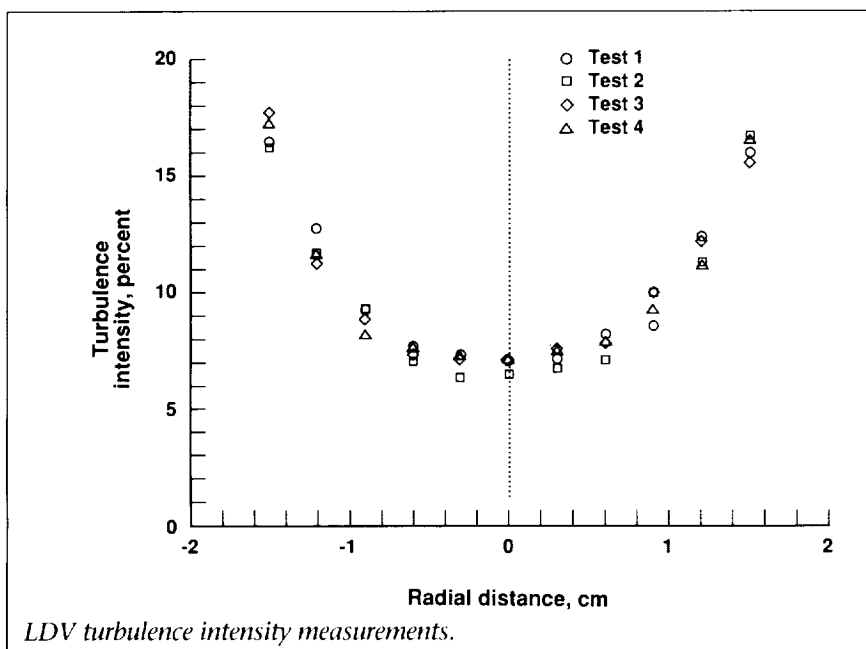
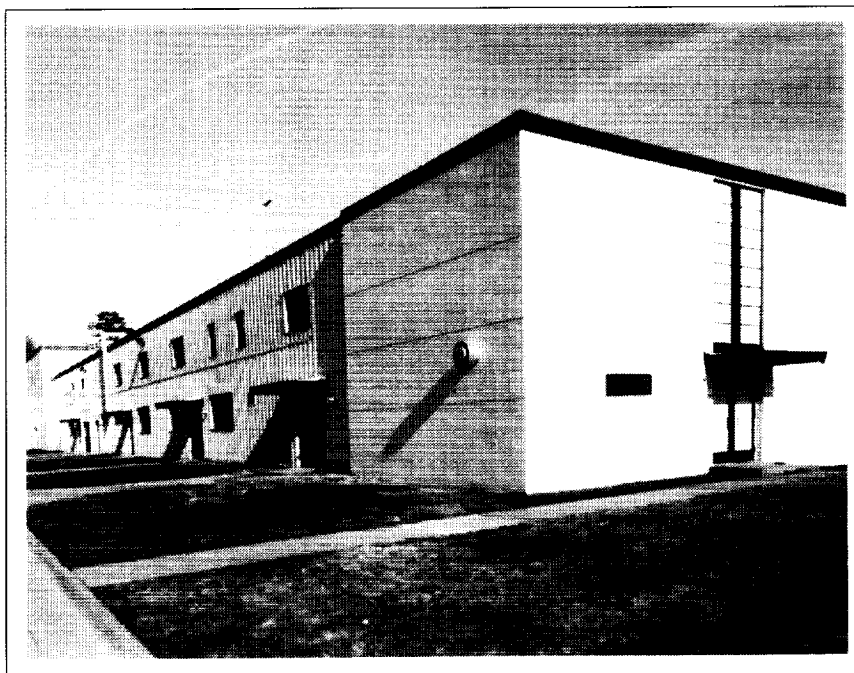


figure are typical velocity and longitudinal turbulence intensity profiles obtained for the 36-mm-diameter laser tube at 86.4 cm downstream of the gas inlet port. (L. R. Gartrell and B. M. Tabibi, 44596)



oxide particles. Detailed flow velocity and longitudinal turbulence intensity profiles were obtained at various locations downstream of the gas inlet port for the 20-mm- and the 36-mm-diameter laser tubes.

The measurement results for the 20-mm-diameter laser tube indicated that the centerline velocity and turbulence level varied from 13 m/s (43 f/s) to 18 m/s (60 f/s) and 25 percent to 6 percent, respectively. Shown in the second



## Advanced Technology Research Laboratory

---

*The Advanced Technology Research Laboratory was dedicated in early 1989 in support of the NASA Space Energy Conversion Research and Technology Program. The laboratory houses multidisciplinary research activities assessing the feasibility of space laser power generation and long-distance transmission for electric power distribution, conducting theoretical studies on galactic and solar cosmic ray exposure and shielding, and developing ultra-high vacuum gas-surface interaction technology. Major facilities include two solar simulators: a single-lamp unit of 100-kW input power and a state-of-the-art single-lamp unit of 160-kW input power. These simulators provide a range of solar irradiance conditions for the multifaceted research into the direct conversion of*

*solar energy to laser power. The research includes investigations using solid, liquid, and gas lasers powered by simulated sunlight; electrically driven diode lasers; and the conversion of laser power into electricity. Theoretical research is supported by a computational capability that includes the latest computer technology. In addition, the facility is fully integrated into the Center's high-speed data network. A group of laboratories house ultra-high vacuum equipment that simulates the space environment and specialized conditions associated with advanced spacecraft. The laboratory also contains a large, multikilojoule capacitor bank that is the energy source for the development of laser-power beaming technology.*

### Diode Laser Laboratory

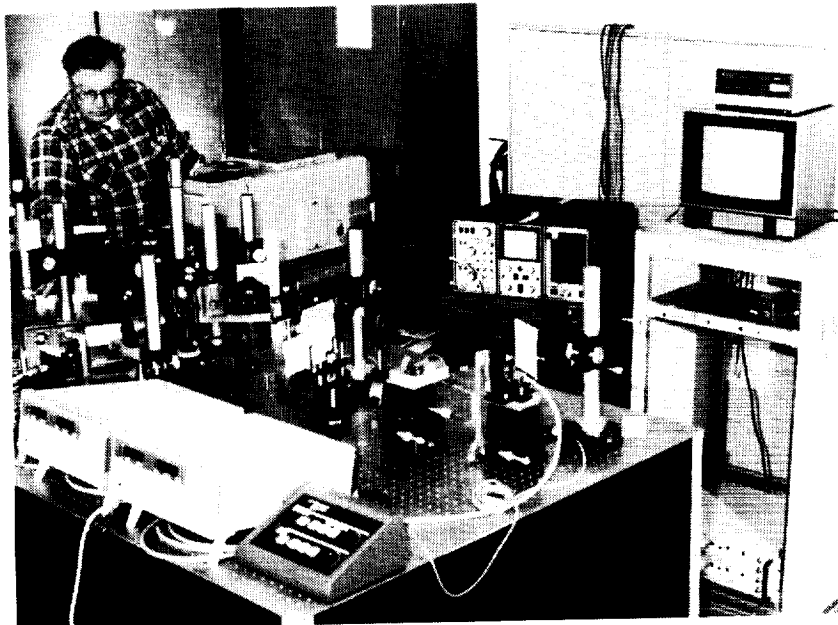
---

Remote laser-power beaming is being considered as an alternative to attached nuclear power sources for lunar/Martian habitats and long-term rover missions. Diode lasers are of interest because of the high efficiencies possible (>70 percent).

Initial experiments for extracting high power from a diode laser system utilize a master-oscillator power amplifier (MOPA) scheme. In the MOPA scheme, the master oscillator beam is split into several less-intense beams, each of which is amplified by an individual amplifier in the first stage of amplifiers. The output from the first stage of amplifiers is again split and ampli-

## Hydrogen Transport Barriers in Ti-Aluminides

Titanium alloys and titanium-aluminide intermetallic alloys are candidate materials for hot structures and heat shields for hypersonic vehicles such as the National Aero-Space Plane (NASP). Establishing an understanding of the fundamental transport properties (permeability, diffusivity, and solubility) of hydrogen is important in these candidate materials such as pure Ti, Ti-14Al-21Nb ( $\alpha_2$ ), and Ti-33Al-6Nb-1.4Ta ( $\gamma$ ). At temperatures  $>650^\circ\text{C}$ , the permeation of hydrogen through the material is diffusion limited at pressures that are below the



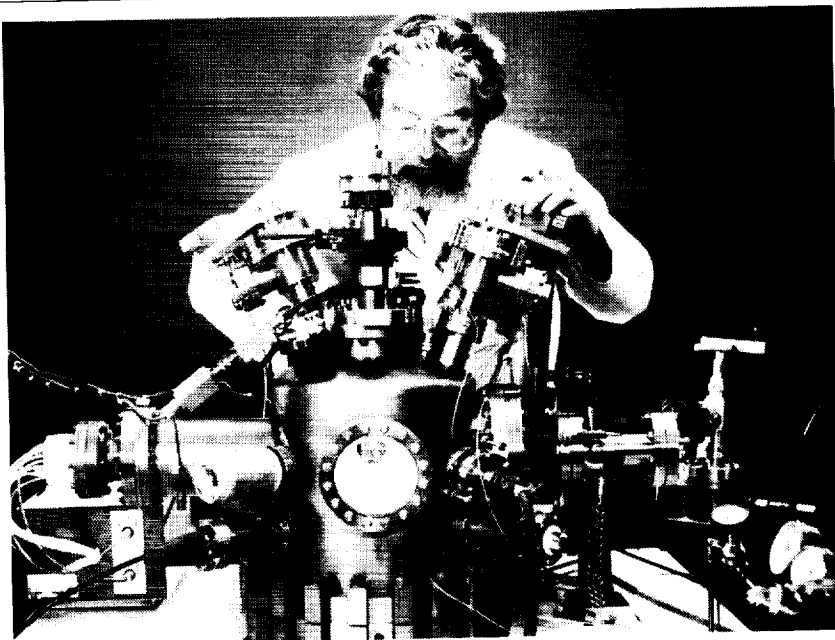
*Photograph of laser diode array test apparatus.*

L-91-02955

fied by the second stage, and this cascading effect is continued until the desired amount of output power is achieved.

Some limiting scaling factors include temperature and current control of individual amplifiers and degradation of beam quality at each amplifier stage. Experiments carried out at Langley Research Center and in joint cooperation with Xerox Corporation have shown that slave laser current control to within 0.1 mA is sufficient and that beam coherence degrades only approximately 1 percent when passing through an individual amplifier.

The diode laser laboratory at Langley currently consists of equipment and instrumentation for testing and characterizing individual diode lasers and amplifiers, for assessing beam quality by measuring near- and far-field profiles, and for measuring the



*Auger AES and ISS test apparatus.*

L-91-02290

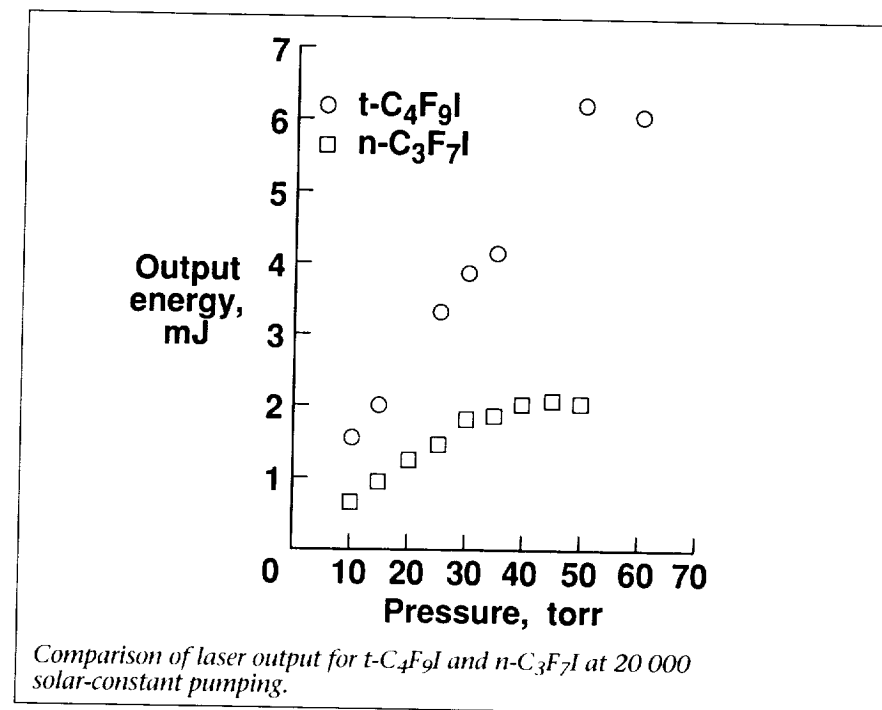
degree of coherence of combined beams from two or more amplifiers.  
(G. L. Schuster, 41486)

threshold for any hydrogen-induced transformations. At temperatures lower than  $650^\circ\text{C}$ , permeation is limited by adsorption processes from the gas phase.

The surface composition of these materials and their variations with temperature (20°C to 1000°C) were studied by Auger electron spectroscopy (AES) and ion scattering spectroscopy (ISS) in order to ultimately correlate the role of surface layers as barriers to hydrogen transport. At room temperature,  $\text{TiO}_2$  on pure Ti and  $\alpha_2$  aluminide is the predominant oxide, but it begins to decompose at 400°C. The  $\alpha_2$  aluminide begins to form some  $\text{Al}_x\text{O}_y + \text{Al}$  at 700°C and, as the temperature is increased further, the metallic Al peak becomes more and more predominant. The oxides on Ti and  $\alpha_2$  aluminide, however, cease to be a surface barrier to hydrogen at temperatures >650°C, but a significant oxide still remains on  $\gamma$  aluminide even above 900°C. Sulfur segregation to the surface occurs on Ti and  $\alpha_2$  aluminide following the dissolution of oxygen, but it does not appear to inhibit the hydrogen transport. (R. A. Outlaw, 41433)

### Efficient Laser Medium for Solar Pumping in Space

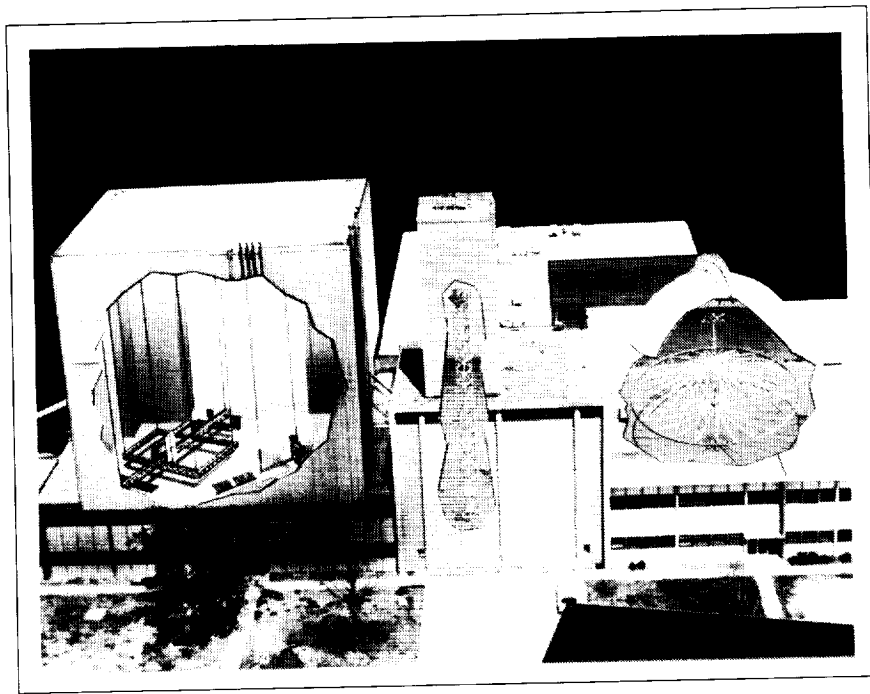
Recent results of a comparative study on laser performance of  $\text{t-C}_4\text{F}_9\text{I}$  and  $\text{n-C}_3\text{F}_7\text{I}$  under closely simulated solar pumping are described. The closely simulated solar irradiance was obtained by using an acetone water filter around the laser tube. The solar concentration on the laser tube was measured to be  $2 \times 10^4$  solar constants (1 s.c. =  $1.35 \text{ kW/m}^2$ ) when the 0.3-m-long flash lamp was energized with two 12.5- $\mu\text{F}$  energy storage capacitors charged



at 6 kV. The flash lamp and the laser cavity were optically coupled in an elliptic cylinder reflector.

A 16-nm red shift of the absorption peak and its broader bandwidth of  $\text{t-C}_4\text{F}_9\text{I}$  ( $\lambda_{\text{peak}} = 290 \text{ nm}$ ) compared with that of  $\text{n-C}_3\text{F}_7\text{I}$  ( $\lambda_{\text{peak}} = 274 \text{ nm}$ ) give significant advantages in the laser efficiency. The solar power absorbed in the laser pump band of  $\text{t-C}_4\text{F}_9\text{I}$  is approximately twice that of  $\text{n-C}_3\text{F}_7\text{I}$ . Consequently, the pumping rate, i.e., photodissociation rate for  $\text{t-C}_4\text{F}_9\text{I}$ , is twice that for  $\text{n-C}_3\text{F}_7\text{I}$ . The first figure gives the laser output comparison from  $\text{t-C}_4\text{F}_9\text{I}$  and from  $\text{n-C}_3\text{F}_7\text{I}$  at different vapor pressures. The laser output from  $\text{t-C}_4\text{F}_9\text{I}$  is three times that from  $\text{n-C}_3\text{F}_7\text{I}$  at 50 torr. The other remarkable difference in performances of  $\text{t-C}_4\text{F}_9\text{I}$  is that the output of the first and second runs for  $\text{t-C}_4\text{F}_9\text{I}$  does not change appreciably because of high chemical reversibility.

These experimental results demonstrate the superiority of  $\text{t-C}_4\text{F}_9\text{I}$  over  $\text{n-C}_3\text{F}_7\text{I}$  in solar spectral utilization and chemical reversibility, indicating that the use of  $\text{t-C}_4\text{F}_9\text{I}$  provides a significantly improved system efficiency that reduces the solar collector size and minimizes the resupply of the fresh iodide in space. (Ja H. Lee, 41473)



# Structural Dynamics Research Laboratory

The Structural Dynamics Research Laboratory (SDRL) is designed to conduct research on the dynamics and controls behavior of spacecraft and aircraft structures, equipment, and materials. The SDRL offers a variety of environmental simulation capabilities, including acceleration, vacuum, and thermal radiation. Improvements are under way which will benefit controls and structures interaction research.

The newest feature of the SDRL is the 5200 ft<sup>2</sup> Space Structures Research Laboratory, which has a 68-ft-high suspension platform from which large space structures may be suspended over any portion of the work area. This laboratory houses a 1/10-subscale space-station-like model and a controls-structures interaction model

for performing structural dynamics and controls research of large space structures. The SDRL also contains a 12-ft by 12-ft backstop area for cantilevered structural tests. A control room houses a state-of-the-art data acquisition capability, which is provided by a 128-channel GenRad 2515/CYTEC scanner and by a 16-channel Zonic system. A CAMAC crate connected via a fiber optic line to the real-time CYBER 175 computer provides computational capability necessary for closed-loop active vibration suppression. The crate has the capacity to handle up to 42 input and 42 output channels.

The dominant feature of the main laboratory is a 38-ft-high backstop of I-beam construction. Test areas available around this facility are 15 ft

by 35 ft by 38 ft high and 12 ft by 12 ft by 95 ft high. The tower presently houses a 66-ft-high space truss. Spiral stairs, ladders, and platforms provide access over the entire main laboratory.

Another feature of the SDRL is the 16-Meter Thermal-Vacuum Chamber, which has a 55-ft-diameter hemispherical dome with a removable 5-ton crane, a 64-ft-high dome peak, a flat floor, and an option for a large centrifuge or a rotating platform. Access is by an airlock door and an 18-ft-high by 20-ft-wide test specimen door. Ten 10-in.-diameter view ports are randomly spaced for visually monitoring tests. A vacuum level of 10 torr can be achieved within 120 min and, with diffusion pumps, 10<sup>-4</sup> torr vacuum can be achieved in 160 min. The centrifuge attached to the

floor of the chamber is rated to 100g, with a 50 000-lbf capacity and a maximum allowable specimen weight of 2000 lb. Six-ft mounting faces for test articles are available at the 16.5-ft and 20.5-ft radii. The tables can accommodate electromagnetic and hydraulic excitation devices. A temperature range of 100°F is obtained from 250 ft<sup>2</sup> of portable radiant heaters and liquid-nitrogen-cooled plates.

A control room for the main laboratory, the tower, and the 16-Meter Thermal-Vacuum Chamber houses state-of-the-art capability for

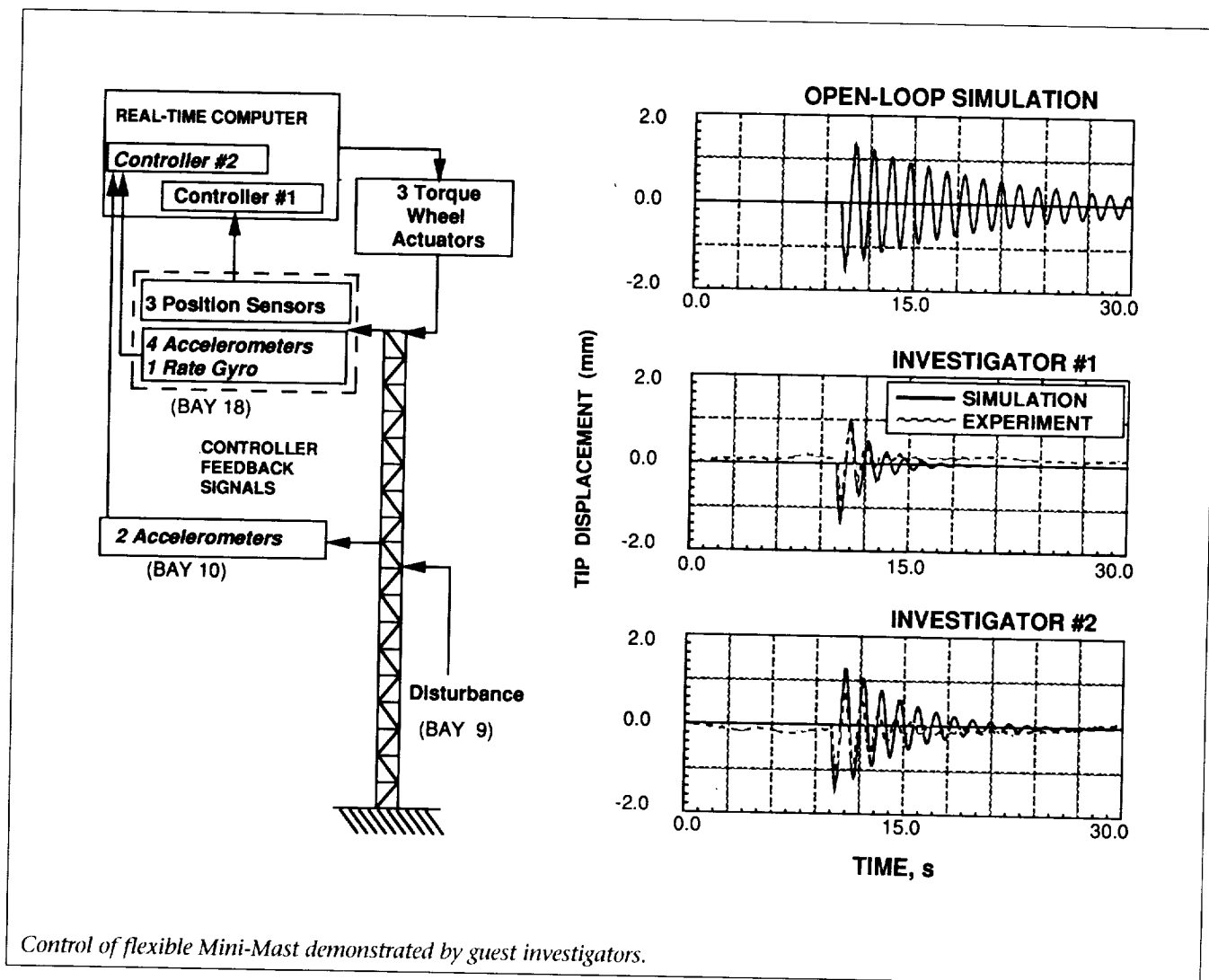
up to 220 channels of signal conditioning and analog and digital data recording. A 128-channel GenRad 2515/CYTEC scanner provides digital signal processing. An EAI 2000 analog computer system for simulation and on-line test control is also available. A CAMAC crate similar to the one in the Space Structures Research Laboratory part of the SDRL is available for closed-loop active vibration suppression testing.

Available excitation equipment includes several types of small shakers. The largest shaker is hydraulic with a maximum of 1200-lbf, a 6-in. stroke,

and a 0-Hz to 170-Hz range. All areas are monitored by closed-circuit television cameras.

## Completion of CSI Mini-Mast Guest Investigator Test Program

The objective of the Controls-Structures Interaction (CSI) Guest Investigator (GI) Program is to verify, on realistic hardware, advanced control law design methods for flexible spacecraft active vibration control. The first



part of the GI Program, involving closed-loop testing of the Langley Research Center Mini-Mast test bed, has been completed.

The GI test program was conducted on a 20-m-long, 1.2-m triangular cross section, deployable, flight-quality truss, known as the Mini-Mast. The structure, mounted vertically and cantilevered at the base, is controlled by three torque wheels mounted orthogonally at the tip. Commands to the torque wheels are generated by a real-time digital computer using signals from sensors mounted on the Mini-Mast. A variety of position, rate, and acceleration sensors are available. Potential investigators were supplied with a mathematical model of the complete system that has been extensively verified by in-house dynamic tests. Investigators designed control laws to satisfy their particular research objectives and submitted them for safety verification (i.e., assurance of stable, nondestructive behavior) on a computer simulation of the system. Once verified in simulation, the control laws were implemented in laboratory tests in which the researcher participated. Investigators have included both in-house researchers and eight guest investigators who were selected in open competition from academe and industry.

More than 15 digital control laws, designed by both NASA and GI researchers, have been subjected to safety simulation. Eight of these laws were approved for test and implemented in the laboratory. The behavior of the integrated system with each controller was examined, and predicted responses were compared with actual re-

sponses. In the figure, simulated and measured results from two control investigations performed by university GI's are shown, along with the simulated open-loop behavior (no feedback control). The first investigator used measurements of the absolute position of the structure during vibration in the control law design. The second investigator used only acceleration and rate sensor measurements because these are more representative of measurements that would be available in a typical on-orbit spacecraft. Both investigators achieved significant improvements in damping the response of the structure because of disturbances. The analytical and experimental results are considered in good agreement because the safety simulation model uses lower-than-measured modal damping values to ensure a conservative "envelope of safety" around the actual response.

With the completion of the Mini-Mast GI Program, the Mini-Mast hardware will be used as a test bed for structural system identification research on nonlinear and joint-dominated structures. (S. E. Tanner, 44353, W. K. Belvin, and R. Smith-Taylor)

### **Fabrication of DSMT Hybrid-Scale Space Station Model for Structural Dynamic Testing**

The objective of Dynamic Scale Model Technology (DSMT) research is to investigate the use of scale models of large spacecraft structures in ground testing. Research areas being addressed include analytical component mode and substructure methods validation, effects of gravity on ground test results, advanced model suspension devices to simulate zero-gravity environ-



*DSMT MB-2 hybrid model.*

L-90-05157

ments, and requirements and methods for on-orbit structural testing of large space structures.

A hybrid-scale structural dynamics model representing a space station class vehicle has been developed and fabricated under contract by the Lockheed Corporation Missiles and Space Group. Hybrid scaling laws were developed to provide a means for designing scale models of very large structures that perform realistically while retaining practical dimensions. These laws were applied to a representative design of the structures of Space Station *Freedom*. The resulting model is denoted a 1/5:1/10 scale model because it employs a 1/10-size truss structure comprised of 1/5-scale truss joints and mass properties to yield a model with global properties of a 1/5-scale dynamic model.

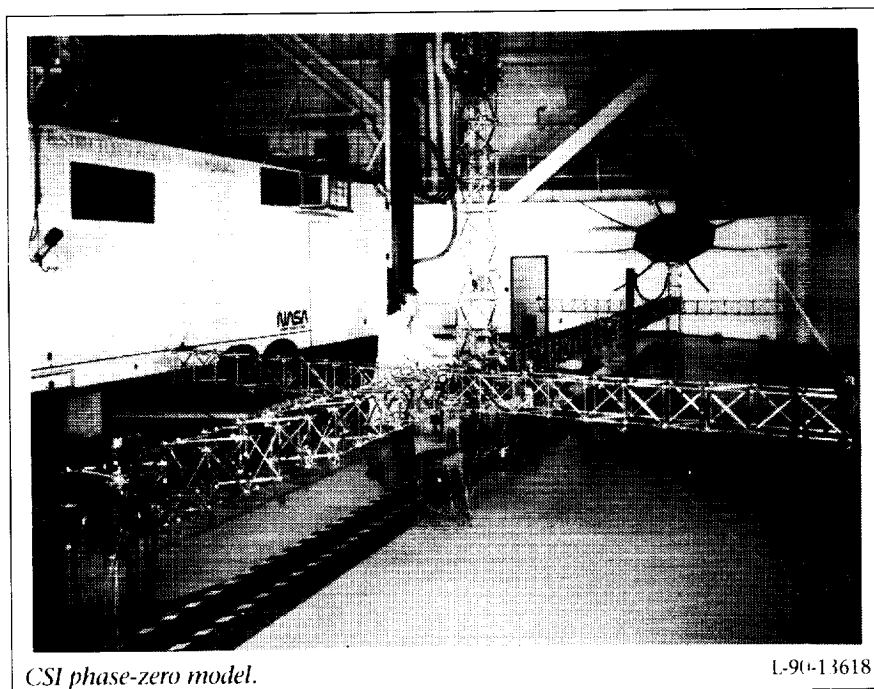
Model hardware for a complete space station configuration has been fabricated. All major space station structural components have been modeled, including the truss, solar arrays and thermal radiators, equipment pallets, nodes, and modules. Some components were simulated (e.g., module-to-truss interconnects) because of insufficient full-scale design information. Because of the evolutionary nature of the space station, the model components were designed for modular attachment to the truss and easy reconfiguration. Shown in the figure is an early flight configuration suspended from cables for dynamic tests. This configuration was selected as the first structure for comparing predictions from component-level synthesized data with that obtained from fully integrated testing.

The DSMT hybrid-scale space station model provides a ground test article with the challenging dynamic characteristics of future large space vehicles. These characteristics include closely spaced and low-frequency vibration modes, potential interactions between flexible components and global truss vibrations, low load capability structural truss elements, and nonlinear rotating joints. In addition, the changes in structural dynamic characteristics during the on-orbit assembly and construction of large vehicles can be simulated. (P. E. McGowan, 44350, V. M. Cooley, and M. Javeed)

### Phase-Zero CSI Evolutionary Model Test-Bed

A new test-bed, the Controls-Structures Interaction (CSI) Evolutionary Model, has been developed

to experimentally evaluate methods for controlling the dynamic response of large flexible spacecraft. This test bed, which is now operational, has been designed to be evolutionary and can be reconfigured and adapted to meet future research needs as dictated by actual spacecraft requirements. The current configuration of the model, denoted phase-zero and shown in the figure, has five major structural components: a 52.5-ft center truss, a 16-ft-diameter reflector, a 9.2-ft tower that supports a laser, and two 16.7-ft cross-member trusses. These structural components have dynamic characteristics (natural frequencies, damping, and mode shapes) that are typical of large spacecraft systems. The model is supported by a steel cable harness from an overhead ceiling support structure, with the cables attached to the model at each end of the two cross members. This method of suspension provides for model transla-





tions, rotations, and structural vibrations that approximate those of a spacecraft on orbit.

Actuators and sensors for feedback control are mounted on the model. The primary actuators are proportional airjet thrusters using a 125 lb/in<sup>2</sup> external air supply. A total of eight actuator pairs, producing 4.4 lb thrust per pair, are placed at four locations along the truss. Eight accelerometers collocated with the thrusters and eight noncollocated angular rate sensors provide feedback signals for control experiments. The tower-mounted laser system is used to measure the relative positioning of the tower with respect to the reflector, an important performance parameter for precise pointing of space science payloads. Light from the laser is bounced by a mirror mounted on the reflector structure to a light detector mounted on the ceiling of the laboratory. The pointing accuracy of the spacecraft is then derived from the sensed position of the laser light on the detector.

Extensive structural dynamic system identification testing has been conducted to determine the actual frequencies, damping, and mode shapes of the structure. These data are being used to update and refine the mathematical dynamics models of the test bed which are then used for control law design. A number of control law designs have been experimentally tested on the model, including nonmodel based controllers, static and dynamic dissipative controllers, virtual passive controllers, and some high-order model-based controllers. Planning for the phase-one evolution of the model,

to incorporate structural changes and new control laws validating integrated control-structure design method benefits, is under way. (W. K. Belvin, 44319, K. Elliott, and L. G. Horta)

---

### Experimental Validation of Dissipative Control Laws for CSI Evolutionary Model

---

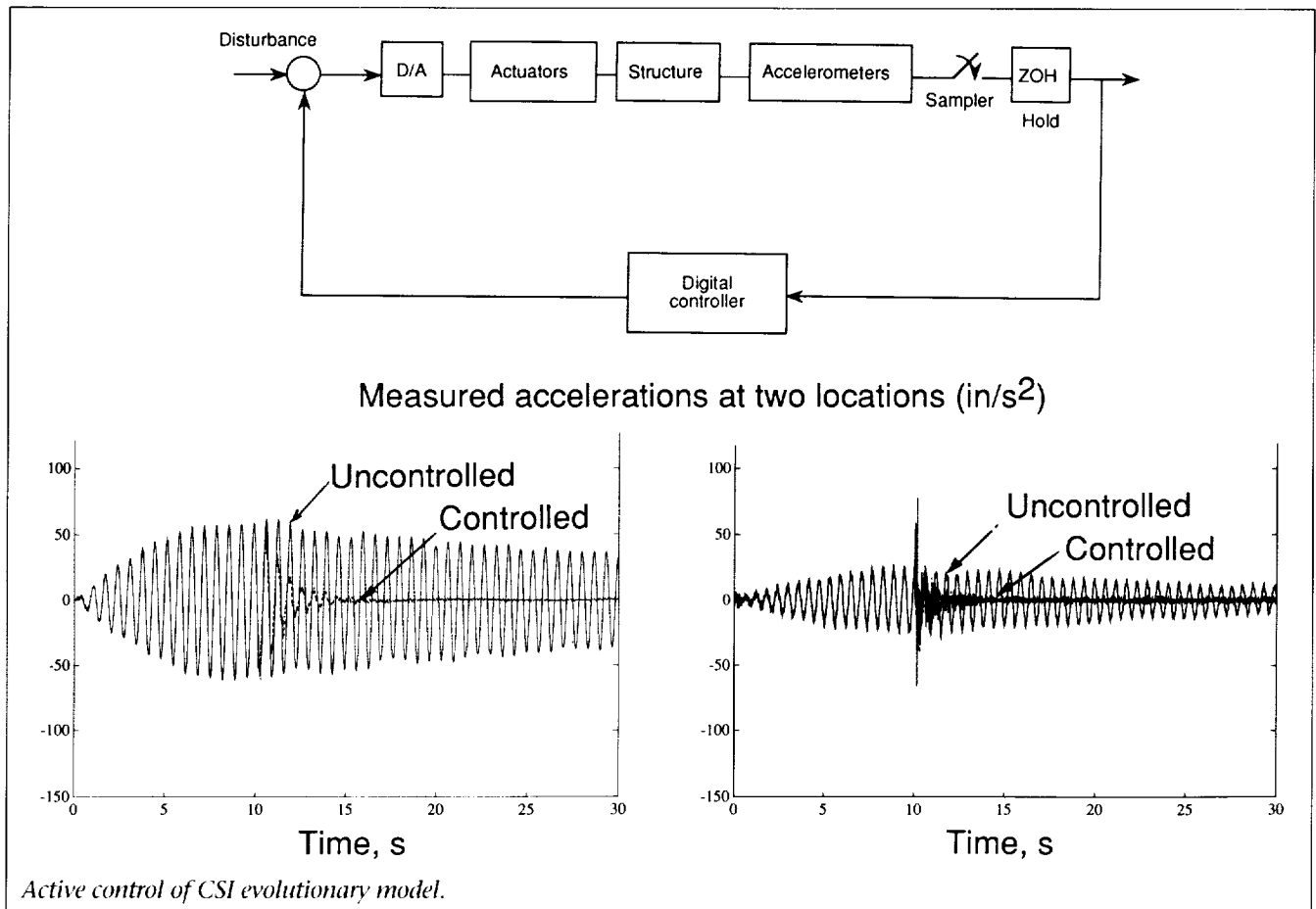
Control system design for flexible space structures is a difficult problem because of their special characteristics, which include a large number of significant elastic modes, low inherent structural damping, and inaccuracies in the mathematical models. The control system must be robust, that is, it must maintain stability and performance despite these problems. One class of controllers, which has been theoretically proved to be robust, consists of dissipative controllers. Dissipative controllers can be divided into two categories: static dissipative controllers (which utilize direct feedback of velocity and position) and dynamic dissipative controllers (which consist of a bank of filters or a state-space equation). Both types of dissipative controllers use collocated compatible actuators and sensors (e.g., force actuators and accelerometers; and torque actuators and attitude/rate sensors).

Both static and dynamic dissipative controllers were designed for the CSI Evolutionary Model and were tested experimentally. Eight force actuators and collocated accelerometers were used for accomplishing control.

The designs were performed via nonlinear programming using the "CSIDESIGN" software package presently under development at Langley Research Center. The design objective was to minimize the average control power in the presence of random disturbance forces at the actuator locations, while constraining the response settling time to be below a certain value. The design variables were the controller parameters. The controllers utilize feedback of velocities, which were obtained by integrating the accelerometer signals. However, a small bias present in an accelerometer, when integrated, would produce an unbounded signal. Therefore, first-order washout (high-pass) filters, one for each accelerometer, were designed to reduce the effect of the biases.

In practical applications, the implementation of the controller is usually accomplished using a digital computer. Two modifications were necessary to incorporate the effect of digital implementation of the control systems. First, in order to compensate for the one-step time delay that is inherently present in all digital implementations, a "one-step-ahead" predictor was incorporated. Second, a low-pass filter was designed to reduce the aliasing problem. A sampling rate of 133 Hz was used in all the experiments.

The control laws were tested by applying a disturbance input signal for 10 s and then turning on the controller. The results showed that the closed-loop damping ratios for the first and second structural modes were about 5 percent and 10 percent, respectively, as com-



pared to their open-loop values of approximately 0.5 percent. The closed-loop damping ratios for the suspension modes (which represent the pendulum motion) were significantly higher.

The second controller design was the dynamic dissipative controller, which consisted of a 16th-order compensator. Although more complex, this compensator has the ability to provide better performance than the static dissipative controller. Accordingly, the dynamic dissipative controller provided a closed-loop damping ratio of approximately 8.5 percent for the first structural mode and 14.5 percent for the second structural mode, accompanied by even higher damping ratios for the suspension modes.

These results were obtained using control system designs that were based solely on a preliminary mathematical model that had significant errors in the parameters. The satisfactory performance obtained in spite of large modeling errors indicates that dissipative controllers are very robust and can deliver high performance in the presence of uncertainties. Furthermore, the potential exists for even better control law designs if more accurate models (e.g., obtained by parameter identification) can be used.

(S. M. Joshi, 46608, P. G. Maghami, and K. B. Lim)



# Materials Research Laboratory

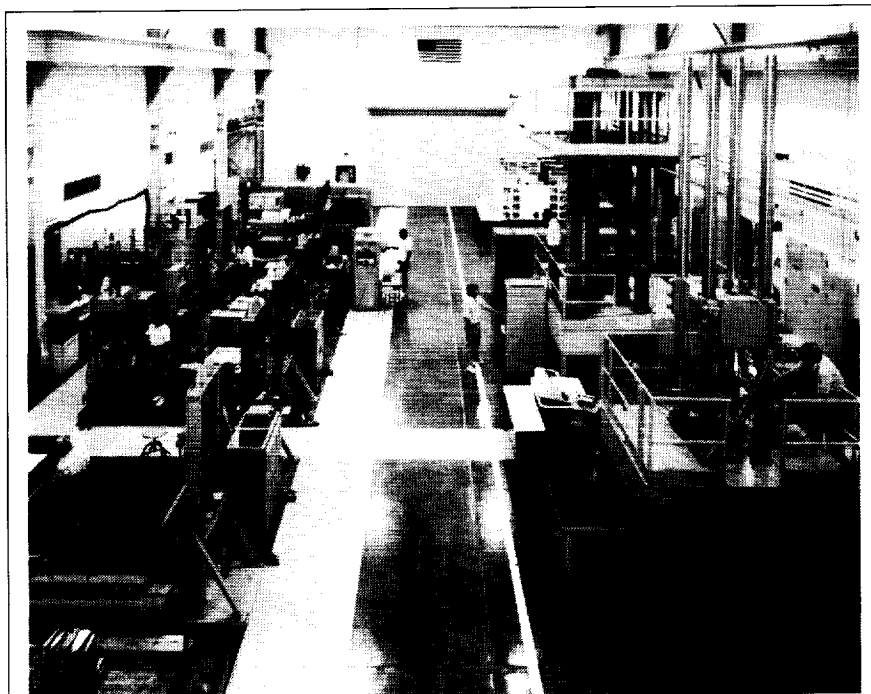
---

*The Materials Research Laboratory houses experimental facilities for conducting a wide range of research to characterize the behavior of structural materials under the application of mechanical and thermal loads. The mechanics of materials research encompasses the study of the deformation characteristics of new materials leading to the development of nonlinear constitutive relationships and the study of damage mechanics leading to the development of strength criteria and fracture-mechanics-based damage tolerance criteria. The facility, which opened in 1968, provides approximately 25 000 ft<sup>2</sup> of laboratory space. The laboratory area rests on a heavy-duty steel-reinforced concrete floor with special isolation pads to support the high-capacity load frames. A high bay area, with a 20-ft clear height and a 7.5-ton traveling overhead crane, houses nine multi-purpose 20-kip to 100-kip servo-*

*hydraulic systems for coupon testing and three high-load capacity systems for testing large panels. Enclosed laboratories around the perimeter of the high bay area are dedicated to specialized research. These laboratories house an additional 18 servohydraulic testing systems, a scanning electron microscope, 3 X-ray radiography systems, 13 high-temperature creep frames, 3 multiparameter test facilities, and 11 load frames for long-term environmental exposure testing.*

*The 27 servohydraulic testing systems are used for monotonic and cyclic loading of material level coupons under tension, compression, combined tension-torsion, and mechanical loading at both cryogenic and elevated temperatures. The load capacities range from 1 kip to 100 kips. A special cryostat and a 100-kip load frame allow testing to approximately*

*-450°F in a liquid-helium environment. Liquid nitrogen is also used when lower cryogenic temperatures are not required. Combined thermal and mechanical loading conditions can be achieved by a variety of methods including convection furnaces (600°F), induction heaters (2000°F+), and quartz lamp heaters (1500°F+). Large specimens and panels can be tested under uniaxial monotonic or cyclic loadings in the 300-kip and 400-kip test facilities. A special biaxial system allows for the testing of flat cruciform panels under monotonic or cyclic inplane loads up to 175 kips. Two tension-torsion testing systems allow for the testing of tubular specimens to investigate the effects of multiaxial stress states. A special multiparameter test facility allows for the simultaneous testing of up to six specimens under combined temperature, cyclic mechanical loads, and partial pressures.*



Laboratory area.

L-88-6247

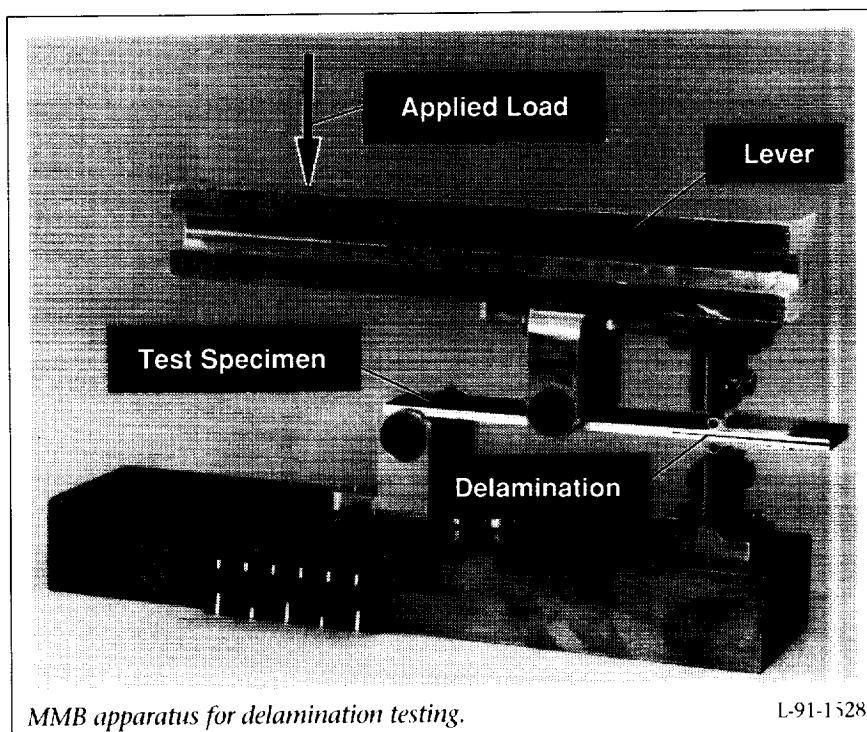
The scanning electron microscope is equipped with a loading stage to permit examination of a growing fatigue crack while the specimen is under load. The crack-tip process zone can also be investigated while the specimen is under load. Basic fracture morphology studies are also conducted in an environmental fatigue laboratory. A vacuum chamber allows for the control of moisture, temperature, and gaseous environment. Fatigue tests can also be conducted in salt water environments. In addition, nine load frames are located outside the building for conducting long-term durability tests in real atmospheric conditions. These hydraulic load frames are electronically controlled to permit mechanical loadings to simulate actual vehicular mission profiles. While not housed in the Materials Research Laboratory, a central analysis laboratory in the Materials Division provides a full range of

fractographic and chemical analysis support for postmortem evaluations of all test specimens.

## Mixed-Mode Delamination Fracture Tests Using MMB Fixture

Laminates are a common form of continuous fiber-reinforced composites, and delaminations are a primary failure mechanism. These delaminations are subjected to opening and shear loads that are referred to as mode I and mode II loading, respectively. To design with composite materials, the energy required to grow a delamination, called the fracture toughness, must be known. Because delaminations are usually subjected to mode I and mode II loadings simultaneously, knowing the mixed-mode fracture toughness is important.

A mixed-mode bending (MMB) test has been developed to measure such delamination toughness. The MMB test apparatus uses a lever to



MMB apparatus for delamination testing.

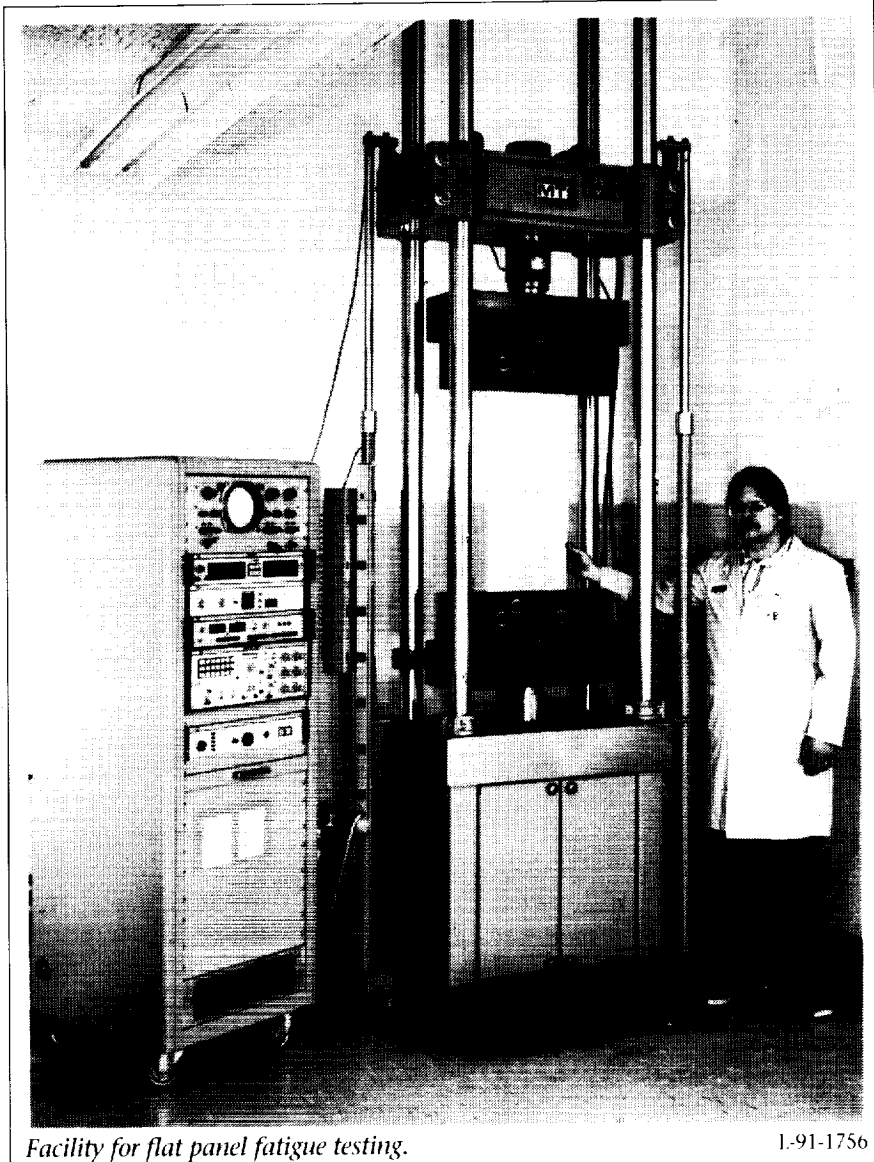
L-91-1528

apply mode I and mode II loadings to the test specimen as shown schematically in the figure. The downward force at the middle of the specimen causes mode II shear stresses at the delamination tip. The upward load at the end of the specimen causes mode I opening stresses. The position of the applied load on the lever determines the relative amounts of the mode I and II loadings. Unlike previous tests, the MMB test can measure toughness with practically any combination of mode I and mode II, using a standard compression test machine. The determination of fracture toughness from the measured loads and displacements only requires a simple calculation based on linear beam theory. The MMB test data can provide a basis for developing new composites with increased delamination fracture toughness so that they are more damage tolerant. The MMB test also can be used to develop the data bases needed to design critical aerospace structures.

(James R. Reeder and J. H. Crews, Jr., 43456)

### Evaluation of Fatigue of Thin-Sheet Aluminum With Multi-Site Damage

The objective of the Airframe Structural Integrity Program is to address issues relevant to the aging commercial transport fleet. One issue of concern is Multi-Site Damage (MSD) fatigue cracking, which has been observed in commercial transport aircraft. The MSD is the formation of a row of cracks, such as along the top line of rivets in a lap-splice joint. The



*Facility for flat panel fatigue testing.*

1-91-1756

critical size of the individual cracks may be relatively small, making their detection with current non-destructive examination (NDE) methods difficult.

An experimental program has been undertaken to investigate the behavior of thin-sheet aluminum with MSD. Flat panel configurations with multiple colinear cracks have been fatigue tested at stress levels typical of commercial transport fuselage skins. The flat

panels were 12 in. wide with cracks propagating from 10 open or riveted holes. A failed open hole specimen is shown in the figure.

The initial tests evaluated the concept of pressure proof testing as a means of detecting MSD cracking in commercial transport aircraft fuselage skin. The proof test concept is based on the assumption that in-flight structural failures precipitated by MSD fatigue can be prevented if the aircraft survives an

overpressurization on the ground. The proof test was simulated by applying an overload to flat panels with MSD cracking. The panels then were fatigue cycled until failure. The results indicated that the required proof test interval, to ensure continued in-flight safety, was too short to make the proof test concept viable. Later experiments were used to verify analytical fracture mechanics models of MSD behavior.  
(David S. Dawicke, 43477)

### Inelastic Stress-Strain Response of Organic Matrix Composites at Elevated Temperatures

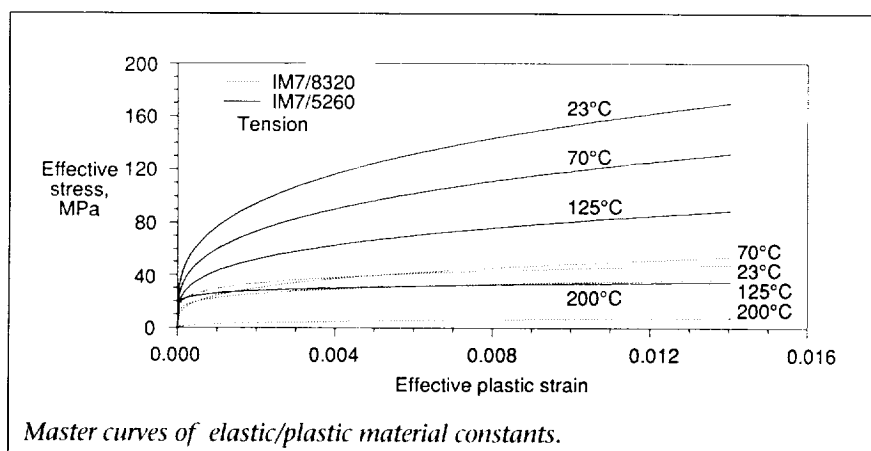
In order to support materials selection for the next generation of supersonic civilian passenger transport aircraft, an experimental investigation is under way to study the nonlinear, time-dependent stress-strain behavior of advanced polymer matrix composites under conditions of high load and elevated temperature. As part of this effort, materials testing was performed to measure the material properties and constants required

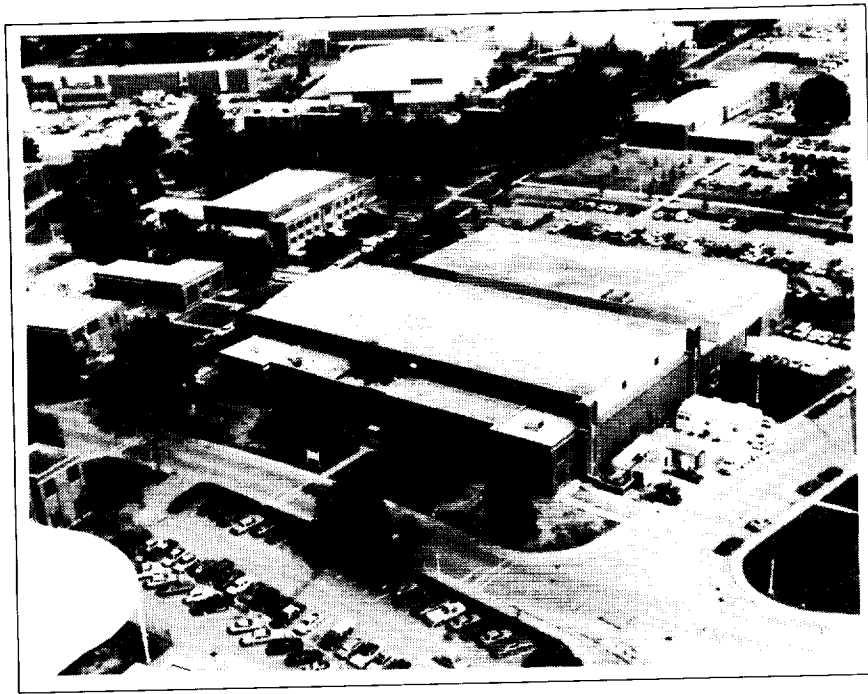
to model the viscoplastic behavior. Utilizing tension and compression test data from stress relaxation of off-axis specimens at elevated temperatures, material constants were measured which can be used in the constitutive model to predict phenomenon such as material nonlinearity, creep, stress relaxation, and variable strain rate loading response. Test methods, laboratory equipment, and data reduction procedures were developed to ensure accurate and repeatable results.

The elastic/viscoplastic constitutive model assumes that a phenomenological understanding of the material behavior can be established by measuring the material constants from off-axis uniaxial tests. Formulations for rate-independent plasticity and rate-dependent viscoplasticity utilize these constants in simple power law expressions. Both graphite/thermoplastic (IM7/8320) and graphite/bismaleimide (IM7/5260) composites were tested, and the resultant material constants were developed for tension and compression over a range of test temperatures. Effective values of stress and strain were used to generate master curves for each

material system. The figure shows the elastic-plastic, tension master curves for the two materials at four different temperatures. Material constants are found from mathematical representations of the master curves. In addition, comparisons between material systems can be found from examination of the master curves. For example, it is apparent that the graphite/bismaleimide material has less tendency toward nonlinear elastic/plastic behavior than the graphite/thermoplastic system. Both systems show a definite trend toward increased ductility as the temperature increases.

(Thomas S. Gates, 43400)





## Structures and Materials Research Laboratory

---

*Built in 1939 to contribute to the development and validation of aircraft structural designs during World War II, this laboratory currently supports a broad range of structural and materials development activities for advanced aircraft, aerospace vehicles, and space platform and antenna structures. Research conducted in this laboratory includes the development, fabrication, and characterization of advanced materials and the development of novel structural concepts. Static testing, environmental testing, and material fabrication and analysis are performed using the unique capabilities of this laboratory. Research results are directly applicable to the development of structures and materials technologies required for future advanced subsonic aircraft, high-speed transports, high-perfor-*

*mance military aircraft, advanced hypersonic and aerospace vehicles, and large space structures and antennas. Emphasis is on the development of structural mechanics technology and advanced structural concepts enabling the verified design of efficient, cost-effective, damage-tolerant advanced composite airframe structural components subjected to complex loading and demanding environmental conditions. This research also emphasizes advanced space-durable materials and structural designs for future large space systems affording significant improvements in performance and economy.*

*A significant feature of the laboratory is its static testing equipment. A 1 200 000-lb-capacity testing machine is used for tensile and*

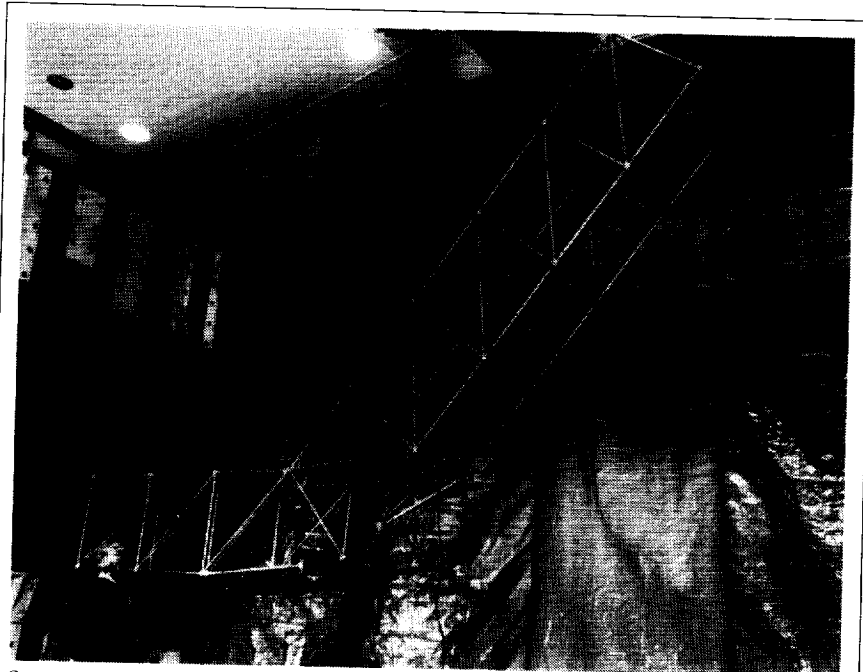
*compressive tests of specimens up to 6 ft wide by 18 ft long. Lower capacity testing machines of 300 000-, 120 000-, 100 000-, and 10 000-lb capacity also are used for smaller specimens. Capability also exists for assembling and testing large structural specimens and components such as the trusses used for Space Station Freedom development and future large space structures.*

*This complex also houses the Langley Research Center state-of-the-art analytical and metallurgical laboratory featuring all aspects of material specimen preparation and examination. Complete, automated metallographic preparation equipment is available for research on light alloys as well as metal matrix and resin matrix composites. Optical microscopy*

includes quantitative image analysis in addition to regular microscopy. Current technology electron microscopy is available including scanning electron microscopy, scanning transmission electron microscopy, and electron microprobe X-ray analysis.

Environmental testing for materials also is performed in this laboratory. Environmental exposure and characterization facilities for space materials research include two thermal cycling chambers ( $\pm 250^\circ\text{F}$ ), three electron irradiation chambers capable of pressures to  $10^{-8}$  torr and energy levels to 85 keV, and four laser interferometers for measuring coefficients of thermal expansion (to 0.05 parts per million (p/m) strain) and surface accuracy (to  $0.2\text{ }\mu\text{m rms}$ ) for elements of precision space structures. A hypersonic materials environmental system is capable of continuous test operation at Mach 5 to a 150 000-ft altitude to simulate operating conditions for future high-speed and hypersonic aircraft. The system is used to study the effects of environment on the materials used for future high-speed and hypersonic aircraft applications.

Carbon-carbon composite materials development for advanced hypersonic vehicles also is conducted. Experimental test materials are fabricated using two high-temperature ovens ( $1300^\circ\text{F}$ ), a vacuum/pressure impregnator with capability to  $500^\circ\text{F}$  at 300 psig, and two inert-atmosphere pyrolysis furnaces ( $2200^\circ\text{F}$ ). Test specimens are heat treated, and oxidation-resistant coatings are applied in a  $4500^\circ\text{F}$  inert-atmosphere furnace.



Space crane with articulating joint candidate emplaced.

1-90-9160

### **Space Crane Articulating Joint Test-Bed**

NASA's new exploration initiatives will require on-orbit assembly and construction using a space crane concept. To determine the positioning accuracy, repeatability, and controllability of space crane articulating joint candidates, a test-bed was designed and fabricated to accommodate different articulating joint designs.

The test-bed (shown in the figure) used 1 in. aluminum-tube, erectable truss hardware, was cantilevered from the Structures and Materials Research Laboratory backstop, and had a total of eight bays of 1 m truss hardware. After initial checkout, the test-bed, which will be mounted on a two-dimensional air suspension system to allow performance characterization of the articulating joint in a simulated 0g environment, is expected to generate technology for a lightweight

space crane capable of rapidly positioning payloads for final assembly. (Harold G. Bush, 43109, Thomas R. Sutter, and Richard Wallsom)

### **Failure Modes of Composite Laminates Subjected to Bending**

To design composite laminated panels as primary structures for aircraft, behavior peculiar to composite materials must be understood. In particular, laminates with holes which are subjected to bending loads are a fundamental design consideration. Graphite/epoxy 48-ply laminates with 6 in. long by 5 in. wide test sections and hole diameters ranging from 0 in. to 3.5 in. were tested to failure in four-point bending. Graphite fiber orientations were at  $\pm 45^\circ$  and  $0^\circ$ ,  $45^\circ$ ,  $90^\circ$  (quasi-isotropic) with the length direction.



Both ply orientations failed progressively through the thickness of the laminate. The  $\pm 45^\circ$  laminates failed in the  $45^\circ$  plies, thus initiating on either the tension or compression side of the specimen. This failure mode was characterized by inplane epoxy matrix shearing. The quasi-isotropic laminates failed in the  $0^\circ$  plies, thus initiating on the specimen compression side. This failure mode was characterized by interlaminar shearing/brooming. The effect of hole size on failure strain for these laminates is plotted in the figure as a function of the hole-diameter-to-plate-width ratio  $d/w$ .

The results for the laminates in this study establish that the initial failure mechanisms for laminates subjected to four-point bending are similar to the initial failure mechanisms for corresponding laminates subjected to uniaxial inplane

loadings, but failure progresses through the laminate thickness rather than having all plies fail in the cross section simultaneously. (M. J. Stuart, 43170, and C. B. Prasad)

### Evaluation of Oxidation-Resistant Carbon-Carbon Composite Materials

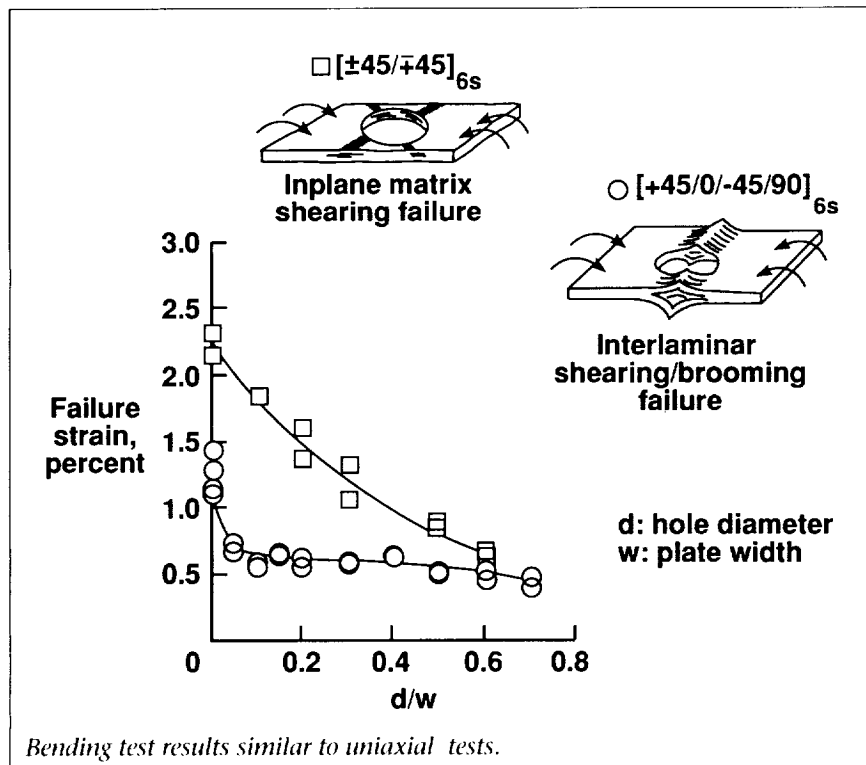
Carbon-carbon (C-C) composites are an emerging class of composites materials which have a unique combination of high-temperature properties and low densities. These properties are attractive for hot structure and thermal protection system applications on advanced aerospace vehicles such as the National Aero-Space Plane (NASP).

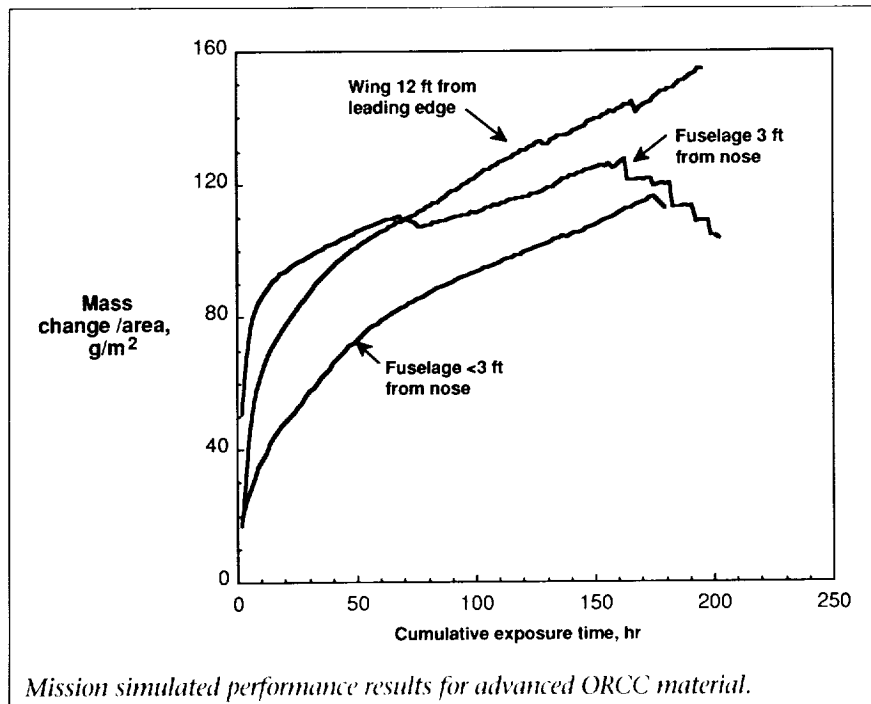


One of three furnaces in Multiparameter Mission Simulation Facility used to evaluate ORCC composite materials. 1-89-00781

A significant problem associated with carbon is that it oxidizes rapidly in air at temperatures above  $1000^\circ\text{F}$ . Hence, for use in oxidizing environments, C-C composites must be protected from oxidation. A first-generation oxidation-resistant carbon-carbon (ORCC) composite material is currently being used for thermal protection on the nose cap and wing leading edges of the Space Shuttle orbiter. Projected applications for NASP require ORCC composites, which have higher strength, higher modulus, and greater oxidation resistance than provided by the first-generation ORCC material. Research is currently being pursued to develop these improved ORCC composite materials.

Extensive evaluations of advanced ORCC composite materials are being conducted at Langley Research Center in the Multiparameter Mission Simulation Facility; these evaluations support the NASP





Program to determine oxidation performance over extended periods of time in simulated airframe environments. Mass change per unit area is plotted in the figure as a function of cumulative exposure time for one ORCC material tested in three environments simulating different locations on the airframe. The fact that no mass loss has occurred out to approximately 170 hours indicates a significant potential for this material. Mass loss data and residual mechanical properties are being measured on this and numerous other ORCC materials.

(Craig W. Ohlhorst, 43502)

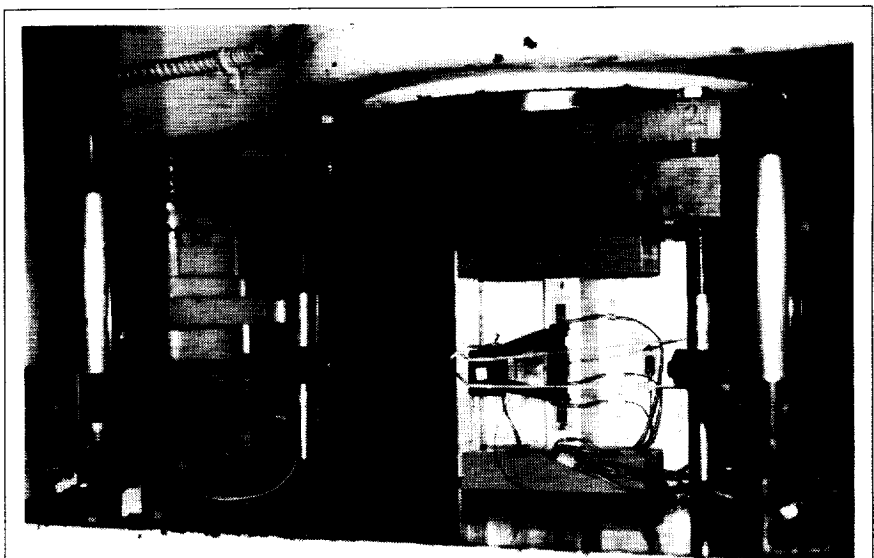
### Aluminum-Lithium Alloy Built-Up Structure Development

Aluminum-lithium alloys offer the potential for significant improvements in structural efficiency

for cryogenic tanks and dry bay structure of future space launch and transportation systems. Several alloy compositions are under continued development with a range of properties to suit a variety of applications. These alloy systems are expected to carry a cost

premium of two to five times that of conventional high-strength aerospace alloys as a result of their different and more complex casting technique and required capitalization of new production casting equipment. As a result, efforts are under way to exploit near-net-shape processing to reduce scrap rate and improve buy-to-fly ratios by a substantial margin.

One approach being explored at Langley Research Center is the development of built-up structure by attaching stiffeners to skins employing resistance welding techniques. The stiffeners are being processed by superplastic forming (SPF) and advanced extrusion techniques, both of which offer the potential for greatly improved structural efficiency. The Langley efforts are part of the development program of the joint NASA and U.S. Air Force Advanced Launch System project. Elements within the Langley program include the development of SPF parameters for a number of emerg-



*Built-up structure single stiffener compression test panel.*

L-89-12157

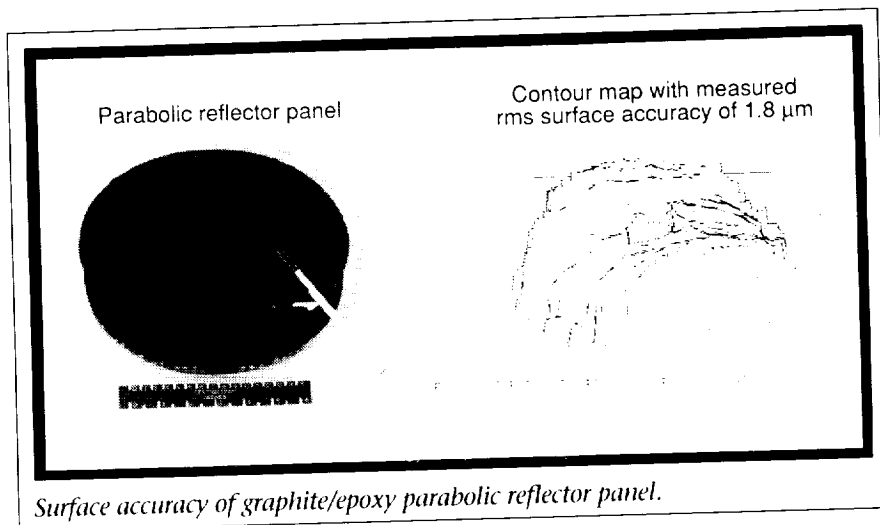
ing alloys of promise and determination of material properties after forming and joining. Also included is the development of resistance spotwelding (RSW) techniques suitable for joining stiffeners to skin and the determination of resulting structural performance.

One test utilized in the evaluation is the single stiffener compression test panel designed to evaluate local buckling and to measure the effectiveness of the RSW technique for attaching stiffener and skin. The figure shows a single stiffener compression test panel fully instrumented with strain gauges, extensometers, and deflectometers in place for testing in a 120 000-lb test machine in the Structures and Materials Research Laboratory. Panels with varying stiffener configurations processed from a number of alloy compositions have been tested; these panels have demonstrated the potential effectiveness of the built-up structure concept. In addition, the incorporation of aluminum-lithium alloys may provide cryogenic tank and dry bay structures with both lighter weight and lower cost for future launch and space transportation vehicles.

(John A. Wagner, 43142)

### Precision Composite Reflector Panels

The Precision Segmented Reflector (PSR) Program is aimed at developing the necessary technology for large-diameter segmented space-based reflectors for a wide variety of scientific missions. An

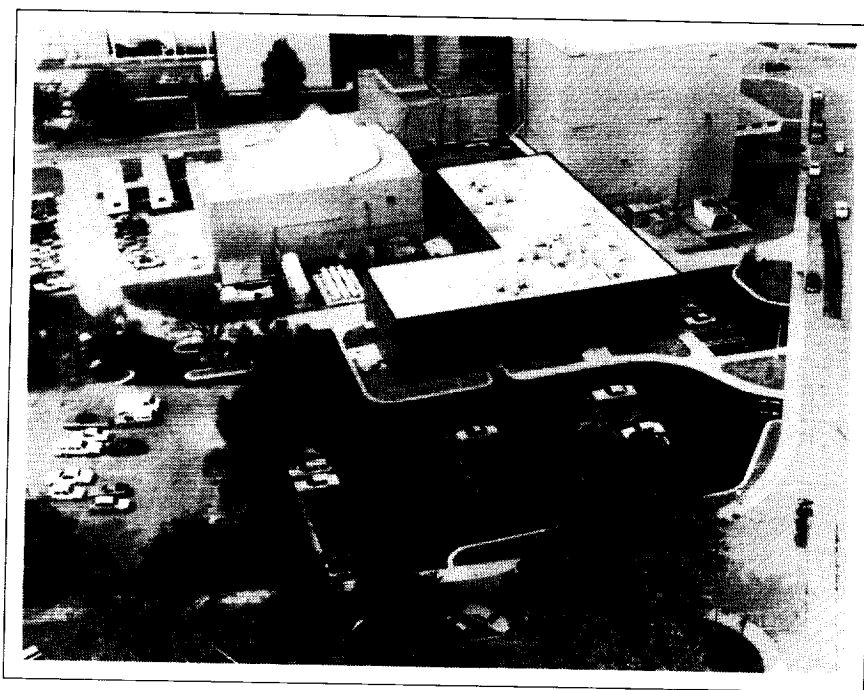


important part of this program is the demonstration of the technology required to fabricate precision, lightweight parabolic reflector panels capable of operating and maintaining their surface accuracies in the space environment. The Materials Division at Langley Research Center is developing and evaluating advanced composite materials and panel concepts for these reflectors. To support this effort, an IR (infrared) laser interferometer system capable of measuring the surface accuracies of flat and parabolic reflector panels over the temperature range of  $\pm 150^\circ\text{F}$  is under development.

The surface accuracy of a 10-in.-diameter parabolic reflector panel has been measured at room temperature in the IR interferometer system. This parabolic panel was fabricated in-house using T50/ERL1962 (Amoco Performance Products, Inc.) graphite/epoxy laminates as facesheets adhesively bonded to a graphite/phenolic honeycomb core. The top facesheet had an in-house developed film of PAEI (polyarylene ether imidazole) cocured to the laminate and subsequently coated

with vapor-deposited aluminum and silicon oxide. This metalized PAEI surface film gives the panel a very smooth surface finish and the desired reflective properties. Measurements on this panel showed an as-fabricated room temperature surface accuracy of 1.8  $\mu\text{m}$  rms (root mean square), which exceeds the PSR panel surface accuracy goal of 3  $\mu\text{m}$  rms. The vacuum-temperature chamber needed for conducting tests at  $\pm 150^\circ\text{F}$  is currently being assembled and will be used to assess the durability of this and other composite reflector panels at temperatures simulating the spacecraft operating environment.

(D. E. Bowles, 43095, S. S. Tompkins, and T. W. Towell)



## Polymeric Materials Laboratory

---

*The Polymeric Materials Laboratory complex, which was completed in 1986, provides 25 000 ft<sup>2</sup> of floor space for the synthesis and characterization of high-performance polymers as well as the development of processing technology and composite fabrication. The building heating, ventilation, and air-conditioning system was designed to provide the highest air pressure in the halls, lower pressures in the office and computer areas, and the lowest pressure in the synthesis and instrument laboratories. This pressure zoning precludes the possibility of chemical fumes escaping from the laboratories to other parts of the building.*

*The complex contains seven synthesis laboratories that can accommodate two persons; each laboratory has two chemical fume hoods and a bench-scale laboratory designed for synthesis of large batches*

*of polymeric materials. An isolated explosion-proof area is provided for safely performing hydrogenations and pressure polymerizations. The facility also contains a film-casting laboratory with environmentally controlled film-casting boxes and forced air ovens for polymer curing. A chemical storage area was constructed to house all needed chemicals, with the highly flammable chemicals stored in flameproof cabinets that are exhausted to the outside of the building through an explosion-proof exhaust manifold system. Another cabinet that is exhausted separately holds highly corrosive acid chlorides. The storage facility is protected by an automatic extinguisher system that will flood the area with CO<sub>2</sub> when triggered by high temperature or smoke.*

*Much of the work of this laboratory is directed toward the synthesis of processible, tough, durable, high-*

*performance matrices and the development of relationships between molecular structure, neat resin properties, and composite properties. Classes of polymers being investigated as matrix resins include amorphous and semicrystalline thermoplastics, lightly crosslinked thermoplastics, semi-interpenetrating networks, and toughened thermosets.*

*Extensive characterization equipment is housed in the instrument laboratories and used for performing chromatography and molecular weight determinations, thermal analyses, X-ray characterizations, rheological and rheometrical evaluations, infrared and mass spectroscopy, and mechanical strength determinations of adhesive bonds, polymer moldings, films, fibers, and composites.*

*The Composites Processing Laboratory located on the first floor of Building 1293A is the focal point at Langley Research Center for research and development of advanced polymer composite systems. The primary function of this laboratory is to determine the potential of newly synthesized and promising commercially available polymers for use as matrix systems for the fabrication of advanced fiber reinforced composites. In addition, novel tooling concepts are employed for the fabrication of a variety of complex structural shapes.*

*Research quantities of graphite-reinforced polymer composite material are fabricated in drum-wound prepreg machines by solvent solution impregnation. Hot rolls are used to manufacture melt-impregnated composite material. Unique dry powder coating/melt fusion equipment is employed to fabricate prepreg from advanced, difficult-to-process polymer matrix materials. Test panels fabricated from these composite systems are scanned ultrasonically to establish structural integrity prior to mechanical testing to determine tensile, shear, and compression properties. Auxiliary equipment utilized to fabricate prepreg and test panels includes a particle-size analyzer, weaving loom, high-temperature autoclave, vacuum press, dry powder spray chamber, heated platen presses, and air-circulating ovens.*

## Characterization of Polymer Molecular Weight

The aerospace community is experiencing an evolutionary movement toward the development of advanced thermoplastics for molding and composite applica-

Sample	M <sub>w</sub>	M <sub>n</sub>	M <sub>v</sub>	M <sub>w</sub> /M <sub>n</sub>	[η]
Neat resin	52,300	15,800	45,700	3.31	0.424
Fractured resin	50,600	15,400	44,000	3.29	0.428
Solvent-cast film	50,200	14,900	43,600	3.38	0.427
Solvent-coated prepreg	54,900	15,900	46,800	3.44	0.430
Hot-melt prepreg	53,200	16,300	45,500	3.27	0.409
Composite	53,200	15,900	45,700	3.34	0.422
Neat resin molding	54,600	16,700	47,500	3.27	0.402

Molecular weights in g/mole; viscosity in dL/g.

*Effect of processing on molecular weight of polysulfone.*

tions. Accompanying this movement is an opportunity for chemical characterization at a level not feasible with thermosetting materials. This opportunity is made possible by the inherent property of solubility exhibited by many thermoplastics. Because they can be dissolved, the most important property (molecular weight) which they possess can be examined. Processibility, structural integrity, and mechanical performance are ultimately related to molecular weight. Many technical advances in these areas have been made possible by the ability to characterize and control the molecular weight of polymers.

Synthetic polymeric materials generally contain a distribution of molecular species. The Solution Property Laboratory developed a number of analytical techniques to examine this distribution. Membrane osmometry, low-angle laser light scattering photometry, differential viscometry, and gel permeation chromatography are used to characterize a number of

molecular weight averages. The laboratory is being upgraded to enable chromatographic analysis at temperatures of 150°C as well as analysis by vapor phase osmometry. Molecular weights from a few hundred to several million can be measured.

The figure summarizes a study that assessed the molecular level effects of processing on a commercially available polysulfone. A characterization of various molecular weight parameters (*w*, *n*, and *v* are weight, number, and viscosity, averaged, respectively) showed very little change at the molecular level as the result of processing, a desirable property for many applications. Other polymers may behave differently. Similar solution property measurements are being used to study synthetic procedures such as offsets in stoichiometry and end-capping sequences and their effects on processibility. (Philip Young, 44265)

---

## LaRC TPI Dry Powder Towpreg Process

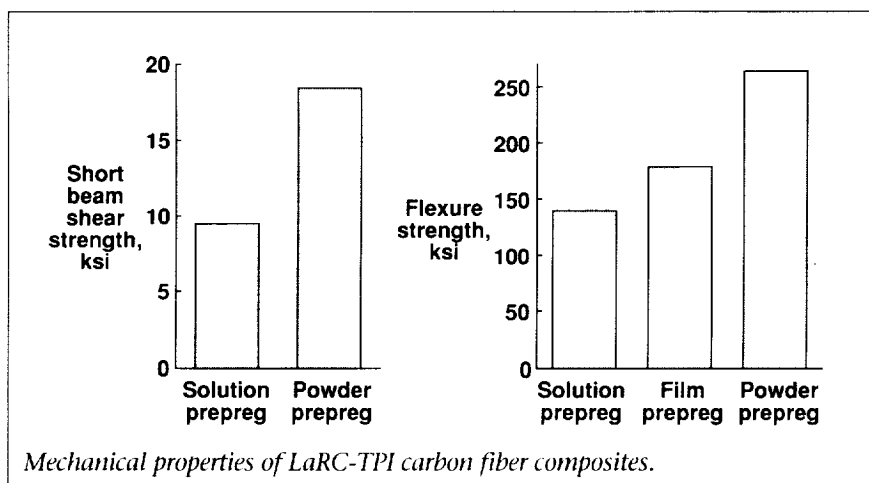
---

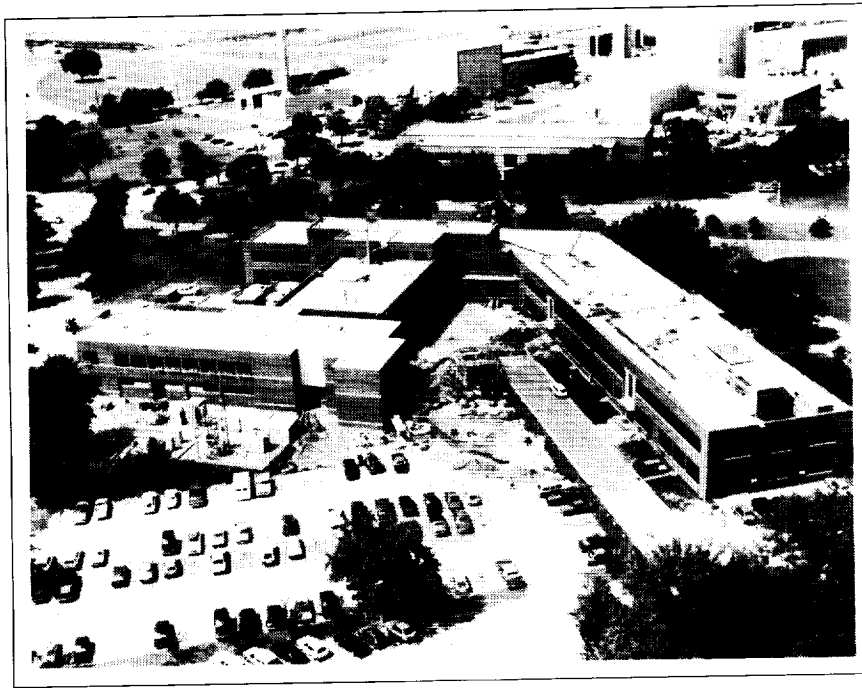
The production of prepreg by the dry powder process overcomes many of the difficulties associated with melt, solution, and slurry prepregging of advanced composite materials. This process has been found to be especially effective in impregnating high-temperature polymers. A pneumatic banding jet is used to uniformly spread 3 k, 6 k, and 12 k carbon tow bundles to desired widths. The spread tow is coated with a controlled mass of dry polymer powder in a recirculating fluidization chamber. The powdered resin then is sintered to the carbon fibers by mild radiant heating.

A unique cylindrical capacitance gauge has been fabricated to continuously monitor the resin mass fraction of the powder-coated towpreg. Over 4000 meters have been fabricated in this facility, and this powder-coated towpreg has been successfully woven into cloth by commercial weavers. The mechanical properties of laminates fabricated from this material appear to be superior to properties of

similar laminates fabricated from prepreg produced by conventional methods as shown in the figure. Development is under way to increase the towpreg line speeds to parallel commercial prepreg production rates. Feedback monitor controls will be employed to automate the powder coating process. Process controls for the dry powder prepreg process will be established to permit commercial vendors to adequately assess this approach for production of industrial quantities of high-quality advanced composite prepreg. (Robert Baucom, 44252)

---





## NDE Research Laboratory

---

*The reliability and safety of materials and structures are of paramount importance to NASA. The assurance of reliability must be based on a quantitative measurement science capability that is nondestructive. The Langley Research Center NDE Research Laboratory has as its prime focus the development of new measurement technologies that can be directly applied to ensuring material integrity. Furthermore, the laboratory activity is strongly directed toward developing physical properties required for structural performance.*

*A new facility has been constructed which added 16 000 ft<sup>2</sup> of laboratory space to the existing nondestructive evaluation (NDE) research area. This new facility was furnished and occupied in January 1989 and will allow for some expansion of NDE efforts over the coming years.*

*The NDE Research Laboratory is a combination of research facilities providing advanced NDE capabilities for NASA and is an important resource for government and industry technology transfer. The laboratory is the Agency's focal point for NDE and combines basic research with technology development and transfer. The activity concentrates on NDE materials measurement science for composites and metals with emphasis in materials characterization as well as impact damage, fatigue, applied and residual stress, and structural NDE with smart sensors/materials. A particular new focus highlights NDE requirements for Space Station Freedom on-orbit NDE and national problems of aging aircraft.*

*The facility is a state-of-the-science measurement laboratory linking 16 separate operations to a central computer consisting of a*

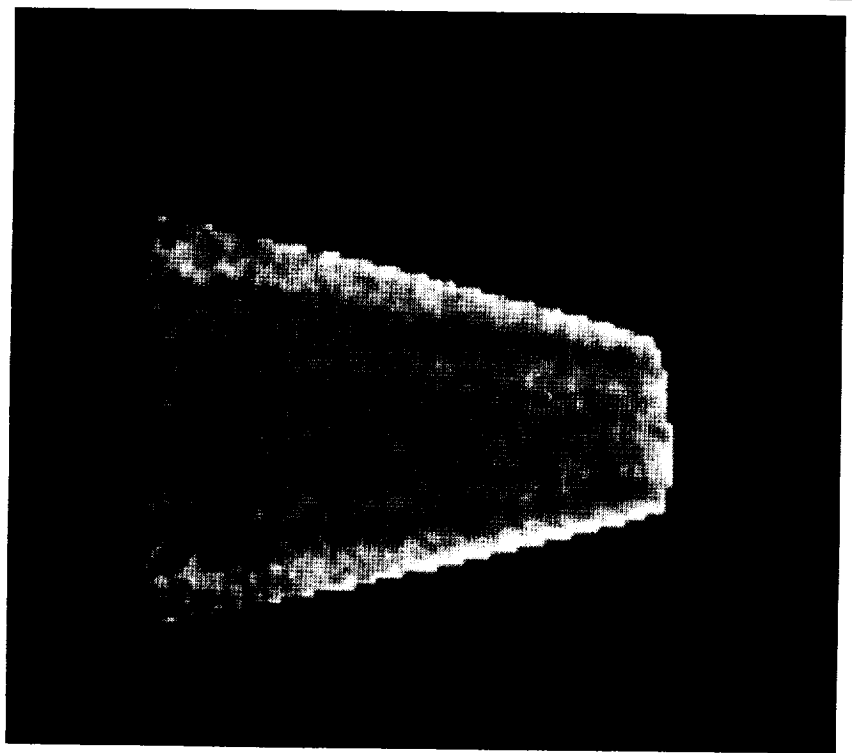
*VAX-750 with 10 megabytes of internal memory and more than 500 megabytes of fast storage tied to staff desktop microcomputers. The system interfaces with a real-time video input-output so that NDE images can be obtained, processed, and analyzed on-line. The major laboratory operations include a 55-kip and a 100-kip load system for stress/fatigue NDE research, a magnetics laboratory for residual stress, three computer-controlled ultrasonic scanners for imaging material properties, a technology transfer laboratory, an electromagnetic impedance characterization laboratory for composite fiber integrity, and a composite cure monitoring laboratory for process control sensor development. Other major laboratory operations include a nonlinear acoustics laboratory for advanced NDE research, a laser modulation applications laboratory for remote sensing and smart materials, a pressure and temperature*

*derivative laboratory for higher order elastic constant measurements, a thermal NDE laboratory, and a signal processing laboratory for improved image resolution and information transfer. An X-ray tomography system is under construction to provide the first view of material or structural failure under load and will be on-line in 1990.*

### **Infrared Measurements of Heat-Transfer Coefficient for Global Imaging of Flow Fields**

The Nondestructive Evaluation Sciences Branch has developed a noncontacting and quantitative technique for assessing flow parameters in wind-tunnel environments. By radiatively injecting heat into the airfoil skins and monitoring the subsequent temperature decay, quantitative heat-transfer coefficients can be imaged rapidly over large fields. Quantitative images of this nature can be used both as a diagnostic tool, e.g., to detect transition from laminar to turbulent flow, and as a research tool to refine and advance state-of-the-art aerodynamic models.

The tests of the infrared flow diagnostic system were performed on a stainless-steel delta wing of  $76^\circ$  with a thin insulating surface coating. Data were taken for Reynolds numbers ranging from  $5 \times 10^5$  to  $1.25 \times 10^6$  at selected angles of attack between  $0^\circ$  and  $28^\circ$ . Flash lamps were used to evenly heat the model, thus allowing the entire wing to be imaged at once. A dedicated microcomputer and video digitizer were used for data acquisition and

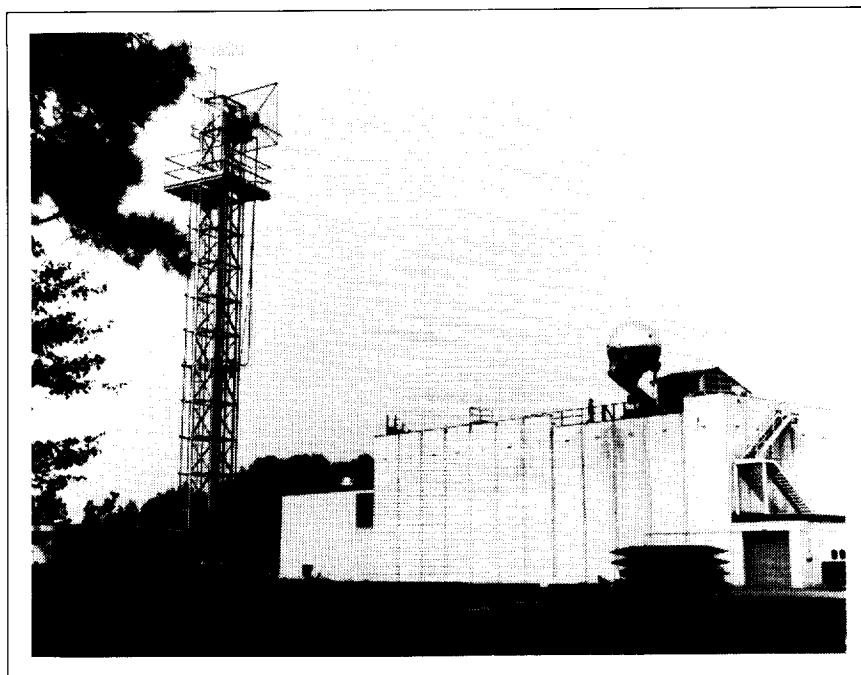


*Heat-transfer image for angle of attack of  $20^\circ$  with 90 mph wind speed.*

processing. An example of the infrared heat-transfer image is shown in the figure with the delta wing at an angle of attack of  $20^\circ$  and a Reynolds number of  $1.25 \times 10^6$ . Extensive flow visualization studies of the complex delta wing flow field have been compared to the infrared results. The comparisons have shown an increase in heat transfer at turbulent transition and a decrease in heat transfer at laminar-vortex separations.

**(D. Michele Heath, 44964)**





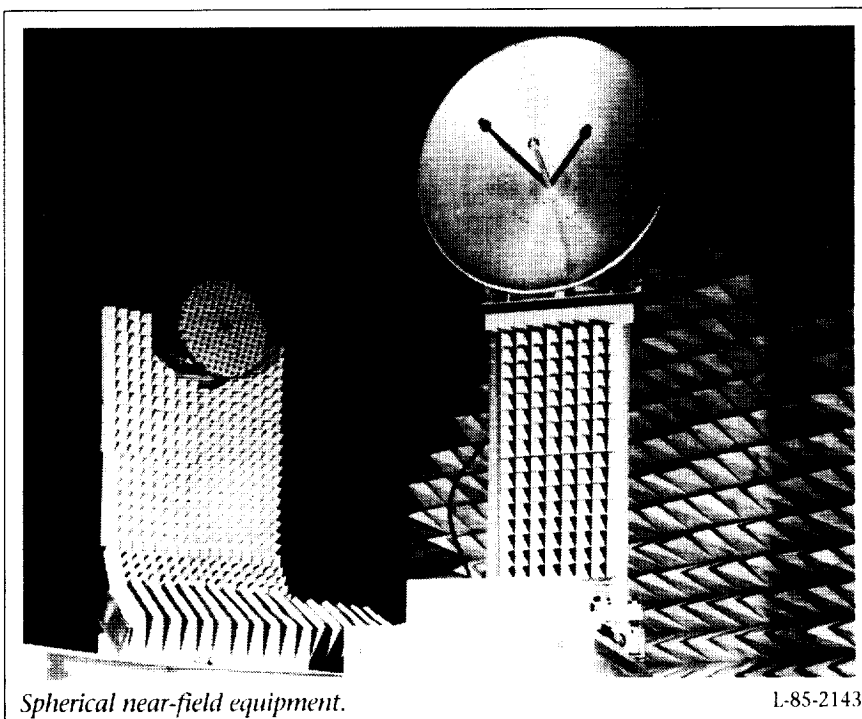
# Vehicle Antenna Test Facility

*The Vehicle Antenna Test Facility (VATF) is a research facility used to obtain data for new antenna performance and electromagnetic scattering data in support of various research programs. The VATF consists of two indoor radio frequency anechoic test chambers and an outdoor antenna range system. The anechoic chambers provide simulated free-space conditions for measurements from 100 MHz to >40 GHz. The anechoic chambers, which are shaped like pyramidal horns to reduce specular reflections of the walls, are more than 100 ft long and have test area cross sections approximately 30 ft by 30 ft.*

*A spherical near-field (SNF) measurement capability was added to the low-frequency anechoic chamber. A precision antenna positioning system, an antenna source tower, and an optical alignment system designed*

*for SNF measurements were installed in the low-frequency anechoic chamber, and the capability now exists for*

*automatic performance of precision SNF measurements up to at least 18 GHz. Antennas with diameters up to*



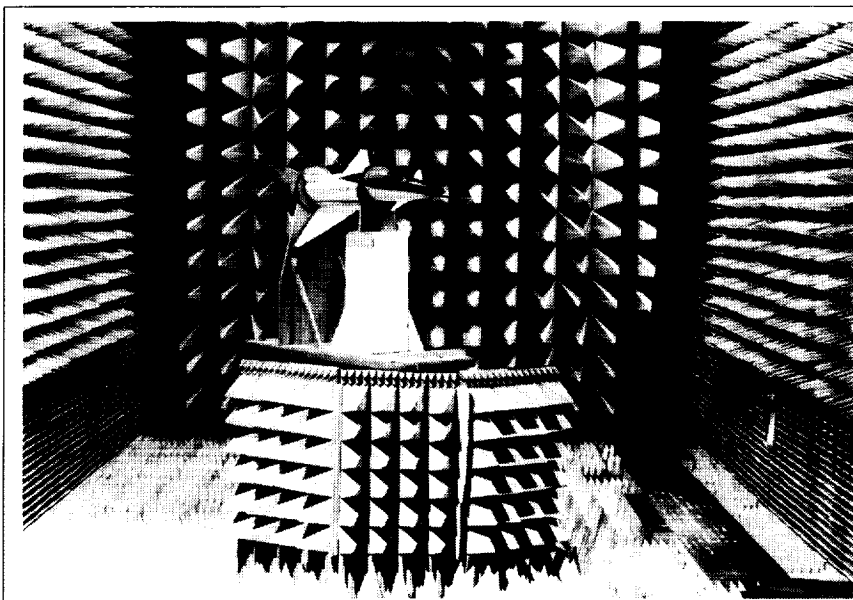
*Spherical near-field equipment.*

L-85-2143

12 ft can be measured if their electrical size is no greater than 100 wavelengths (i.e., diameter/wavelength  $\leq 100$ ). This limitation is imposed by the SNF system software, which transforms the near-field data to obtain the desired far-field data. Measured data stored on disc can be processed to provide antenna directivity, polar or rectangular plots of the radiation patterns, and three-dimensional contour plots of the antenna radiation characteristics.

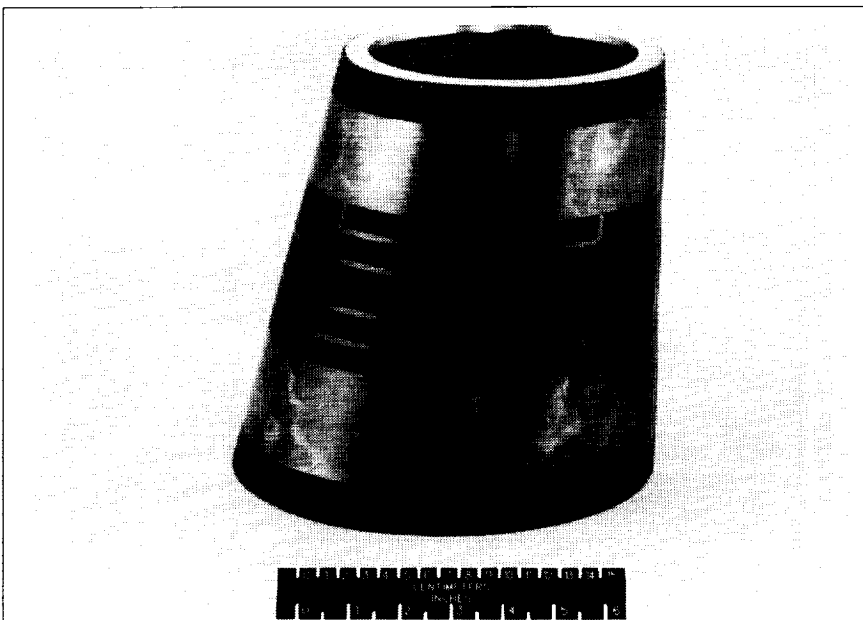
The high-frequency anechoic chamber was used to establish a Compact Range Facility. The compact range is an electromagnetic measurement system used to simulate a plane wave illuminating an antenna or scattering body. The plane wave is necessary to represent the actual use of the antenna or scattering from a target in a real-world situation. The compact range utilizes an offset-fed parabolic reflector to create the simulated plane wave test conditions. The standard commercially available compact range is limited to the measurement of antennas or models with maximum dimensions of 4 ft over the frequency range of 4 GHz to 100 GHz.

The outdoor antenna range system is available for use when the antenna or test model size or frequency precludes the use of the anechoic chambers. The outdoor range consists of two remote transmitting towers that are spaced 150 ft and 350 ft from the test positioner mounted on the VATF roof. The VATF has several electronic laboratories with the extensive measurement capability needed to support the design of unique antennas prior to their evaluation in the antenna chambers or on the outdoor antenna range system.



X-31 Aircraft Drop Model during antenna testing in Low-Frequency Antenna Test Facility.

1-91-00626



Printed circuit antenna for command, control, and telemetry subsystems on X-31 Aircraft Drop Model.

1-90-5242

### Design and Testing of X-31 Aircraft Drop Model Antenna System

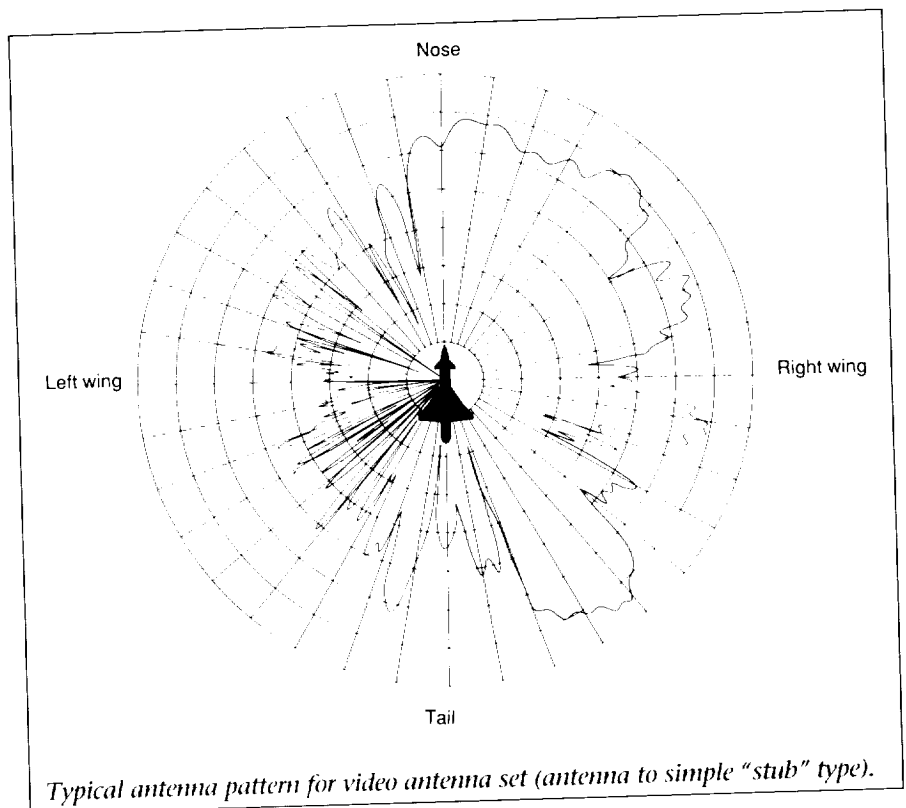
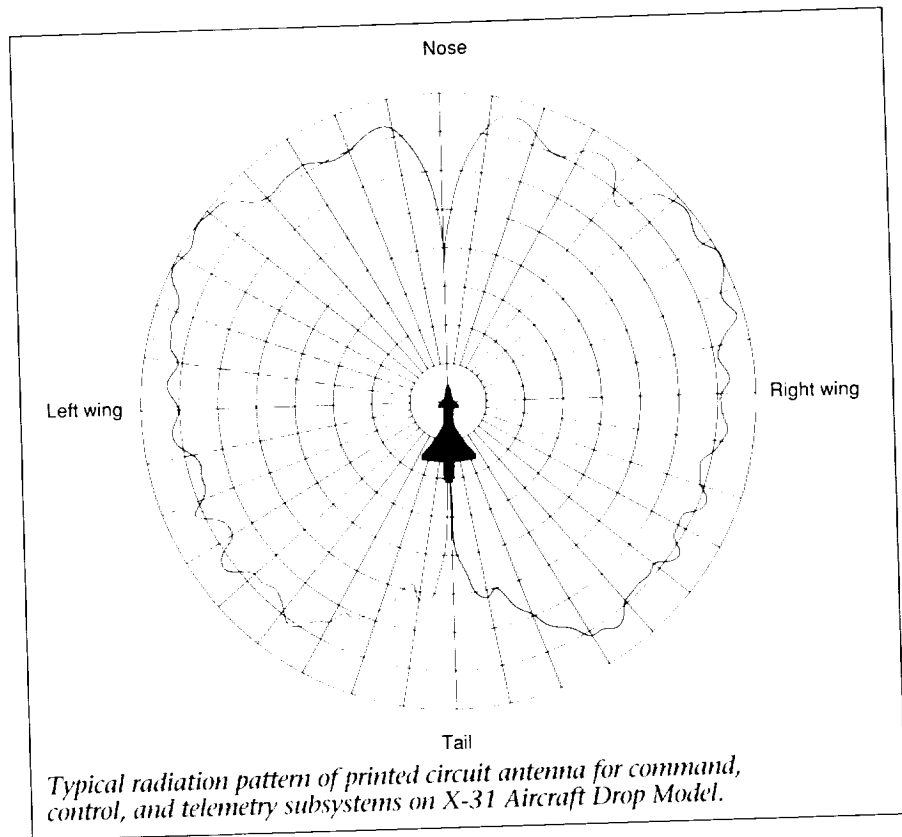
Antenna pattern measurements of the command, control, telemetry, and video antenna systems of

the X-31 Aircraft Drop Model were conducted in the Low-Frequency Antenna Test Facility as shown in the first figure. The electronic subsystems operate at radio frequencies 1804.5 MHz, 1835.5 MHz, 1496.5 MHz, and 2220.5 MHz,

respectively; therefore, the antenna pattern measurements were conducted at these frequencies to verify system performance. The objective of this particular test was to verify antenna system performance when integrated with the complete aircraft system configuration.

Because the command, control, and telemetry antenna systems are the most critical to successful flight operation, Langley Research Center personnel designed and developed a printed circuit antenna array system (as shown in the second figure) which would provide near-optimum electrical characteristics for these applications. This assembly was located in the nose of the X-31 fuselage. The printed circuit antenna consists of two antenna arrays that are designed to accommodate all three frequencies associated with the electronic subsystems mentioned previously. Drawings of the power dividers and antenna elements were produced using a Computer Aided Design (CAD) system that allowed the artwork to be generated directly. This artwork was then used to photo-etch both arrays with their respective power dividers on the outside of a single piece of 1/16-in. thick teflon fiberglass board with a thick layer of copper clad on each side. A heat treating process was used to wrap this board to the shape required to fit the complex cone support structure.

The third figure shows a measured antenna pattern for the command antenna and is typical of other patterns measured for the command, control, and telemetry antenna systems. Test results indicate that these antennas



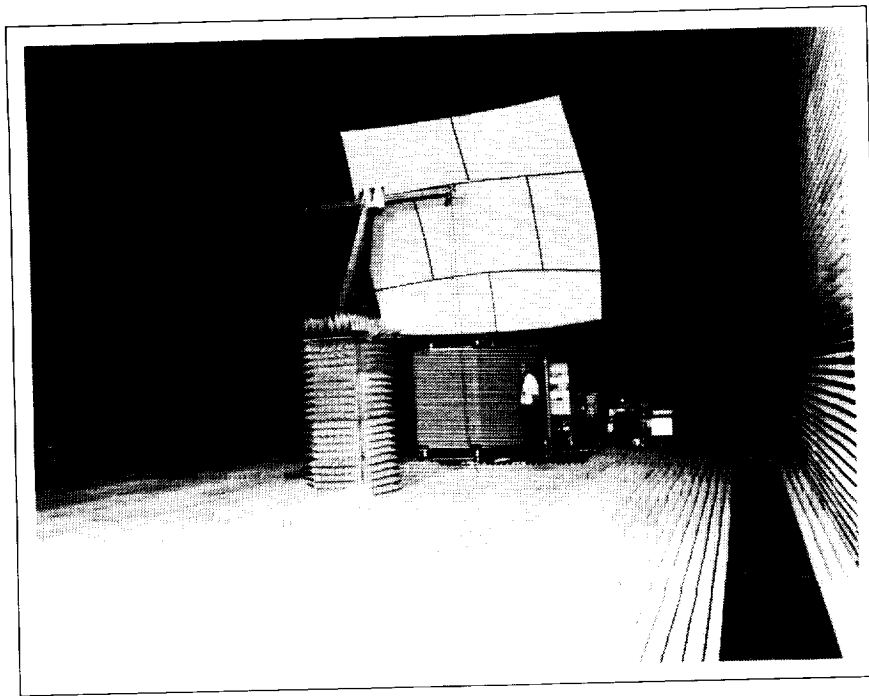
---

provide excellent coverage for practically all possible aircraft attitudes.

The fourth figure shows an antenna pattern measured for the video antenna set. This antenna is a simple, commercially produced "stub" type antenna, and its patterns show numerous deep nulls that are locations where signal dropouts are likely to occur. However, the video channel is a noncritical link.

**(W. Robert Young, 41824)**

---



## Experimental Test Range

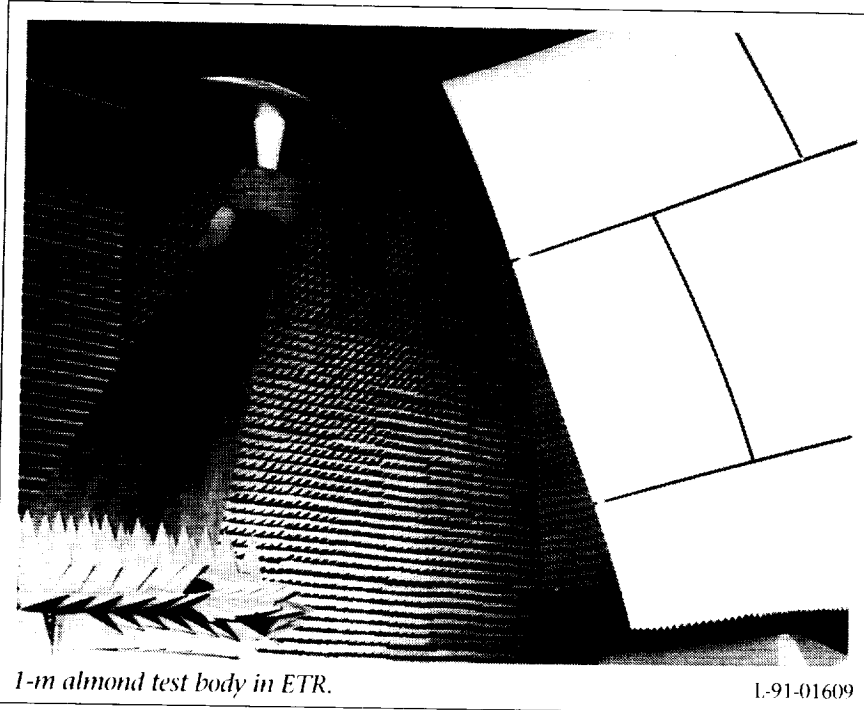
---

The Experimental Test Range (ETR) is an indoor radio frequency (RF) anechoic laboratory designed to improve existing compact range technology through research and to support ongoing electromagnetic measurements at the Antenna and Microwave Research Branch (AMRB). The ETR is capable of simulating free space conditions for microwave measurement research using anechoic pyramidal and wedge-shaped absorber material that completely covers the interior of the RF shielded 40-ft by 40-ft by 80-ft chamber. Currently, a large 16-ft by 16-in. cosine-squared blended rolled edge main reflector is used along with a Gregorian subreflector for a novel approach to compact range designs.

The antenna feed, subreflector, and main reflector along with strategically placed absorber material form a reflector system that generates a uniform plane wave in a volume of

space near the center of the chamber. The uniform plane wave is necessary to simulate far-field conditions for the actual use of antennas or scattering bodies in real-world situations.

In addition to the chamber and reflector systems, a state-of-the-art radar and data processing system is in use. The pulsed continuous wave (CW) radar developed at Ohio State University is capable of continuously sweeping over the frequency range of 2 GHz to 18 GHz and can be outfitted with a Ka-band frequency doubler giving the radar the potential of making measurements up to 36 GHz. A Hewlett-Packard 386 Vectra computer located outside the chamber controls all aspects of the radar with menu-driven software. After the data have been collected by the 386 computer, they may be sent directly to a Tektronix XD88 workstation for signal processing and display.



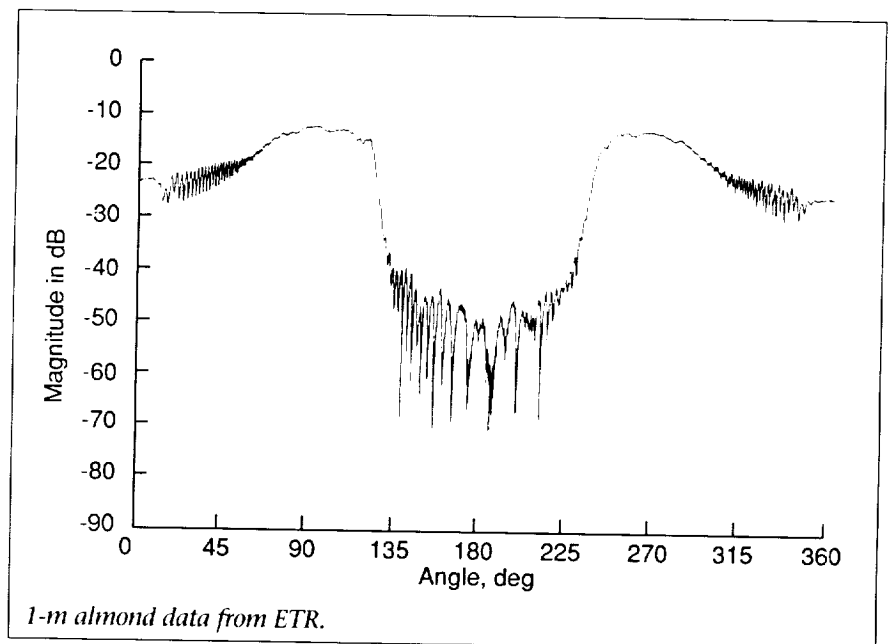
### Measurements of 1-m Almond Test Body Radar Backscatter

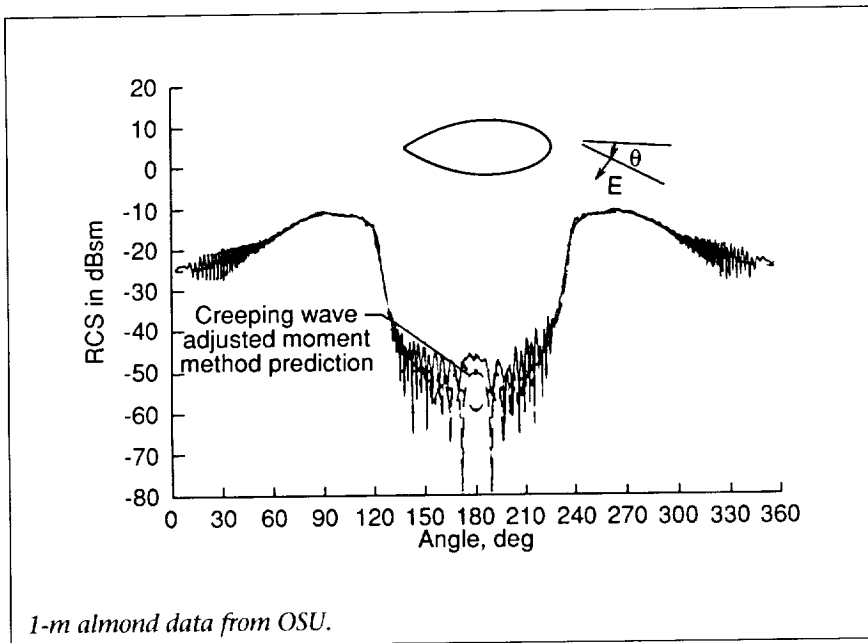
An important characteristic property of a radar backscatter measurement laboratory is the dynamic range. The dynamic range is the difference measured in decibels between the receiver noise floor and its saturation level. An almond test body (shown in the first figure) was chosen as a range performance and calibration target for part of the preliminary evaluation of the ETR. The almond is a standard target used in many ranges because of its large radar cross section (RCS) variation as a function of aspect angle (for example, it is a good target for dynamic range estimation). The almond is also a target whose RCS has been analyzed and computed theoretically.

The 1-m almond was constructed of a high-density foam and painted with silver for use as one of the calibration targets for the ETR.

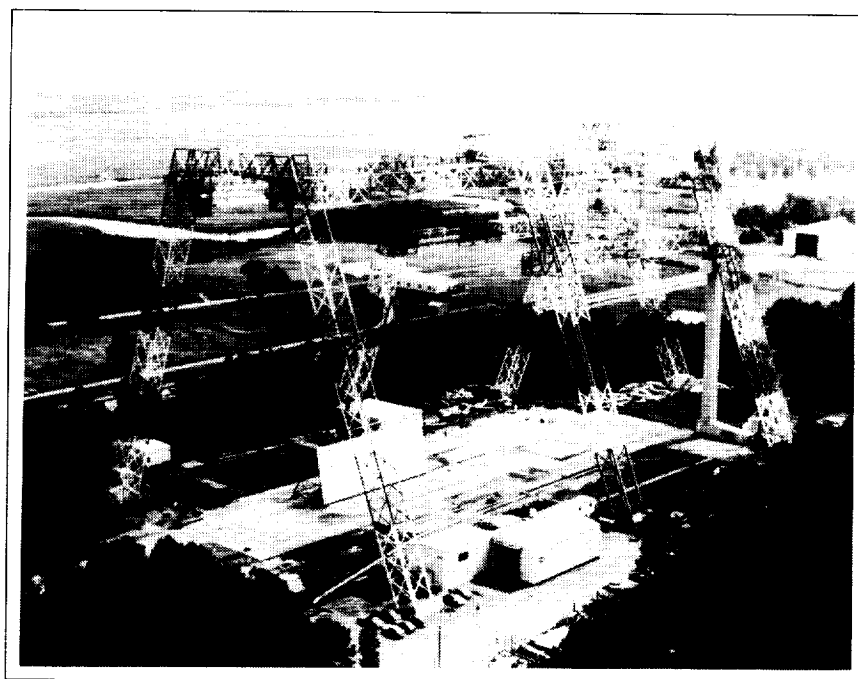
Shown in the second and third figures is a comparison between measurements made in ETR (second figure) and those made at the Ohio State University (OSU) ElectroScience Laboratory (third figure). In both cases, the data were taken at 10 GHz with the electric field parallel to the plane of rotation (E-plane). Below 40 dB relative to a square meter (dBsm), the quality of the surface of the almond, the conductive paint, the model positioning, and the ability of the range electronics to subtract background clutter become critical. By measuring various different models, the ability to assess the background subtraction and range sensitivity improves.

The line overlaying the OSU measurement represents a moment method solution to the magnetic field integral equation computing the expected RCS and can be used





to extract various scattering mechanisms such as specular returns and creeping waves.  
(Erik Vedeler, 41825)



## Impact Dynamics Research Facility

---

*This facility, which was originally used by the astronauts during the Apollo Program for simulation of lunar landings, has been modified to simulate crashes of full-scale aircraft under controlled conditions. The aircraft are swung by cables, pendulum-style, into the concrete impact runway from an A-frame structure approximately 400 ft long and 230 ft high. The impact runway can be modified to simulate other ground crash environments, such as packed dirt, to meet a specific requirement.*

*Each aircraft is suspended by swing cables from two pivot points 217 ft off the ground. It is then pulled back along an arc to a predetermined height by a pullback cable from a movable bridge on top of the A-frame, released from the pullback cable, and allowed to swing, pendulum-style, into the ground. An instant before impact,*

*the swing cables are separated from the aircraft by pyrotechnics. The length of the swing cables regulates the aircraft impact angle from 0° (level) to approximately 60°. Impact velocity can be varied to approximately 65 mph (governed by the pullback height). Variations of aircraft pitch, roll, and yaw can be obtained by changes in the aircraft suspension harness attached to the swing cables. Onboard instrumentation allows data to be obtained through an umbilical cable attached to the top of the A-frame. Photographic data are obtained by onboard cameras, ground-mounted cameras, and cameras mounted on top of the A-frame. The maximum weight of the aircraft is 30 000 lb.*

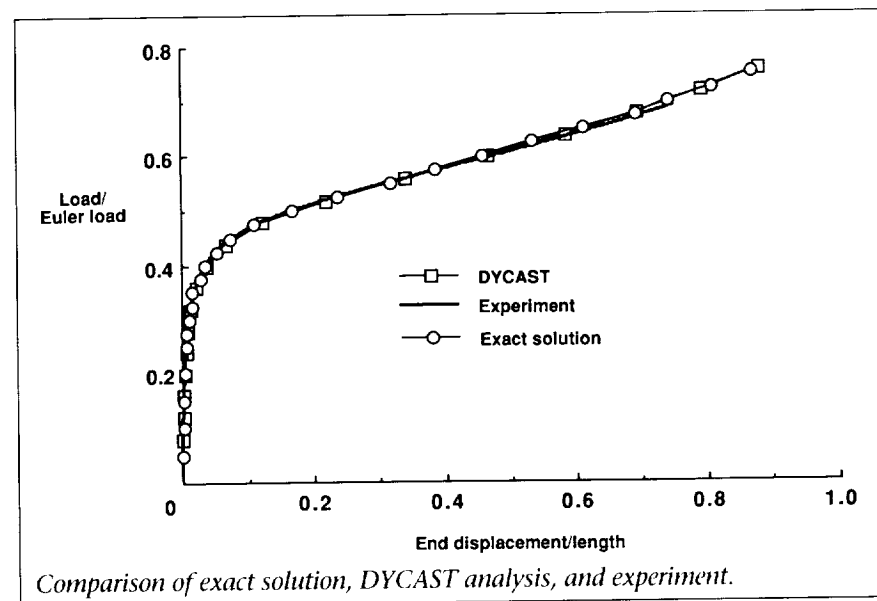
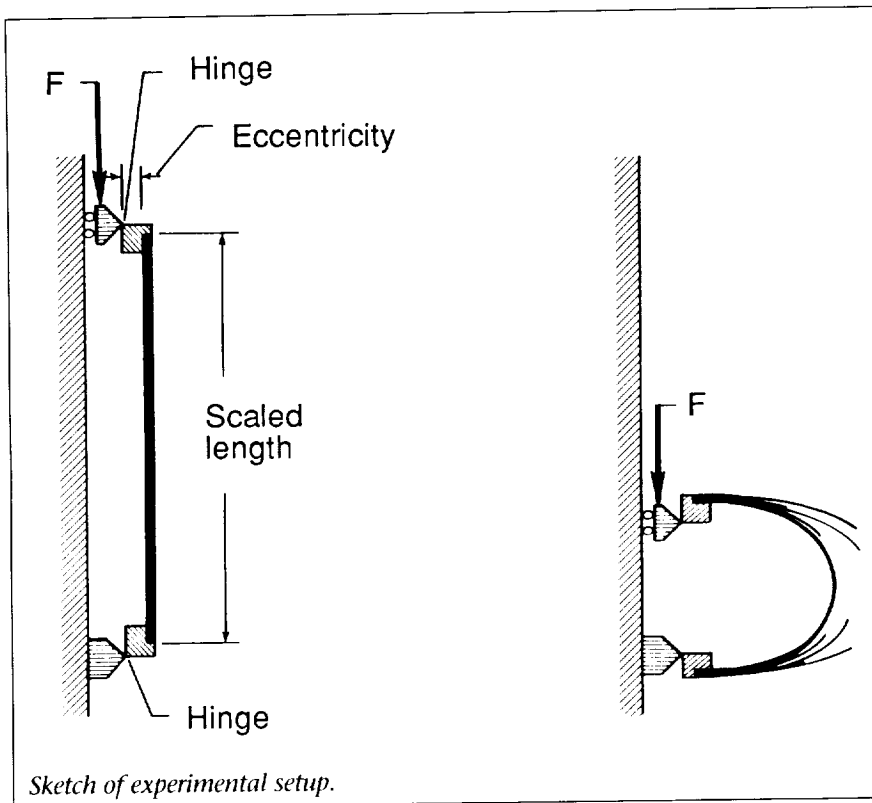
### **Beam Column Data to Verify Analysis Tools**

---

A series of parametric experimental studies were conducted to provide a data base for evaluating the accuracy and ease of implementation of nonlinear finite-element codes in analyzing complex structural impact problems.

In the study, an eccentrically loaded 24-ply unidirectional graphite/epoxy (AS4/3502) beam with a gauge length of 15 in., width of 1.5 in., and thickness of 0.13 in., shown in the first figure, was chosen for comparison of the analytical codes because the beam-column exhibits similar fundamental bending and failure characteristics observed in the lower portion of an aircraft fuselage during a crash. In addition, an exact solution of the static beam-column exists, and data are avail-



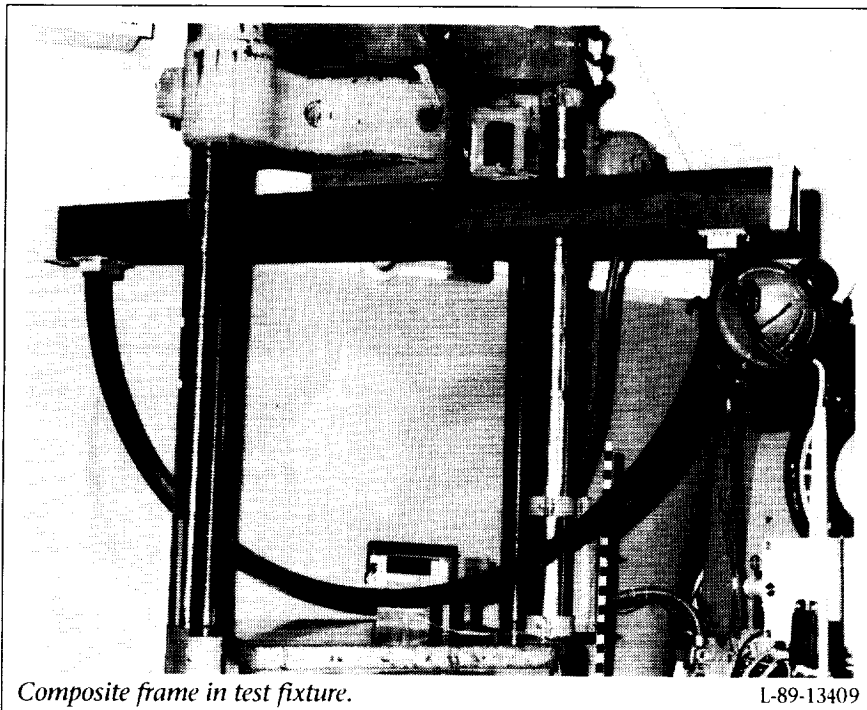


able for various size composition beams with different laminate stacking sequences. A sketch of the experimental setup is shown in the first figure. Offset hinge supports at the top and bottom generated a

combined bending and axial loading state. The bottom hinge allowed one rotational degree of freedom, while the top hinge allowed vertical translation and rotation. The finite-element code

DYCAST (Dynamic Crash Analysis of Structures), developed by Grumman Corporation, and the NIKE/DYNA codes, developed by the Lawrence Livermore National Laboratories, were used in this study.

Experimental data are compared to the DYCAST beam model and the exact solution in the second figure. The DYCAST beam results correspond almost identically with the exact solution and are in excellent agreement with the test data, even for very large displacements and loads. Additional load-deflection responses (not shown) from plate models were generated using NIKE and DYCAST codes and a beam model using NIKE. The DYCAST plate model, with triangular members, was considerably stiffer than the DYCAST beam solution and consistently overpredicted the static load-deflection response by approximately 10 percent. The NIKE rectangular plate model showed good agreement with the exact solution for small deflections. However, as the load increased, the solution stiffened and deviated from the exact response. In contrast, the NIKE beam model overpredicted the small deflection beam response by approximately the same amount as the DYCAST plate model, but for larger displacements, the NIKE model approached the exact solution. Of the beam models, DYCAST gave the best correlation with the exact solution with little computational effort; of the plate models, NIKE provided the next best correlation with the exact solution, but it required considerable computational effort. (Edwin L. Fasanella and Karen E. Jackson, 44150)



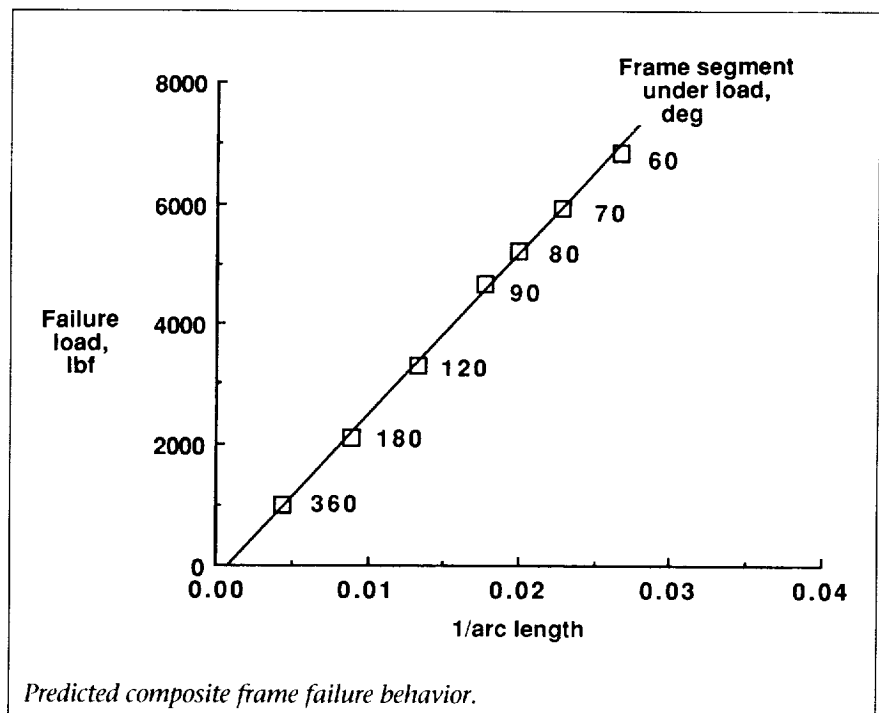
### Effect of Floor Location on Failure of Composite Fuselage Frame

Experimental and analytical studies are part of the composite impact dynamics research to generate a data base on the behavior of composite structures under crash loads. Analysis and experimental static and dynamic tests of frames such as the one shown in the first figure are being used to verify the analytical predictions for the composite fuselage frame concepts. Part of the effort has been the determination of the effect of the floor vertical attachment position on the response and failure of generic composite fuselage frame concepts.

Nonlinear finite-element models of a 6-ft-diameter composite fuselage frame concept were formulated. Static loads were applied to the frame/floor simulation to determine the load-deflec-

tion response of the composite frames. Failure loads and strain distributions were determined using the models in which the location of the simulated floor was

moved to several locations on the circumference of the frame. As is shown by the data in the second figure, the load that produced failure of a composite I-frame varies linearly as a function of  $1/\text{arc}$  length of the loaded lower portion of the frame. The linear variation with  $1/\text{arc}$  length of the ring or arch is also predicted by closed-form solutions for loaded rings/arches. Note that the shorter frame segments produced the highest failure loads. Typical circumferential strain distributions (at a 500 lbf load) for the composite fuselage frame for different floor locations were similar to the distribution for the floor located at the diameter (Position 1). Although the strain distributions associated with the lower floor locations were compressed horizontally between the ends of the floor attachment points, failure still occurred at the point of ground contact and at plus and minus positions up the frame from the point of ground contact.

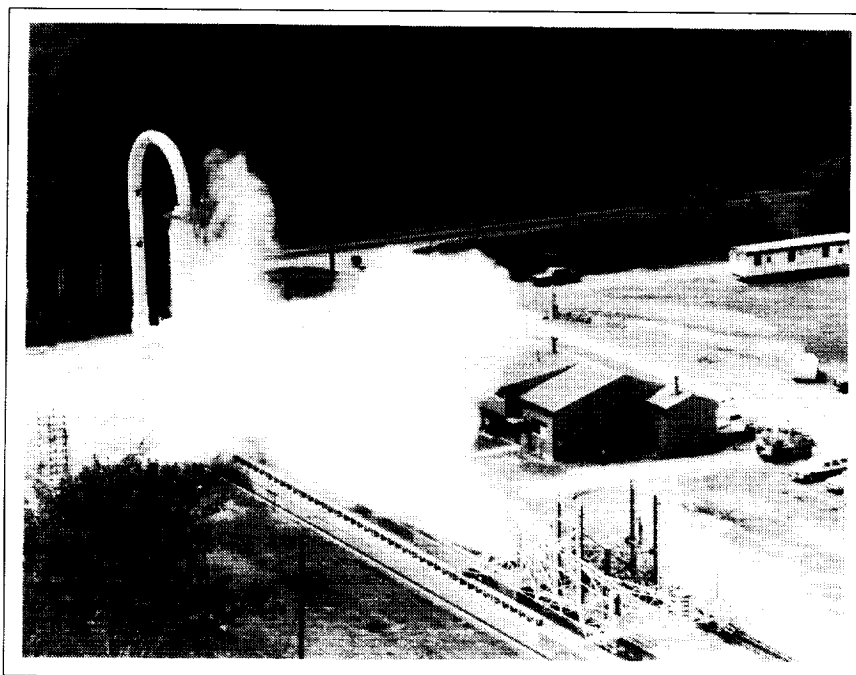


---

With the widely separated, discrete failure locations associated with the composite frame concepts, a need exists to provide innovative structural concepts that have some inherent, more efficient energy absorbing mechanisms in the subfloor design.

(Lisa E. Jones and Huey D. Carden, 44151)

---



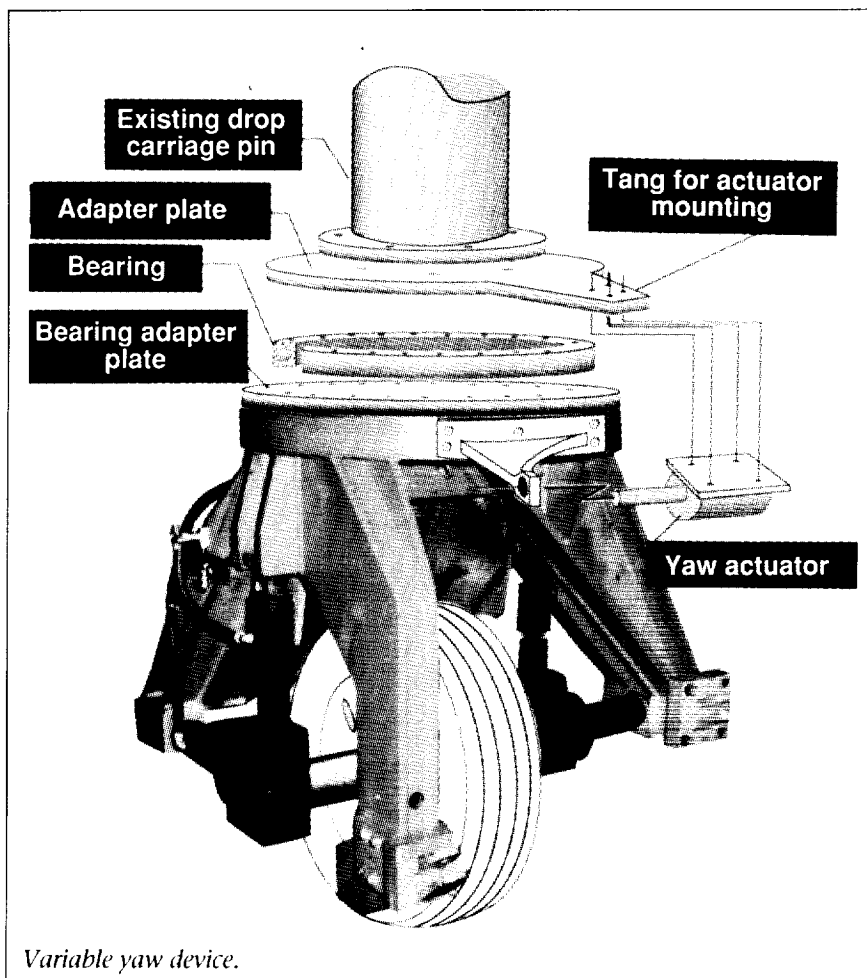
## Aircraft Landing Dynamics Facility

*In 1985, Langley Research Center upgraded the landing loads track to the Aircraft Landing Dynamics Facility (ALDF) to improve the capability for low-cost testing of wheels, tires, and advanced landing systems. The main features of the updated facility are the propulsion system, the arresting gear system, the high-speed carriage, and the track extension. In 1988, the capability of ALDF was enhanced by the addition of a Rain Simulation System (RSS). The ALDF-RSS is a 500-ft-long, 44-ft-wide overhead distribution system comprised of three parallel 10-in.-diameter irrigation pipes aligned lengthwise along the track and supported every 100 ft at a height of 42 ft above the track. The RSS can be configured with as many as 1590 nozzles and can simulate rainfall intensities as high as 40 in/hr.*

*The ALDF uses a high-pressure water jet system to propel the test carriage along the 2800-ft track. The propulsion system consists of an L-shaped vessel that holds 28 000 gal of water pressurized up to 3150 lb/in<sup>2</sup> by an air supply system. A timed quick-opening shutter valve is mounted on the end of the "L" vessel and releases a high-energy water jet, which catapults the carriage to the desired speed. The propulsion system produces a thrust in excess of 2 000 000 lb force, which is capable of accelerating the 54-ton test carriage to 220 knots within 400 ft. This thrust creates a peak acceleration of approximately 20g. The carriage coasts through the 1800-ft test section and decelerates to a velocity of 175 knots or less before it intercepts the five arresting cables that span the track at the end of the test section. The arresting system brings the test carriage to a stop in 600 ft or less.*

*Essentially any landing gear can be mounted on the test carriage, including those exhibiting new or novel concepts, and virtually any runway surface and weather condition can be duplicated on the track.*

*Since 1985, ALDF has been used to evaluate the friction and wear characteristics of the Space Shuttle orbiter main- and nose-gear tires, to define modifications to the runway at the John F. Kennedy Space Center Shuttle Landing Facility, and to demonstrate the ability of the orbiter to safely complete a landing following tire and wheel failures. During 1990, tests were conducted on the joint NASA/FAA (Federal Aviation Administration) Surface Traction and Radial Tire (START) Program and the Heavy Rain Simulation Program.*



Variable yaw device.

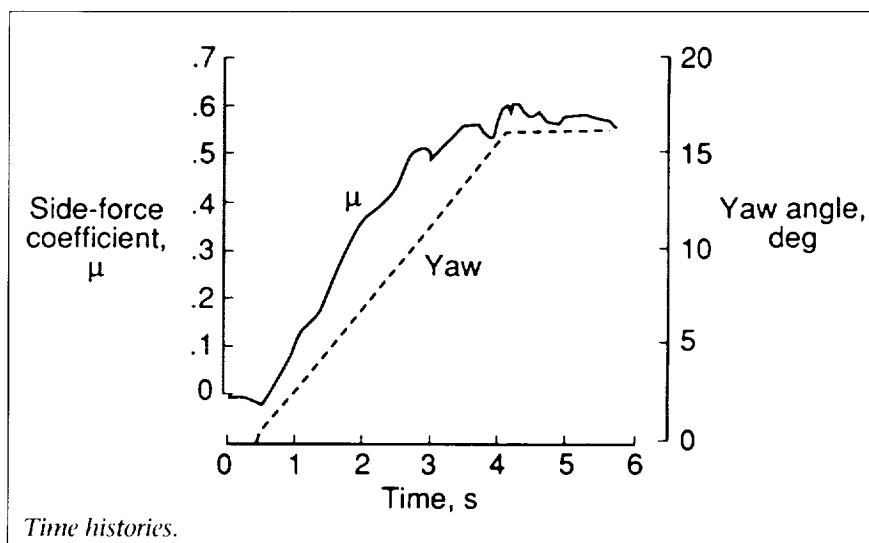
run and also can be configured for constant yaw angle testing. The second figure shows time history plots of the yaw angle and the resulting side-force coefficient  $\mu$  for the DC-9 nose-gear tire during a recent test on ALDF. The data in the figure indicate that the dynamic response of the tire is adequate to handle a yaw rate of  $5^\circ/\text{s}$ . A typical set of tire cornering tests may involve five or six yaw angle settings and three or four vertical load values; thus, this variable yaw system can reduce the number of carriage runs in a typical ALDF test program by 40 percent. (Robert H. Daugherty, 41309)

### Definition of Cornering Characteristics of Radial-Belted and Bias-Ply Aircraft Tires

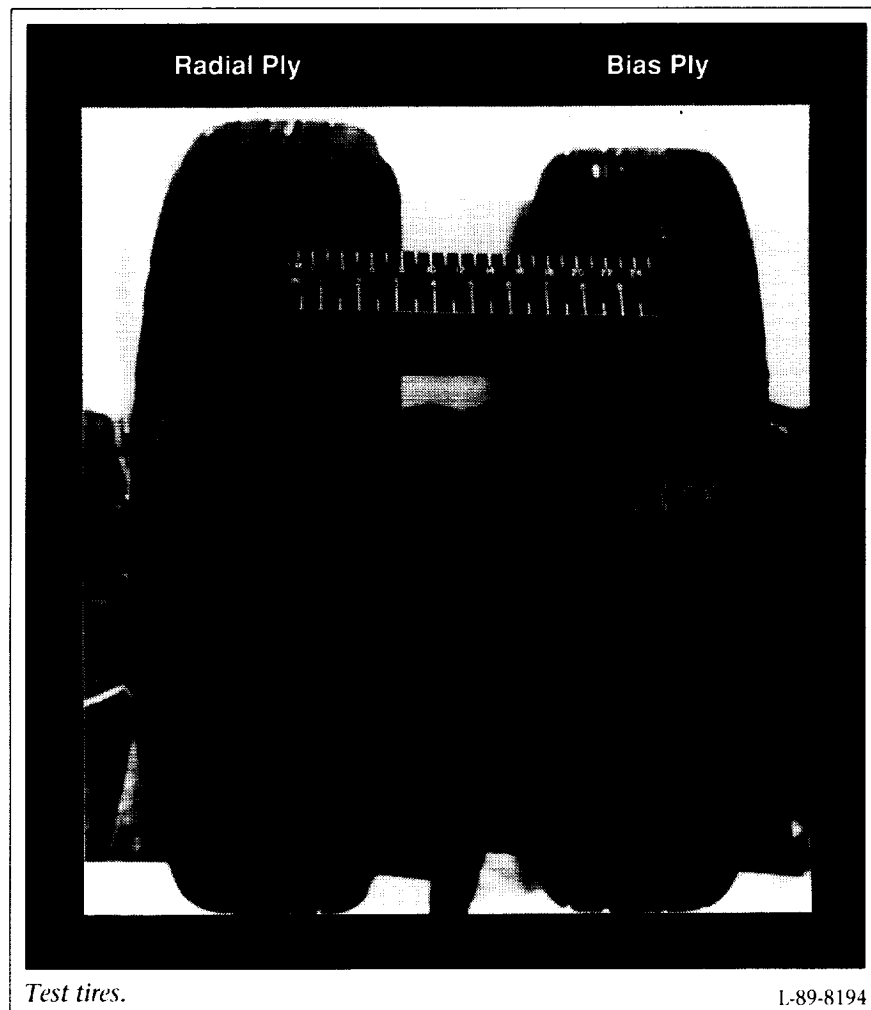
The object of the joint NASA/FAA START Program is to develop a national data base of tire mechanical properties and frictional

### Variable Yaw System

With the implementation of the joint NASA/FAA START Program on ALDF, demand for facility operation time is at an all-time high. Consequently, improving the operational efficiency of the facility whenever possible is desirable. One improvement that has been made in 1990 is the installation of a variable yaw system on the test carriage. A schematic of the components of this system is shown in the first figure; this system permits a range of yaw or steering angles to be tested during a single run. The variable yaw system allows a variation in steering angles ranging from  $0^\circ$  to  $16^\circ$  during a test



Time histories.



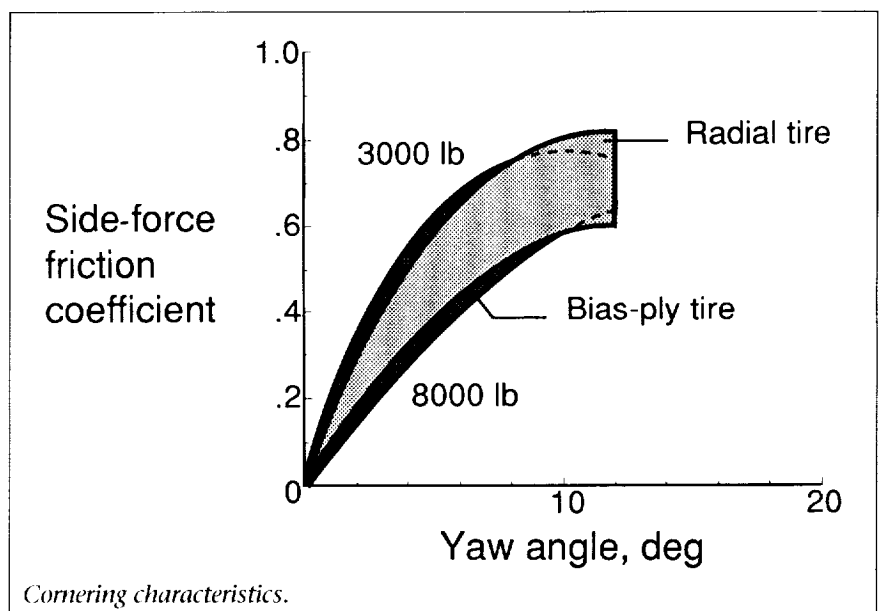
on ALDF. The inflation pressure for each tire was 185 lb/in<sup>2</sup>. The second figure shows the side-force friction coefficient for each tire plotted as a function of yaw angle. The cornering characteristics of both tires are sensitive to changes in the vertical load, which suggests that the ground-handling characteristics of the aircraft will be a function of its weight. The cornering properties of the radial-belted tire are comparable to those of the conventional bias-ply tire, thus indicating that radial-belted nose-gear tires can be installed on the airplane without compromising ground-handling safety. (Pamela A. Davis, Sandy M. Stubbs, and Thomas J. Yager, 41308)

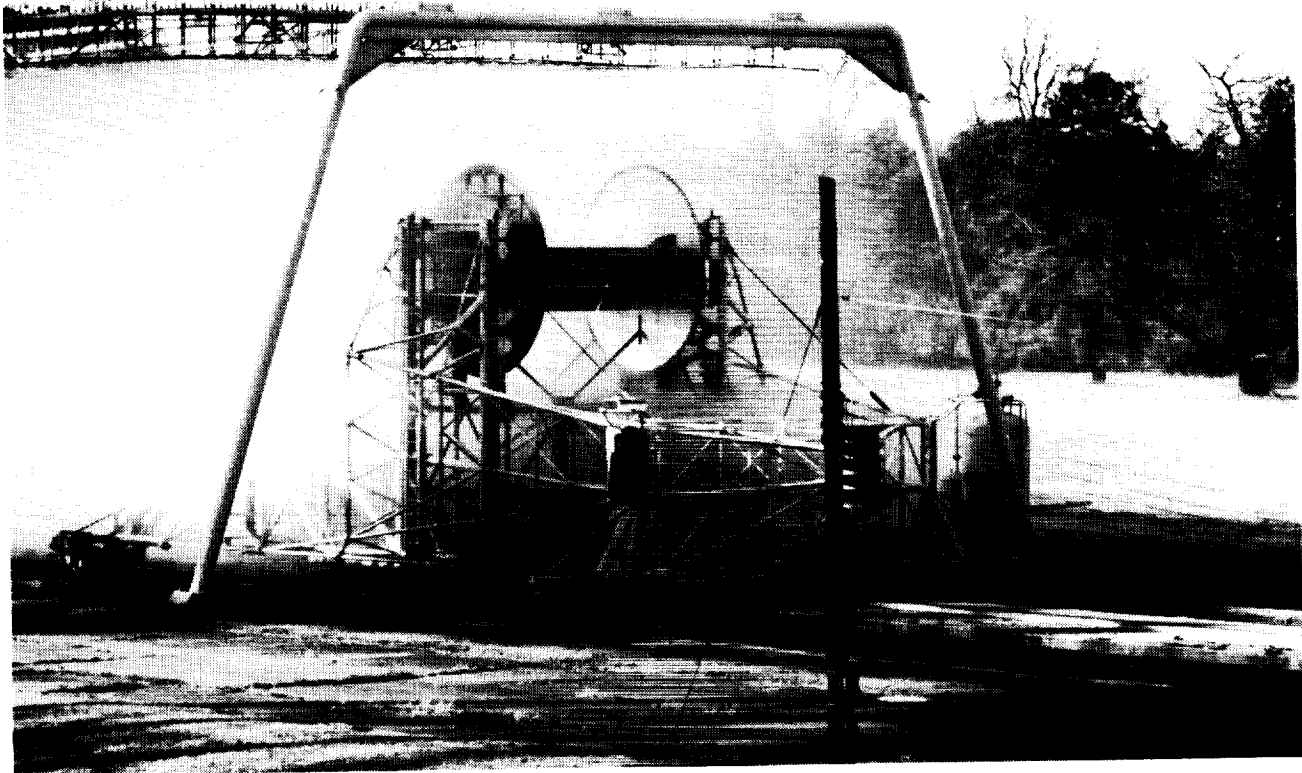
### Effect of Rain on Airfoil Performance at Large Scale

Large-scale heavy rain effects testing in ALDF ended in December 1990, after a 2-year cooperative

characteristics for radial-belted aircraft tires and to compare these properties with those of comparable bias-ply aircraft tires. Static and dynamic testing of several tire sizes representing the full range of aircraft load and speed requirements is under way on ALDF.

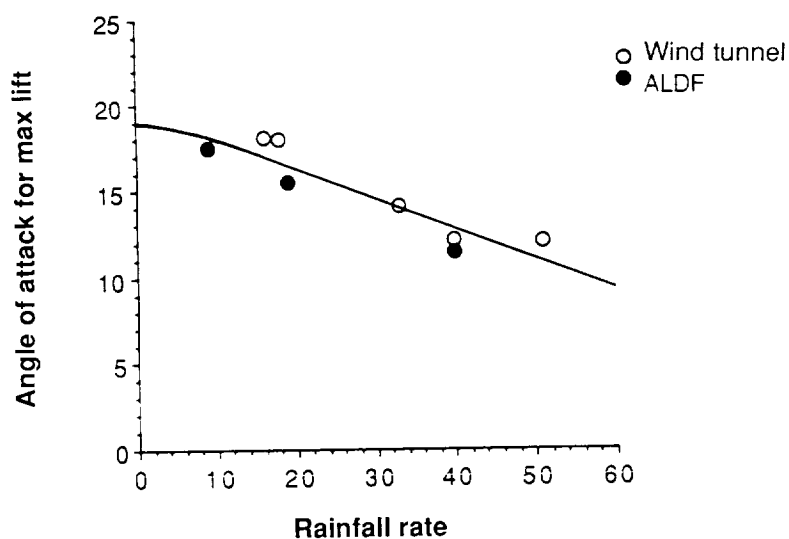
A photograph of two of the test tires is shown in the first figure. These tires are 26 x 6.6 aircraft tires that are used as nose-gear tires for the McDonnell Douglas Corporation DC-9 aircraft. The second figure presents the cornering properties of these tires on a smooth, dry concrete surface during testing at 100 knots





View of modified ALDF test carriage exiting 19-in/hr simulated rain field.

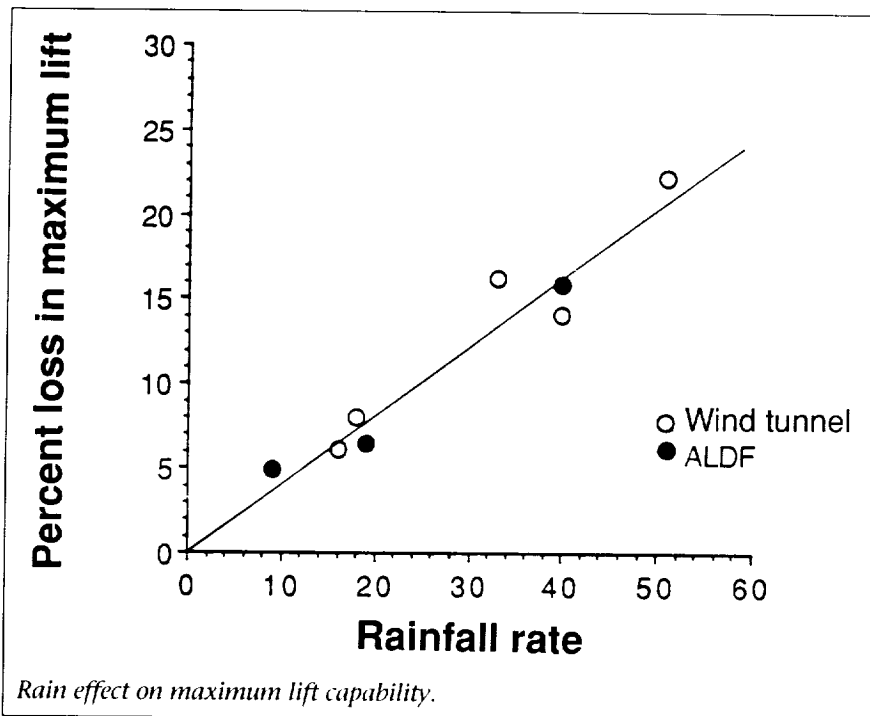
1-90-14620



Rain effect on stall angle of attack.

effort involving the Aeronautics and Structures Directorates. A large-scale ground test capability for acquiring aerodynamic data was developed to assess the actual effect of heavy rain on airfoil performance. Large-scale confirmation of the wind-tunnel results was required to eliminate uncertainties with regard to the sensitivity of the experimental process to the rain scaling relationships involved.

The ALDF test carriage was modified to transport a large-scale NACA 64-210 wing section, representative of a commercial transport, along a 3000-ft track at



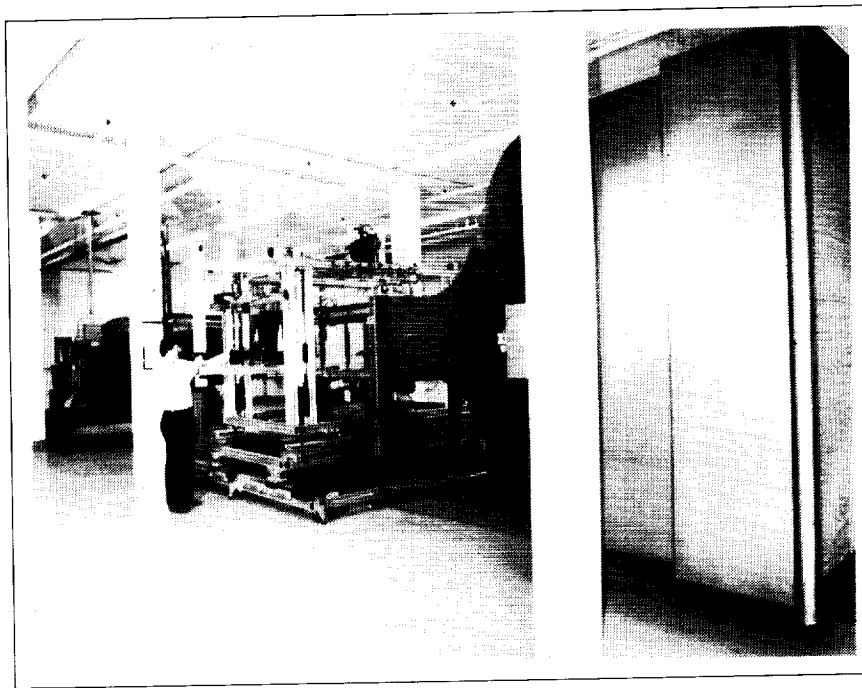
full-scale airplane approach speeds. An overhead rain spray system along a 500-ft section of the track test section produced rainfall rates of 9 in/hr, 19 in/hr, and 40 in/hr. The 10-ft chord NACA 64-210 wing section was tested with high-lift devices deployed to simulated landing conditions. Aerodynamic lift data were acquired with and without the rain simulation system activated. Tests were conducted at a maximum speed of 160 knots and an angle-of-attack range from 7.5° to 19.5° for all three rain environments.

Preliminary large-scale test results indicate that the effect of rain on the aerodynamic lift performance is significant for angles of attack near or at stall. The lift loss is a function of rainfall rate and angle of attack. The magnitude of the loss in maximum lift capability and the reduction in the stall angle of attack are a

function of rainfall rate. A comparison between the wind-tunnel and large-scale results shows a good correlation with respect to the behavior of the airfoil near or at stall in simulated heavy rain environments.

(Gaudy M. Bezos and Bryan A. Campbell, 45083)





# Basic Aerodynamics Research Tunnel

---

Computational methods are progressing rapidly toward the prediction of the three-dimensional flow field about complex geometries at high angles of attack. These computational methods require a large number of grid points to adequately model the flow field, and they produce large amounts of information. To validate these methods, detailed experimental flow field measurements are required. The Basic Aerodynamics Research Tunnel (BART) is a flow diagnostic facility dedicated to the task of acquiring the detailed data required for code validation and investigating the fundamental character of complex flow fields.

The BART is an open-return wind tunnel with a closed test section 28 in. high, 40 in. wide, and 10 ft long. The maximum test section velocity is 220 ft/s, which yields a Reynolds number per ft of  $1.4 \times 10^6$ . The airflow

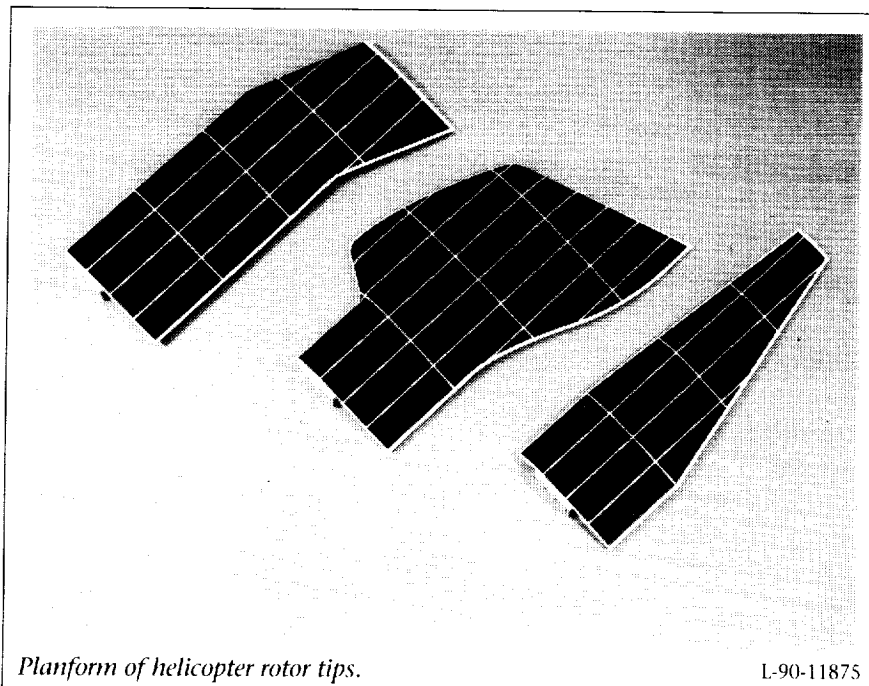
entering the test section is conditioned by a honeycomb, four antiturbulence screens, and an 11-to-1 contraction ratio. These flow conditioners provide a low-turbulence flow in the test section. The level of the longitudinal component of turbulence intensity ranges from 0.05 percent at low speeds to 0.08 percent at a test section dynamic pressure of 45 lb/ft<sup>2</sup>.

The timely acquisition of the detailed data required for code validation dictates the use of a highly integrated and fully automated Data Acquisition and Control System (DACS). The BART DACS consists of a computer system that monitors and controls all test instrumentation. The BART instrumentation includes a three-dimensional probe traverse system, an electronic scanning pressure system, a three-component hot wire, and a three-component laser velocimeter.

## Experimental and Computational Study of Helicopter Rotor Tips

---

Helicopter rotors operating in hover and forward flight encounter a number of dynamic aerodynamic phenomena. Much of the physics related to these aerodynamic phenomena are not completely understood. Computational fluid dynamics (CFD) methods are under development for use in the prediction of the complex rotor aerodynamics. These methods include full-potential and Reynolds-averaged Navier-Stokes codes. The current investigation is a combined CFD and experimental study of three helicopter rotor tip shapes. The experimental data will be used to provide physical insight into the process of the tip vortex formation and serve as a data base for evaluation of several advanced CFD codes.



*Planform of helicopter rotor tips.*

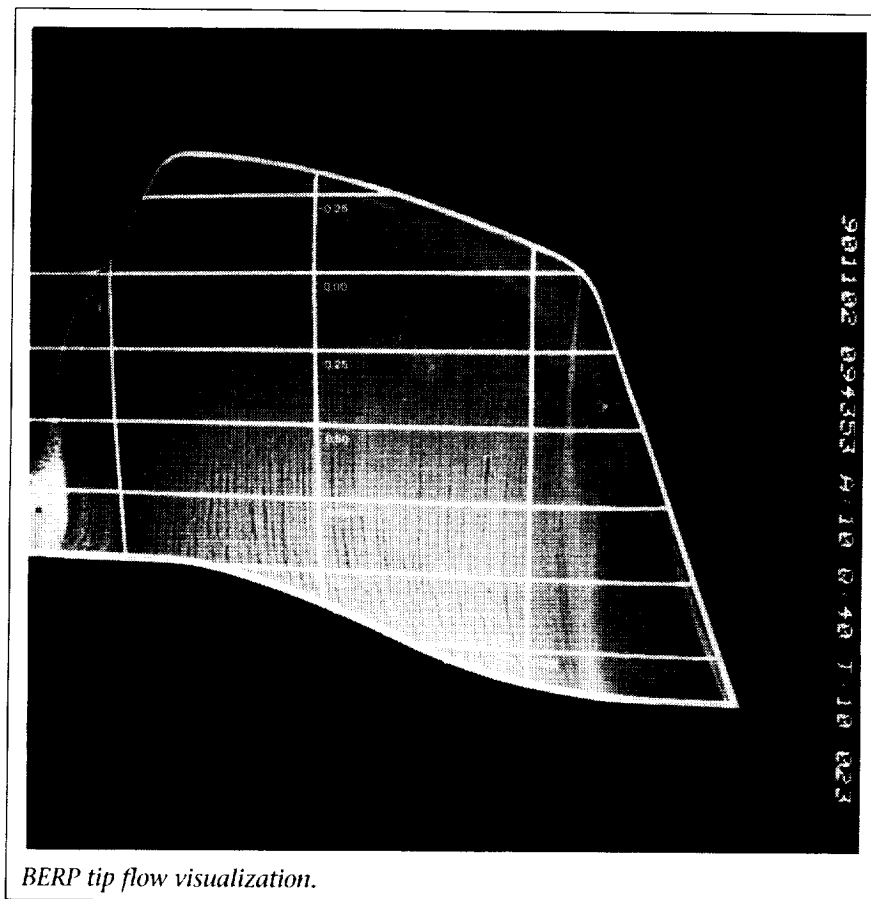
L-90-11875

are digitized for comparison with preliminary CFD calculations.  
(Greg Jones, 41065)

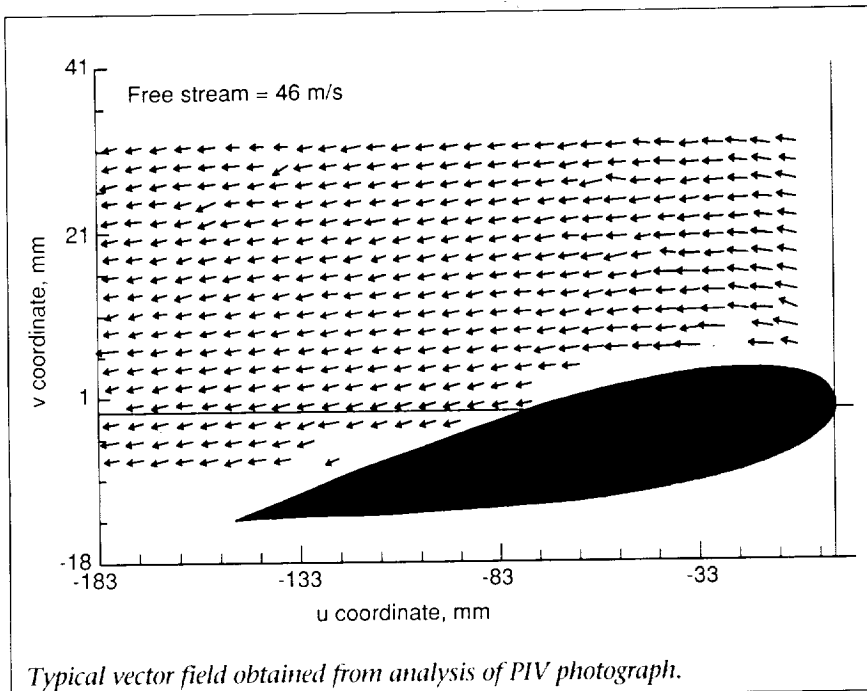
### NACA 0012 Flow Field Survey Using Particle Image Velocimetry

The global velocimetry technique of Particle Image Velocimetry (PIV) has been successfully used to perform two-dimensional flow field surveys in the BART. The technique consists of illuminating the seeded flow field with a 1-mm-thick double-pulsed lightsheet. The pulsed lightsheet is formed using two frequency doubled, 140-

Because of the multiple goals of the test program and the detailed nature of the data being sought, the experiment is being conducted in three phases. The first phase of the experimental testing has been completed in the BART for three helicopter rotor tips that included the BERP tip, the GBH tip, and the UH60A tip (see the first figure). This flow visualization phase of the experiment concentrated on the global flow field features of the different rotor tips which will be measured in detail in the next two phases of testing. The flow visualization techniques utilized during this first phase included fluorescent oil techniques and multiple laser lightsheet techniques. The data from these techniques have been used to identify both the near-wake tip vortex formation and the complex three-dimensional separation associated with stall at the higher angles of attack (see the second figure). The photographs



*BERP tip flow visualization.*



mJ Nd:YAG lasers fired in sequence. The illuminated region of the flow is imaged onto a film plate, resulting in a photograph containing a myriad of double exposed particle images with the image separation dependent on both the pulse separation and the local velocity of the flow during image acquisition. Individual velocity vectors in the flow field are ascertained by interrogating small regions of the photograph to determine the displacements of the individual particle image pairs.

The test model used for the surveys consisted of an NACA 0012 airfoil with a 152.5-mm chord length oriented at angles of attack of 0°, 5°, and 15°. The tunnel was operated at a free-stream velocity of 46 m/s (corresponding to a tunnel  $Q$  of approximately 25.5), and the flow was seeded with 0.8  $\mu\text{m}$  polystyrene latex microspheres. A field of view of the illuminated region with dimensions of 100 mm

by 125 mm was used for the surveys. The figure shows a typical resultant velocity vector field obtained for an angle-of-attack case of 5°. The vector field shown is constructed from more than 10 000 individual velocity vectors that have been projected onto a uniform grid using weighted averages. The analysis of each 100-mm by 125-mm photograph required the examination of approximately 2500 four-mm<sup>2</sup> interrogation regions over a 3-hour period.

This test represents the first use of PIV in a large air facility at Langley Research Center. The results indicate that the technique is a viable method of mapping two-dimensional model flow fields with direct application to computational fluid dynamics code validation.  
(William M. Humphreys, Jr., 44601, and Scott M. Bartram)



## Flight Research Facility

*The truss-supported roof of the huge hangar of the Flight Research Facility provides a clear floor space with nearly 300 ft in each direction (over 87 000 ft<sup>2</sup>).*

*Door dimensions will allow entry of a Boeing 747. Features such as floor air and electrical power services, radiant floor heating to eliminate corrosion-causing moisture, a modern deluge fire suppression system, energy-saving lighting, modern maintenance spaces, and entry doors and taxiways on either side of the building make this structure equal or superior to any hangar in the country. Significant in-house capabilities for design, construction, and quality assurance of flight hardware allow Langley to build and test new concepts in flight at minimal cost. Extensive and modern maintenance equipment makes it possible to maintain, repair, and modify aircraft ranging in sophistication from modern*



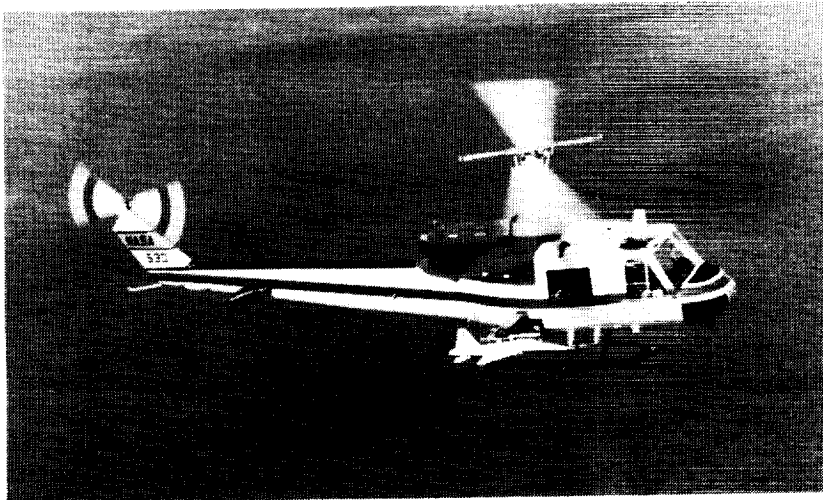
*B-737 with flaps instrumented for high-lift research.*

L-89-13501



F-5F research support aircraft.

1-90-4788



Bell 204B configured for model drop mission.

1-76-6425

metal and composite airliners, fighters, and helicopters to fabric-covered light airplanes. Surrounding the hangar are ramp areas with load-bearing capacity sufficient to handle the largest current wide-body jet. The high-power turnup area can also handle a wide variety of aircraft.

The present array of research and research support aircraft includes an airliner, military fighters, trainers, experimental one-of-a-kind designs, helicopters, and single and multiengine light airplanes. This variety enables research to be carried out over a wide range of flight conditions, from hover to Mach 2 and from the surface to 60 000 ft. Research

pilot currency in this wide spectrum of aircraft is important in safely conducting in-flight experiments as well as in-flight simulator assessments. A variety of research can be conducted in such areas as terminal traffic flow, microwave landing system (MLS) approach optimization, airfoil properties, handling qualities, performance, engine noise, turbulence research, natural laminar flow, winglet studies, stall/spin, and severe storm hazards.

One of the support helicopters is used to drop unpowered remotely controlled models of high-performance airplanes to study high-angle-of-attack control characteristics. The Radio-Controlled Drop Model Facility is used to study the low-speed flight dynamic behavior of aerospace vehicles with particular emphasis on high-angle-of-attack characteristics of combat aircraft. The technique consists of launching an unpowered, dynamically scaled, radio-controlled model into gliding flight from the support helicopter, controlling the flight of the model from the ground, and recovering the model with a parachute.

The models are constructed primarily of molded fiberglass and are typically 10 ft long with weights in the range of 200 lb to 500 lb. A comprehensive onboard instrumentation system provides measurements of key flight dynamics parameters that are transmitted to the ground via telemetry and recorded for analysis. The model control loop involves a combination of ground-based and onboard equipment and the required communication links. The heart of the system is a ground-based digital computer into which the control laws are programmed. The processor accepts downlinked feedback signals from the model and commands from



Radio-Controlled Drop Model Facility.

L-83-11167

*the pilot and computes the control surface commands that are then transmitted to the model. Very-high bandwidth electromechanical servactuators are used to drive the model control surfaces. The pilot flies the model from a ground station that provides the required information on a number of displays. These displays include a high-resolution video image of the model, a map display showing model ground track, and conventional analog instruments presenting key parameters such as angle of attack and airspeed.*

*The tests are conducted at the Plum Tree Site located approximately 5 miles from Langley Research Center. The test site is a marsh approximately 2 miles long and 1 mile wide.*

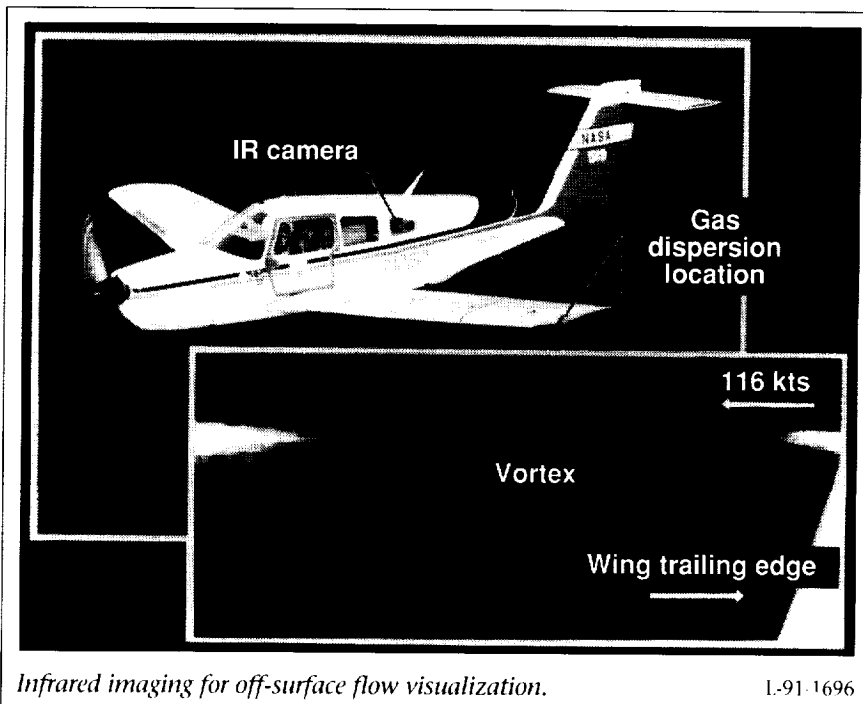
### In-Flight Off-Surface Flow Visualization Using Infrared Imaging

A new method for off-surface flow visualization in aerodynamic testing has been developed. Recent flight experiments explored the

ability to detect off-surface flow phenomena using infrared imaging. This technique is based on the infrared detection of a gas with strong infrared-absorbing and -emitting characteristics. For these experiments, the wing tip vortex was seeded with sulfur hexafluoride ( $\text{SF}_6$ ) gas so that the strong infrared-emitting gas entrained would

appear white (warmer) to the cooler surrounding air. Wing tip vorticity was chosen to be visualized because it is a well-understood aerodynamic phenomenon and its off-surface location in reference to the wing tip is well known.

A single-engine, low-wing, light airplane was used for the experiments. This airplane was equipped with an infrared imaging system, a video recording system, and an  $\text{SF}_6$  gas seeding system. The imager was mounted in the rear cabin to provide a field of view downstream of the left wing tip of the airplane. The gas was dispensed from the left wing tip and entrained into the wing tip vortex. The figure shows the airplane with an inset photograph of the recorded infrared image. The image shown in the figure was obtained with a clear-sky background. Other backgrounds such as clouds, haze, water, and Earth were investigated, but the sky background resulted in the clearest recorded image.



Infrared imaging for off-surface flow visualization.

L-91-1696

Infrared imaging offers a new research tool to further the understanding of off-surface flow phenomena through dynamic off-surface flow visualization.

(Greg Manuel, Kamran Darybeigi, David Alderfer, and Cliff Obara, 43864)

## Boeing 757 Hybrid Laminar-Flow Control Flight Tests

One of the most significant events in the history of boundary-layer control occurred during 1990, when a Boeing 757 aircraft (see the figure) achieved laminar boundary-layer flow to 65 percent wing chord through the use of a Hybrid Laminar-Flow Control (HLFC) system.

With this accomplishment, the feasibility of the HLFC concept was demonstrated in flight for the first time. The HLFC system provides suction boundary-layer control to the front spar. Downstream of the

front spar, the surface pressure distribution is used to stabilize the laminar boundary-layer flow to the wing shock. A 22-ft span section of the Boeing 757 wing outboard of the left-engine pylon was modified for the flight test. The leading-edge suction surface was a micro-perforated titanium skin with over  $15 \times 10^6$  tiny, laser-drilled, closely spaced holes. A leading-edge Krueger flap was integrated into the high-lift system and also served as an insect shield. The design incorporated innovations made in earlier NASA laminar-flow programs, such as the JetStar Leading-Edge Flight Test (which first used perforated titanium suction skin). Flight tests were conducted over a 5-month period to altitudes of 40 000 ft, Mach numbers to 0.82, and chord Reynolds numbers to  $30 \times 10^6$ . Laminar flow was achieved the first time the suction system was used.

The program is jointly funded by NASA, the U.S. Air Force, and Boeing Commercial Airplane Company. NASA and industry researchers believe that HLFC

technology could be introduced in new aircraft designs during this decade.

(Dal V. Maddalon, 41909, and Richard D. Wagner)

## Airborne Wake Vortex Detection

Airport capacity is often limited during poor visual conditions by the spacing between airplanes that are approaching to land on a runway. These spacing requirements are presently dictated in part by the hazard due to the violent motions of an airplane encountering the trailing vortices from a preceding airplane. If the occasional dangerous wake vortex could be detected far enough away for the pilot to avoid the hazard, the spacing requirements might be safely reduced and airport capacity increased. In order to determine whether a wake vortex could be detected using low-cost, conventional, airborne instrumentation, an exploratory flight experiment was conducted.

Three airplanes were used in the experiment, which was conducted at the Wallops Flight Facility. A Wallops-based P-3 airplane (90 000-lb, four-engine turboprop transport) was used to generate the wake vortex. Smoke produced by a smoke generator mounted near the wing tip of the P-3 was used to make the wing tip vortex visible. Sensors carried on a Langley-based PA-28 airplane (four-place, single-engine) were used to measure the airplane motions and pilot inputs needed to detect the wake vortex. The third airplane, a T-34C based at Langley Research



Hybrid Laminar-Flow Control Boeing 757 research aircraft.

1-90-9548



*PA-28 airplane with wing tip flow vanes used to detect presence of wake vortex.*

L-90-9548

Center, flew above the other two airplanes with video cameras to photograph and measure the relative horizontal distance between the P-3's wake vortex and the PA-28 detecting airplane. Data from the video cameras and from the sensors of the detecting airplane were analyzed after the flight tests. Algorithms were developed to remove the effects of the pilot's control inputs from the motions of the PA-28 airplane and to produce detection parameters due solely to the presence of the vortex. Three useful detection parameters were identified from several investigated. These parameters made it possible to detect the presence of the wake vortex at a substantial distance. (Eric C. Stewart, 43939)

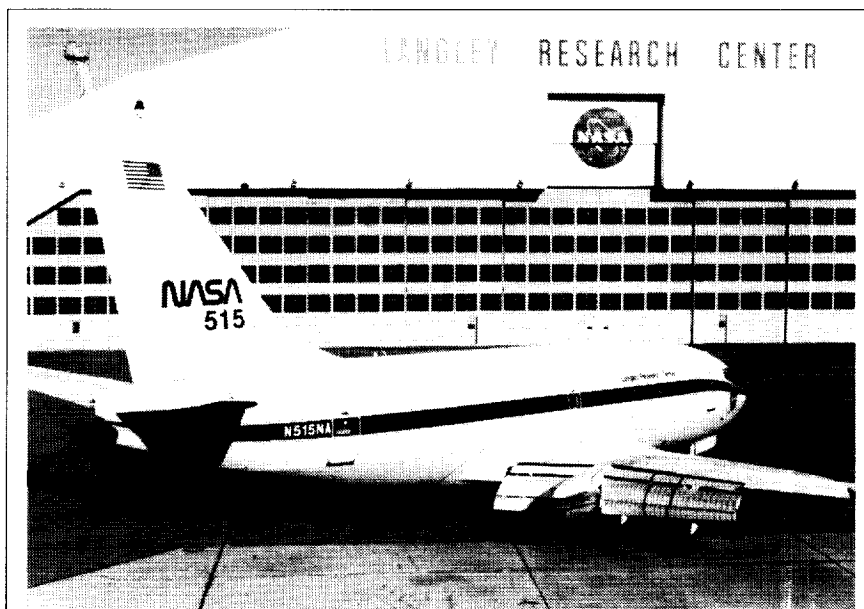
### Transport High-Lift Flight Experiment

The need for advanced high-lift design methodology for subsonic

transport aircraft has long been recognized. Progress in computational techniques has been difficult and slow because of the aerodynamic and structural complexity of high-lift systems. The availability of data appropriate for code

validation has been limited because of the sensitivity of slat/flap flow to Reynolds number and compressibility effects. As part of an overall research program to improve high-lift design methodology, flight experiments are planned to provide detailed flow measurements of transport high-lift systems to correlate with wind tunnel and computational fluid dynamics (CFD) results.

Flight tests have been conducted on the NASA 515 research aircraft (shown in the figure) as part of the first phase of this high-lift flight research program. The first phase of the program includes flight tests to visualize the flow field with surface tufts and to measure pressure distributions and flow separation characteristics of the flap system. Flight tests have been conducted to obtain the flow visualization of the flap at flap settings of 15°, 30°, and 40°. The aircraft was flown to the minimum



*NASA 515 research aircraft with pressure belts and tufts installed on high-lift flap system.*

L-91-01052

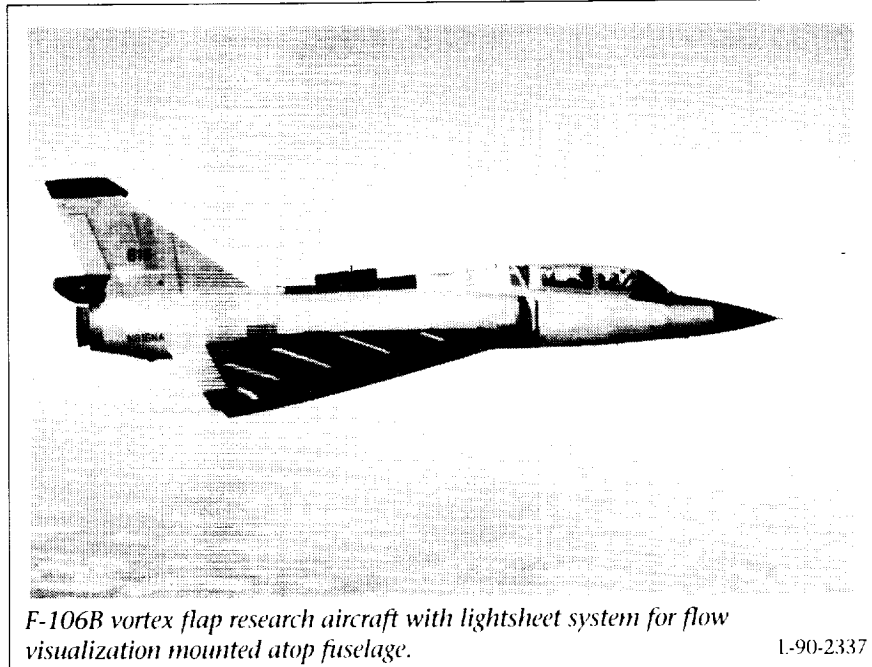


normal operating speed at each of the flap settings to determine the degree of spanwise and separated flow on the flap surface. The data were recorded with still and video photography. This information was useful in planning future experiments with instrumentation sensors for pressure distributions and boundary-layer characteristics. The second phase of the high-lift flight research program will incorporate advanced flight instrumentation for pressure distributions, boundary-layer characteristics, wake characteristics, and structural deformation measurements. These flight experiments are expected to contribute to the state of technology for high-lift design of transport aircraft by providing detailed flow characteristics for correlation with CFD and wind-tunnel results. In addition to improved aircraft performance, advanced high-lift design methodology has potential payoffs in noise reduction and wake vortex minimization.

(L. P. Yip, 43866, P. M. Vijgen, and N. A. Strain)

### Wing Leading-Edge Vortex Flap Flight Experiment

An F-106B is currently being used to flight test a wing leading-edge vortex flap concept developed at Langley Research Center. This flap concept can improve the performance and maneuver capabilities for aircraft with highly swept wings. The wedge-shaped flap has been tested with deflection angles of 40° and 30°; these tests included measurements of wing and flap surface pressures, struc-



tural loads and accelerations, and other pertinent aerodynamic data. The data have been acquired over a flight test envelope that encompasses speeds up to Mach 1, altitudes up to 40 000 ft, and maneuver loads up to 4g's. Significant data also have been obtained using vapor-screen and oil-flow techniques to visualize the flow field on and above the wing of the aircraft to help understand the aerodynamics associated with such vortical flow. Preliminary results from the tests of the flap configuration of 40° have been compared with similar data from flight tests of the unmodified wing and wind-tunnel experiments. An overview of these results was presented at the High-Angle-of-Attack Technology Conference held in 1990 at Langley Research Center.

Following a short series of on-surface flow visualization flights currently under way, the vortex flap will be removed from the aircraft for the final element of the

flight experiment. This final element will be to reevaluate selected flight conditions for the baseline wing configuration. Flight tests with the F-106B research airplane will be completed in 1991. (D. J. DiCarlo, 43870, and J. B. Hallissy)



## 16- by 24-Inch Water Tunnel

*The Langley 16- by 24-Inch Water Tunnel, which is used for flow visualization studies at low Reynolds numbers, has a vertical test section with an effective working length of approximately 4.5 ft. The test section is 16 in. high by 24 in. wide, and all four sidewalls are plexiglass to provide optical access. The test section velocity can be varied from 0 ft/s to 0.75 ft/s. The unit Reynolds number range for water at 78°F for this velocity range is 0 to  $7.7 \times 10^4$ /ft. The normal test velocity that produces smooth flow is 0.25 ft/s.*

*A sting-type model support system positions the model, and the model attitude can be varied in two planes over angle ranges of  $\pm 33^\circ$  and  $\pm 15^\circ$ . Operator-controlled electric motors are mounted outside of the test section to control the model position. Semispan models are mounted on a splitter plate supported by a sting with a lateral offset.*

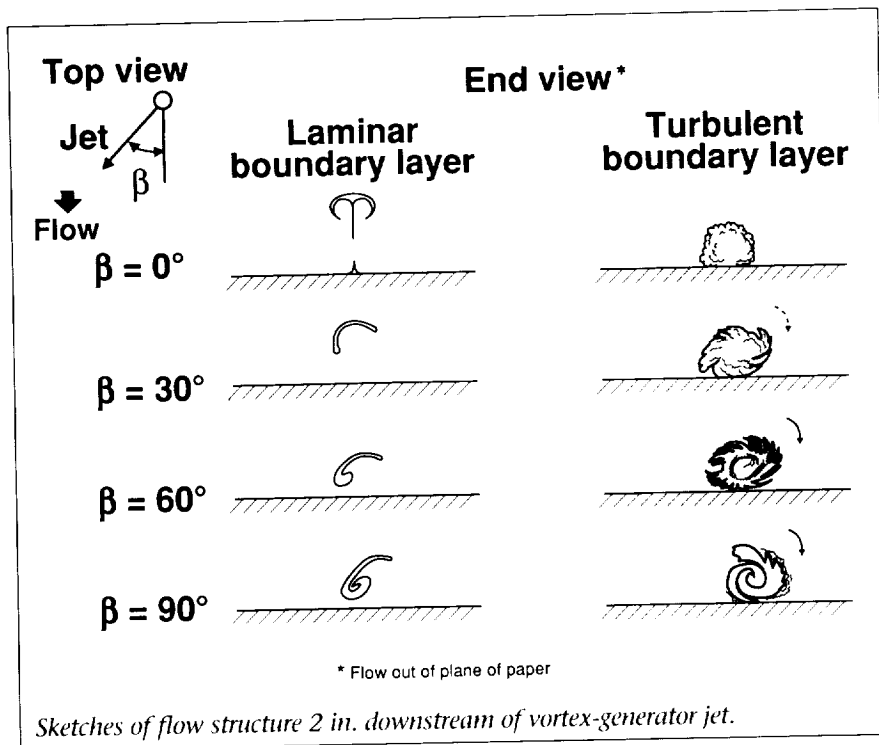
*Ordinary food coloring is used as a dye to visualize the flow. The dye is supplied by three reservoirs under pressure so that up to three dye colors may be used. Dye may be ejected from small orifices on the model surface or injected upstream of the test section. A three-dimensional laser fluorescence anemometer is available for quantitative studies. The water tunnel was placed in operation in 1987.*

### **Flow Visualization Study of Vortex-Generating Devices**

Flow phenomena associated with several vortex-generating devices for controlling turbulent separated flow were investigated through dye-flow visualization in the Langley 16- by 24-Inch Water Tunnel. The flow-control devices

examined included submerged vortex generators (Wheeler doublet and wishbone types), spanwise cylinders, large-eddy breakup devices (LEBU's) at small angle of attack  $\alpha$ , and vortex-generator jets (VGJ's).

The flow visualization study was performed on a splitter plate surface for both a laminar boundary layer (free-stream velocity of 0.08 ft/s) and a turbulent boundary layer (free-stream velocity of 0.69 ft/s). Both food coloring (red) and fluorescent (fluorescein) dyes were used. The colored dye visualization tests produced a global picture of the flow structure, while fluorescent dye illuminated by a laser sheet provided a cross-sectional view of the flow structure. A 200-mW argon laser with a cylindrical lens produced the lightsheet used to illuminate both the side view (x-y plane) and the end view (y-z plane).

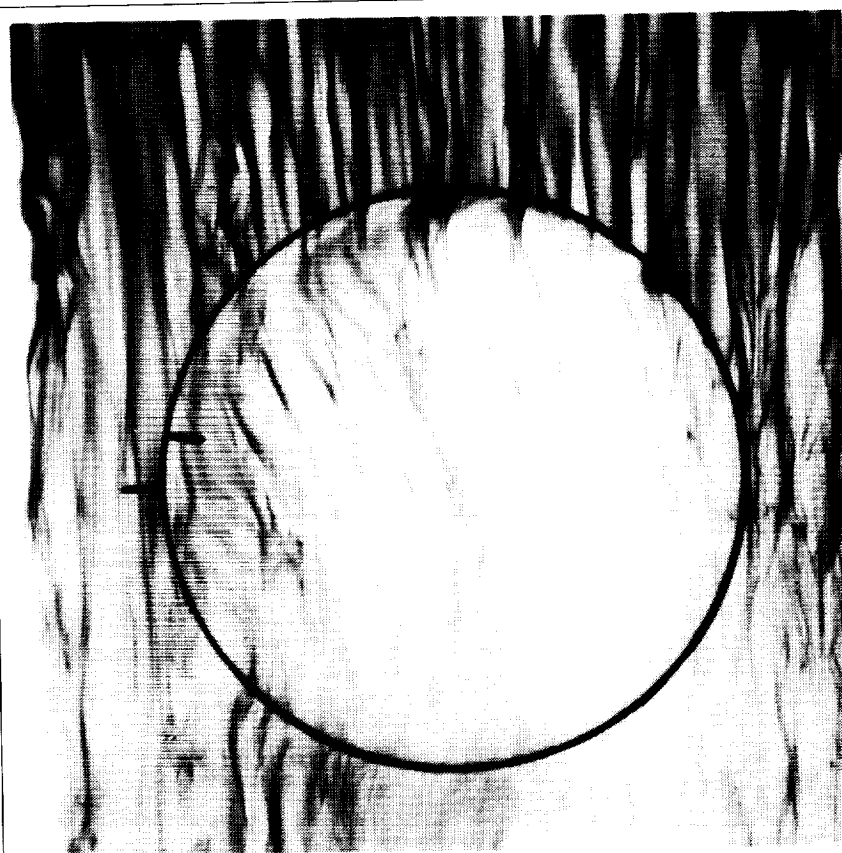


## Shear-Driven Three-Dimensional Boundary-Layer Studies

Limited studies have been conducted on three-dimensional (3-D) turbulent boundary layers mainly because of the complexity of their flow fields. Instead, attention has been focused primarily on the much simpler two-dimensional layers. Recently, however, increased interest has existed in 3-D boundary layers due to their abundance in everyday engineering applications, computer modeling deficiencies for these types of flows, and possible drag reduction benefits from 3-D induction of a naturally two-dimensional (2-D) turbulent boundary layer.

The dye flow visualization tests indicated that wishbone vortex generators in the forward orientation shed horseshoe vortices; wishbone vortex generators oriented in the reverse direction and doublet vortex generators shed streamwise counterrotating vortices. A spanwise cylinder located near the wall and LEBU's at  $\alpha = -10^\circ$  produced eddies that rotated with the same sign as the mean vorticity in a turbulent boundary layer, and the most effective VGJ's produced streamwise corotating vortices. The figure shows that as azimuthal angle  $\beta$  of the jets increased from  $0^\circ$  to  $90^\circ$ , both the downstream rotational speed and vortex core size increased for the longitudinal (corotating) vortices. For  $\beta \gg 0^\circ$ , the signs of observed vorticity for laminar and turbulent jets were opposite each other. The VGJ's seem to perform best for  $\beta$  near  $90^\circ$ .

(John C. Lin, Gregory V. Selby, and Dan H. Neuhart, 45556)



Flat plate model with rotating disk.

---

To more fully characterize these boundary layers (specifically through flow visualization techniques), studies were conducted in the Langley 16- by 24-Inch Water Tunnel. The model consisted of a 4-ft-long flat plate with a flush-mounted 4-in.-diameter disk located 3 ft from the leading edge. The disk was rotated at  $r/\text{min}$ 's between 4 and 24 to add a shear-driven third velocity component to the 2-D boundary already established. Structures within the boundary layer were visualized using dye injected from a slot 2 in. upstream of the disk. The figure is a normal view of the disk rotating at 12  $r/\text{min}$  showing the shear-driven skewness of the near-wall structures.

Results from this study indicate a possible reduction in eruptive fluid motions from the wall in the 3-D region which might account for previously observed lower drag values in such boundary layers. Further point measurements of each velocity component are to be conducted in the same facility as soon as instrumentation is in place. (Barry Lazos, 45731, and Dan Neuhart)

---



## Scientific Visualization System

---

A Scientific Visualization System has been brought on line in the Analysis and Computation Division Graphics Laboratory to support video tape recording of computer graphics generated on the Supercomputing Network Subsystem or on high-performance graphic workstations. Dynamic video displays are essential for accessing, understanding, analyzing, documenting, and displaying the vast numerical data bases resulting from computer simulations of time-dependent physical phenomena or from detailed measurements in ground-based or inflight experimental facilities.

The central component of the system is the DF/X Composium, a digital component video editing suite. The Composium menu-driven software offers a fully featured video processing and special effects capability including three-dimensional fonts,

paint box, layering, and compositing. The Composium provides centralized control of all ancillary equipment, including the ability to handle multiple video input sources. An A-60 real-time digital disc provides on-line working storage for up to 25 s of video. The A-60 is on the Langley Research Center Ethernet network and can accept raster image files in multiple formats directly from a remote workstation. A digital video tape drive is available for archive storage and as a high-capacity working store. An IRIS 4D/340 high-performance graphics workstation running the FAST computational fluid dynamics software and WAVEFRONT modeling and animation software is available on site for users familiar with these graphics packages. The system includes analog tape recorders in the VHS, S/VHS, Umatic, Umatic/SP, BetaCam, and BetaCam/SP formats which may be used as either sources of

video input or as a means of recording a completed video for distribution.

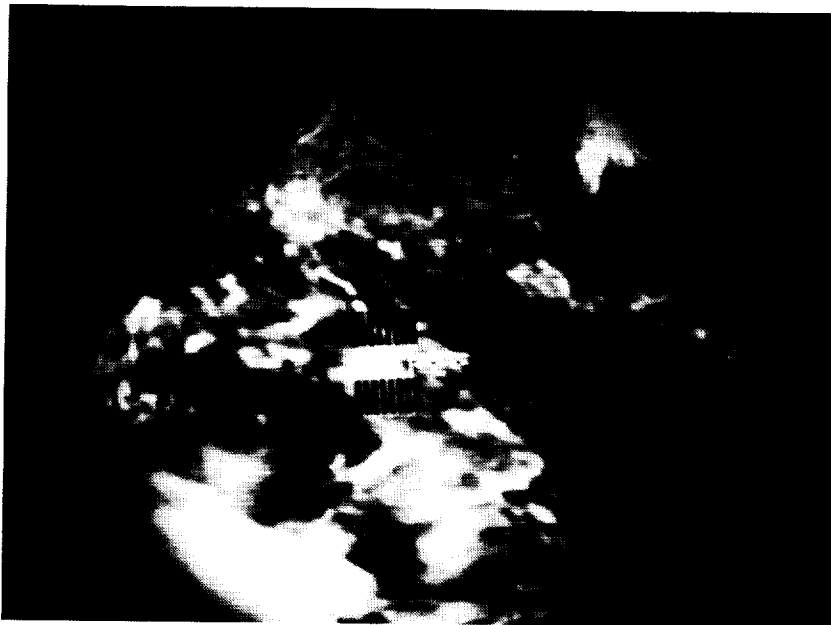
This system makes it possible to create a professional, self-contained video technical report to document and explain the results of Langley's theoretical or experimental research.

### Applications of Scientific Visualization System

---

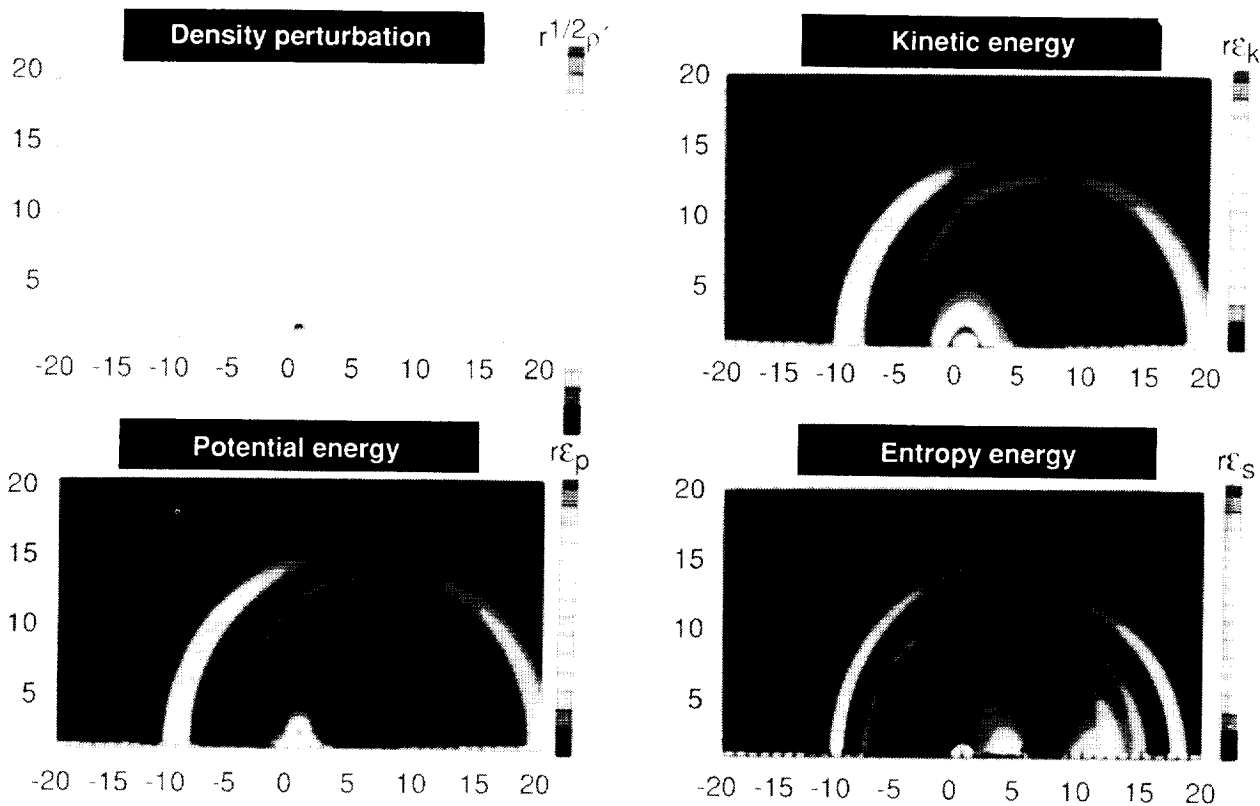
The use of the Scientific Visualization System is illustrated by the two still frames (shown in the figures) extracted from video sequences made with it.

A visual presentation prepared by the Space Station Freedom Office examines solar array shadowing for the Lyndon B. Johnson Space Center restructured Space Station



*Solar array shadowing.*

(see the first figure). Several animated sequences demonstrate the amount of shadowing that is present at the spring equinox ("worst-case" shadowing) and the winter solstice ("best-case" shadowing), and they depict Space Station *Freedom* in Earth orbit. The ray tracing capabilities of the WAVEFRONT Advanced Visualizer software together with several in-house programs were used in this analysis to determine quantitatively how much of the solar array area was shadowed during an orbit as well as the consequent power reduction. The animated sequences clearly show the resulting thermal gradients on this configu-



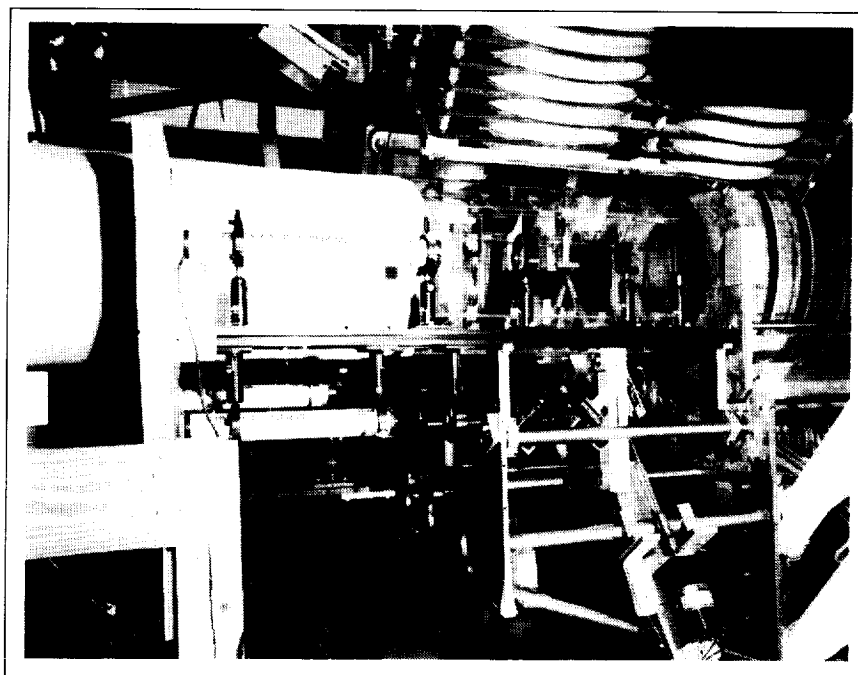
*Computational aeroacoustics.*

---

ration and provide a basis for making a judgment of their acceptability.

The second example (see the second figure), from the Acoustics Division, comes from the new field of computational aeroacoustics. This video sequence visualizes the intense sound generated by an impulsively started circular cylinder. The sound field has been calculated numerically using a two-dimensional Euler code. The segment of the video highlighted here shows the propagation of the density perturbation and the kinetic, potential, and entropy components of the acoustic energy. In this calculation, the entropy energy is a measure of the numerical error in the solution because acoustic propagation is an isentropic process. The video makes it clear that as the acoustic waves propagate, energy is transferred from the kinetic and potential components into the nonphysical entropy component. During the startup, a shock forms temporarily which generates entropy and a vortex. This process accounts for a physically real source of entropy, which can be seen moving downstream at the convection velocity rather than the acoustic speed.  
**(Don Lansing, 46714)**

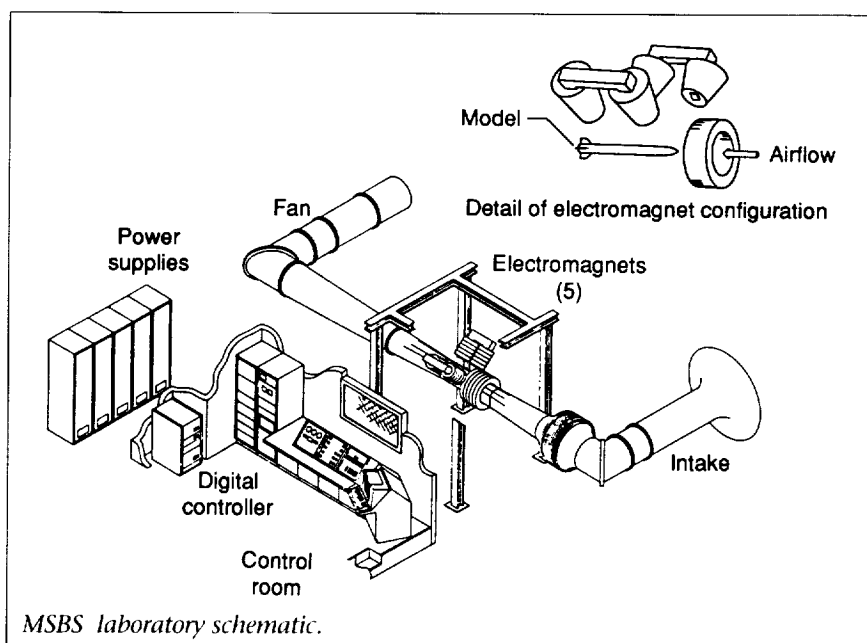
---



## 13-Inch Magnetic Suspension and Balance System

*The Langley 13-Inch Magnetic Suspension and Balance System (MSBS) is a laboratory established to develop technology required for wind-tunnel testing that is free of model-support interference. In 1984, the laboratory began operation as a combination of a magnetic suspension and balance system.*

*For this system, four electromagnets (arranged in a "V" configuration) above the wind-tunnel test section provide the lift force, pitching moment, side force, and yawing moment. A drag electromagnet opposes the drag force. Motion is controlled in these five degrees of freedom with no provision for generation of controlled magnetic roll torque on the model. The 13-Inch MSBS has a lift force capability of approximately 6 lb*



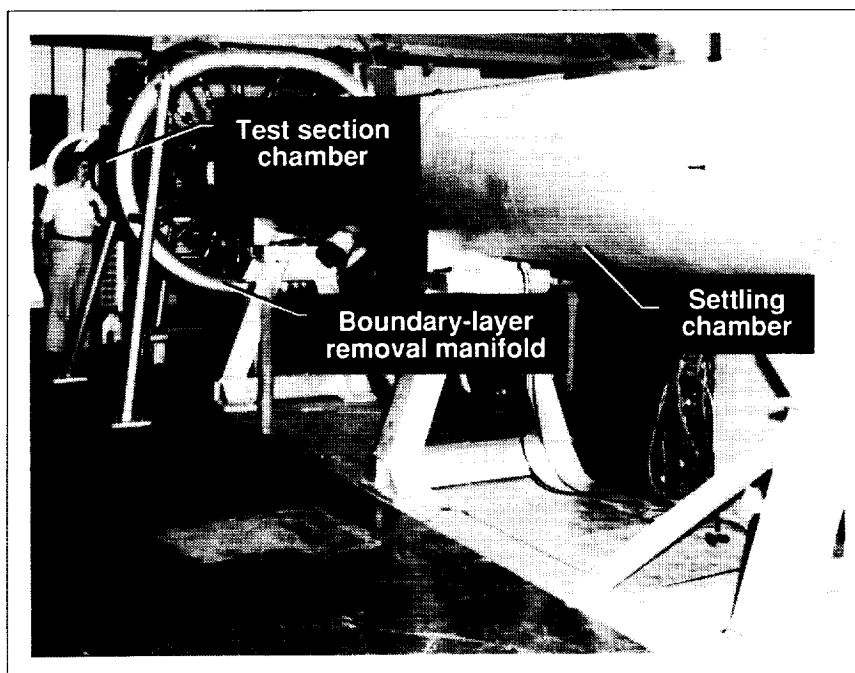


---

*depending on the size and shape of the iron core in the model. The test section passes through the drag electromagnet.*

*The tunnel is a continuous-flow, closed-throat, open-circuit design. Ambient air enters the tunnel from the outside through a large bellmouth intake protected from outside contaminants by a screen enclosure. At the end of the tunnel, the flow exhausts to the outdoors. The tunnel is capable of speeds up to Mach 0.5. The transparent test section measures approximately 12.6 in. high and 10.7 in. wide.*

*The tunnel has not been in operation during 1990, but it is scheduled to resume research studies during the summer of 1991.*



## Supersonic Low-Disturbance Pilot Tunnel

The Supersonic Low-Disturbance Pilot Tunnel (formerly called the Langley Mach 3.5 Low-Disturbance Pilot Tunnel) has been in operation since 1981. The tunnel, which is located in the Gas Dynamics Laboratory, uses high-pressure air from a 4200-psi tank field that is dehydrated to a dew point temperature of  $-52^{\circ}\text{F}$ , reduced in pressure by control valves located upstream of the settling chamber, and filtered to remove all particles larger than  $1\text{ }\mu\text{m}$  in size.

The predicted locations of transition from laminar-to-turbulent flow in the boundary layers of high-speed, high-altitude flight vehicles are critical design considerations because both friction drag and aerodynamic heating may be greatly affected by uncertainties in these predictions. Unfortunately, transition phenomena

are extremely sensitive to noise, which is a known contaminant in conventional high-speed wind tunnels. For Mach numbers  $>2.5$ , the predominant sources of this wind-tunnel noise are acoustic disturbances radiated into the free stream from the supersonic turbulent boundary layers on the tunnel walls. Other sources of noise in blowdown wind tunnels are pressure-reducing control valves that regulate the settling chamber pressure. The tunnel is a part of an ongoing Langley Research Center program to develop and test methods for eliminating or reducing severe noise problems.

The main figure shows the settling chamber (visible on the right-hand side) and the open-jet test section chamber (visible on the left-hand side). The tunnel flow exhausts to a vacuum sphere complex that provides

up to approximately 1-hr run times for stagnation pressures from 25 psia to 100 psia. At higher pressures, the flow is exhausted to the atmosphere. The settling chamber contains seven antiturbulence screens along with a number of dense porous plates that function as acoustic baffles to attenuate the high-level noise from the control valves and the piping system. These porous plates reduce the incoming noise from approximately 0.2 percent of stagnation pressure to approximately 0.01 percent. The antiturbulence screens reduce the normalized rms velocity fluctuations to approximately 1 percent.

With the input disturbances reduced to these low levels, research has shown that the most successful technique to eliminate the radiated noise is to laminarize the nozzle wall

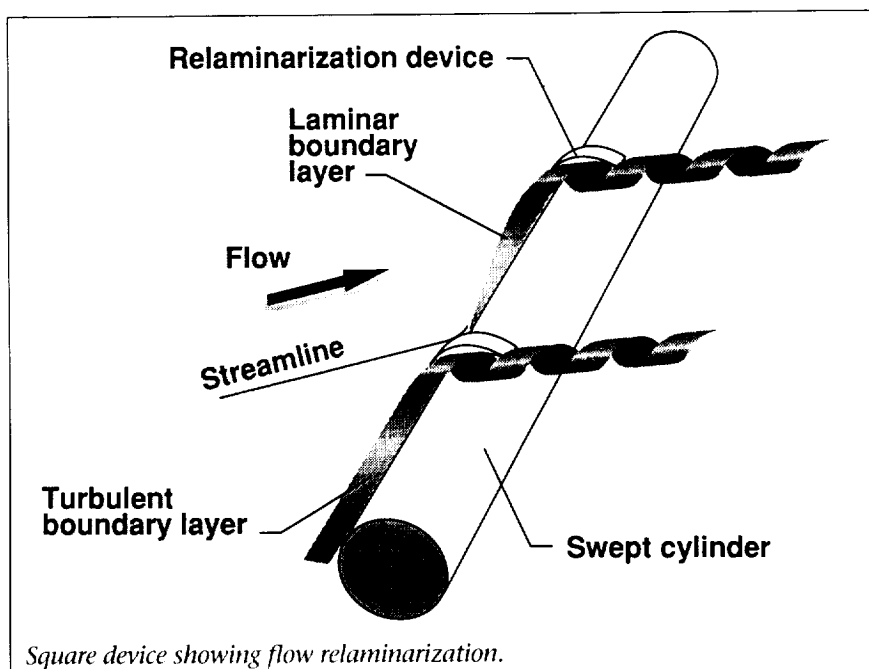
boundary layers by using boundary-layer removal slots just upstream of the nozzle throat and properly tailored expansion nozzles with highly polished walls. The large circular manifold shown in the figure is connected to a vacuum sphere and is used to remove the nozzle inlet boundary layer through a series of 1-in.-diameter pipes. By the use of these techniques, all disturbances have been practically eliminated in three different nozzles for Mach numbers of 3 and 3.5.

### Relaminarization of Supersonic Attachment-Line Boundary Layers

Laminar flow on the upper surface of swept wings at high Reynolds numbers is only possible if turbulent contamination on the leading-edge attachment line is minimized or alleviated. The objective of the current research is to investigate passive leading-edge modifications designed to relaminarize the attachment-line boundary layer in supersonic flows.

The leading edge of a supersonic swept wing was simulated by a swept cylinder mounted in the Supersonic Low-Disturbance Pilot Tunnel. A variety of leading-edge devices were mounted on the cylinder, and the attachment-line boundary layer was determined to be laminar or turbulent by the temperature distribution along the attachment line, as measured by embedded thermocouples.

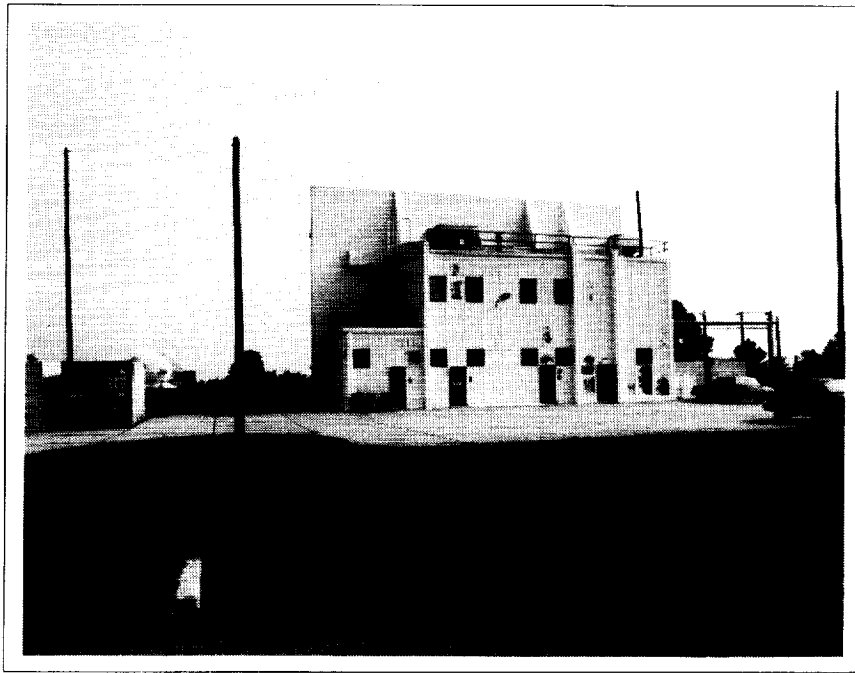
For a sweep angle of  $76^\circ$ , several devices display the ability to relaminarize the turbulent attachment-line boundary layer.



This effect is hypothesized because of the induction action of a stream-wise vortex system generated by the leading-edge device, which sweeps the contaminating turbulent flow downstream over the top of the wing rather than spanwise along the leading edge (see the figure).

The availability of simple, low-cost passive devices that provide a laminar attachment-line flow on swept wings will be useful and possibly critical to the practical achievement of laminar flow on swept wings at supersonic speeds.

Optimization of device shapes is currently under way, as is a companion study to investigate the flow mechanisms responsible for the observed results. Numerical studies also are planned.  
(Theodore R. Creel, 45554)



## Pyrotechnic Test Facility

---

*The Pyrotechnic Test Facility (Building 1159) contains the Langley Research Center space simulation environmental and functional test equipment used for the handling and testing of small-scale potentially hazardous materials. This facility includes three test cells and a general-purpose work area.*

*The environmental test equipment includes a 2000-lbf vibration machine, a thermal-vacuum chamber, which is 35 in. in diameter and 48 in. long and is capable of pressures to  $1 \times 10^{-7}$  torr at temperatures of  $-320^{\circ}\text{F}$  to  $+200^{\circ}\text{F}$ , and a mechanical shock apparatus, which is capable of producing up to a 30 000g pulse for 0.2 ms. This facility also includes thermal chambers with a capability of  $-320^{\circ}\text{F}$  to  $+600^{\circ}\text{F}$ , a centrifuge with a capability of 200g's, a 25 000-V electrostatic discharge apparatus, and a high-pressure pump with a capabil-*

*ity of 40 000 lb/in<sup>2</sup>. The functional test capabilities are programmable electrical firing circuits, measurements of acceleration, force, pressure, and temperature, and a variety of explosive performance monitoring systems. A high-frequency (40-kHz) analog recording/playback system is used for dynamic measurements.*

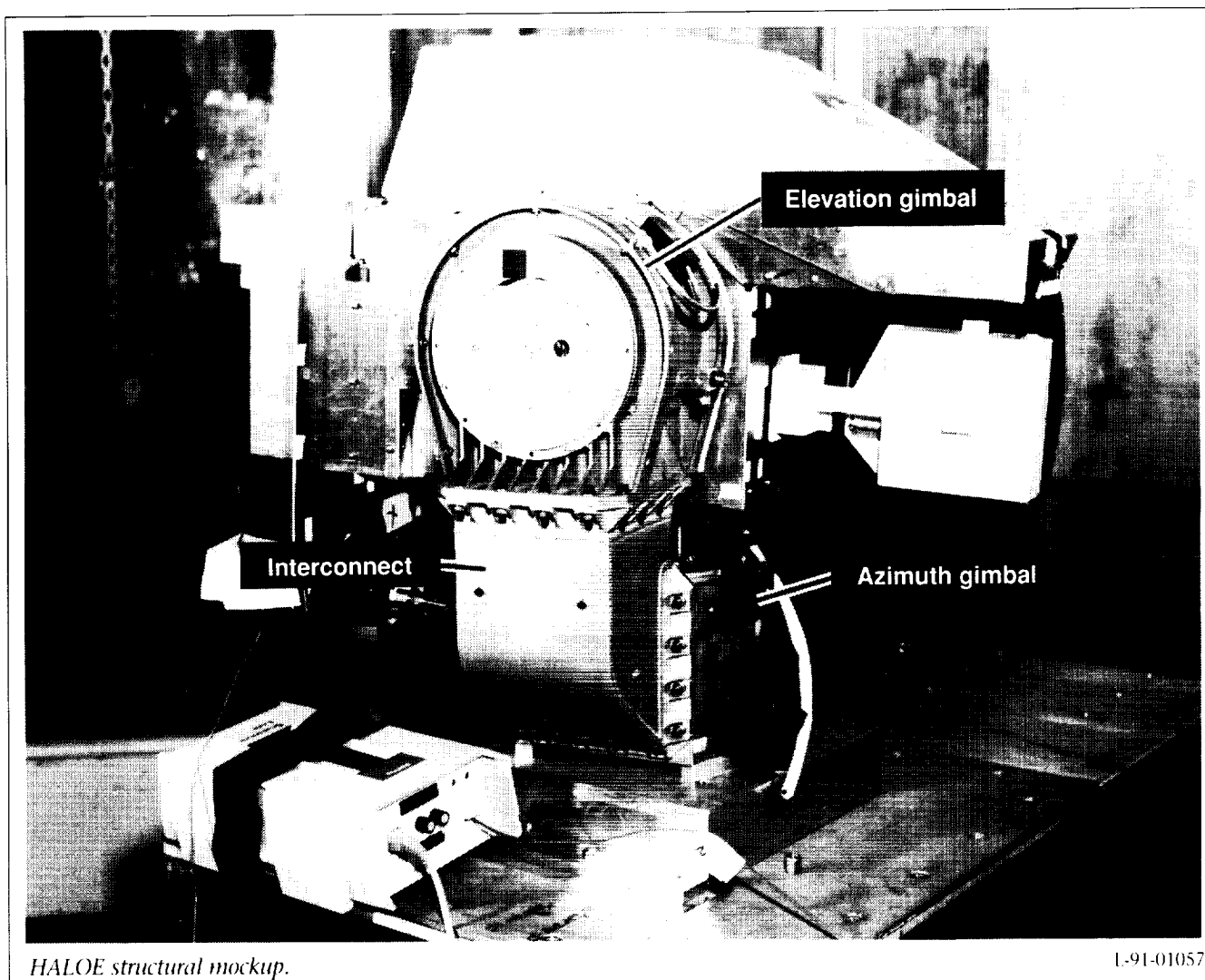
*The general-purpose open work area has a 30-ft by 60-ft floor space with a vertical working height of 35 ft. Two explosion-proof pneumatic gantry cranes are available to handle the heavier loads. The three reinforced concrete test cells are designed with lightweight external walls to relieve overpressures in an outboard manner. These test cells serve three separate functions. Environmental testing is performed in cell one, and temporary storage of potentially hazardous materials and test article assembly and checkout are performed in cell two. Cell*

*three is used for explosives functional testing because this cell contains an exhaust fan, which is used for the purge of smoke or other caustic products, and a mobile steel containment box, which is used for testing and may produce explosive fragments.*

### **Hazardous Testing of HALOE Hardware**

---

*In qualifying and certifying flight hardware for the HALOE instrument, a number of tests were conducted which were potentially hazardous to personnel. These tests, which included functioning pyrotechnically actuated pin pullers and pneumatically pressurized portions of primary structure, were conducted in facilities designed for remote testing and containment of blast pressures and fragmentation.*



The HALOE development and qualification required more than 100 firings of pyrotechnically actuated pin pullers in both component and system-level tests. The figure shows a mockup of the HALOE instrument on which the system-level test firings were made. Both proper release of the gimbals that are pinned during launch and the levels of pyrotechnically induced mechanical shock into the structure were demonstrated.

A pneumatic test was conducted on the closed-volume interconnect structural adapter

between the gimbals to determine the potential for rupture or mechanical deformation during ascent to orbit. A structural margin was demonstrated by pressurizing the volume to 20 lb/in<sup>2</sup>, which induced no permanent deflections. Bleed-down data were also obtained to accurately predict the equivalent orifice size of the venting at the assembled interfaces. (Laurence J. Bement, 47084)



## Report Documentation Page

1. Report No. NASA TM-104090	2. Government Accession No.	3. Recipient's Catalog No.	
4. Title and Subtitle Langley Aerospace Test Highlights—1990		5. Report Date May 1991	
		6. Performing Organization Code	
7. Author(s)		8. Performing Organization Report No.	
		10. Work Unit No.	
9. Performing Organization Name and Address NASA Langley Research Center Hampton, VA 23665-5225		11. Contract or Grant No.	
		13. Type of Report and Period Covered Technical Memorandum	
12. Sponsoring Agency Name and Address National Aeronautics and Space Administration Washington, DC 20546-0001		14. Sponsoring Agency Code	
		15. Supplementary Notes	
16. Abstract The role of the NASA Langley Research Center is to perform basic and applied research necessary for the advancement of aeronautics and spaceflight, to generate new and advanced concepts for the accomplishment of related national goals, and to provide research advice, technological support, and assistance to other NASA installations, other government agencies, and industry. This report highlights some of the significant tests that were performed during calendar year 1990 in the NASA Langley Research Center test facilities, a number of which are unique in the world. The report illustrates both the broad range of the research and technology activities at the NASA Langley Research Center and the contributions of this work toward maintaining United States leadership in aeronautics and space research. Other highlights of Langley research and technology for 1990 are described in <i>Research and Technology 1990—Langley Research Center</i> . Further information concerning both reports is available from the Office of the Chief Scientist, Mail Stop 105-A, NASA Langley Research Center, Hampton, Virginia 23665 (804-864-6062).			
17. Key Words (Suggested by Author(s)) Research Technology Wind tunnels Simulators Laboratories Facilities Aeronautics		18. Distribution Statement Unclassified—Unlimited  Subject Category 99	
19. Security Classif. (of this report) Unclassified	20. Security Classif. (of this page) Unclassified	21. No. of Pages 183	22. Price A09